Age-related changes in CNS and PNS neuronal structures within C57BL / 6J male mice that regulate continence

Emily Helen Doogan (E.H.D)

PhD

2020

Age-related changes in CNS and PNS neuronal structures within C57BL / 6J male mice that regulate continence

Emily Helen Doogan

Biomedical Science (BSc)

A thesis submitted in partial fulfilment of the requirements for a Doctor of Philosophy of the University of Northumbria at Newcastle

Research undertaken in the School of Applied Sciences, University of Northumbria at Newcastle

March 2020

ABSTRACT

The prevalence of urinary incontinence (UI), faecal incontinence (FI) and chronic constipation increases with age. Sufferers tend to have reduced quality of life, with treatments being far from ideal. Furthermore, treatment costs place significant financial burden on the economy. The lumbosacral somatic dorsolateral nucleus (DLN) and spinal nucleus of the bulbospongiosus (SNB), and the sacral parasympathetic nucleus (SPN), exert control over the external urethral sphincter (EUS) external anal sphincter (EAS), and bladder detrusor / colorectal smooth muscle, respectively. Pontine nuclei, including the pontine micturition centre (PMC), locus coeruleus (LC) and laterodorsal tegmental nucleus (LDTg), and the hypothalamic paraventricular nucleus (PVN) share connection pathways and exert control over defaecation and micturition.

In this work, lumbosacral spinal structures were immunolabelled alongside inhibitory methionine-enkephalin (met-ENK) and gamma aminobutyric acid (GABA) boutons; pontine structures were immunolabelled alongside inhibitory met-ENK boutons; and the PVN was immunolabelled alongside inhibitory GABA and excitatory glutamate. The density of GABA and met-ENK in the SPN significantly decreased with age; the density of glutamate significantly increased in the PVN periventricular region (PVNpv); and the number of GABA inputs onto OXY^+ and VP^+ parvocellular soma within the PVN medial parvocellular dorsal division (PVNmpd) significantly increased with age. In all other nuclei the density / number of inputs from immunolabelled boutons remained unchanged with age. Furthermore, soma size and cell number (observed in pontine and spinal nuclei) were maintained with age. The distal colon (DC) is also extensively controlled by the intrinsic enteric nervous system (ENS) which is known to be subject to age-related structural changes. Protein was extracted from the whole DC with the future aim of extracting proteins specifically from the myenteric plexus (MP). Subsequently, whole DC protein extract was subject to downstream protein analysis to determine expression changes with age. Forty-four proteins showed age-associated change in regulation. These findings indicate that age-associated changes occur at all levels of nervous and non-nervous structures that may contribute to age-related voiding dysfunctions.

TABLE OF CONTENTS

ACKNOWLEDGMENTS

Firstly, I will extend my gratitude to Northumbria university of Newcastle for providing me the opportunity and the funding to undertake this PhD. This university has given me many fun and challenging experiences that will set me up well for the future.

I would like to express my gratitude towards members of my supervisory team. To my principal supervisor, Dr Rachel Ranson, for helping to develop my research skills from undergraduate level through to the completion of three projects and the submission of a PhD thesis. Thank you for taking the time to encourage me when I lacked confidence in my work. To Dr Jill Saffrey, Prof Gary Black and Dr Meng Zhang for providing support and for their collaborative advice on final chapter write-up and the development of methodologies that were entirely new to me.

I would like to show my appreciation to all research members who helped me in the lab. Thank you to fellow PhD student, Jennifer Wright for taking the time to demonstrate lab techniques that I had not previously undertaken. To fellow PhD student, Jon Thompson and post-doctoral researcher, William Cheung for assisting me with protein analysis and providing me with additional helpful advice.

Furthermore, I would like to thank several people who provided support outside of academic guidance. To my amazing friend, and fellow PhD student Joey Atkinson for having study days with me, making work on the weekend a lot more fun. The most entertaining parts of my PhD always involved you. To my sister, Olivia Doogan and my father, Paddy Doogan for listening to me complain about the work-life struggles I faced; even though I imagine the gloomy conversations were not overly entertaining. To my mother, Jenny Doogan for encouraging me to continue when I was finding the stress of completion almost overwhelming.

I would also like to extend this gratitude to all my family and friends who cheered me up and kept me going. The fun I had with you all gave me the work-life balance that was sometimes difficult to achieve during times of great pressure. Additionally, seeing pictures

and videos of my funny little nephew and godson, Finlay Cameron could brighten up any day.

Finally, I would like to give a massive thank you to my wonderful boyfriend, Phil Reed who provided me with every form of support possible outside of academia. I cannot express my gratitude enough for having you there when work got on top of me. From every small thing, including taking over household chores to the emotional support you gave me when I felt like giving up. Even during incredibly tough days in the lab or library I was secure in the knowledge that when I got home you would make me laugh and put a smile on my face.

DECLARATION

I declare that the work contained in this thesis has not been submitted for any other award and that it is all my own work. I also confirm that this work fully acknowledges opinions, ideas and contributions from the work of others.

Any ethical clearance for the research presented in this thesis has been approved. Approval has been sought and granted by the University Ethics Committee under project reference BMS36UNNEDRNR2015 on 02 / 12 / 2015.

Word count: 43,491

Name: Emily Helen Doogan

Signature:

Date: 01 / 03 / 2020

ABBREVIATIONS

5-HT: 5-hydroxytryptamine

AAT: Aspartate aminotransferase

ACh: Acetylcholine

ACN: Acetonitrile

AOI: Area of interest

APS: Ammonium persulphate

ASC: Anal sphincter complex

ATP: Adenosine triphosphate

BCA: Bicinchoninic acid

BSA: Bovine serum albumin

ChAT: Choline acetyltransferase

CM: Circular muscle

CNS: Central nervous system

CRC: Colorectal cancer

CRH: Corticotrophin releasing hormone

DC: Distal colon

DCV: Dorsal vagal complex

DGC: Dorsal grey commissure

DH: Dorsal horn

DI: Dual incontinence

DLN: Dorsolateral nucleus

DMV: Dorsal motor nucleus of the vagus

DOR: Delta opioid receptor

DRG: Dorsal root ganglia

DSD: Detrusor sphincter dysnergia

DTT: Dithiothreitol

EAS: External anal sphincter

EEC: Enteroendocrine cells

EEG: Electroencephalography

ELISA: Enzyme-linked immunoassay

ENK: Enkephalin

ETC: Electron transport chain

EUS: External urethral sphincter

FA: Formic acid

FFPE: Formalin-fixed paraffin-embedded

FI: Faecal incontinence

FIC: Faecal incontinence with concurrent constipation

FLCs: Fibroblast-like cells

FMRI: Functional magnetic resonance imaging

GABA: Gamma-Aminobutyric acid

GADPH: Glyceraldehyde 3-phosphate dehydrogenase

GH: Growth hormone

GHRH: Growth hormone releasing hormone

GIT: Gastrointestinal tract

GLAST: Glutamate aspartate transporter

GLT-1: Glutamate transporter-1

GLP1: Glucagon like peptide-1

GLP2: Glucagon like peptide-2

GnRH: Gonadotrophin releasing hormone

GO:BP: Gene Ontology: Biological Processes database

GO:CC: Gene Ontology: Cellular Component database

GO:MF: Gene Ontology: Molecular Function database

H&E: Haematoxylin and eosin

HNT: Hypothalamo-neurohypophysial tract

IAA: Iodoacetamide

IAS: Internal anal sphincter

IC: Interstitial cell

ICC: Interstitial cells of cajal

ICC-IM: Intramuscular interstitial cells

ICC-MP: Interstitial cells of the myenteric plexus

ICC-SMP: interstitial cells of the submucous plexus

ICS: International Continence Society

IDH: isocitrate dehydrogenase

IHC: Immunohistochemistry

IMA: Inferior mesenteric artery

IML: Intermediolateral spinal column

IAS: Internal anal sphincter

IPANs: Intrinsic primary afferent neurons

IUS: Internal urethral sphincter

KEGG: Kyoto Encyclopedia of Genes and Genomes database

KOR: kappa opioid receptor

LC / MS / MS: Liquid chromatography / mass spectrometry / mass spectrometry

LC: Locus coeruleus

LDTg: Laterodorsal tegmental nucleus

Leu-ENK: Leucine-enkephalin

LM: Longitudinal muscle

LMDC: Laser capture microdissection

LUT: Lower urinary tract

MDH: Malate dehydrogenase,

Met-ENK: Methionine enkephalin

MGF: Mascot generic format

MOR: Mu opioid receptors

MP: Myenteric plexus

MPG: Major pelvic ganglion

MPO: Medial preoptic area

MUI: Mixed urinary incontinence

NAD: Nicotinamide adenine dinucleotide

NADH: Nicotinamide adenine dinucleotide + hydrogen

NE: Norepinephrine

NHS: National Health Service

NO: Nitric oxide

NOS1: Nitric oxide synthase 1

OAA: Oxaloacetate

OAB: Overactive bladder

OXY: Oxytocin

p.a.: Per annum

PAG: Periaqueductal grey

PBS: Phosphate buffered saline

PDGFRα: Platelet-derived growth factor receptor alpha

PFA: Paraformaldehyde

PK: Pyruvate kinase

PMC: Pontine micturition centre

PNS: Peripheral nervous system

PVN: Paraventricular hypothalamic nucleus

PVNam: Paraventricular nucleus, anterior magnocellular

PVNap: Paraventricular nucleus, anterior parvocellular

PVNdp: Paraventricular nucleus, dorsal parvocellular

PVNlp: Paraventricular nucleus, lateral parvocellular

PVNmm: Paraventricular nucleus, medial magnocellular

PVNmpd: Paraventricular nucleus, medial parvocellular, dorsal zone

PVNmpv: Paraventricular nucleus, medial parvocellular, ventral zone

PVNpml: Paraventricular nucleus, posterior magnocellular, lateral zone

PVNpmm: Paraventricular nucleus, posterior magnocellular, medial zone

PVNpv: Paraventricular nucleus, periventricular part

PYY: Peptide YY

QOL: Quality of life

RAIR: Rectal anal inhibitory reflex

RDLN: Retrodorsolateral nucleus

REAC: Reactome Pathways database

SCI: Spinal cord injury

SCN: Suprachiasmatic nucleus

SMC: Smooth muscle cell

SMP: Submucous plexus

SNB: Spinal nucleus of the bulbospongiosus

SON: Supraoptic nucleus

SPN: Sacral parasympathetic nucleus

SUI: Stress urinary incontinence

TCA: Tricarboxylic acid

TEMED: N,N,N’,N’-Tetramethylethylenediamine

TF: Transcription Factor database

TRH: Thyrotropin-releasing hormone

UI: Urinary incontinence

UTI: Urinary tract infection

UUI: Urge urinary incontinence

VGAT: Vesicular GABA transporter

VGLUT2: Vesicular glutamate transporter 2

VP: Vasopressin

WP: WikiPathways database

1 INTRODUCTION

1.1 BRIEF INTRODUCTION AND AIMS OF THESIS

The prevalence of UI, FI, and chronic constipation increases with age (Searcy, 2017; Shah et al., 2012; Vazquez Roque and Bouras, 2015). This has a major impact on the quality of life for the elderly population (Baffy et al., 2017; Bartlett et al., 2009; Ko et al., 2005). Treatment of bladder and bowel dysfunction are currently far from ideal and often involve symptom management (e.g. incontinence pads). Some pharmaceutical treatment options for UI show no symptom improvement in some patients and others (anti-cholinergics) causing adverse side effects including constipation (Samuelsson et al., 2015). Therefore, treatment has a long way to come, with the cost of current treatments placing significant financial burden on individuals and the economy (Coloplast., 2016; NHS England., 2018; NHS England., 2016). Furthermore, UI, FI, and constipation are associated with an increased mortality rate in older adults (Jamieson et al., 2017; John et al., 2014).

The age-associated changes resulting in bladder and terminal bowel dysfunction are likely multifactorial. These include ageing of effector cells (smooth muscle of the bladder and terminal bowel / striated muscle of external sphincters) and neurons that regulate their function (located in the both the central and peripheral nervous systems). The main aim of this PhD was to determine potential neurogenic mechanisms that may contribute to age-associated bladder and bowel dysfunction in mice. This was undertaken via immunohistochemical labelling of mouse central nervous structures (in the lumbosacral spinal cord, brainstem, and hypothalamus) that control bladder / bowel function (see Chapters 2-4). Additionally, protein analysis of mouse DC was undertaken (see Chapter 5). This methodology was applied to various age groups for structural and proteomic comparisons between young and aged mice that may contribute to age-associated problems with storage / elimination of urine and faecal matter.

1.2 BLADDER AND TERMINAL BOWEL DYSFUNCTION AND PREVALENCE IN THE ELDERLY POPULATION

Ageing of the bladder and terminal bowel may result in problems with storage and elimination of urine and faecal matter (Searcy, 2017; Shah et al., 2012; Vazquez Roque and Bouras, 2015). UI is defined by the International Continence Society (ICS) as involuntary loss of urine and can occur for different reasons. Stress UI (SUI) is involuntary leakage as a consequence of events such as sneezing, coughing or physical exertion and reflects the inability of the bladder outlet to remain closed. Urge UI (UUI) is leakage preceded or accompanied by a sudden compelling desire to urinate and reflects over-activity of detrusor muscles. SUI and UUI can co-occur in the same individual and is known as mixed UI (MUI) (Abrams et al., 2002). UI can be secondary to urinary retention, of which the prevalence in the general population is unknown; however, it is thought to be more prevalent in aged males. Urinary retention is defined as the inability to completely empty the bladder of urine and can be caused by detrusor underactivity or urethral obstruction (Dougherty and Aeddula, 2019; Emberton and Anson, 1999). Regarding the terminal bowel, involuntary loss of faeces is known as faecal incontinence; and difficulty expelling faecal matter is known as constipation (less than three bowel movements per week) and can result in faecal impaction (Bharucha et al., 2006; Mounsey et al., 2015). FI can occur secondary to constipation or faecal impaction (Read and Abouzekry, 1986).

The prevalence of UI has been observed to increase with age in both sexes (Campbell et al., 1985; Collerton et al., 2009; Condon et al., 2019; Irwin et al., 2009; Jerez-Roig et al., 2016; Kok et al., 1992; Lasserre et al., 2009; Nakanishi et al., 1997; Shaw et al., 2006; Song and Bae, 2007; Teunissen et al., 2004; Wehrberger et al., 2012; Wu et al., 2015; Xu and Kane, 2013). It should be noted that the majority of studies did not provide details on the type of bladder dysfunction e.g., SUI vs UUI etc.; and that studies had varying sample sizes and sex / age-groups. Additionally, due to social stigma, it is likely that UI (and bowel dysfunction) is underreported by sufferers. UI was consistently found to be more prevalent in 80+ year old individuals confined to nursing homes (58.9-69 %) compared with community dwellers (31-47 %) (Jerez-Roig et al., 2016; Lasserre et al.,

2009; Nakanishi et al., 1997; Song and Bae, 2007; Wehrberger et al., 2012; Xu and Kane, 2013). Furthermore, in a study with 32,285 participants, UI was determined as a significant risk factor for elderly residential care admission (Schluter et al., 2017). Where studies distinguish between males and females, UI prevalence was higher in women of 80+ (26.7 %) and 85+ years (26.6-36.4 %) than males of 80+ (13 %) and 85+ years (12.6-24 %) (Collerton et al., 2009; Song and Bae, 2007; Wehrberger et al., 2012; Wu et al., 2015).

Studies that distinguished between types of UI in elderly community dwellers reported differing results. Of women over 80 years of age, 25.9-62 % suffered MUI, 9.3-26 % SUI, and 9-9.3 % UUI (Lasserre et al., 2009; Shaw et al., 2006). Of male and females aged 85+, 62 % suffered MUI, 4 % SUI and 34 % UUI (Song and Bae, 2007). In 85+ women, UUI (35 %) and SUI (39.1 %) were more prevalent than in men (25.5 % and 13.8 % respectively). Whereas, nocturia (waking to void one or more times during the night) had a higher prevalence in males (69 %) than females (49 %) (Wehrberger et al., 2012). Jerez-Roig et al. (2016) sought to distinguish between types of UI in institutionalised elderly individuals (mean age: 81.5 years). Of those suffering UI, 3.7 % suffered SUI and 13.8 % suffered UUI. These relatively small figures can be attributed to the inclusion of two additional categories of UI— functional UI (physical impairment) and functional UI (cognitive impairment) of which 56.1 % and 54 % of individuals suffered from respectively. Functional UI is the loss of urine due to inability or unwillingness to access toilet facilities as a result of physical or cognitive impairment or psychological unwillingness. The extent of UI and co-morbidities associated with functional UI likely made it difficult to differentiate between SUI and UUI.

Like UI, the prevalence of FI and dual incontinence (DI– the co-occurrence of UI and FI in the same individual) is increased with age (Chassagne et al., 1999; Chughtai et al., 2019; Schnelle et al., 2009; Teunissen et al., 2004; Tobin and Brocklehurst, 1986; Wu et al., 2015). It should be noted, as was the case for UI, data collection methods were not consistent across studies; and FI / DI were likely underreported due to social

embarrassment. Separate studies observed a consistently greater prevalence of FI in nursing homes ranging from 20 % in those aged 60+ to 52 % in those aged 80+ (Chassagne et al., 1999; Chughtai et al., 2019). In community dwellers, FI prevalence was as low as 4.2 % in those aged 60+ and was 16.9 % in those aged 85 + (Kok et al., 1992). Risk factors for the development of FI or DI include older age, cognitive impairment, limitations in daily activities, prolonged institutionalisation, history of UI, and spinal cord injury (Bliss et al., 2018; Chassagne et al., 1999; Obokhare, 2012; Shamliyan et al., 2007; Tobin and Brocklehurst, 1986). Where studies distinguish between males and females, the prevalence of FI was observed to be slightly higher in women than men. In individuals aged 65+ confined to a nursing home, 43.9 % of women suffered FI compared to 37.5 % of men (Saga et al., 2013). In a sample study of both community dwellers and nursing home residents, 9.3 % of women aged 85+ suffered FI compared to 7.4 % of men (Collerton et al., 2009). In a cohort of individuals aged 50+ measuring both FI and DI prevalence, women had slightly lower prevalence of FI at 8.2 % compared to men at 8.4 %. However, the prevalence of DI was much greater in women at 6 % than men at 1.9 % (Wu et al., 2015). The increased prevalence of UI, FI, and DI observed in females has been linked to injuries during childbirth, often associated with pudendal nerve damage (Jiang et al., 2009; Snooks et al., 1985).

The prevalence of constipation and laxative use increases with age. Over a 14-year period, a study using a cohort of 2,087 males and females aged 65+ saw constipation increase from 13.8 % to 20.9 %, and laxative use increase from 6.3 % to 15.1 % (Werth et al., 2015). In a study comparing free-living (mean age: 74 years) to institutionalised elderly (mean age: 84 years), laxative use was greater in nursing home residents (65 %) compared to community dwellers (20 %) (Marfil et al., 2005). In community-dwelling individuals aged 65+, a higher prevalence of constipation and laxative use was reported in women at 14.6 % and 16.6 %, than men at 6.3 % and 12.8 %, respectively (Werth et al., 2017). Constipation / faecal impaction can lead to FI as elderly patients with faecal impaction showed impaired anorectal sensation during distension and a lower rectal volume required for anal relaxation compared to healthy controls (Read and Abouzekry,

1986). Furthermore, in a study of faecally incontinent nursing home residents with a mean age of 86 years, 81.1 % were found to suffer from constipation (Schnelle et al., 2009). Additionally, effective treatment of constipation in institutionalised elderly resulted in 35 % fewer episodes of FI (Chassagne et al., 2000). Prevalence of neurogenic constipation as a result of spinal cord injury (SCI) has been observed to increase with age. In a study cohort of individuals who had suffered SCI (median age beginning at 55 years), constipation and laxative use increased from 21 % and 19 % to 39 % and 31 %, respectively over a 19-year period (Nielsen et al., 2017). Furthermore, age-associated neurodegenerative diseases are linked to increased prevalence of UI, FI, and constipation (Campbell et al., 1985; Emmanuel, 2019; Tobin and Brocklehurst, 1986).

1.3 IMPACT OF BLADDER AND BOWEL DYSFUNCTION ON QUALITY OF LIFE

Incontinence negatively impacts a sufferer's psychological well-being and overall quality of life (QoL) (Choi et al., 2020; Farage et al., 2008; Markland et al., 2010; Meyer et al., 2019; Molinuevo and Batista-Miranda, 2012; Ugurlucan et al., 2019). Both UI and FI have been associated with symptoms of anxiety and depression (Coyne et al., 2012; Molinuevo and Batista-Miranda, 2012). Anxiety symptoms can manifest from fear of urinary or faecal leakage and can result in adoption of coping strategies including restriction of food / fluid intake and toilet mapping (Anders, 2000; Andy et al., 2019; Anger et al., 2011; Hansen et al., 2006; Kuhn et al., 2006; Thomas and Morse, 1991). Furthermore, anxiety can result in reduction of daily activities, particularly activities in a social setting, which can impact self-confidence and promote feelings of social isolation and loneliness (Hunskaar and Sandvik, 1993; Stickley et al., 2017). The belief that incontinence is an inevitable aspect of ageing combined with the shame / embarrassment of disclosing personal matters prevents people from seeking help and likely worsens feelings of social isolation (Horrocks et al., 2004).

Overactive bladder (OAB) and urinary retention have also shown co-occurrence with depression and anxiety (Drossaerts et al., 2016; Jairam et al., 2018). However, the

causality between bladder symptoms and mental conditions is unclear and may involve a mechanism in the bladder–brain-axis. Some studies observed the new onset of OAB in already depressed patients. Whilst other studies lack evidence of causality and suggest that OAB and depression / anxiety are bidirectional in nature (Vrijens et al., 2015). Constipation has also been linked with a decreased QoL (Belsey et al., 2010; Dennison et al., 2005; Wald et al., 2007). Patients with FI and concurrent constipation (FIC) reported worse overall QoL in comparison to patients with FI alone, and QoL scores were further declined with increased constipation severity. Additionally, FIC patients had higher rates of mental (depression) and physical impairments (pelvic organ prolapse, UI, pelvic pain, bladder pain, and abdominal pressure) (Cauley et al., 2019). Mental and physical impairments experienced alongside constipation are worsened with increased age (Wald et al., 2007).

1.4 ECONOMIC BURDEN OF BLADDER AND BOWEL DYSFUNCTION

With improvements in healthcare and lifestyle, the population is living longer. 18.3 % of the UK population was 65+ in 2018, which is projected to increase to 24.2 % in 2038 (Office for National Statistics., 2019). The prevalence of bladder and bowel dysfunction is increased with age and thus treatment of incontinence will likely place a greater financial burden on the National Health Service (NHS) in the future. The annual NHS cost for incontinence pad usage is around 80 million per annum (p.a.) in England (NHS England., 2018). In 2015, GP prescribing data observed that the cost of catheters was £115.1 million p.a. (NHS England., 2016). Hospitalised patients with incontinence are at increased risk of acquiring a urinary tract infection (UTI) due to catheterisation, with costs of additional bed days and treatment at around £90 million p.a. Furthermore, poor continence care is a contributory factor to the development of pressure ulcers, of which it costs an average of £4,638 per pressure ulcer (NHS England., 2018). OAB / UUI are predisposing risk factors for falls, and the risk of falling is increased in individuals aged 65+ (Szabo et al., 2018). Elderly individuals suffering incontinence are 26 % more likely to

fall and 34 % more likely to fracture (Soliman et al., 2016). Falls from fragility fractures cost the NHS £4.4 billion p.a. in England (NHS England., 2017). Regarding constipation, GP prescription of laxatives costs £101 million p.a. across the UK. Additionally, unplanned hospital admissions due to constipation was £145 million in 2014 / 15. The figure for NHS expenditure on constipation is likely to be much higher when including GP visits and home visits (Coloplast., 2016). Furthermore, the cost of treating anxiety and depression as a result of bladder and bowel dysfunction likely places further financial burden on the NHS. However, at present, this cost has not been estimated.

1.5 BASIC STRUCTURE OF THE BLADDER AND TERMINAL BOWEL

The bladder and terminal bowel perform similar functions, namely the storage and voluntary expulsion (developed after 2-3 years of age) of urine and faecal matter, respectively. Additionally, they have a similar basic cellular structure consisting of smooth muscle with an inner lining of specialised epithelial cells. Further cell types and tissue structures include nervous and vascular supplies, connective tissue, interstitial cells (ICs), and immune system cells; the composition and properties of these cell types, however, are vastly different between the two organs (Merrill et al., 2016; Saffrey, 2014). The main focus of this thesis is the nervous control of these structures and therefore a detailed discussion of non-nervous / sensory cell types in the bladder will not be included. However, protein analysis of the DC is undertaken in whole gut sections (encompassing all cells types) and therefore a more detailed description of cell structure in the DC wall is included (see section 1.7).

1.6 ANATOMY, CELLULAR ORGANISATION AND NERVOUS CONTROL OF THE BLADDER

1.6.1 Functional anatomy of the bladder

The urinary bladder is a hollow muscular organ made up of smooth detrusor muscle surrounding the bladder body. Urine is excreted from the kidneys and passes through the

ureters into the bladder until activation of the micturition reflex in which urine exits via the urethra (Lanzotti and Bolla, 2019). The storage phase is supported by the contraction of the smooth and striated muscle of the internal urethral sphincter (IUS) and EUS respectively, and the surrounding pelvic floor musculature; whilst the smooth detrusor muscle remains relaxed allowing bladder distension as it fills. During the micturition reflex, the EUS and IUS relax and seconds later the bladder smooth muscle contracts causing urine expulsion (Fowler et al., 2008). Storage and voiding reflexes are elicited by nervous activity. The human bladder is partially controlled by intramural cells grouped into small ganglia (Dixon et al., 1983). However, the majority of bladder activity is derived from external innervation from neurons located outside the bladder wall (Gilpin et al., 1983). In mice (used in the present study), only intramural nerve fibres have been observed to course through the bladder wall. Thus, the majority (if not all) bladder innervation is from extrinsic nerve supply (Koh et al., 2012).

The muscle fibres that make up detrusor muscle are arranged arbitrarily. Individual cells within muscle fibres are interconnected with the presence of gap junctions between each cell. This muscular arrangement allows the bladder to contract in a coordinated manner and helps to rapidly spread nervous signals, despite multiple cells having no direct autonomic input (Andersson and Arner, 2004; Karicheti and Christ, 2001). Certain cells in the bladder are thought to play an intermediary role in its nervous control, including interstitial and urothelial cells (bladder epithelium) (Merrill et al., 2016). Urothelial cells are located in close proximity to efferent and afferent nerve endings (Birder et al., 2002). They express a variety of receptor subtypes (including purinergic, adrenergic, cholinergic etc.) which indicates that urothelium can respond to diverse stimuli (from bladder distension to noxious stimuli). In response to chemical / mechanical stimuli, they release a variety of neuroactive mediators [adenosine triphosphate (ATP), acetylcholine (ACh), nitric oxide (NO) etc.] (Merrill et al., 2016). ATP appears as the main messenger released during purinergic mechanosensory transduction and acts on $P2X_3$ receptors on afferent neurons to generate signals indicative of bladder fullness or pain (Burnstock, 2009; Cockayne et al., 2000). Urothelial cells have been hypothesised to interact with ICs

due to their close anatomical location (in the lamina propria) and their expression of purinergic receptors (Merrill et al., 2016). Interstitial cells of cajal (ICCs), present in the GIT, are implicated in the regulation of smooth muscle contractility. In the bladder, like ICCs, sub-populations of cells express c-kit, vimentin and platelet-derived growth factor receptor alpha (PDGFRα). However, their exact function is more ambiguous at present. In addition to presence in the lamina propria, ICs are intermingled with detrusor muscle cells and have been suggested to play a role in modulation of smooth muscle activity, sensory processing (via contact with bladder afferents), and integration of signalling between bladder layers. For further explanation of the potential functions of bladder ICs, see review by Koh et al. (2018).

1.6.2 Innervation of the bladder and urethral sphincters at spinal level

1.6.2.1 Spinal efferents

The bladder receives indirect (preganglionic) innervation from sympathetic and parasympathetic autonomic neurons and the EUS receives direct innervation from somatic motor neurons in the spinal cord (Chancellor and Yoshimura, 2004). The cholinergic SPN promotes detrusor contraction and bladder emptying (Ni et al., 2018; Papka et al., 1995). It is located in Lamina V in spinal segments' S2-S4 in humans and L5-S1 in rodents, and projects via the pelvic nerve to the pelvic ganglion in humans / major pelvic ganglion (MPG) in rodents (Banrezes et al., 2002; Chancellor and Yoshimura, 2004). Preganglionic parasympathetic neurons excite postganglionic neurons by ACh release that is mediated by nicotinic receptors (Somogyi and de Groat, 1993; Yoshimura and de Groat, 1997). Postganglionic neurons then excite smooth muscle fibres by ACh transmission mediated via muscarinic receptors (M_2 and M_3 subtypes). Although ACh is the main neurotransmitter that excites detrusor muscle, ATP has also been observed to stimulate bladder contractions via purinergic receptors (de Groat and Yoshimura, 2001). Additionally, some postganglionic parasympathetic neurons innervate

the IUS and cause smooth muscle relaxation likely via transmission of NO (Bennett et al., 1995).

Spinal sympathetic innervation of the IUS derives from the intermediolateral cell column (IML) and the dorsal grey commissure (DGC), at spinal segments' T12-L2 in humans and L1-L2 in rodents (Chancellor and Yoshimura, 2004; Ranson and Saffrey, 2015). Sympathetic preganglionic neurons project via the hypogastric and pelvic nerves towards the hypogastric / pelvic ganglia in humans, or the MPG in rodents. This sympathetic innervation promotes urine storage via bladder neck IUS contraction and detrusor relaxation (de Groat and Wickens, 2013; Shefchyk, 2002). Preganglionic sympathetic neurons excite postganglionic neurons via ACh transmission mediated by nicotinic receptors (Chancellor and Yoshimura, 2004; Somogyi and de Groat, 1993). Postganglionic neurons then excite IUS smooth muscle via transmission of norepinephrine (NE) mediated by α_1-adrenoreceptors. Additionally, detrusor relaxation is initiated by postganglionic transmission of NE mediated by β_2- and β_3-adrenoreceptors (Nomiya and Yamaguchi, 2003).

Onuf's nucleus provides somatic innervation to the EUS and is located in lamina IX, segments S2-S4 (Mannen, 2000). The rodent homologues of onuf's nucleus are two separate nuclei termed the SNB and the DLN and are located in lamina IX, segments' L5-L6. The DLN projects to the EUS and ischiocavernosus (related to anal flexion and reproductive reflexes), and the SNB projects to the EAS, ventral bulbospongiosus (related to sexual reflexes), and levator ani (forms main part of the pelvic floor musculature) (Schrøder, 1980). These motor neurons project via the pudendal nerve and excite the EUS by the release of ACh that acts on nicotinic receptors (Bierinx and Sebille, 2006; von Heyden et al., 1998). During bladder filling, EUS-projecting neurons are tonically active to evoke EUS contraction (Thor and de Groat, 2010).

Parasympathetic and somatic LUT and terminal bowel spinal efferents (located in the lumbosacral spinal cord) were structurally compared for age-associated changes. This

was done by immunohistochemically labelling neurons in mice of different age groups. Analyses and results of this research are discussed in Chapter 3.

1.6.2.2 Spinal afferents

Sensory information is carried from the bladder via afferent fibres in the pelvic, hypogastric, and pudendal nerves (de Groat and Yoshimura, 2009). Afferents comprise of myelinated Aδ fibres and unmyelinated C fibres. Aδ fibres are present in the detrusor muscle layer and respond to detrusor stretching to convey bladder fullness sensations. C fibre afferents are more abundant and are present in the detrusor muscle layer, the lamina propria and in the urothelial layer. C fibres discharge during bladder distension, but at a higher threshold compared to Aδ fibres (de Groat and Yoshimura, 2009). The soma of pseudounipolar pelvic and pudendal afferents are located in the dorsal root ganglia (DRG) with afferents terminating in the sacral spinal cord (S2-S4 in humans; L4-S2 in rodents). The soma of hypogastric afferents are located in the DRG of neurons projecting to thoracolumbar spinal segments (T10-L2 in humans; T8-L1 in rodents) (Brumovsky et al., 2012; Tennyson et al., 2016). Transganglionic transport of tracers show that bladder afferents project into Lissauer's tract and pass rostrocaudally giving off collaterals where sympathetic, parasympathetic, and somatic LUT efferent soma and / or dendrites are located. These regions include, (in sympathetic, parasympathetic, and somatic spinal segments), the dorsal horn (DH) in laminae I, laminae V-VII where the SPN and further rostral IML are located, and the DGC in laminae X. The most prominent projection site for bladder afferents is the SPN (de Groat and Yoshimura, 2009). Additionally, bladder afferents input onto spinal interneurons that make excitatory or inhibitory synaptic connections with preganglionic neurons. Some bladder afferents synapse with second-order neurons that project to nuclei in the brain involved in micturition (discussed below) (Fowler et al., 2008).

1.6.3 Supraspinal control of bladder function

The process of micturition is partially controlled by reflexes and is partially under conscious control. An integral part of this process involves communication with higher brain centres so urination only occurs when it is appropriate (de Groat et al., 2015). Neuronal tracing, electrical nerve stimulation, and functional imaging studies have shown that a wide variety of brain centres are involved in the control of the LUT emphasising its complexity (Blok and Holstege, 1997; Duong et al., 1999; Griffiths and Fowler, 2013; Kuipers et al., 2007; Roy and Green, 2019). These include nuclei situated in the brainstem, cerebellum, limbic system, hypothalamus, thalamus, basal ganglia, and cerebral cortex.

Brainstem nuclei, including the periaqueductal grey (PAG) and the PMC are a fundamental part of the spinobulbospinal voiding-reflex pathway. This pathway acts as a binary switch between ‘off’ (urine storage) or ‘on’ (voiding) (de Groat and Wickens, 2013). Higher brain centres involved in micturition control are likely associated with assessment of voiding safety (since an organism is vulnerable during voiding) and assessment of social appropriateness of voiding (Griffiths and Fowler, 2013). Brain structures that have been immunohistochemically labelled and analysed in the present study include the PMC, LC, and LDTg of the brainstem and the PVN of the hypothalamus. Therefore, these nuclei are one of the focuses of this thesis and are discussed below. For further explanation of other brain centres / nuclei involved in the control of micturition see listed reviews (de Groat et al., 2015; Drake et al., 2010; Griffiths and Fowler, 2013; Malykhina, 2017; Roy and Green, 2019).

1.6.3.1 Brainstem nuclei

The LC, PMC, and LDTg brainstem nuclei that are involved in the micturition reflex are located within the pontine tegmentum. These brainstem nuclei were immunohistochemically labelled (in mice) and structurally compared for age-associated changes. Analyses and results are discussed in Chapter 3. All three nuclei are situated in

close apposition to each other on the ventrolateral edge of the fourth ventricle. The LC is the furthest lateral with the PMC medial to the LC and LDTg. Nuclei are bilateral, located in each hemisphere (Paxinos and Franklin, 2007). In a study where retrograde tracer was injected into the rat urethra, the PMC and LC had the greatest number of immunopositive neurons in comparison to all other brain nuclei (Vizzard et al., 1995). Also known as the Barrington's nucleus, the PMC was first discovered in the cat as the centre for efferent control of the bladder due to the blockade of micturition reflex following bilateral lesioning (Barrington, 1925). An electrophysiological study reported that 79 % of PMC neurons are active during bladder distension and the PMC is active during bladder voiding (in rodents and humans) (Blok et al., 1997b; Nour et al., 2000; Rouzade-Dominguez et al., 2003b; Tai et al., 2009; Yao et al., 2019), with the injection of glutamate or electrical current into the PMC triggering micturition (Kruse et al., 1991; Mallory et al., 1989; Mallory et al., 1991; Nishizawa et al., 1988; Sugaya et al., 1987). Recent studies in unanaesthetised rats and mice have shown the PMC exhibits slow background activity during bladder filling, with bursts of activity during and up to 20 seconds after urination (Hou et al., 2016; Manohar et al., 2017). The purpose of neuronal firing after urination is unknown but suggests that the PMC plays a more complex role in bladder emptying than a simple on/off switch.

The PMC exerts visceral control over the micturition reflex via descending fibres that synapse onto spinal sympathetic IML and parasympathetic SPN neurons. Additionally, the PMC synapses onto inhibitory GABAergic / Glycinergic interneurons in the DGC that project to (somatic) onuf's nucleus / DLN. This results in coordinated relaxation of the EUS and contraction of detrusor muscle during micturition (Blanco et al., 2014; de Groat, 1998; Guo et al., 2013; Keller et al., 2018; Nuding and Nadelhaft, 1998; Verstegen et al., 2017). A wide variety of afferents project (directly and indirectly) to the PMC (Valentino et al., 1994). Known direct projections to the PMC include layer 5 neurons in the primary motor cortex, the ventromedial pontomedullery field, ventromedial and dorsomedial PAG, medial preoptic area, posterior hypothalamus, and the lumbosacral spinal cord (SPN and DGC) (Blok and Holstege, 1994; Ding et al., 1999; Ding et al., 1997; Kuipers et al., 2006; Yao et al., 2018). Recently, the PMC has been observed to have very

long dendritic arbours and thus potentially receive additional afferent inputs (Verstegen et al., 2017). Lumbosacral spinal afferents have also been observed to project to relay neurons in the PAG before reaching the PMC to evoke micturition in rats (Matsuura et al., 2000). However, this pathway does not evoke micturition in cats (Ding et al., 1997; Takasaki et al., 2010). Inputs from higher brain afferents likely relay conscious information on whether it is safe or appropriate for micturition to occur (Tai et al., 2009).

Aside from efferent influence over spinal micturition, the PMC sends collateral projections to the noradrenergic LC, which may serve to coordinate visceral and neurobehavioral aspects of the micturition (Valentino et al., 1996). The LC sends its widely distributed axonal network to various regions of the forebrain including the cortex where its noradrenergic input results in cortical electroencephalographic (EEG) activation (Berridge and Foote, 1991; Carter et al., 2010; Vazey and Aston-Jones, 2014). This likely leads to arousal and shift of focus i.e. awareness of bladder fullness. Furthermore, bladder distension has been linked to cortical EEG activation (Page et al., 1992; Valentino et al., 2011). The LC also sends direct descending projections to spinal LUT efferents including the sympathetic IML, the parasympathetic SPN, and the DLN / onuf's nucleus (Jones and Yang, 1985; Nygren and Olson, 1977; Westlund et al., 1983). The LC's influence over spinal micturition is modulatory. NE derived from LC projections can mediate excitatory and inhibitory spinal influences on the LUT via adenoreceptors. Excitation of either α_{1-} and α_2-adrenoreceptors in the sacral spinal cord have been observed to both cause and inhibit bladder contractions (de Groat et al., 2015). More specifically NE innervation of α_{1A}- and α_{1D}-adrenoreceptors is excitatory only, resulting in bladder contractions (Kadekawa et al., 2013; Sugaya et al., 2002; Yokoyama et al., 2010). In the IML, NE effect is more well-defined with tonic excitation occurring via α_1-adrenoreceptors and inhibition occurring via α_2-adrenoreceptors. Similarly, the DLN is tonically excited (EUS contraction) via α_1-adrenoreceptors and inhibited (EUS relaxation) via α_2-adrenoreceptors (de Groat et al., 2015). The LC receives innervation from a variety of higher brain centres. Aside from the PMC, direct projections to the LC that are implicated in micturition control include the LDTg (caudal region) PAG (ventrolateral part),

rostral ventral medulla, and the preoptic area (Drolet et al., 1992; Jones and Yang, 1985; Luppi et al., 1995; Samuels and Szabadi, 2008).

The LDTg's function in LUT control is less well-defined in comparison to the LC and PMC. The LDTg projects to and receives innervation from the LC (Cornwall et al., 1990; Jones and Yang, 1985). Additionally, the LDTg has been observed (in rats) to have a reciprocal relationship with the sacral spinal cord whereby it sends efferents to and receives afferents from the SPN (Hamilton et al., 1995; Hida and Shimizu, 1982). Electrical stimulation of dorsal pontine tegmentum sites in anaesthetised rats showed that the LDTg (and PAG) were the optimum sites for evoking bladder contractions (Noto et al., 1989). Distinct sites of the LDTg have been implicated in bladder function. Electrical stimulation (in rats) of a small region on the ventrolateral edge of the nucleus resulted in bladder contractions only; a further caudal region evoked sphincter contractions only; and a further lateral and caudal region evoked both bladder and sphincter contractions (Yamao et al., 2001). The LDTg has been observed to have a wide variety of efferent and afferent networks in higher brain centres including sites involved in the control of micturition (Cornwall et al., 1990).

1.6.3.2 The PVN of the hypothalamus

The PVN is a complex nucleus within the hypothalamus that is known to be the coordinator of neuroendocrine and autonomic functions, including micturition and defaecation. The PVN was immunohistochemically labelled (in mice) and structurally compared for age-associated changes. Analyses and results are discussed in Chapter 4. The PVN lies bilateral to the dorsal portion of the third ventricle in the periventricular region (Paxinos and Franklin, 2007). The PVN has three main cell types— magnocellular (larger soma) neuroendocrine, parvocellular (smaller soma) neuroendocrine, and parvocellular autonomic-projecting neurons. Magnocellular neuroendocrine neurons project to the posterior pituitary where they release hormones directly into the bloodstream. Parvocellular neuroendocrine neurons project to the median eminence for

controlled hormone release into the circulation via the hypophyseal portal system of the anterior pituitary. Parvocellular autonomic projecting neurons innervate numerous regions of the brain and spinal cord that are involved in the control of various autonomic functions including micturition (Swanson and Sawchenko, 1980). Neuronal tracing studies (in rats) have consistently observed that PVN parvocellular neurons indirectly project to the bladder and urethra (Grill et al., 1999; Marson, 1997; Rouzade-Dominguez et al., 2003a; Sugaya et al., 1997). Neurons within the PVN are highly immunocytochemically diverse and are immunopositive for numerous neuroactive substances including oxytocin (OXY), vasopressin (VP), corticotrophin releasing hormone (CRH), thyrotropin-releasing hormone (TRH), somatostatin, growth hormone-releasing hormone (GHRH), dopamine, and enkephalin (ENK) (Biag et al., 2012; Bruhn et al., 1987; Sawchenko and Swanson, 1982a; Swanson et al., 1981). Based on location and cell type, the PVN is divided into ten subnuclei in mice (discussed in Chapter 4).

PVN neuroendocrine neurons can indirectly impact bladder function via hormone circulation. For example, circulating VP dose-dependently increases EUS contractility (in mice) which can result in bladder retention (Ito et al., 2018). Regarding autonomic-projecting neurons there are several efferent and afferent connections to regions heavily involved in the micturition reflex. The rat PVN sends direct efferent projections via the lateral funiculus to the thoracic IML and DGC, and to the lumbosacral spinal DH, DGC, SPN, SNB, and potentially the DLN (Gerendai et al., 2001; Gerendai et al., 2003; Nadelhaft and Vera, 1996; Puder and Papka, 2001a; Puder and Papka, 2001b; Swanson and McKellar, 1979; Tang et al., 1999; Wagner and Clemens, 1993; Zheng et al., 1995). The PVN directly projects to brainstem sites involved in LUT control including the ventrolateral PAG, scattered fibres at the rostral LC, and the medullary raphe nuclei (which project to the lumbosacral spinal cord for partial LUT control) (Geerling et al., 2010; Zheng et al., 1995). Additionally, the PVN projects to some forebrain sites involved in micturition control including the MPO (Silverman et al., 1981). Hence, the PVN is thought to be a modulator between conscious (forebrain nuclei projections) and reflex micturition (brainstem and spinal nuclei projections). The PVN also receives afferents from various

regions that are involved in micturition control including the pre-frontal cortex, LC, caudal LDTg, and caudal dorsal raphe nucleus (Cornwall et al., 1990; McKellar and Loewy, 1981; Petrov et al., 1994; Sawchenko and Swanson, 1982b; Spencer et al., 2005).

The PVN's role in LUT function still has knowledge gaps and is more complex than that of spinal and brainstem nuclei discussed above. However, studies of PVN-derived inputs at spinal level provide some insight. CRH in the lumbosacral spinal cord (derived from both the PMC and PVN) causes decreased detrusor contractions (in rats) (Pavcovich and Valentino, 1995; Puder and Papka, 2001a; Wood et al., 2013). Whilst OXY intrathecally injected into the rat lumbosacral spinal cord increases bladder pressure and the number of non-voiding contractions (Pandita et al., 1998; Puder and Papka, 2001b). Therefore, PVN-derived OXY may act as a modulator in the spinal micturition reflex. Additionally, the PVN may partially control the EUS, as activation of vasopressinergic receptors (V_{1A}Rs) present on lumbosacral motor neurons results in increased EUS closure (Ueno et al., 2011).

1.7 ANATOMY, CELLULAR ORGANISATION AND NERVOUS CONTROL OF THE TERMINAL BOWEL

For the purpose of this thesis, the terminal bowel is defined as the region spanning the DC (descending and sigmoid colon), the rectum and anal sphincter complex (ASC), since these parts of the gastrointestinal tract (GIT) are the key regions in the maintenance of faecal continence (Brading and Ramalingam, 2006; Palit et al., 2012). The DC and rectum function in faecal storage and as conduits during defaecation (Hardcastle and Mann, 1968; Proano et al., 1990). The ASC is composed of an internal anal sphincter (IAS) comprised of smooth muscle and an EAS comprised of striated muscle. The main function of the EAS is to stop involuntary expulsion of faecal matter by remaining contracted during prolonged periods between defaecation (Fritsch et al., 2002; Gibbons et al., 1988). The GIT is unique as it is the only organ to have its own complex nervous system, known as the enteric nervous system (ENS) (Furness et al., 2014). Although the

ENS has a significant degree of autonomy, some extrinsic nervous control (originating from the CNS) is necessary for regulation, modulation, and control of GIT functions (Browning and Travagli, 2014). Furthermore, like micturition, defaecation (after the age of 2-3) is a partially conscious process and therefore requires (indirect) input from higher brain centres (Palit et al., 2012).

1.7.1 Faecal storage and defaecation

Distal gut distention inhibits proximal gut motor activity and therefore rectal distension results in decreased colonic motility and tone— a process which inhibits faecal overload in the rectum and contributes to continence (Law et al., 2002). The process of defaecation is initiated by a burst of activity in the DC which results in a ‘mass movement’ of faecal matter into the rectum (Sarna, 1991). Rectal distension results in the initiation of the rectal anal inhibitory reflex (RAIR), whereby the rectal contents descends into the upper anal canal due to IAS relaxation (Bajwa and Emmanuel, 2009). This is rapidly followed by contraction of the EAS and pelvic floor musculature (Cheeney et al., 2012; Frenckner, 1975). ‘Anal sampling’ occurs during this period to distinguish between faecal matter and flatus. Slow wave activity in the IAS results in contents being moved back to rectum in a cyclic fashion over a period of less than 10 seconds (Bajwa and Emmanuel, 2009; Kumar et al., 1990). Tone is greatest at the distal end of the IAS where slow wave frequency and amplitude is greatest (Keef and Cobine, 2019). Sensory information is relayed to higher brain centres for perception and assessment of appropriateness of defaecation (Knowles, 2018). If inappropriate, the ASC remains contracted and faeces may move from the rectum to the colon as a result of retrograde contractions (Keef and Cobine, 2019; Rao and Welcher, 1996; Rao, 2004). When appropriate, defaecation is initiated by Valsalva straining, which increases colon intraluminal pressure. Additionally, EAS is voluntarily relaxed alongside IAS relaxation (Ranson and Saffrey, 2015; Winge et al., 2003).

1.7.2 Anatomy and cellular composition of the terminal bowel

In Chapter 5, whole tissue sections from the mouse DC underwent protein analysis whereby changes in protein regulation between young and aged tissue was compared. Therefore, a description of the cellular composition of the GIT wall is described below. The GIT wall has similar cellular composition throughout (from the oesophagus to ASC). Generally, the wall of the GIT is arranged into four main tissue layers with each layer composed of a variety of cell types. The outermost layer (known as the adventitia) is composed of loose connective tissue coating the organ and serving to maintain organ structure. The following adjacent layer (known as the muscularis externa) consists of longitudinal (LM) and circular muscle (CM) between which a complex network of ganglia, the MP, is located (Cheng et al., 2010; Furness et al., 2014). The third layer (known as the submucosa) is a connective tissue layer with vascular and lymphatic supply and contains a network of smaller ganglia known as a submucous plexus (SMP) (Cheng et al., 2010). In rodents, the submucosa contains a single layer of ganglia in comparison to human intestines, which comprise of two layers (Brehmer et al., 2010; Timmermans et al., 1997). The SMP and the MP comprise the ENS. The innermost layer is the mucosa which consists of three layers within itself— the muscularis mucosa (directly adjacent to submucosa), the lamina propria (thin layer of connective tissue) and the epithelial monolayer. Nerve fibres extensively innervate the smooth muscle layers (alongside other GIT layers) and are of both intrinsic (ENS) and extrinsic (CNS) origin (Furness et al., 2014). See Table 1.1 for an in-depth description of the composition of the terminal bowel wall.

Table 1.1: Cellular composition of DC wall and main functions of each cellular component

Layer	**Cellular composition**	**Main functions**
Mucosa		
Epithelial monolayer	Mature and immature colonocytes (colon epithelium)	Metabolic processes
	Goblet cells	Mucous secretion
	BEST4-OTOP2 cells	pH regulation
	Intraepithelial T cells	Immune response
	B-cells	Immune response

	EECs	Hormone and peptide release
	Stem cells	Cell differentiation
Lamina propria	Macrophages	Immune response
	Connective tissue	Structure
	Lymphatics	Toxin and waste removal
	Vasculature	Oxygen and nutrient supply
Muscularis mucosa	SMCs	Aid contraction and relaxation of GIT
Submucosa		
	Neurons (submucosal plexus)	Innervation of structures
	Connective tissue	Structural
	Lymphatics	Toxin and waste removal
	Vasculature	Oxygen and nutrient supply
	Glial cells	Neuronal support
Muscularis externa	Smooth muscle cells (circular alignment)	Colonic motility
	Neurons (myenteric plexus)	Innervation of structures
	Glial cells	Neuronal support
	ICCs	Smooth muscle contractility
	Smooth muscle cells (longitudinal alignment)	Colonic motility
Adventitia	Connective tissue	Structural

Abbreviations: EECs, Enteroendocrine cells; GIT, Gastrointestinal tract; ICCs, Interstitial cells of Cajal; SMCs, Smooth muscle cells.

The DC and rectal wall have the same general cellular structure as described above. However, the IAS has the distinct anatomical feature of a thickened CM layer within the muscular externa. Skeletal muscle external to the GIT wall surrounds the IAS and makes up the EAS and the pelvic floor musculature (Ranson and Saffrey, 2015). The IAS is controlled involuntarily and contributes to 50-85 % of total anal sphincter tone (Bajwa and Emmanuel, 2009; Bharucha, 2008; Lestar et al., 1989). The voluntarily controlled EAS contributes to the remaining sphincter tone (Krogh and Christensen, 2009).

1.7.3 Intrinsic nervous control of the terminal bowel

The ENS is the main nervous supply to the GIT, with an estimated neuronal count of 200-600 million in humans. They are functionally diverse, including intrinsic sensory neurons, interneurons, and motor neurons. Intrinsic sensory neurons, also known as intrinsic primary afferent neurons (IPANs) comprise 10-30 % of submucosal and

myenteric neurons (Furness et al., 2014). They are multi-axonal neurons that project to CM and mucosa for response to alterations in luminal chemistry and mechanical changes i.e. stretch (Bertrand et al., 1998; Bertrand et al., 1997; Brookes et al., 1995; Furness et al., 1998; Kirchgessner et al., 1992; Kunze et al., 1998; Neunlist et al., 1999; Smolilo et al., 2019; Song et al., 1991). Based on recent findings from an immunohistochemical labelling study (in mice), IPANs have been proposed to project to ascending (excitatory) and descending (inhibitory) interneurons in the MP (Smolilo et al., 2020). This likely causes gut contraction oral to the stimulus and relaxation aboral to promote movement of luminal content in the direction of the ASC (Bayliss and Starling, 1901).

Enteric interneurons are single axon neurons that project in an ascending (orally) and descending (anally) manner in both the SMP and MP (Pompolo and Furness, 1993; Portbury et al., 1995; Song et al., 1997; Young and Furness, 1995). In addition to control of local motility reflexes, descending interneurons are potentially involved in activity associated with migrating myoelectric complexes (waves of electrical activity during the interdigestive period) (Portbury et al., 1995). Additionally, some interneurons have been observed to have mechanosensitive properties and respond directly to stretch without IPAN input (Costa et al., 2019; Smith et al., 2007).

Enteric motor neurons are a diverse neuronal group which regulate the functions of smooth muscle, intestinal blood vessels, epithelium, EECs, immune cells, and intestinofugal neurons (afferent neurons with soma residing in the GIT wall, but whose axons project to CNS ganglia) (Ranson and Saffrey, 2015). They excite and inhibit smooth muscle layers (muscularis externa and muscularis mucosa) via release of acetylcholine and tachykinins (excitatory), and NO, vasoactive intestinal polypeptide, and ATP-like transmitters (inhibitory) (Furness et al., 2014). In mice, the soma of neurons supplying the muscularis externa (CM and LM) are located in the MP, making it a major region for the nervous control of gastric motility (Furness et al., 2014; Steele et al., 1991). In the muscularis mucosa of the colon, the nervous supply is thought to originate from neurons in the SMP (Furness et al., 1990).

Some cells play an intermediatory role in nervous control of the bowel including ICCs, fibroblast-like cells (FLCs), and EECs. C-kit^{+} ICCs and PDGFRα^{+} FLCs partially form an integrated cell network (known as SIP syncytium) that generates and regulates phasic and tonic GIT contractions (Sanders et al., 2014). ICCs are stellate or spindle shaped and are mainly located on the surface of the SMP (ICC-SMP) and the MP (ICC-MP). Intramuscular ICCs (ICC-IM) also exist in the circular and longitudinal muscle (LM) layers. (Wang et al., 2018; Ward and Sanders, 2006; Yang et al., 2012). Additionally, ICCs have been observed in the lamina propria and are thought to regulate secretion and absorption (Yang et al., 2012). ICC-MP serve as pacemakers, generating and propagating electrical slow waves to form phasic contractions of smooth muscle (Huizinga et al., 1995; Ward et al., 1994). ICC-IM form gap junctions with smooth muscle cells and are in close synaptic contacts with terminals of enteric motor neurons. They express receptors and second messenger pathways necessary for enteric motor neurotransmission (Blair et al., 2012; Drumm et al., 2019; Durnin et al., 2017; Groneberg et al., 2013; Sung et al., 2018). In the (mouse) IAS, ICC-IM contribute to muscle tone via the generation of slow wave contractions (Cobine et al., 2017).

EECs form the largest endocrine organ in the body and play a key role in the control of GIT secretion and motility in addition to regulation of food intake and metabolism. In the colon, sub-types of EECs include L-cells and enterochromaffin cells, which both release 5-hydroxytryptamine (5-HT) otherwise known as serotonin. In addition to 5-HT, colonic L-cells release peptide YY (PYY), glucagon like peptide-1 (GLP1), and glucagon like peptide-2 (GLP2) (Habib et al., 2012). EECs possess various types of cell surface receptors (mainly on the luminal side) allowing them to respond to a variety of stimuli (Latorre et al., 2016; Ye and Liddle, 2017). In mice EECs were observed to have contact with ‘neuropods’ (on the lamina propria side) which consist of axonal process and glial cells (cells which nurture and provide support to neurons) likely providing efferent and afferent neuronal connections (Bohorquez et al., 2014; Bohorquez et al., 2015). Neural connections have been observed between EECs and vagal afferents connecting indirectly to higher brain centres (Dockray, 2013). Specifically, PYY / GLP1 cells coming into

luminal contact with protein, carbohydrates etc. send food-associated signals to brain regions including the hypothalamus (Bradley, 2007; Engelstoft et al., 2008; Geraedts et al., 2012; Thomas et al., 2009). PYY and GLP1 is secreted as a result of contact with short chain fatty acids produced by microbial fermentation (Psichas et al., 2015). Importantly, ECCs can affect gut motility through 5-HT release (Nozawa et al., 2009). Furthermore, enterochromaffin cells have been observed to release histamine, which causes periodic gastric contractions via ICCs (Naganuma et al., 2018).

1.7.4 Innervation of the terminal bowel at spinal level

As noted previously, the majority of the nervous supply to the bowel as a whole originates from the intrinsic ENS. However, extrinsic connections with the CNS are necessary for conscious control of defaecation. Furthermore, the ASC requires conscious control and (in humans) the major nerve supply to the IAS is arises from the spinal pelvic plexus (Kinugasa et al., 2014). CNS efferent and afferent control of the terminal bowel has overlaps with that of the LUT described in section 1.6.

1.7.4.1 Spinal efferents

Spinal efferent innervation of the terminal bowel is more complex than innervation of the LUT. In guineapigs, the rectum was observed to receive a much greater extrinsic innervation (4,177 ± 987 extrinsic neurons on average) than the DC (649 ± 125 extrinsic neurons on average); of which 49 % of projections to the rectum were parasympathetic, whilst in the DC only 17 % were (Olsson et al., 2006). Coinciding with innervation of the LUT, parasympathetic preganglionic neurons projecting to the terminal bowel are present within the SPN (described in section 1.6.2.1) (Dorofeeva et al., 2009; Payette et al., 1987). These preganglionic neurons project through the pelvic nerve via two pathways— directly to intrinsic GIT neurons, or indirectly to intrinsic GIT neurons via the MPG (Browning and Travagli, 2014; Olsson et al., 2006). Pelvic nerve efferents have been observed to densely innervate the MP and externa muscle layers, and (to a lesser extent) deeper layers

including the SMP, mucosa, and blood vessels, suggesting functional control beyond colorectal motility (Brumovsky et al., 2014). Parasympathetic innervation of the terminal bowel increases contractions via muscarinic receptors. Whilst sympathetic innervation inhibits contractions via beta-adrenoreceptors. This is also the case for IAS innervation in rodents (Cobine et al., 2007; Tong et al., 2010). However, in higher species (including humans and monkeys) sympathetic innervation of the IAS is excitatory, with parasympathetic inputs likely to be inhibitory (Carlstedt et al., 1988; Cobine et al., 2007). This must be considered when interpreting present results (in mice) for human application.

Sympathetic preganglionic neurons arise from lumbar spinal (L1-S1 in guineapigs) and project to prevertebral (celiac, inferior mesenteric, and superior mesenteric) and paravertebral ganglia which project via the splanchnic nerves to the rectum and DC (Janig and McLachlan, 1987; Luckensmeyer and Keast, 1994; Olsson et al., 2006; Trudrung et al., 1994). In the guinea-pig DC, pre-vertebral efferent projections are more abundant that paravertebral. 17 %, 17 %, and 31 % of efferent projections arose from the celiac ganglion, the superior mesenteric ganglion and the inferior mesenteric ganglion respectively; whilst 18 % of efferent projections arose from the paravertebral sympathetic ganglia. However, paravertebral sympathetic ganglia provided the majority sympathetic projections to the rectum making up 37 % of efferent projections. Whilst the celiac ganglion (1.5 %), superior mesenteric ganglion (3 %) and inferior mesenteric ganglion (9.2 %) only accounted for a small amount of efferent innervation (Olsson et al., 2006).

The EAS is separate from the GIT and therefore has no intrinsic enteric nervous input, with all nervous input derived from spinal motor neurons. As described in section 1.6.2.1, the EAS (in addition to the ventral spongiosus) in rodents is innervated by lumbosacral SNB motor neurons projecting via the pudendal nerve (McKenna and Nadelhaft, 1986; Schrøder, 1980).

1.7.4.2 Spinal afferents

Sympathetic afferents innervating the DC, rectum, and IAS project from DRG cell bodies in the thoracolumbar DRG (T8-L1 in mice) via the splanchnic nerve. Parasympathetic afferents project from DRG soma via the pelvic nerve (L6-S1 in mice) (Brierley et al., 2018; Christianson et al., 2007; Robinson et al., 2004). There is also evidence of vagal afferent supply to the DC in rats (Berthoud et al., 1990; Berthoud et al., 1997; Herrity et al., 2014; Wang and Powley, 2007). In mice, 20 % of DC and bladder spinal afferents (of which 12 % are lumbosacral) dually innervate both structures suggesting convergent regulation of the two organs (Christianson et al., 2007). Colorectal spinal afferents respond to muscle stretch / distension, mucosal distortion, noxious stimuli, and immune / inflammatory signals (Brierley et al., 2018). Thoracolumbar spinal afferents project from the wall of the DC and send collaterals to lamina I and V. Whereas, lumbosacral spinal afferents originate from both the DC wall (45 %) and lumen (25 %), with 31 % of afferents dually innervating the wall and lumen. Lumbosacral afferents from the DC wall send collaterals to lamina I, the DGC, and SPN. Projections from the DC lumen terminate in lamina I, lamina III, and the DGC, and dual (DC wall and lumen) projections send collaterals to lamina I and the DGC (Harrington et al., 2019). Spinal afferents synapse onto second order neurons in the form of reflex interneurons or ascending neurons projecting to the brain (De Groat and Krier, 1978; Sadeghi et al., 2018).

1.7.5 Supraspinal control of the terminal bowel

As previously mentioned, the process of defaecation requires conscious control from higher brain centres. In patients with supraconal spinal injuries, FI is prevalent and conscious control of sphincter activity is abolished. Furthermore, discriminant rectal sensation during rectal distension is lost, emphasizing the importance of supraspinal control for the initiation of the RAIR and defaecation (Macdonagh et al., 1992; Rasmussen et al., 2013).

Functional magnetic resonance imaging (FMRI) and neuronal tracing studies have observed a wide variety of brain centres involved in the control of the rectum and ASC including the brainstem, cerebellum, limbic system, hypothalamus, thalamus, and the cortex (He et al., 2018; Mayer et al., 2009; Moisset et al., 2010; Mugie et al., 2018; Silverman et al., 1997). Brain structures that have been immunohistochemically labelled and analysed in the present study include the PMC, LC, and LDTg of the brainstem and the PVN of the hypothalamus. Therefore, their role in rectal and anal control will be discussed. For further explanation of CNS control of defaecation, see listed reviews (Drake et al., 2010; Greenwood-Van Meerveld et al., 2017; Jones et al., 2006).

1.7.5.1 Brainstem nuclei

The location and efferent and afferent connections of the LC and PMC have been described in section 1.6.3.1. To our best knowledge, the LDTg does not appear to be involved in terminal bowel control and therefore will be discussed with reference to its impact on LUT control in Chapter 3. Transneuronal tracer injected into the DC shows consistent labelling of the PMC and LC (Pavcovich et al., 1998; Rouzade-Dominguez et al., 2003a; Valentino et al., 2000). Furthermore, PMC and LC neurons are active during DC and rectal distension (Elam et al., 1986; Lechner et al., 1997; Rouzade-Dominguez et al., 2001; Rouzade-Dominguez et al., 2003b; Wang et al., 2009). The PMC has been observed to project to the LC when retrograde tracer is injected into the DC (Pavcovich et al., 1998). The activity in the LC during colorectal distension is caused by CRH inputs, since CRH antagonist injected into the LC (during colonic distension) abolishes activity (Kosoyan et al., 2005; Lechner et al., 1997). One third of PMC-LC-projecting neurons are CRH-immunopositive suggesting the PMC as the source of LC excitation (Valentino et al., 1996).

Activation of the PMC via glutamate injection results in increased DC intraluminal pressure (Pavcovich et al., 1998). This is also potentially mediated by CRH, as CRH^+ PMC neurons have been observed to project dually to the SPN and LC (Valentino et al.,

1996). In addition, dual labelling with transneuronal tracer (injected into the DC) and CRH displays direct CRH^+ projections from the PMC to the SPN (Valentino et al., 2000). This pathway may serve to bring attention to a mass movement of faecal matter in the bowel (initiated by the PMC) and therefore the urge to defaecate, since the colonic distension results in LC induced cortical EEG activity (Lechner et al., 1997). Additionally, CRH injected into the LC and SPN results in increased colonic motility (Lechner et al., 1997; Monnikes et al., 1994; Schwarz et al., 2015; Valentino et al., 1999; Wang et al., 2010). However, electromyogram activation of the LC during colorectal distension (in rats) has shown that the LC inhibits external abdominal oblique muscle contraction (Tsuruoka et al., 2005). Therefore, the LC has been observed to increase visceral activity, but inhibit visceromotor activity. This implies that the LC has a dual function whereby it increases arousal / awareness during colonic transit (mediated by PMC dual CRH projections to the LC and SPN); however, during RAIR it may impede initiation of defaecation likely as a result of inappropriateness of defaecation at that time.

Furthermore, the LC and PMC have also been implicated in the control of the EAS. The LC sends noradrenergic projections to the SNB (Thor and de Groat, 2010). In cats, stimulation of the LC was observed to increase and decrease pudendal nerve firing and EAS contraction. Therefore, the LC likely plays a modulatory role in EAS control (Abysique et al., 1998). In rats, tracing studies have shown (indirect) projections from the PMC to the SNB, likely via interneurons in the DGC and SPN (Dobberfuhl et al., 2014; Tang et al., 1999). However, to our best knowledge, information on how the PMC may affect EAS excitability is currently unavailable.

The PMC has also been implicated in dual innervation and functioning of the bladder and terminal bowel. In rats, 53 % of PMC neurons are activated during both bladder and colon distension (but not colon distension alone) (Rouzade-Dominguez et al., 2003b). A separate study (in rats) whereby transsynaptic tracer was injected into the DC and bladder revealed that 70 % of PMC neurons were double-labelled, with only 10 % of neurons single labelled for DC injections (Rouzade-Dominguez et al., 2003a).

1.7.5.2 The PVN of the hypothalamus

The location, immunocytochemistry, and efferent and afferent connections of the PVN have been described in section 1.6.3.2. Transneuronal tracer injected in the DC has displayed PVN labelling, particularly in the dorsal portion (in rats) (Pavcovich et al., 1998; Rouzade-Dominguez et al., 2003a; Valentino et al., 2000). Furthermore, the PVN is active during colonic distension, with 81 % of OXY neurons, 18 % of VP neurons and 16 % of CRH neurons showing activity (Martínez et al., 2006; Wang et al., 2009). The exact function of the PVN in colonic control is not fully understood. Adding to this, it is difficult to determine projection sites of subsets of PVN neurons i.e. projection to the hypophysis (for circulatory hormone release); or projection to various CNS sites involved in terminal bowel control. The PVN has been observed to project to brainstem and spinal sites involved in DC efferent control including the LC, PAG, nucleus tractus solitaries (NTS), dorsal motor nucleus of the vagus (DMV), and the lumbosacral spinal cord (Geerling et al., 2010; Portillo et al., 1998; Zheng et al., 1995).

Within the LC, CRH inputs increase colonic motility and these inputs may partially be derived from the PVN (as well as the PMC) (Lechner et al., 1997; Monnikes et al., 1994; Schwarz et al., 2015; Valentino et al., 1999). Furthermore, CRH inputs onto the SPN have been observed to increase colonic motility, and PVN-derived CRH inputs have been observed in the lumbosacral spinal cord (Puder and Papka, 2001a; Wang et al., 2010). However, dual labelling with transneuronal tracer (injected into the DC) and CRH showed that CRH^+ inputs in the SPN derived solely from the PMC (and not the PVN) (Valentino et al., 2000). PVN-derived CRH may impact colonic motility via circulatory release, as CRH delivered to the inferior mesenteric artery (IMA) (main blood supply to the DC and rectum) and intraperitoneally (in rats) results in increased colonic motility and defaecation via activation of myenteric neurons (Maillot et al., 2000; Maillot et al., 2003; Million et al., 2000).

In addition, PVN-derived VP may impact colonic motility via circulatory release as VP delivered to the IMA in the monkey resulted in inhibition of phasic contractions at lower

doses and caused giant migratory contractions at higher doses (Zhu et al., 1992). A similar phenomenon was observed when VP was applied directly to the guineapig colon (Botting and Turmer, 1966). Therefore, VP may be partially responsible for faecal ‘mass movement’ prior to or during defaecation. Furthermore, PVN-derived OXY has been observed to increase colonic motility (in mice) via circulatory release and does so via activation of OXY receptors present of MP neurons (Xi et al., 2019).

PVN OXY neurons have also been observed to project to the lumbosacral spinal cord (Puder and Papka, 2001b). However, there has been no evidence reported thus far of these projections in direct control of colon or rectal function, with most studies reporting OXY inputs onto the SNB resulting in penile erection (Giuliano et al., 2001; Tang et al., 1998; Veronneau-Longueville et al., 1999). However, PVN-derived OXY inputs onto the lumbosacral SNB have been observed to innervate the pubococcygeus muscle of the pelvic floor and likely results in muscle contraction (Perez et al., 2005). The pubococcyceus muscle is a key striated muscular structure connected to the EAS and thus OXY input onto the SNB likely aids faecal storage and continence during rectal distension (Garavoglia et al., 1993). Therefore, PVN control of DC contractility is likely mainly via circulatory release of hormones at the hypophysis, with control of pelvic floor contractility via central pathways. See Figure 1.1 for projection pathways of nuclei of interest involved in controlling the LUT and terminal bowel.

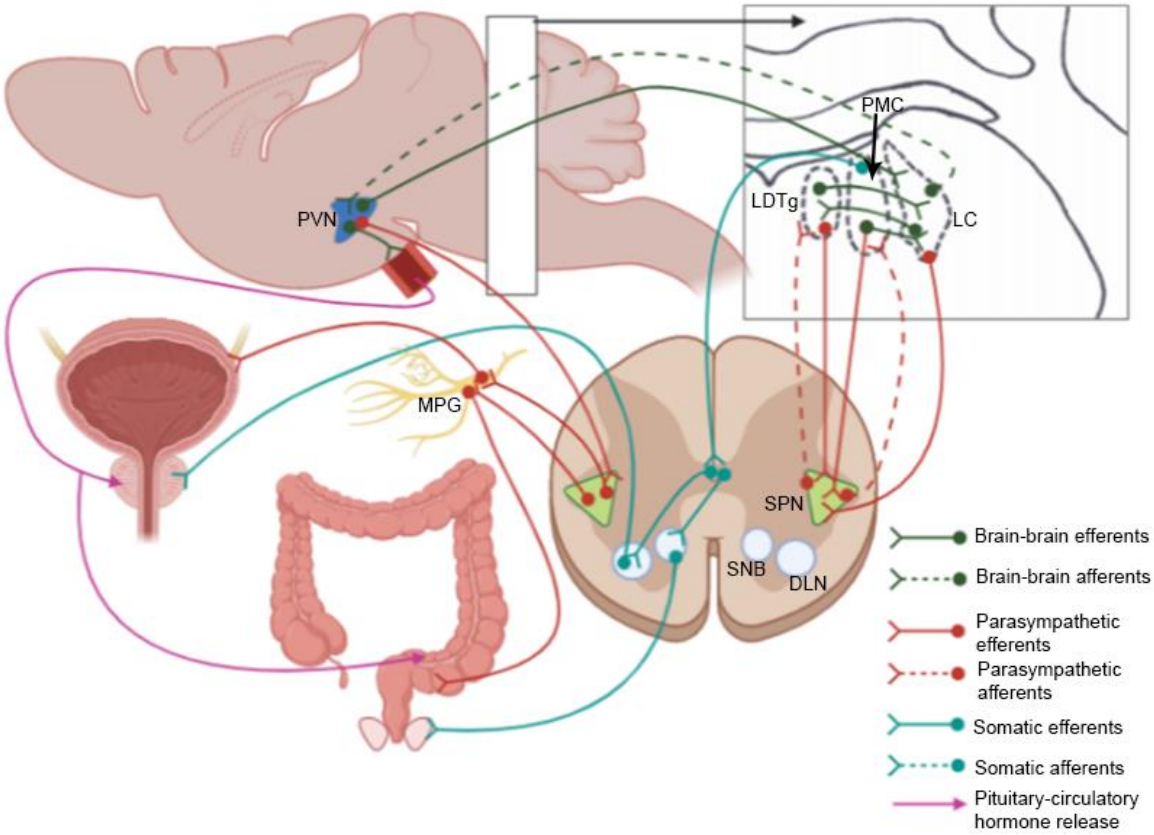

Figure 1.1: Connections between nuclei of interest that directly and indirectly innervate the LUT and terminal bowel. Brain connections: the PVN projects to the pituitary for circulatory hormone release (that controls EUS and DC smooth muscle); the PVN projects to and receives innervation from the LC; the LC projects to and receives innervation from the LDTg; and the PMC sends collateral projections to the LC and SPN. Brain-spinal connections: the PVN projects to the SPN; the PMC projects to and receives innervation from the SPN; the PMC projects to the inhibitory neurons in the DGC which project to the DLN and SNB; the LDTg projects to and receives innervation from the SPN; and the LC projects to the SPN. Spinal efferents: the SPN projects to the MPG which innervates the bladder detrusor and DC smooth muscle; the DLN projects directly to the EUS; and the SNB projects directly to the EAS. DC, Distal colon; DLN, Dorsolateral nucleus; LC, Locus coeruleus; LDTg: laterodorsal tegmental nucleus; EAS, External anal sphincter; EUS, External urethral sphincter; MPG, Major pelvic ganglion; PMC, Pontine micturition centre; PVN, Paraventricular nucleus; SNB, Spinal nucleus of the bulbospongiosus; SPN, Sacral parasympathetic nucleus.

1.8 NEUROACTIVE SUBSTANCES INVOLVED IN BRAIN AND SPINAL CONTROL OF LUT / TERMINAL BOWEL

Many neuroactive substances have been previously discussed that impact CNS and PNS outflow for LUT and terminal bowel function. In the present study, specific neuroactive substances have been immunohistochemically labelled. These include met-ENK inputting onto brainstem (LC, PMC, and LDTg) and lumbosacral spinal (SPN, DLN, and SNB) nuclei; gamma-Aminobutyric acid (GABA) within the lumbosacral spinal cord and the PVN of the hypothalamus; and glutamate within the PVN. The roles of these neuroactive substances in the control of micturition and defaecation are discussed below.

1.8.1 Met-Enkephalin

Enkephalin is a neuropeptide that exists in two forms— met-ENK and leucine-enkephalin (leu-ENK), which are both products of the proenkephalin gene. ENK is expressed in neurons in various regions of the CNS and binds to delta opioid (DOR), mu opioid receptors (MOR), and kappa opioid receptors (KOR) which are inhibitory G-protein-coupled receptors (Takahashi, 2016). Activation of opioid receptors results in inhibition of adenylyl cyclase and voltage-gated calcium channels, and the opening of inward rectifying potassium channels (Waldhoer et al., 2004).

1.8.1.1 Met-ENK in the lumbosacral spinal cord (Chapter 3)

In Chapter 3, the impact of ageing on of met-ENK density was observed in the lumbosacral spinal cord within the SPN, SNB, DLN, DH (lamina I), DGC, and VH (ventral portion of lamina VIII). Intrathecal administration of ENK in the lumbosacral spinal cord (of rats and cats) inhibits bladder, DC, and EAS contractions (Abysique et al., 1998; Dray and Metsch, 1984; Hisamitsu and de Groat, 1984; Kennedy and Krier, 1987). Furthermore, it likely inhibits EUS contractions (at spinal level) as subcutaneously administered ENK (in humans) results in decreased urethral pressure (Vaidyanathan et al., 1989). In the lumbosacral spinal cord (of rats), ENK fibres are present in the SPN, DLN, SNB, DGC,

DH, and VH (Katagiri et al., 1986; Micevych et al., 1986; Romagnano and Hamill, 1985; Sasek and Elde, 1986; Shimosegawa et al., 1987). Furthermore, ENK inputs appose SNB, DLN, and SPN soma and neuronal processes, and likely influence spinal outflow to the terminal bowel and LUT resulting in inhibition of contractions (Micevych et al., 1986; Sasek and Elde, 1986). Additionally, SPN soma and neuronal processes are immunopositive for MORs in rats (Dou et al., 2013).

Knowledge of ENK$^+$ fibre origin is incomplete. However, mid-thoracic spinal transections (in rats) have shown no change in lumbosacral ENK fibre density, suggesting intraspinal origin (Micevych et al., 1986; Romagnano et al., 1987). Therefore, lumbosacral ENK fibres are likely to be derived from spinal afferents or interneurons. In rats, ENK$^+$ bladder and penis afferents are present, but sparse. Retrograde tracer injected into the DRG shows that ENK$^+$ afferents are mainly derived from the colon (in comparison to the bladder and penis) (Keast and de Groat, 1992). Therefore, ENK fibres likely present in the DH, SPN, and / or DGC partially derive from colon (and to a less extent) bladder and penis DRG afferents (de Groat and Yoshimura, 2009; Harrington et al., 2019). The remaining lumbosacral spinal afferents are likely from spinal interneurons caudal to the mid-thoracic region. Indeed, ENK$^+$ soma have been observed in the DH (L3-L5), DGC (L1-L5), and SPN in rodents (Huang et al., 2010; Nicholas et al., 1999; Sasek and Elde, 1986; Shimosegawa et al., 1987). Furthermore, ENK$^+$ fibres extend between the SPN and DGC, indicating interactions between neuronal populations (Sasek and Elde, 1986).

1.8.1.2 ENK in the pontine tegmentum (Chapter 3)

ENK tonically inhibits pre-sympathetic and pre-parasympathetic PMC neurons (via MORs) and regulates bladder capacity (in rats and cats) (Fowler et al., 2008; Guo et al., 2013). The impact of ENK inputs onto PMC neurons on colonic function, to our best knowledge, is unknown. However, since it tonically inhibits bladder-projecting SPN neurons, it likely has a similar effect on DC and rectum-projecting SPN neurons (Guo et al., 2013). The source of ENK inputs onto PMC neurons is unknown. However, PAG,

MPO, and lumbosacral DGC and SPN all contain ENK^+ neurons and are CNS sites that innervate the PMC for bladder control (Blok and Holstege, 1994; Ding et al., 1999; Ding et al., 1997; Moss et al., 1983; Nicholas et al., 1999; Sasek and Elde, 1986; Shimada et al., 1987; Shimosegawa et al., 1987). Therefore, these nuclei are possible regions of ENK projections to the PMC.

ENK innervation of the LC (via MORs) inhibits bladder contractions (in cats) and increases bladder capacity (Guyenet and Aghajanian, 1979; Matsuzaki, 1990). ENK-LC and impact on colorectal motility has, to our best knowledge, not been reported. However, ENK injected into the (cat) LC results in decreased EAS contraction and tone (Abysique et al., 1998). ENK inputs in the LC are derived from the rostral medulla in the nucleus prepositus hypoglossi and the nucleus paragigantocellularis (Drolet et al., 1992). In addition, ENK^+ neurons have been observed in the PMC (in rats) and may be a source of LC innervation (Morita et al., 1990).

LDTg neurons are DOR^+ and inhibit neuron firing (Arvidsson et al., 1995; Capece et al., 1998). The effects of ENK-LDTg on LUT function are unknown. Additionally, the source of ENK inputs onto LDTg neurons are currently unknown.

1.8.2 GABA

GABA is the principle inhibitory neurotransmitter in the CNS. GABA inhibits neurons via ionotropic ($GABA_AR$) and metabotropic ($GABA_BR$) receptors. $GABA_ARs$ are selective cation channels that open upon GABA binding resulting in Cl^- influx. $GABA_BRs$ are G-protein-coupled receptors that decrease Ca^{2+} intracellular concentration and inhibit cAMP production (Jembrek and Vlainic, 2015). Vesicular GABA transporters (VGATs) are present in the plasma membrane of synaptic vesicles, which release GABA upon neuronal stimulation (Albers et al., 2017). Anti-VGAT antibodies were used to label GABAergic synaptic boutons in the present study.

1.8.2.1 GABA in the lumbosacral spinal cord (Chapter 3)

Intrathecal administration of bicuculline ($GABA_AR$ antagonist) in the lumbosacral spinal cord increases bladder and colorectal contractions (in rats) (Nakamori et al., 2018; Sugaya et al., 2019). Therefore, GABA decreases contractile responses in the bladder and colorectum at lumbosacral spinal level (via $GABA_ARs$). This likely occurs via GABAergic inputs onto the SPN, since immunolabelled GABA synaptic boutons have been observed in contact with rat SPN soma and dendrites (Ranson et al., 2006; Santer et al., 2002). The PMC (in cats) projects to GABAergic sacral spinal interneurons in the DGC, which are thought to project to onuf's nucleus / DLN for EUS inhibition (during PMC-induced bladder contractions via the SPN) (Blok et al., 1997a; Sie et al., 2001).

GABAergic projections from the rostral ventromedial medulla have been observed to synapse in the DH and DGC of the lower lumbar spinal cord (in rats) (Antal et al., 1996; Holstege, 1991). The remainder of GABAergic inputs (to SPN and motor neurons) are likely derived from spinal interneurons projecting from the DH and DGC (in the rat and cat) (Blok et al., 1997a; Polgar et al., 2003).

1.8.2.2 GABA in the PVN (Chapter 4)

GABA is the principle inhibitory neurotransmitter in the PVN (Johnson et al., 2018). It inhibits PVN neurons via $GABA_ARs$ and $GABA_BRs$ (Chen and Pan, 2006; Herman et al., 2004; Park et al., 2007; Yamaguchi et al., 2019). GABA synaptic boutons in the (rat) PVN have been observed to project from hypothalamic structures including the PVN itself (rostral portion), supraoptic nucleus (SON), suprachiasmatic nucleus (SCN) and the perifornical region (Hermes et al., 1996; Roland and Sawchenko, 1993). However, these studies only account for local GABAergic connections, mainly observed inputting onto parvocellular neurons. Therefore, there are likely further brain GABAergic connections to the PVN, particularly for magnocellular neuronal control.

1.8.3 Glutamate in the PVN (Chapter 4)

Glutamate is the principle excitatory neurotransmitter in the PVN (and CNS in general) (Brann, 1995; Platt, 2007). Glutamate excites neurons via metabotropic (mGluRs- Group I-III) and ionotropic (iGluRs- NMDA, kainite, and AMPA) receptors. IGluRs are non-selective cation channels that open upon glutamate binding resulting in cation influx (e.g. Na^+, K^+, and Ca^{2+}). Group I mGluRs are present in the PVN and are G-protein-coupled receptors whose activation results in generation of diacylglycerol and inositol 1,4,5-trisphosphate, which eventually activates protein kinase C (Herman et al., 2000; Mahato et al., 2018; Reiner and Levitz, 2018; van den Pol, 1994; Van Den Pol et al., 1995). Vesicular glutamate transporters (VGLUTs) are present in the plasma membrane of synaptic vesicles, which release glutamate upon neuronal stimulation. Three types of VGLUTs exist, VGLUT1-3 (Liguz-Lecznar and Skangiel-Kramska, 2007). In the PVN, VGLUT1 and VGLUT2 are present in pre-synaptic terminals. However, anti-VGLUT2 antibodies label the vast majority of glutamate terminals in the mouse PVN and therefore were used in the present study (Nakamura et al., 2005). Glutamate afferents projecting to the PVN (in rats) are derived from a variety of nuclei of which the majority are hypothalamic (including from interneurons within the PVN itself), while the remainder are from telencephalonic, thalamic, and midbrain projections (including substantial VGLUT2-containing projections from the PAG) (Csáki et al., 2000; Hermes et al., 1996; Ulrich-Lai et al., 2011; Ziegler et al., 2012).

1.9 AGEING OF THE LUT, TERMINAL BOWEL, AND CNS STRUCTURES INVOLVED IN THE CONTROL OF PELVIC VISCERA

1.9.1 Ageing in the bladder

Changes in bladder function with age varies between species and gender. Age-associated detrusor underactivity and overactivity have both been reported. Increased pressure threshold for voiding with age appears to be a widespread phenomenon across various species (Birder et al., 2018). Studies have shown age-associated changes in

intrinsic nervous and non-nervous tissue, and in extrinsic innervation of the bladder. In humans, fMRI has revealed an age-associated decrease in cortical activation during bladder filling indicating decreased conscious control (Griffiths et al., 2007; Griffiths et al., 2009) In this thesis, the impacts of ageing on LUT function were observed at specific CNS regions [lumbosacral (SPN, DLN, and SNB), brainstem (LC, PMC, and LDTg) and hypothalamic (PVN)]. Therefore, age-associated changes within these specific AOIs are discussed below. See listed reviews for further description of age-associated changes within the LUT and other nervous structures involved in its control (Birder et al., 2018; Finkbeiner, 1993; Ranson and Saffrey, 2015).

1.9.2 Ageing in the terminal bowel

As the GIT is one of the most complex organs with a vast cellular diversity, it is subject to a variety of age-associated changes. Analysis of the ENS suggests that enteric neurons (in the MP and SMP) may be more susceptible to age-associated degeneration than neurons in other parts of the nervous system (Saffrey, 2013). This likely impacts GIT motility and defaecation, potentially resulting in constipation and / or FI (Wiskur and Greenwood-Van Meerveld, 2010). For a more in-depth discussion of how ageing affects the DC and GIT as a whole, see listed reviews (Merchant et al., 2016; Saffrey, 2014; Saffrey, 2013; Soenen et al., 2016; Wiskur and Greenwood-Van Meerveld, 2010).

1.9.3 Ageing in the lumbosacral spinal areas of interest controlling the LUT and terminal bowel

As discussed previously, the lumbosacral SPN is the main source of spinal parasympathetic innervation to the bladder and terminal bowel. Whilst the DLN and SNB provide somatic control of the EUS and EAS, respectively. Some studies have reported the impact of ageing on these neuronal structures and their synaptic inputs, which may contribute to LUT / terminal bowel dysfunction. In male rats (but not females), DLN and SNB dendritic length are decreased with age (Fargo et al., 2007). However, neuron

number and cell size in rats show differing results. Neuron number has been observed to be decreased and maintained with age, whilst soma size has been observed to be both increased and decreased with age (Fargo et al., 2007; Jacob, 1998). In aged rats where soma size was increased, a significant build up of lipofuscin was noted (Jacob, 1998). Lipofuscin is an aggregate formed by lipids, metals, and misfolded proteins and is thought to contribute to free radical[1] formation by preventing the degradation of oxidised proteins (Moreno-García et al., 2018).

Changes in motor neuron innervation have been noted with age. The density of (unlabelled) synaptic inputs in apposition to SNB soma and glutamate inputs to SNB / DLN dendrites decrease with age (in rats) (Matsumoto, 1998; Ranson et al., 2007). These changes likely diminish EUS and EAS contractile properties since glutamate excites sphincter muscles at the level of the spinal cord (Furuta et al., 2009). Additionally, tyrosine hydroxylase^{+} (representing dopamine and NE) and serotonin^{+} synaptic density within DLN was declined with age. This likely results in diminished EUS control, since duloxetine[2] is used to treat UI and increases EUS contractility (Thor and de Groat, 2010).

In the rat SPN no age-associated changes have been observed regarding neuron numbers or size / complexity of dendritic arbors (Dering et al., 1998; Dering et al., 1996; Santer et al., 2002). Whole (unlabelled), serotonergic, GABAergic, and glycinergic boutons inputting onto (rat) SPN neurons have also been observed to remain unchanged in rats with age (Ranson et al., 2003a; Santer et al., 2002). Furthermore, the density of $GABA_{B}$Rs within the SPN remain unchanged with increased age (Dorfman et al., 2006). Therefore, SPN structures in the rat appear to remain largely intact with age. However, the density the substance P and tyrosine hydroxylase immunoreactive boutons in the SPN show an age-associated decrease (Ranson et al., 2003a; Ranson et al., 2005). Since NE both excites and inhibits SPN firing via different adrenergic receptors, the impact on detrusor contractility is ambiguous. However, substance P has been observed to induce

[1] Free radicals are highly reactive unpaired electrons associated with oxidative damage which occurs via removal of electrons from biologically functional molecules rendering them dysfunctional.
[2] Duloxetine is a selective NE and serotonin-reuptake inhibitor.

immediate bladder contractions at the level of the SPN and thus an age-related decrease may contribute to delayed contractile response and bladder retention (Mersdorf et al., 1992).

1.9.4 Ageing in brainstem nuclei that control LUT and terminal bowel

Within brainstem AOIs (LC, PMC, and LDTg), the vast majority of age-associated studies have been carried out in the LC due to its implication in the pathophysiology of Parkinson's disease (Bari et al., 2020). The age-associated changes that may impact LUT and terminal bowel dysfunction are summarised below. Despite exerting major influence over spinal micturition and defaecation pathways, few studies have observed age-associated changes in the PMC. A study using fMRI showed diminished PMC activity during bladder filling in elderly women suffering detrusor overactivity (Griffiths et al., 2007; Griffiths and Fowler, 2013). This is suggestive of a lack of coordination between reflex and conscious micturition as suprasacral spinal cord injury (i.e. reduced / absent PMC-lumbosacral input) results in detrusor overactivity and detrusor sphincter dysnergia (DSD)[3] (Taweel and Seyam, 2015). Therefore, lack of PMC activity in ageing suggests reduced 'switch' from bladder filling to conscious urination.

In the LC and LDTg, age-associated changes in neuron number and morphology have been reported. In the LDTg, soma size, dendritic length, and number (in mice and cats) is decreased with age. However, neuron numbers are maintained (in mice, rats, and cats) (Kawamata et al., 1990; Lolova et al., 1996b; Zhang et al., 2005). In the LC, neuron size is reported to decrease or be maintained with age (in humans) (Lohr and Jeste, 1988; Mouton et al., 1994). Some studies (in mice and humans) show age-associated neuronal loss, whilst others (in rats and humans) show no change (Goldman and Coleman, 1981; Lohr and Jeste, 1988; Manaye et al., 1995; Mouton et al., 1994; Ohm et al., 1997; Sturrock and Rao, 1985; Vijayashankar and Brody, 1979; Wree et al., 1980). Where LC age-associated neuronal loss was observed, a significant increase in intracellular

[3] DSD: involuntary contractions of the EUS during involuntary detrusor contractions.

neuromelanin labelling was noted (Lohr and Jeste, 1988; Manaye et al., 1995). Neuromelanin provides neuronal protection from oxidative stress and accumulation and is indicative of the build-up of high levels of toxins in aged LC neurons. Furthermore, neuromelanin released by degenerating neurons activates microglia which results in an accompanying inflammatory response (Zucca et al., 2017). Increased activation of microglia occurs in normal ageing and is associated with neurodegenerative diseases including Parkinson's disease (Akiguchi et al., 2017; Zucca et al., 2017). Lipopolysaccaride-induced inflammation in the mouse LC resulted in a variety of age-associated pathophysiologies including constipation and thus LC neuroinflammation may play a significant role in age-associated terminal bowel dysfunction (Song et al., 2019).

Additional age-associated changes have been observed in the LC including synaptic inputs and projection pathways as discussed below. Noradrenergic innervation of sympathetic preganglionic boutons in the spinal cord, that are likely LC-derived, are diminished in aged rats (Ko et al., 1997; Lyons et al., 1989). This may impact sympathetic bladder outflow since LC lesioning results in bladder retention in cats (Yoshimura et al., 1990). Furthermore, ageing affects LC innervation of parasympathetic and somatic pathways, since NE density is decreased in the SPN and DLN of aged rats (Ranson et al., 2003a), with potential the impact on bladder outflow discussed in section 1.9.3. Additionally, lesioning of LC to spinal projections results in loss of diurnal rhythm micturition patterns in aged, but not young rats suggesting alterations in micturition circuitry with age (Ranson et al., 2003b). Furthermore, LC innervation of the cortex shows age-associated changes including electrophysiological changes and decreased LC inputs (Ishida et al., 2001a; Ishida et al., 2001b; Shirokawa et al., 2000). This may impact conscious control of the urination / defaecation. Innervation of the LC has shown age-associated changes whereby synaptic inputs onto LC soma had increased levels of synaptic vesicle protein (Iwanaga et al., 1996). Synaptic vesicle protein is involved in regulation of neurotransmitter release and therefore may be indicative of increased age-associated post-synaptic innervation of LC neurons (Madeo et al., 2014).

1.9.5 Ageing in the PVN and potential impacts on LUT and terminal bowel function

Various studies have observed age-associated changes in the PVN. The PVN is involved in a variety of autonomic and neuroendocrine functions, and thus emphasis will be placed upon age-associated changes that may impact functional micturition and defaecation. Changes in PVN neuron numbers have shown differing results in species. In monkeys, whole PVN neuron numbers increase with age (Roberts et al., 2012). In humans, an age-associated increase in select PVN cell populations including VP^+ and CRH^+ neurons was observed (Zhou and Swaab, 1999). However, in mice and rats, whole PVN numbers have been observed to be maintained, whilst selected OXY^+ and VP^+ neuron numbers and area occupied by OXY and VP magnocellular neurons were decreased (Calza et al., 1990; Hsu and Peng, 1978; Lolova et al., 1996a; Peng and Hsü, 1982; Sartin and Lamperti, 1985; Sturrock, 1992). Considering present study PVN work was carried out in mice, implications of age-associated neuron number change in mice and rats will be considered. A decrease in OXY and VP neuron numbers and area of magnocellular neurons in the PVN would likely result in decreased hormone circulatory release and a potential decrease in lumbosacral spinal projections of parvocellular neurons. Since both OXY and VP (in circulation) contribute to terminal bowel motility this could potentially result in constipation (Xi et al., 2019; Zhu et al., 1992). Furthermore, decreased spinal-projecting OXY would likely result in bladder underactivity and diminished awareness of bladder filling since intrathecal OXY administration results in non-voiding contractions (Pandita et al., 1998). Spinal-projecting OXY and VP, and circulatory VP decrease would also contribute to a decrease in EUS and EAS contractility and associated decrease in continence (Perez et al., 2005; Ueno et al., 2011; Wagner and Clemens, 1993).

In terms of morphological and ultrastructural changes in PVN neurons, an age-associated swelling of dendritic spines has been observed (in rats) in addition to an overall decrease in dendritic spine number (Itzev et al., 2003). Additionally, OXY and VP soma size increase with age (in rats) (Lolova et al., 1996a). Ultrastructural changes with

increased age include mitochondrial aberration and chromatolysis[4] (Verbitskaia and Bogolepov, 1984). Furthermore, Ageing in rats results in decreased (unlabelled) synaptic inputs onto PVN neurons (Itzev et al., 2003). These changes likely impact neuronal function and projection pathways. Indeed, a decrease in PVN–vagal output has previously been reported and this potentially impacts DC motility since vagal nerve stimulation elicits DC contractions (Calza et al., 1990; Tong et al., 2010).

1.10 C57BL / 6J MALE MICE: A MODEL FOR AGE-RELATED BLADDER AND TERMINAL BOWEL DYSFUNCTION

The present study has utilised C57BL / 6J male mice for immunohistochemical studies of central nervous structures that control bladder / bowel function, and protein analysis of the DC. They are the most widely used inbred strain in research and are often used as a model of ageing (Birder et al., 2018). C57BL / 6J show bladder / bowel dysfunction with increasing age. Cystometric studies have shown that aged mice (27-30 months) have weaker detrusor contractile responses followed by weaker relaxant responses compared to middle-aged mice (12 months). These impairments are more pronounced in males (Kamei et al., 2018). Additionally, male C57BL / 6J mice (up 24 months old) have shown impaired colonic motility and increased faecal impaction with increasing age (Patel et al., 2014).

1.11 AIMS AND OBJECTIVES

Chapter 3:

- Immunohistochemically double-label brainstem (LC, PMC, and LDTg) and lumbosacral spinal nuclei (SPN, DLN, and SNB) alongside met-ENK (brainstem

[4] Chromatlysis is the dissolution of nissl bodies in the soma which is often associated with increased soma and nucleus size and is frequently a precursor to apoptosis.

and spinal cord) and VGAT (spinal cord only) boutons in different age groups (3-5, 12-14, 24-26, and 29-30 months).

- Analyse age-associated changes in brainstem structures including soma size, neuron number, ENK density, and number of ENK-soma inputs.
- Analyse age-associated changes in lumbosacral spinal structures including soma size, ENK / VGAT immunoreactivity, and number of ENK / VGAT-soma inputs.

Chapter 4:

- Immunohistochemically double-label OXY or VP PVN neurons alongside VGAT or VGLUT2 boutons in different age groups (3-4, 12-14, 24-25, and 30 months).
- Categorise OXY and VP-immunolabelled soma into subnuclei (based on location) and parvocellular or magnocellular cell types (based on soma size) utilising previous work in the mouse PVN (Biag et al., 2012; Castel and Morris, 1988; Kadar et al., 2010).
- Analyse age-associated changes in VGAT / VGLUT2 density (within PVN subnuclei), and number of VGAT / VGLUT2 inputs onto OXY / VP parvocellular / magnocellular soma (within PVN subnuclei).

Chapter 5:

- Develop methodology for successful extraction of protein from formalin-fixed paraffin-embedded (FFPE) mouse DC tissue and apply to different age-groups (3 and 30 months).
- Apply extracted proteins to in-gel trypsin digestion and downstream analyses using liquid chromatography / mass spectrometry / mass spectrometry (LC / MS / MS).
- Analyse DC whole mouse proteome using Mascot™ (Matrix Science, London, UK) software.
- Analyse age-associated change in protein regulation between 3 and 30 months using Progenesis™ LC-MS data analysis software (Nonlinear Dynamics, Newcastle upon Tyne, UK).

2 GENERAL MATERIALS AND METHODS

Main methodology used in present study included immunohistochemical labelling and protein analysis. Immunohistochemical labelling was undertaken in mouse CNS structures (detailed in Chapter 3 and 4) and therefore techniques are described collectively in this chapter. Protein analysis was undertaken in formalin fixed paraffin embedded (FFPE) mouse gut tissue. Method development was required when extracting proteins for downstream analysis from FFPE samples. Therefore, all methods (aside from ethics approval and animal housing) for protein analysis are detailed in Chapter 5.

2.1 ETHICS APPROVAL

This study required ethical consideration as perfusion fixed and FFPE animal tissue was used. Experiments were designed to minimise the number of animals used and sacrifices were performed with accuracy to minimise duration of suffering. The '1986 Animal Science Procedures act' governs animal experimentation and laboratory care stated by UK national law. Murine brains, spinal cords and gut samples were obtained from the Open University. Harvesting was either made following schedule 1 terminal anaesthesia or post perfusion fixation licensed by UK Home Office. Animal licensing was held by supervisor's Dr R.N.Ranson (UK Home Office personal licence) and Dr M.J.Saffrey (UK Home Office project licence). Samples were transported to Northumbria University for immunofluorescence labelling and microscopy analyses, or for extraction of proteins and downstream protein analyses. See Appendix A for letter detailing ethical approval.

2.2 ANIMALS AND HOUSING

Housing maintenance and experimentation were performed in accordance with UK Home Office regulations under the animals (Scientific Procedures) Act 1986. Male C57BL / 6J mice were obtained from Harlan, UK at 8 weeks of age. Mice were housed in groups of five within a designated facility at the Open University where

Veterinary and Home Officials performed inspections on a regular basis. Mice were maintained under 12-hour light / dark photoperiods at a temperature of 21 ± 2°c and 50 ± 10% humidity. Mice were fed *ad libitum* with RM1 (E) 801002 (Special Diet Services) chow and UV sterilised mains water.

2.3 GENERAL TISSUE PREPARATION

2.3.1 Dissection and fixation of paraformaldehyde fixed mouse brain and spinal cord

Once mice had reached the required age ranges of 3-5, 12-14, 24-25 and 30-31.5 months old, they were terminally anaesthetized using sodium pentobarbital. Animals were initially exsanguinated with heparinized saline before transcardial perfusions with 4 % paraformaldehyde (PFA) in 0.1 M phosphate buffered saline (PBS) (pH = 7.4). Spinal cords and whole brains from each animal were removed and further fixed for four hours at 21 ^{o}C. Tissues were then rinsed three times with PBS at one hour intervals prior to storage at 4 ^{o}C in PBS until use.

2.3.2 Sectioning

All sections collected were separated by 90 µm or more so that neither neurons, nor boutons could be counted twice in subsequent analysis.

2.3.2.1 Sectioning of the lumbosacral spinal cord (Chapter 3)

Spinal cords were washed three times in PBS at one-hour intervals. Spinal cord segments L5-S1 were excised and the rostral end (with larger surface area) was fixed to the vibratome specimen base (VT1000S, Leica Microsystems, UK) and immersed in PBS. The spinal cord was sectioned serially at 45 µm at 0.5-0.125 mm / s at a frequency of 70 Hz. Sections were viewed under the light microscope until the rostral-most end (since sections were collected caudal-rostral) of the DLN, SNB and RDLN motor neurons were observed at L5, and two additional sections were collected as controls. Twenty sections

prior to the caudal-most end of motor neurons at L6 were collected as SPN-containing sections[5] (L6-S1), and two additional sections were collected as controls. Sections containing motor neurons were placed alternately in two separate vials containing PBS— one for VGAT and one for met-ENK bouton staining. The same collection method was applied for SPN-containing sections.

2.3.2.2 Sectioning of brainstem (Chapter 3)

Brains were removed from storage buffer and washed in PBS as described previously. Using the Mouse Brain Atlas (Paxinos and Franklin, 2007) as a guide, and Bregma as a measuring point[6], a transverse cut was made adjacent to the cerebellum (Bregma: -5.88 mm). Another transverse cut was made 5 mm rostral to that to ensure entirety of pontine AOIs (LC, PMC and LDTg) were retained. The larger, rostral end was fixed to the vibratome base and sectioned at 45 µm as described previously. Sections were collected in order in PBS-filled 24-well plate. Sections were viewed under the light microscope and structures were cross-reference with those imaged in the Mouse Brain Atlas until the rostral-most end of pontine nuclei was collected (Paxinos and Franklin, 2007). Two additional sections were collected as controls. The sections were alternately separated (maintaining rostral to caudal order) into 24-well plates— one for combined LC and met-ENK and one for combined LDTg and met-ENK staining.

2.3.2.3 Sectioning of hypothalamus (Chapter 4)

Using the Mouse Brain Atlas, a transverse cut was made at Bregma -0.3 mm and 5 mm caudal to ensure entirety of PVN was retained. The larger caudal end of the hypothalamus was fixed to the vibratome specimen base, sectioned at 45 µm, and collected as described previously. Sections were viewed under light microscope until the

[5] SPN neurons are not visible under the light microscope (unless labelled) and therefore, the visible motor neurons were used as a guide.
[6] Bregma is the anatomical point on the skull where the coronal suture is intersected perpendicularly by the sagittal suture.

rostral-most end of the PVN was observed. Four additional sections were collected as controls. Sections were separated into four separate plates in order, for example, in the first plate, the first, fifth and ninth sections etc. were collected. This was so that combined OXY and VGAT, OXY and VGLUT2, VP and VGAT, and VP and VGLUT2 antibody labelling regimes could be applied.

2.3.3 Immunohistochemistry and microscopy

All sections (from spinal cord, pons and hypothalamus) were washed with PBS three times for five minutes. Sections were subsequently incubated in blocking solution consisting of of 10 % normal donkey serum (NDS, 017-000-121, Stratech Scientific, Suffolk) and 0.3 % Triton™ X-100 (X-100, Sigma-Aldrich, Dorset) in PBS for 2 hours at 21 ^{o}C. Tissue sections were then incubated in primary antibody combinations in Table 2.3 (for concentrations and catalogue numbers see Table 2.1) in diluent containing 1 % normal donkey serum and 0.03 % Triton™ X-100 in PBS for 48 hours at 4 ^{o}C. After washing in PBS (as described above), labelling was visualised using secondary antibody combinations in Table 2.3 (for concentrations and catalogue numbers see Table 2.2) for 1.5 hours at 21 ^{o}C in darkness to avoid light-induced fluorophore bleaching. In order to reduce autofluorescence attributable to age-pigment accumulation, sections were washed in PBS and treated with 2 mM copper sulphate and 50 mM ammonium acetate in distilled water (dH_2O) for 10 minutes at 21 ^{o}C. Sections were subsequently washed in PBS and were mounted on microscope slides before coverslipping with Vectashield mounting medium (H-1000, Vector Lab Ltd, Peterborough). In control sections, the omission of primary antibodies abolished any significant labelling other than autofluorescence.

Table 2.1: Primary antibodies used for immunofluorescence labelling of structures in the lumbosacral spinal cord, brainstem, and hypothalamus.

Optimal concentrations were tested and confirmed as suggested by manufacturer.

Primary antibody	**Host species**	**Catalogue number, company and country**	**Optimal concentration**
Lumbosacral Spinal cord:			
Anti-MAP2	Chicken	AB5392, Abcam, Cambridge, UK	1.5000
Anti-ChAT	Goat	AB144P, Merck Millipore, Watford, UK	1.200
Anti-ENK, methionine antibody	Rabbit	AB5026, Merck Millipore, Watford, UK	1.1000
Anti-VGAT	Guinea pig	131-308, Synaptic Systems, Goettingen, Germany	1.500
Brainstem:			
Anti-TH	Sheep	AB152, Merck Millipore, Watford, UK	1.1000
Anti-ChAT	Goat	AB144P, Merck Millipore, Watford, UK	1.200
Anti-ENK, methionine antibody	Rabbit	AB5026, Merck Millipore, Watford, UK	1.1000
Hypothalamus:			
Anti-OXY	Rabbit	AB911, Merck Millipore, Watford, UK	1.5000
Anti-VP	Rabbit	AB1565, Merck Millipore, Watford, UK	1.5000
Anti-VGAT	Guinea pig	131-308, Synaptic Systems, Goettingen, Germany	1.500
Anti-VGLUT2	Guinea pig	AB2251, Merck Millipore, Watford, UK	1.5000

Abbreviations: ChAT, Choline acetyle transferase; ENK, enkephalin; MAP2, Microtubule-associated proteion 2; OXY, Oxytocin; TH, Tyrosine Hydroxylase; VGAT, Vesicular GABA transporter; VGLUT2, Vesicular glutamate transporter 2; VP, Vasopressin.

Table 2.2: Secondary antibodies with conjugated fluorophores used for immunofluorescence labelling of structures in the lumbosacral spinal cord, brainstem, and hypothalamus.

Secondary antibody	**Fluorophore**	**Catalogue number, company and country**	**Concentration**
Lumbosacral Spinal cord:			
Donkey anti-chicken	Alexa Fluor® 488	703-545-155, Jackson ImmunoResearch, Cambridgeshire, UK	1.200
Donkey anti-goat	Cy3	A21432, Thermo Fisher Scientific, Loughborough, UK	1.400
Donkey anti-rabbit	Alexa Fluor® 488	711-545-152, Jackson ImmunoResearch, Cambridgeshire, UK	1.200
Donkey anti-guinea pig	Fluorescin isothiocyanine (FITC)	AP193F, Merck Millipore, Watford, UK	1.200
Donkey anti-rabbit	Cy3	711-545-152, Jackson ImmunoResearch, Cambridgeshire, UK	1.400
Donkey anti-guinea pig	Cy3	706-165-148, Jackson ImmunoResearch, Cambridgeshire, UK	1.400
Brainstem:			
Donkey anti-sheep	555	A21436, Thermo Fisher Scientific, Loughborough, UK	1.400
Donkey anti-goat	Cy3	A21432, Thermo Fisher Scientific, Loughborough, UK	1.400
Donkey anti-rabbit	Alexa Fluor® 488	711-545-152, Jackson ImmunoResearch, Cambridgeshire, UK	1.200
Hypothalamus:			
Donkey anti-rabbit	Alexa Fluor® 488	711-545-152, Jackson ImmunoResearch, Cambridgeshire, UK	1.200

Donkey anti-guinea pig	Cy3	706-165-148, Jackson ImmunoResearch, Cambridgeshire, UK	1.400

Table 2.3: Double immunofluorescence labelling combinations for nuclei and surrounding neurotransmitter terminals of AOIs in spinal cord, brainstem and hypothalamus.

Nucleus	**Neuronal marker**	**Secondary antibody**	**Terminal Marker**	**Secondary antibody**
Lumbosacral spinal cord:				
DLN, SNB and RDLN	MAP2	Donkey anti-chicken 488	ENK	Donkey anti-rabbit Cy3
			VGAT	Donkey anti-guinea pig Cy3
SPN	ChAT	Donkey anti-goat Cy3	ENK	Donkey anti-rabbit 488
			VGAT	Donkey anti-guinea pig FITC
Brainstem:				
LC	TH	Donkey anti-sheep Cy3	ENK	Donkey anti-rabbit 488
LDTg	ChAT	Donkey anti-goat Cy3		
Hypothalamus:				
PVN	OXY	Donkey anti-rabbit 488	VGAT	Donkey anti-guinea pig Cy3
			VGLUT2	
	VP		VGAT	
			VGLUT2	

Abbreviations: ChAT, Choline acetyle transferase; DLN, Dorsolateral nucleus; ENK, enkephalin; LC, Locus coeruleus; LDTg, Laterodorsal tegmental nucleus; MAP2, Microtubule-associated proteion 2; OXY, Oxytocin; PVN, Paraventricular nucleus; RDLN, Retrodorsolateral nucleus; SNB, Spinal nucleus of the bulbospongiosus; SPN, Sacral parasympathetic nucleus; TH, Tyrosine Hydroxylase; VGAT, Vesicular GABA transporter; VGLUT2, Vesicular glutamate transporter 2; VP, Vasopressin.

2.3.3.1 Primary antibody validation and optimisation of immunolabelling

All primary antibodies were validated by the manufacturers via western blot to confirm that the antibody binding was only at the expected molecular weight of the target protein. Additionally, IHC / ICC was used by manufacturers to confirm expected

subcellular localization of the target protein. Where available, manufacturers further validated antibody specificity using knockout / knockdown cell lines. Furthermore, manufacturers undertook consistency testing to confirm antibody quality remained stable during the manufacturing process (Abcam, 2020; Merck, 2020; Synaptic-Systems, 2020).

In-house antibody validation was based on IHC and comparison to literature. For example, Biag et al. (2012) provides a detailed cyto- and chemoarchitecture of the C57BL / 6J mouse PVN, including the location of OXY and VP immunopositive cells. This was then cross-referenced with the cellular localization of OXY and VP immunolabelled neurons that were observed in the present study. Additionally, primary antibodies were initially tested within the concentration ranges suggested by manufacturers for IHC to produce optimal immunolabelling.

2.3.3.2 Immunofluorescence light microscopy in Leica DM 5000B

The presence of nuclei of interest and neurotransmitter presumed terminals in spinal, brainstem and hypothalamic sections were identified on a Leica DM 5000B fluorescence microscope (Leica Microsystems, Milton Keynes, UK) at a 5x magnification prior to capturing images for analyses. Sections with inconsistent staining, folds, or tears in the AOIs were excluded from the study. Images were captured using a Leica DFC 310 FX digital camera (Leica, Milton Keynes, Uk) in overlay format to merge the image of immunolabelled neurons with immunolabelled presumed terminals at x20, x40 and x63 magnification. In pontine sections, images were taken in the region medial to the TH-immunolabelled LC and the ChAT-immunolabelled LDTg and this region was presumed to be the PMC in accordance with the Mouse Brain Atlas (Paxinos and Keith B. J. Franklin, 2007). Additionally, VGAT and met-ENK presumed terminals in spinal sections, were also captured in the DGC, DH and VH.

3 EFFECTS OF AGEING ON INHIBITORY INPUTS TO NEURONAL STRUCTURES OF THE BRAINSTEM AND THE LUMBOSACRAL SPINAL CORD

3.1 INTRODUCTION

The prevalence of LUT and terminal bowel dysfunction increases with age resulting in UI, FI, and / or constipation (as discussed in section 1.2). Cystometric studies and studies of contractility of isolated bladder strips suggest that age-related changes are largely associated with changes in bladder innervation as opposed to alterations in bladder contractility and this is potentially also the case with the terminal bowel and defaecation (Chun et al., 1988; Chun et al., 1989; Chun et al., 1990; Hotta et al., 1995). Brainstem and spinal nuclei are involved in the control of reflex micturition and defaecation and have shown age-associated changes within these structures which is discussed in detail in section 1.9. The present study aim was to establish any age-associated structural changes by immunohistochemically labelling select pontine and spinal regions involved in the control of micturition and defaecation in male C57BL / 6J mice.

Nuclei within the lumbosacral spinal cord exert parasympathetic and somatic control over the bladder and colorectal smooth muscle, and somatic control over the EUS and EAS (as described in sections 1.6.2.1 and 1.7.4.1). The SPN is the main source of (indirect) spinal parasympathetic control of the bladder detrusor and colorectal smooth muscle (Dorofeeva et al., 2009; Ni et al., 2018; Papka et al., 1995; Payette et al., 1987), whilst the DLN and SNB are spinal motor neurons that directly innervate the EUS and EAS respectively (McKenna and Nadelhaft, 1986; Schrøder, 1980). The PMC, located in the brainstem, exerts direct and indirect control over all three nuclei. The PMC initiates micturition by exciting the SPN via direct projections and simultaneously relaxes the DLN via projections to inhibitory GABAergic / glycinergic neurons in the DGC (Blanco et al., 2014; de Groat, 1998; Guo et al., 2013; Keller et al., 2018; Nuding and Nadelhaft, 1998;

Verstegen et al., 2017). This results in detrusor muscle contraction and EUS relaxation allowing for urine expulsion via the urethra. Excitation of the PMC causes DC contraction via the SPN (Pavcovich et al., 1998). Like the micturition reflex, the PMC likely simultaneously excites the SPN and inhibits the SNB during defaecation, since indirect projections have been observed from the PMC to the SNB (Dobberfuhl et al., 2014; Tang et al., 1999).

Other brainstem nuclei involved in the control of micturition and defaecation include the LC and LDTg. The PMC sends projections to the adjacent LC (Valentino et al., 1996) which controls conscious micturition and defaecation via cortical connections (Berridge and Foote, 1991; Carter et al., 2010; Lechner et al., 1997; Page et al., 1992; Valentino et al., 2011; Vazey and Aston-Jones, 2014). Furthermore, the LC exerts modulatory control over micturition and defaecation via projections to the SPN, DLN, SNB and sympathetic IML (in the thoracic spinal cord) (Jones and Yang, 1985; Nygren and Olson, 1977; Thor and de Groat, 2010; Westlund et al., 1983). Additionally, the LC sends projections to and receives innervation from the LDTg, which has been implicated in the control of micturition only (Cornwall et al., 1990; Jones and Yang, 1985). The LDTg also sends and receives projections from the SPN (Cornwall et al., 1990; Jones and Yang, 1985). Furthermore, LDTg stimulation evokes detrusor and EUS contractions (Noto et al., 1989; Yamao et al., 2001).

The neuropeptide met-ENK has been implicated in LUT and terminal bowel control within pontine nuclei. ENK inhibits PMC, LC and LDTg neuron activity. Some studies have reported inhibitory effects of ENK on these structures that are directly linked to LUT and terminal bowel control, whereby ENK regulates bladder capacity within the PMC and decreases detrusor contraction within the LC (Capece et al., 1998; Fowler et al., 2008; Guo et al., 2013; Guyenet and Aghajanian, 1979; Matsuzaki, 1990). Furthermore, it inhibits EAS contraction when injected into the LC (Abysique et al., 1998).

ENK and GABA-immunolabelling have been observed at lumbosacral level (in the SPN, DLN, SNB, DGC, DH and RDLN) and input onto SPN, DLN and SNB soma and

neuronal processes (Katagiri et al., 1986; Micevych et al., 1986; Ranson et al., 2006; Romagnano and Hamill, 1985; Sasek and Elde, 1986; Shimosegawa et al., 1987). ENK and GABA inhibit bladder, colorectal, EAS, and likely EUS contraction at this level (Abysique et al., 1998; Dray and Metsch, 1984; Hisamitsu and de Groat, 1984; Kennedy and Krier, 1987; Nakamori et al., 2018; Sugaya et al., 2019; Vaidyanathan et al., 1989).

Since pontine and lumbosacral spinal nuclei are heavily involved in the control of micturition and defaecation, they may be subject to age-associated structural changes. Furthermore, ENK and GABA both exert major inhibitory influences on nuclei of interest and thus may also be subject to change with age. Indeed, the PMC shows decreased activation with age (in humans) (Griffiths et al., 2007; Griffiths and Fowler, 2013), and this may be modulated by an increase in enkephalinergic inhibitory input. The SNB, DLN, LC, and LDTg have shown structural changes with increased age including changes in neuron number, soma size and dendrite length in cats, rats and mice (discussed in detail in section 1.9). For direct comparison to the present study, changes in mice include decreases in LC and LDTg neuron number and decreases in LDTg soma size and neurite length (Kawamata et al., 1990; Sturrock and Rao, 1985).

Change in density or number of ENK inputs to nuclei of interest have not been observed. However, ENK density at lumbar level is unchanged with age in rats (Missale et al., 1983) and this likely incorporates enkephalinergic interneurons that potentially project to spinal nuclei of interest (Huang et al., 2010; Nicholas et al., 1999; Sasek and Elde, 1986; Shimosegawa et al., 1987). In the SNB, a decrease in unlabelled synaptic inputs have been observed in rats and may reflect a change in ENK innervation (Matsumoto, 1998). Number of GABAergic inputs and $GABA_BRs$ on SPN neurons remains unchanged with age in rats (Dorfman et al., 2006; Santer et al., 2002). However, this may differ in present study mice due to interspecies variability.

In order to establish age-associated changes that may result in voiding dysfunction, brainstem and spinal structures were immunohistochemically labelled and compared across age groups. In lumbosacral spinal sections, percentage area measurements of

GABA and ENK were taken in additional regions to spinal nuclei of interest, including the DH, VH and DGC. These structures were included since ENK bladder and DC afferents, project to these regions (Keast and de Groat, 1992). Furthermore, GABAergic and enkephalinergic interneuron fibres likely project through the DH and DGC to the SPN and motoneurons (Blok and Holstege, 1994; Ding et al., 1999; Ding et al., 1997; Huang et al., 2010; Kuipers et al., 2006; Micevych et al., 1986; Nicholas et al., 1999; Sasek and Elde, 1986; Shimosegawa et al., 1987; Yao et al., 2018). The SNB and DLN are sexually dimorphic nuclei that respond to changes in testosterone (Breedlove and Arnold, 1981; Jordan et al., 1982; Kurz et al., 1991; Matsumoto, 2001; Matsumoto, 1997; Matsumoto et al., 1988). Therefore, the RDLN[7], an additional motor neuron structure that is largely unaffected by age-associated decrease in circulating testosterone was analysed, to help account for any age-associated changes that are testosterone-induced (Leslie et al., 1991; Nicolopoulos-Stournaras and Iles, 1983).

The main study hypothesis is that LUT and terminal bowel-controlling CNS structures are subject to age-associated changes that result in voiding disorders. Analysis of immunocytochemically labelled spinal and brainstem structures was undertaken to help determine if this is the case.

3.2 MATERIALS AND METHODS

3.2.1 Measurement parameters

Measurement parameters undertaken in pontine immunolabelled neurons in the LC (TH-immunopositive), LDTg (ChAT-immunopositive) and PMC (unstained) were compared across four age ranges: 3-5, 12-14, 25-26 and 29-31 months (n=3 for 12-14 and 25-26 months; n=4 for 3-5 and 29-31 months). Measurement parameters undertaken in lumbosacral spinal immunolabelled neurons in the SPN (ChAT-immunopositive), DLN, SNB, RDLN (MAP2-immunopositive), DGC, VH, and DH (unstained) were quantified and

[7] The RDLN contains motor neurons that innervate the flexor digitorium brevis muscle within the foot.

compared across two age ranges: 3-5 and 29-31 months (n=4 per age group). Analyses was undertaken using captured overlay images of sections. Over 4,100 images were analysed.

3.2.1.1 Cell counts

Cell counts were carried out in images taken at x20 magnification (see section 2.3.3.2 for imaging methodology) in immunolabelled nuclei including the LC, LDTg, SPN, DLN, and SNB. The mean number of labelled soma per section was calculated by counting immunolabelled neurons from the rostral to caudal extent of the nucleus and dividing the sum by the number of sections[8]. Abercrombie's correction factor was applied to avoid double counts of soma in consecutive sections (Abercrombie, 1946).

3.2.1.2 Soma perimeter measurements

Soma perimeter was carried out in images taken at x40 magnification in immunolabelled nuclei including the LC, LDTg, SPN, DLN, and SNB. All neurons (containing a visible nucleolus) were numbered in a section and up to six neurons were randomly selected using a random number generator. Perimeter measurements were undertaken using Image-pro Plus 7.0 (Media Cybernetics, Inc., Rockville USA) whereby soma were drawn around and the length was recorded. The mean soma perimeter of each nucleus was calculated per animal.

3.2.1.3 Percentage area coverage of ENK and VGAT within pontine and spinal areas of interest

Image-pro Plus 7.0 (Media Cybernetics, Inc., Rockville USA) was used to determine the percentage area coverage (per area) of ENK and VGAT in pontine and spinal areas of

[8] Quantification of neurons across entire nuclei was not possible in LC / LDTg due to alternate section labelling with TH or ChAT (see Chapter 2). Cell counts per section in spinal nuclei were continued for consistency.

interest (AOIs). ENK per area was measured in all spinal and brainstem regions mentioned in section 3.2.1. VGAT immunolabelling was undertaken in the lumbosacral spinal cord only and thus VGAT per area was measured in all spinal regions. Thresholds for fluorescence intensity were applied to reduce aberrant signalling. These were set manually by the same experimenter so only fluorescently labelled terminals were included. The percentage area coverage was determined in all sections containing set AOIs and the average per section was calculated in each animal.

In order to maintain consistency, shapes of a set size were placed over each nucleus or AOI for measurement of VGAT or ENK percentage coverage within each shape's boundaries (see Figure 3.1) The boundaries of each shape were mapped out to be roughly the average size of the nucleus from its rostral to caudal extent. To reduce the chance of shape boundaries overlapping into peri-nuclear regions, shapes were placed in the most central regions of AOIs.

Images of ENK and VGAT presumed terminals were taken at x40 magnification and analysed. Every section containing immunolabelled nuclei was measured using the corresponding shape. This resulted in roughly 9 measurements being taken per nucleus per animal within one antibody labelling regime in brainstem material, and 7 measurements being taken per nucleus in lumbosacral spinal material. In spinal sections, for every section containing labelled neurons in nuclei of interest (SPN, DLN and SNB) the per area of the RDLN, DH, VH and DGC was also measured within the same section. The mean percentage area coverage of VGAT and ENK in AOIs was then calculated per mouse.

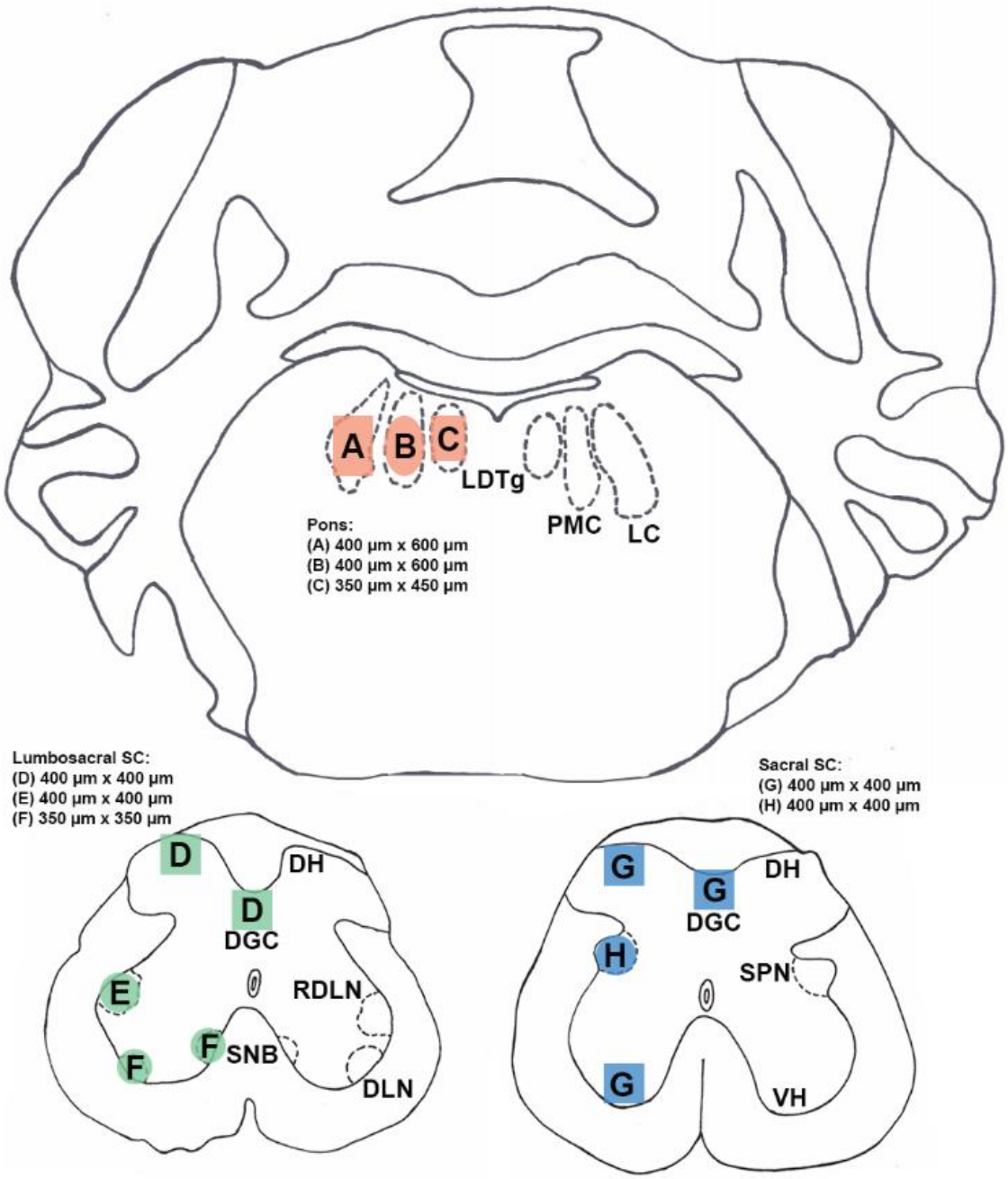

Figure 3.1: Shapes applied to pontine and lumbosacral spinal AOIs for per area measurement within AOI boundaries. A-H show the varying heights, widths, or diameters (µm), and types of shapes (rectangular, square or ellipses) applied to each AOI. AOI, Area of interest; DGC, Dorsal grey commissure; DH, Dorsal horn; DLN, Dorsolateral nucleus; LC, Locus coeruleus; LDTg, Laterodorsal tegmental nucleus; PMC, Pontine micturition centre; RDLN, Retrodorsolateral nucleus; SNB, Spinal nucleus of the bulbospongiosus; SPN, Sacral parasympathetic nucleus; VH, Ventral horn.

3.2.1.4 Quantifying ENK and VGAT terminal inputs in apposition to immunopositive cells within each nucleus

Overlay images of pontine and spinal nuclei showed ENK and VGAT presumed terminals making contact with immunolabelled neurons. Using overlay images at x63 magnification, the number of VGAT / ENK inputs in apposition to soma were counted on up to six randomly selected soma per section. All neurons (containing a visible nucleolus) were numbered in a section and six soma were randomly selected using a random number generator. Although a worthwhile measurement parameter, input counts onto neurites could not be done reliably. This was due to few neurites visibly extending from soma. Therefore, conditions were not replicable across neurons.

3.2.2 Tabulation, graphical representation, and statistical analyses

Means of each parameter were calculated per animal. Animals were then grouped into age groups. The mean for each sample group was then calculated ± standard error of the mean (SEM). For all parameters measured, data distribution was tested for using an Anderson-Darlington test, which allows determination of whether data samples came from a population with a specific distribution. The Anderson-Darling test is a goodness-of-fit test of distribution of a random variable and is one of the most powerful statistical tools for testing divergence from normality (Stephens, 1979). Its null hypothesis is that data follow a specified distribution i.e. a bell-shaped curve. It is based on empirical distribution function (EDF) statistics which is a non-parametric statistical estimation of distribution modelled on sample data. The Anderson Darling places more weight on tails than other statistical tests for normality e.g. the Kolmogorov-Smirnoff test.

3.2.2.1 Data derived from brainstem nuclei

To test for equal variance, a Bartlett’s test was used for all brainstem data. All brainstem results were observed to have abnormal distribution or unequal variance and

thus assumptions of a one-way ANOVA were defied. Therefore, to determine data significance a Kruskal-Wallis test was applied.

3.2.2.2 Data derived from spinal nuclei

To test for equal variance, an F-test was used for all spinal data. For parameters displaying homogenous variance a two-sample t-test assuming equal variance was performed. For parameters that showed heterogeneity of variance, a two-sample t-test with Welch's correction factor was used to test significance of data.

3.3 RESULTS

3.3.1 Pontine AOIs

The LC was present between Bregma -2.00 to -1.54 mm and was a crescent-shaped nucleus. It was located just ventral to fourth ventricle and sat bilateral to the ventrolateral edge of the fourth ventricle. The LDTg was present between Bregma -1.88 to -1.16 mm. It was ventral to the fourth ventricle and was located more medially than the LC. There was a gap between the LC and the LDTg where the PMC was presumed to reside (Paxinos and Franklin, 2007). Antibodies to TH consistently labelled 1-46 soma per section within the LC, and antibodies to ChAT consistently labelled 1-18 soma per section within the LDTg in all age groups (see Figure 3.2).

LC neurons appeared unipolar with spindle or oval shaped soma. LDTg neurons appeared multipolar with spindle or oval shaped soma. Neurite labelling was evident in both the LC and LDTg. Neurites were more prominent within the LC and appeared to have ventromedial projections towards the PMC. Although more sparse, LDTg neurites were still evident, with projections appearing more arbitrary in direction. Cell packing density in the LC was greater than that of the LDTg. Control sections, where primary antibodies had been omitted, showed no specific fluorescent labelling (see Appendix B, Figure 8.3).

3.3.1.1 Neuron counts and soma perimeter

The number of immunolabelled neurons in both regions was consistent across age groups. There was no significant change in the number of LC or LDTg neurons across age groups. Similarly, no significant differences were observed in LC/LDTG soma perimeter with age (Table 3.1).

Table 3.1: cell counts and soma perimeters of TH immunolabelled LC and ChAT immunolabelled LDTg neurons ± standard error of the mean (SEM).

	LC		**LDTg**	
Age (months)	**Cell count**	**Soma perimeter (µm)**	**Cell count**	**Soma perimeter (µm)**
3-5	15.31 ± 1.23	53.48 ± 1.14	7.52 ± 1.30	61.32 ± 2.87
12-14	9.87 ± 1.14	53.06 ± 2.97	5.91 ± 0.59	54.81 ± 3.18
24-26	10.76 ± 0.37	52.84 ± 1.79	7.31 ± 0.93	53.97 ± 2.77
29-31	9.57 ± 2.52	59.82 ± 2.12	9.27 ± 1.61	60.85 ± 1.68

Abbreviations: LC, Locus coeruleus; LDTg, Laterodorsal tegmental nucleus.

3.3.1.2 Per area measurement of ENK immunolabelling

Immunofluorescence labelling of ENK terminals comprised of punctate labels depicting neuron terminal boutons. ENK terminals were distributed across the entirety of whole brainstem sections. However, terminals were particularly concentrated within the region of the medial parabrachial nucleus and PMC. ENK terminals appeared to input onto immunolabelled LC and LDTg soma and neurites. Control sections (omission of primary antibodies) showed no specific labelling (see Appendix B, Figure 8.1 and Figure 8.2).

The distribution of ENK across entire sections allowed for the quantification of the percentage ENK immunofluorescence within individual pontine nuclei. ENK per area immunofluorescence within the PMC, LC and, LDTg displayed consistent concentrations across all age groups, with no significant changes across age groups (Figure 3.2.H).

3.3.1.3 ENK inputs onto LC / LDTg soma

Widespread distribution of ENK presumed terminals in apposition to consistently labelled LC / LDTg soma allowed for quantitative comparisons across age groups of presumptive ENK inputs onto soma. There were a similar number of soma appositions in each nucleus with the means for both falling between 0.5-2.7 (Figure 3.2.I). The number of ENK terminals in appostion to LC / LDTg soma showed no significant change across age groups.

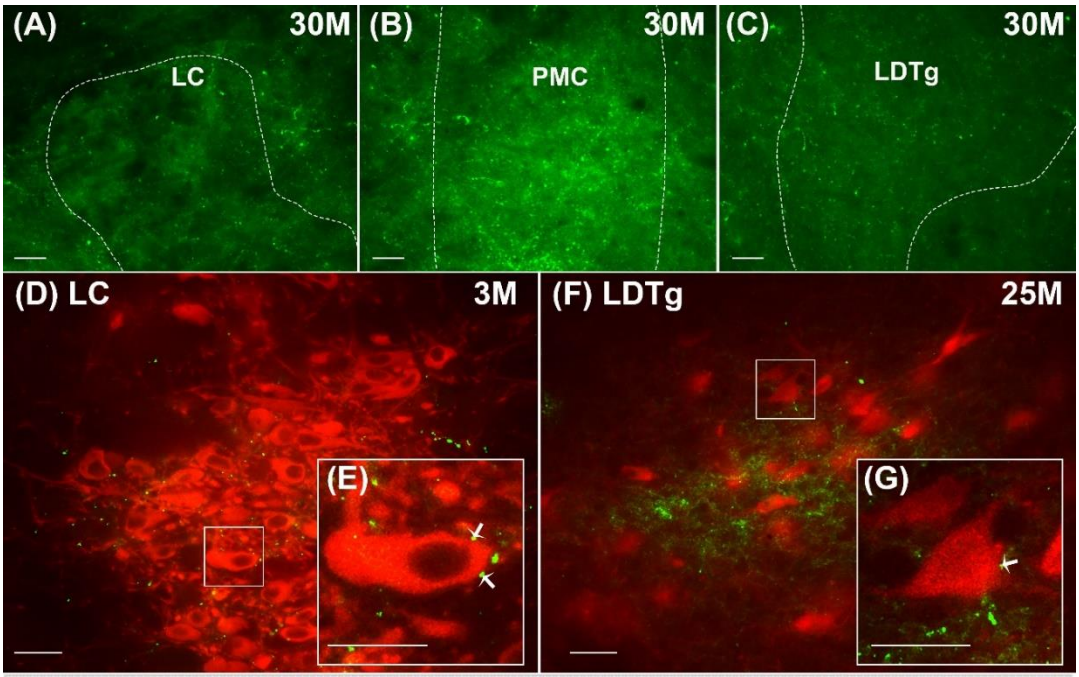
(A)
30M
LC
(B)
30M
PMC
(C)
30M
LDTg
(D) LC
3M
(E)
(F) LDTg
25M
(G)

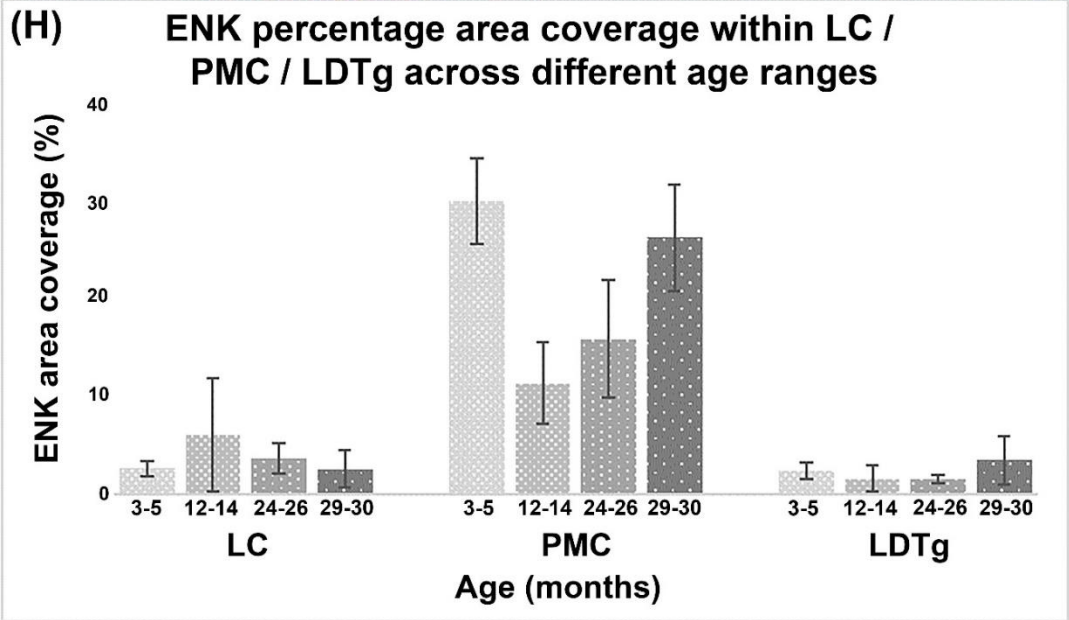
(H)
ENK percentage area coverage within LC / PMC / LDTg across different age ranges
ENK area coverage (%)
40
30
20
10
0
3-5
12-14
24-26
29-30
LC
PMC
LDTg
Age (months)

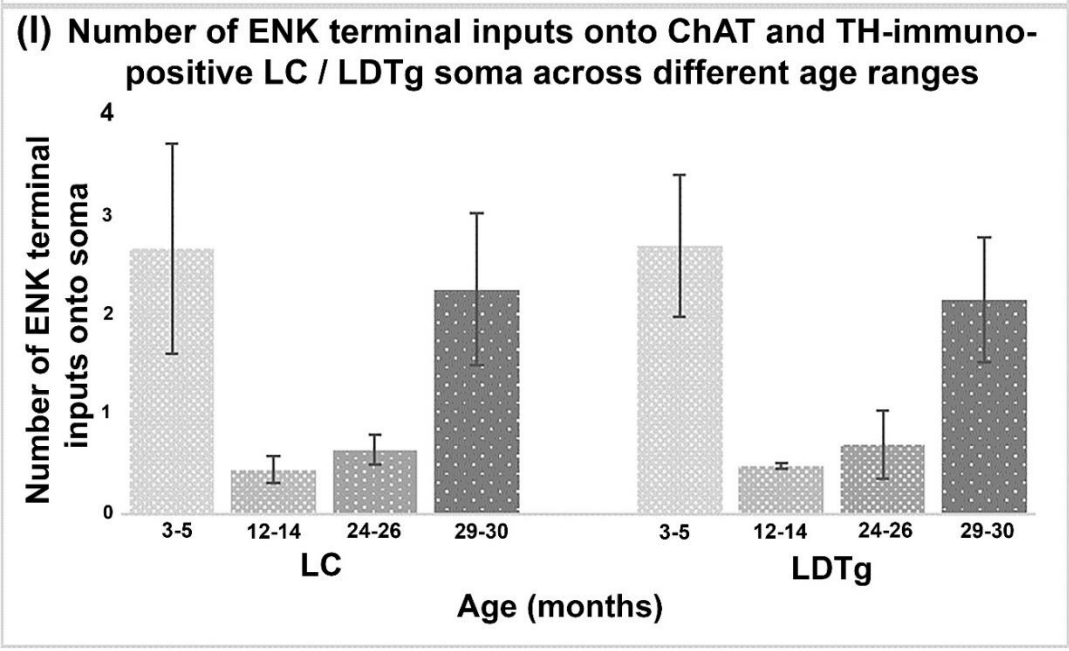
(I) Number of ENK terminal inputs onto ChAT and TH-immuno-positive LC / LDTg soma across different age ranges
Number of ENK terminal inputs onto soma
4
3
2
1
0
3-5
12-14
24-26
29-30
LC
LDTg
Age (months)

Figure 3.2 A-I: Immunolabelling of pontine nuclei and ENK terminals. A-C show ENK labelling within the LC, PMC, and LDTg. Graph H reflects the increased ENK immunolabelling density in the PMC. D-E show ENK inputs in apposition to LC soma; F-G show ENK inputs in apposition to LDTg soma. Arrows depict ENK inputs in apposition to soma. Group means ± SEM; n=3 (12-14 & 24-26 months); n=4 (3-5 & 29-31 months). All data were determined to have abnormal distribution and/ or unequal variance when Anderson-Darling and the Bartlett's test were applied, respectively. Data was tested for significant differences between age groups with a Kruskal Wallis test. Scale bars = 10 µm. ChAT, Choline acetyltransferase; ENK, Met-enkephalin; LC, Locus coeruleus; LDTg, Laterodorsal tegmental nucleus; M, Months; PMC, Pontine micturition centre; TH, Tyrosine hydroxylase.

3.3.2 Lumbosacral spinal AOIs

The DLN and SNB (in lumbosacral sections) were located in the ventral horn in lamina IX. The SPN (in sacral sections only) was located at the dorsolateral edge of lamina VII. Antibodies to MAP2 consistently labelled 1-5 SNB and 1-6 DLN soma per section. Antibodies to ChAT consistently labelled 1-8 SPN soma per section in both age groups (Figure 3.5). DLN and SNB soma were oval in shape with labelled neurites that were dense within each nucleus. These neurites surrounded labelled soma, but few were observed to visibly extend from soma and projected in varying directions. SPN soma were spherical in shape, a nucleolus often was not visible. SPN neurites were sparse and often not visible within individual sections.

3.3.2.1 Neuron counts and soma perimeter

The number of immunolabelled neurons within each nucleus was consistent across both age groups (Table 3.2). Soma perimeter also showed no significant difference between age groups. DLN / SNB soma perimeter was larger than SPN perimeter (Table 3.2).

Table 3.2: Age-associated changes in cell counts and soma perimeters of ChAT immunolabelled SPN neurons and MAP2 immunolabelled DLN/SNB neurons ± SEM.

	SPN		**DLN**		**SNB**	
Age (months)	**Cell count**	**Soma perimeter (µm)**	**Cell count**	**Soma perimeter (µm)**	**Cell count**	**Soma perimeter (µm)**
3-5	2.91 ± 0.63	46.85 ± 8.41	3.15 ± 0.27	92.28 ± 3.73	3.18 ± 0.13	78.90 ± 4.99
29-31	3.41 ± 0.26	60.40 ± 4.56	3.31 ± 0.21	91.11 ± 5.97	3.03 ± 0.18	82.48 ± 4.89

Abbreviations: DLN, Dorsolateral nucleus; SNB, Spinal nuclues of the bulbospongiosus; SPN, Sacral parasympathetic nucleus.

3.3.2.2 Per area measurement of VGAT and ENK immunolabelling

Antibodies to VGAT and ENK produced punctate labelling depicting terminal boutons that were spread ubiquitously across entire spinal cord sections. There was more concentrated immunolabelling of VGAT / ENK within the DH / DGC of both age groups (see graphs in Figure 3.3-2.4). SPN VGAT per area immunoreactivity showed a significant decrease of 66.4 % with age (see Figure 3.3). Similarly, SPN ENK per area immunoreactivity showed a significant decrease of 57.4 % with age (see Figure 3.4).

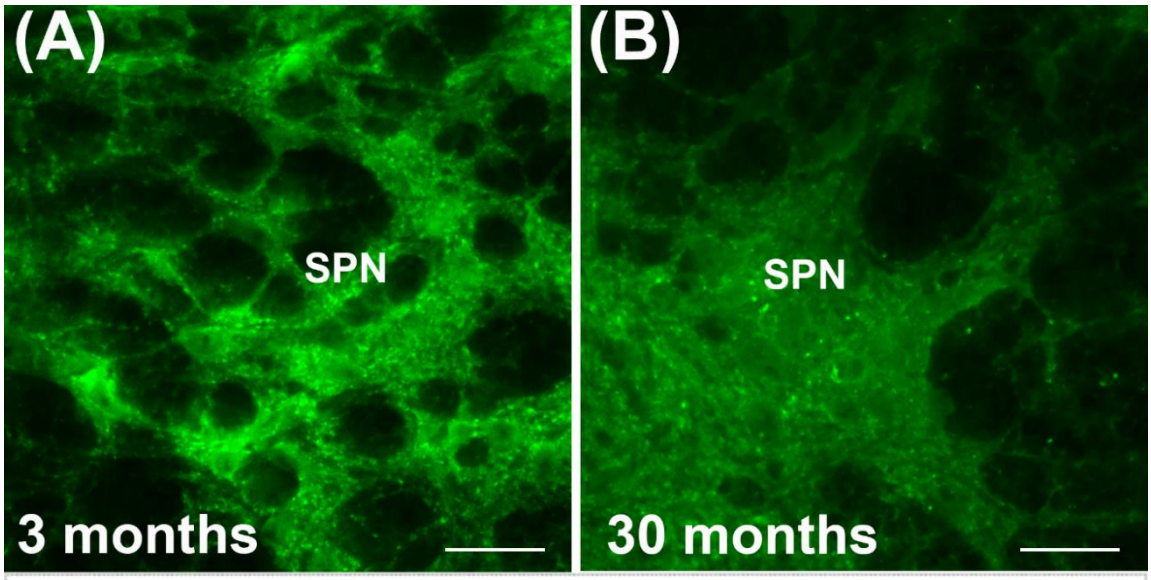
(A)
SPN
3 months
(B)
SPN
30 months

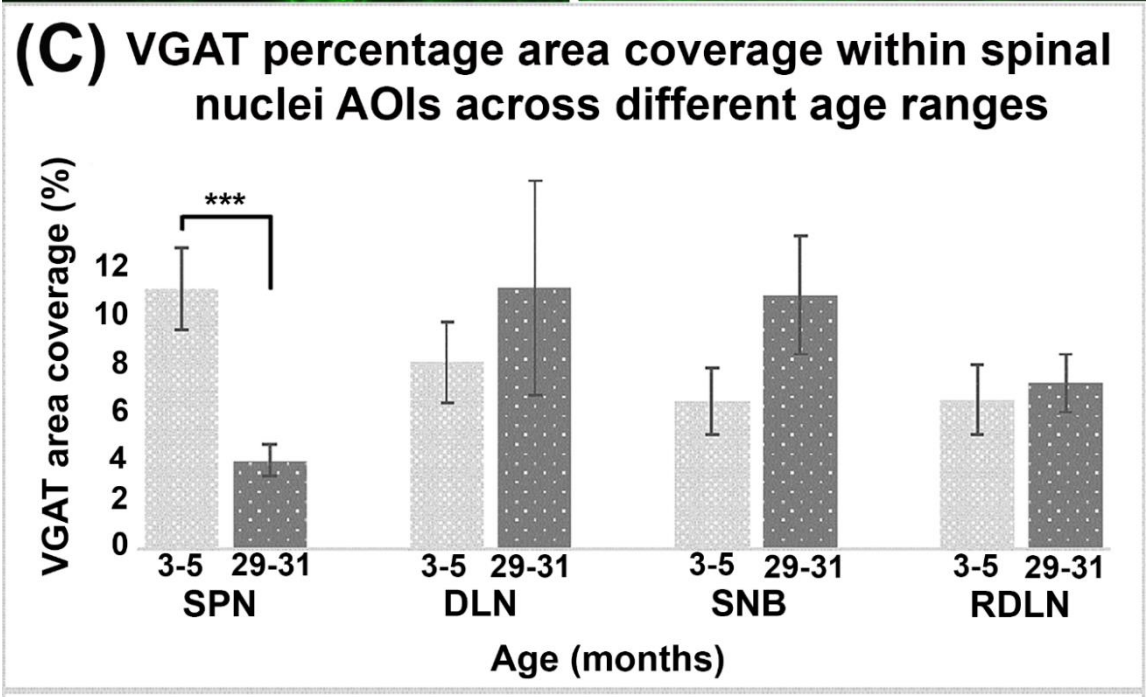
(C) VGAT percentage area coverage within spinal nuclei AOIs across different age ranges
VGAT area coverage (%)
***
12
10
8
6
4
2
0
3-5
29-31
SPN
DLN
SNB
RDLN
Age (months)

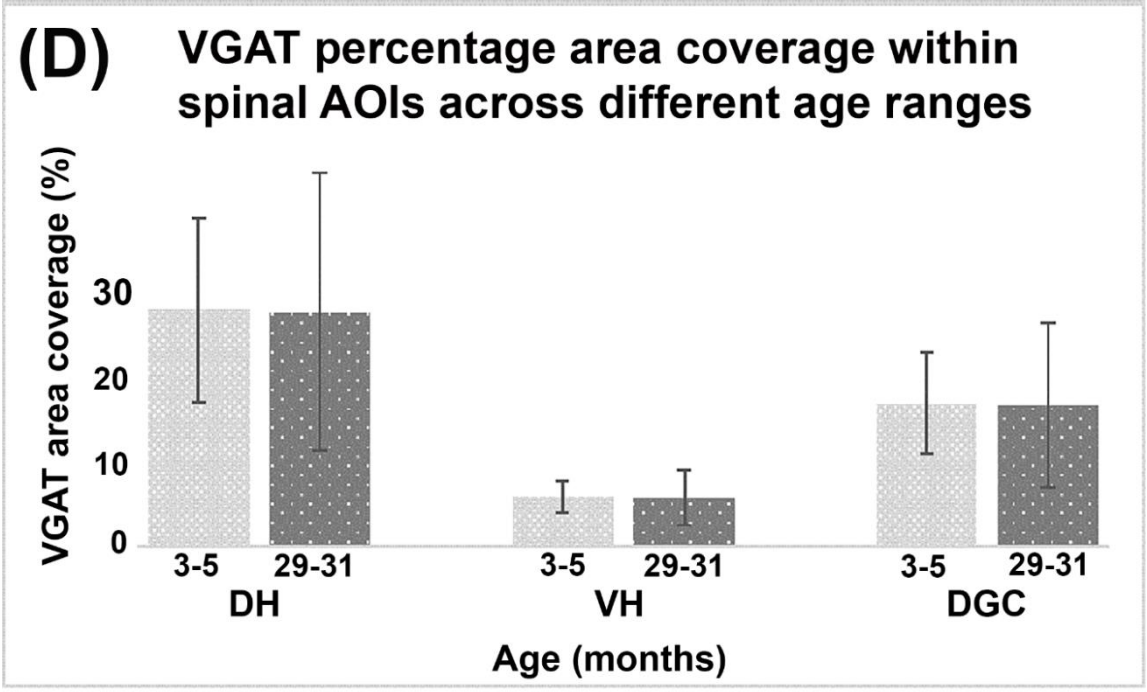
(D) VGAT percentage area coverage within spinal AOIs across different age ranges
VGAT area coverage (%)
30
20
10
0
3-5
29-31
DH
VH
DGC
Age (months)

*Figure 3.3 A-D: VGAT per area in lumbosacral spinal AOIs, with a decrease in VGAT immunoreactivity in the SPN with age. A-B shows VGAT immunolabelling in 3- and 30-month SPN. C-D show graphs depicting VGAT immunolabelling per area in spinal AOIs across age groups. Group means ± SEM; n=4 per age group; ***p≤0.01. Anderson Darling and F-tests were applied to test for normality and variance, respectively. To test for significant differences between age groups, two-sample t-tests assuming equal variance were applied to data with an equal variance; two-sample t-tests with Welch's correction factor were applied to data with unequal variance. Scale bars = 20 µm. AOIs, Areas of interest; DLN, Dorsolateral nucleus; DGC, Dorsal grey commissure; DH, Dorsal horn; RDLN, Retrodorsolateral nucleus; SNB, Spinal nucleus of the bulbospongiosus; SPN, sacral parasympathetic nucleus; VGAT, Vesicular GABA transporter; VH, Ventral horn.*

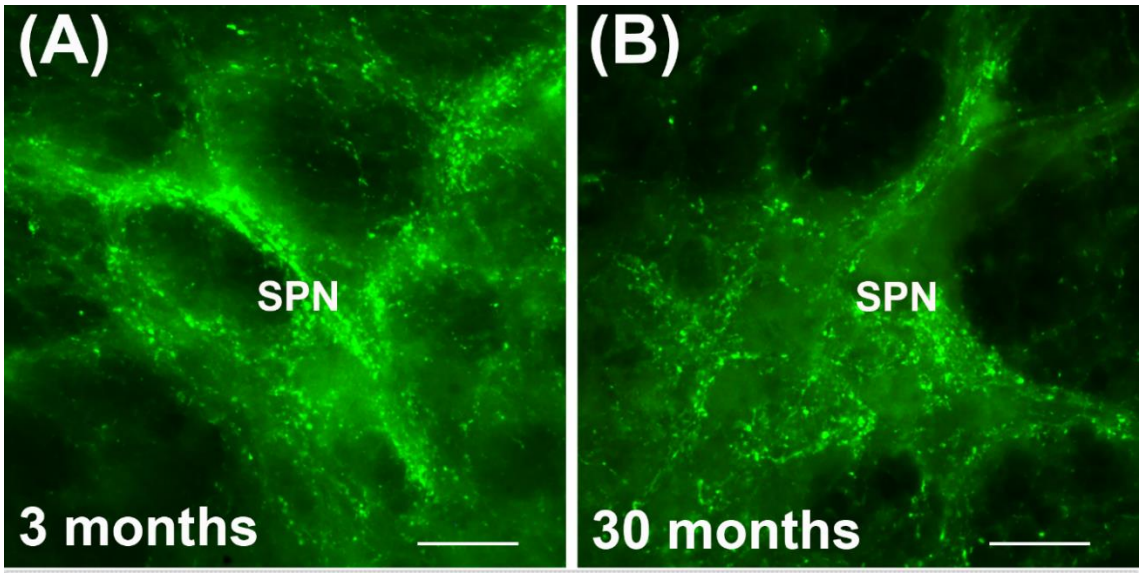
(A)
SPN
3 months
(B)
SPN
30 months

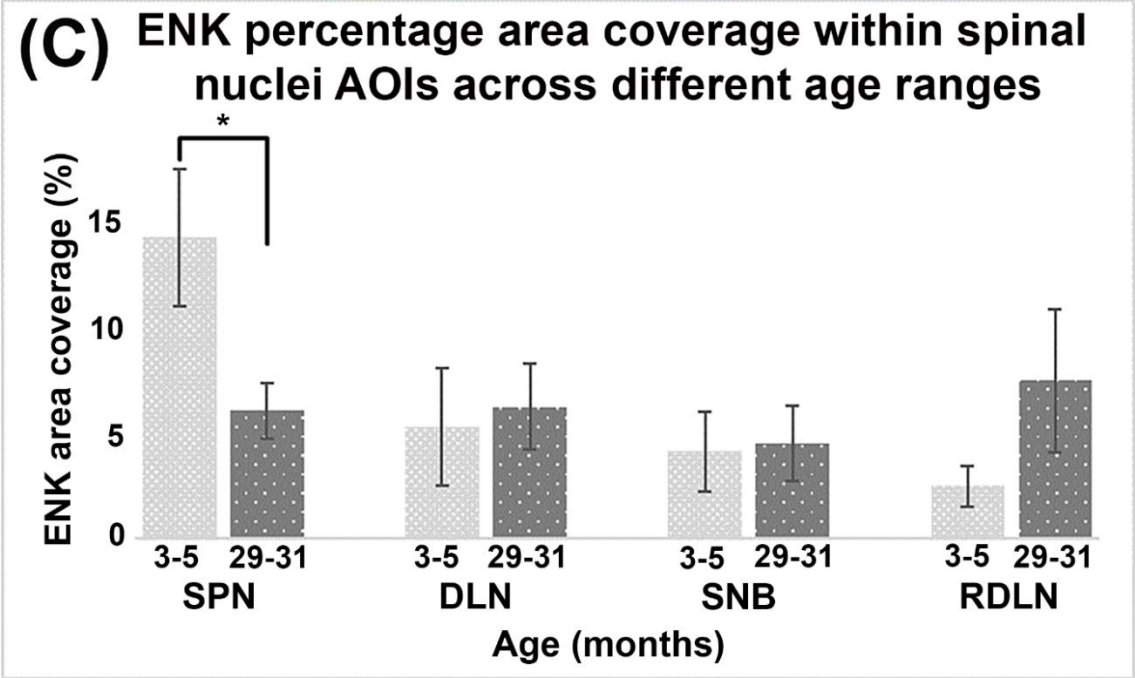
(C)
ENK percentage area coverage within spinal nuclei AOIs across different age ranges
*
ENK area coverage (%)
15
10
5
0
3-5
29-31
SPN
DLN
SNB
RDLN
Age (months)

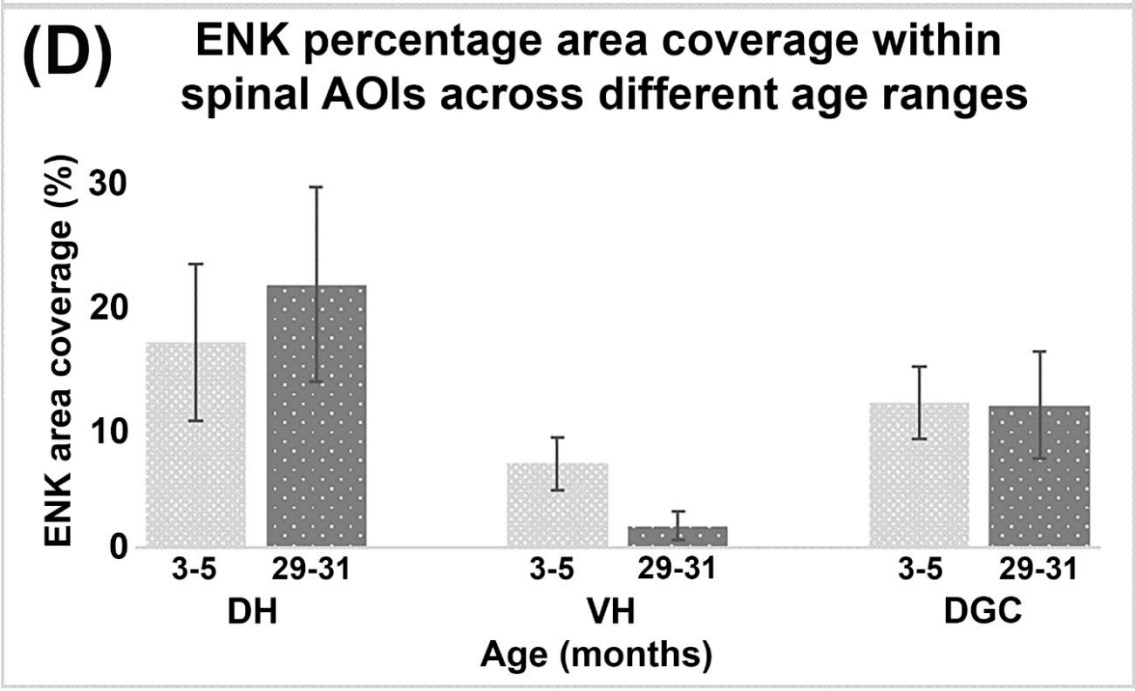
(D)
ENK percentage area coverage within spinal AOIs across different age ranges
ENK area coverage (%)
30
20
10
0
3-5
29-31
DH
VH
DGC
Age (months)

*Figure 3.4 A-D: ENK per area in the lumbosacral spinal AOIs. A-B show ENK immunolabelling in 3- and 30-month SPN. C-D show graphs depicting ENK immunolabelling in spinal AOIs across age groups. Group means ± SEM; n=4 per age group; *p≤0.1. Anderson Darling and F-tests were applied to test for normality and variance, respectively. To test for significant differences between age groups, two-sample t-tests assuming equal variance were applied to data with an equal variance; two-sample t-tests with Welch's correction factor were applied to data with unequal variance. Scale bars = 20 µm. AOIs, Areas of interest; DLN, Dorsolateral nucleus; DGC, Dorsal grey commissure; DH, Dorsal horn; ENK, Met-enkpehalin; RDLN, Retrodorsolateral nucleus; SNB, Spinal nucleus of the bulbospongiosus; SPN, sacral parasympathetic nucleus; VH, Ventral horn.*

3.3.2.3 VGAT/ ENK inputs onto spinal motoneurons

Presumptive ENK and VGAT terminals in apposition to DLN, SNB, and SPN immunolabelled soma allowed for quantitative comparisons across age groups. SPN soma had more ENK inputs in apposition than motor neuron soma (see Figure 3.5.H). In terms of age-associated changes, there was no significant differences in the number of VGAT / ENK inputs in apposition to SPN, DLN, or SNB some (Figure 3.5).

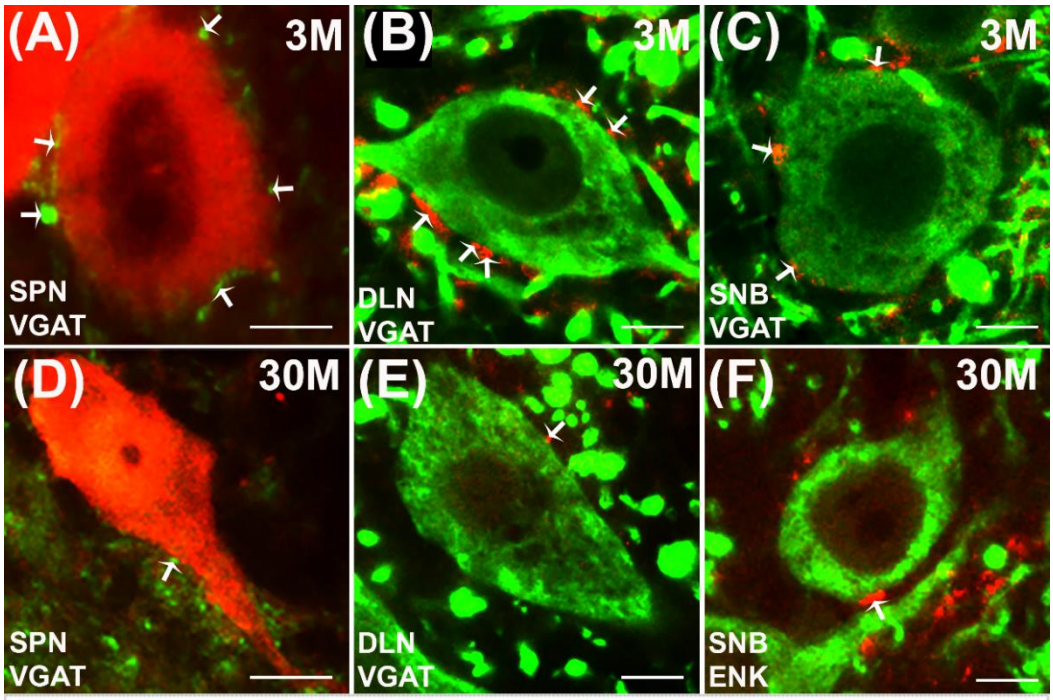
(A)
3M
SPN
VGAT
(B)
3M
DLN
VGAT
(C)
3M
SNB
VGAT
(D)
30M
SPN
VGAT
(E)
30M
DLN
VGAT
(F)
30M
SNB
ENK

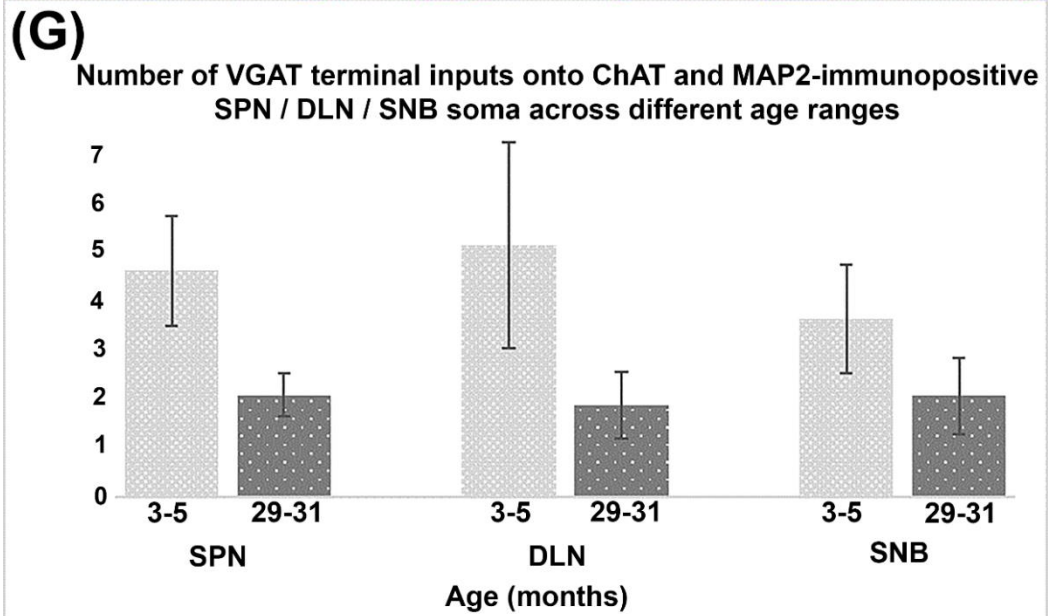
(G)
Number of VGAT terminal inputs onto ChAT and MAP2-immunopositive SPN / DLN / SNB soma across different age ranges
0
1
2
3
4
5
6
7
3-5
29-31
SPN
DLN
SNB
Age (months)

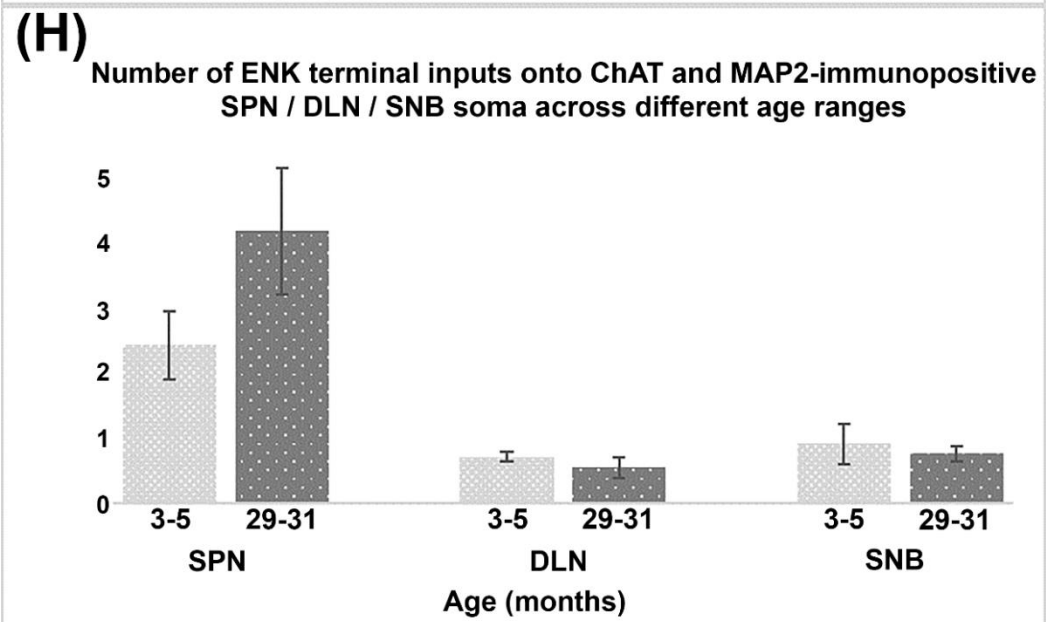
(H)
Number of ENK terminal inputs onto ChAT and MAP2-immunopositive SPN / DLN / SNB soma across different age ranges
0
1
2
3
4
5
3-5
29-31
SPN
DLN
SNB
Age (months)

Figure 3.5: ENK and VGAT inputs onto lumbosacral spinal nuclei showing decreased VGAT inputs onto SPN and DLN soma with age; results were not significant. A & D show VGAT inputs in apposition to SPN soma (3 and 30 months). B and E show VGAT inputs in apposition to DLN soma (3 and 30 months). C shows VGAT inputs in apposition to SNB soma (3 months). F shows ENK inputs in apposition to SNB soma (30 months). G-H show graphs depicting the mean number of VGAT / ENK inputs in apposition to SPN/DLN/SNB soma. Group means ± SEM; n=4 per age group. Anderson Darling and F-tests were applied to test for normality and variance, respectively. To test for significant differences between age groups, two-sample t-tests assuming equal variance were applied to data with an equal variance; two-sample t-tests with Welch's correction factor were applied to data with unequal variance. Scale bar = 10 µm. ChAT, Choline acetyltransferase; DLN, Dorsolateral nucleus; ENK, Met-enkpehalin; MAP2, Microtubule associated protein 2; SNB, Spinal nucleus of the bulbospongiosus; SPN, sacral parasympathetic nucleus; VGAT, Vesicular GABA transporter.

3.4 DISCUSSION

3.4.1 Summary of main findings

In this chapter, application of immunohistochemistry allowed for the identification of age-associated changes in ENK and VGAT immunoreactivity in lumbosacral spinal nuclei. There was a significant 66.5% decrease in ENK immunoreactivity in the aged (29-31 month) mouse SPN compared with young (3-5 month). Additionally, there was a significant 57.5% decrease in VGAT immunoreactivity in the aged SPN compared with young. No age-associated changes in soma size, neuron number or ENK / VGAT inputs onto to spinal or brainstem nuclei of interest were noted.

3.4.2 Immunolabelled structures

Immunolabelling of LC (TH) and LDTg (ChAT) neurons agreed with previous literature regarding cell shape, neurite projection and cell packing density (Armstrong et

al., 1983; Holets et al., 1988; Pickel et al., 1977; Standaert et al., 1986). Putative ENK punctate terminals were ubiquitous throughout the LC, PMC, and LDTG suggesting rostro-caudal projection of ENK fibres. This has been observed in previous studies of the rat LC and PMC using anti-met-ENK antibodies (Drolet et al., 1992; Van Bockstaele et al., 1995). ENK-immunoreactive cells were also observed in the rat PMC and were not observed in the present study (Drolet et al., 1992). This difference may be due to interspecies variability between mice and rats; or may be due to partially masked ENK^+ antigen loci meaning that ENK^+ soma often go undetected with standard immunohistochemical techniques (Huang et al., 2010; Todd et al., 1992). ENK immunoreactivity has not previously been reported in the LDTg. However, δ-opioid receptor (DOR) immunopositive cells have been observed in the rat LDTg (and LC), and ENKs are the endogenous ligands for DORs (Arvidsson et al., 1995). Within the PMC, the mean ENK-immunoreactive percentage ranged between 11.4-30.2 % which was more concentrated than LC (2.6-6.1 %) and LDTg (1.5-3.5 %) ENK-immunoreactivity. Consequently, ENK appears more closely associated with autonomic control of the bladder than control of other behaviours linked with LC / LDTg activation.

VGAT and ENK punctate labelling was ubiquitous throughout lumbosacral spinal grey matter, which has been previously reported. VGAT and ENK immunoreactivity showed the highest density of immunolabelling within the DH and DGC which also corresponds with previous literature (Gibson et al., 1981; Magoul et al., 1987; Marvizon et al., 2009; Snow et al., 1996). ChAT-immunoreactivity in rat SPN neurons is reflective of that in the present study labelling. Additionally, like present work, ENK inputs have been observed in apposition to ChAT-immunoreactive SPN neurons (at ultrastructural level) (Kohno et al., 1989).

3.4.3 Ageing in pontine AOIs

The present study observed that ageing did not impact the soma size or neuron number within ChAT-immunolabelled LDTg and TH-immunolabelled LC nuclei.

Furthermore, ENK per area within pontine nuclei remained robust with age, indicating that age-associated dysfunction of structures within the peritoneum cavity is unlikely to be attributed to changes in ENK levels within these nuclei. Similarly, ENK inputs observed in apposition to LC and LDTg soma were also maintained with increasing age. The mean number of ENK inputs onto LC and LDTg soma in general fell within the same range of 0.5-2.7 inputs onto each nuclei's soma. To the best of our knowledge, age-associated changes in ENK input numbers, density, or concentration have not previously been observed within these structures.

ENK inputting onto PMC neurons plays an important role in regulating bladder capacity. Stimulation of MORs in rats results in decreased firing of pre-sympathetic and pre-parasympathetic spinal-projecting neurons of the PMC (Guo et al., 2013), and PMC-injected ENK has been observed to reduce bladder contraction in cats (Hisamitsu and de Groat, 1984; Jubelin et al., 1984). Furthermore, microinjection of opioid blocking naloxone into the PMC of decerebrated cats and dogs reduced bladder capacity by 17-57 %, with effects reversed by the microinjection of the opioid fentanyl (Matsumoto et al., 2004). Thus, ENK likely plays an important role in setting the bladder volume threshold for which micturition should occur. Studies of the impact of ENK-PMC inputs and defaecation have not been undertaken; however, it likely has an inhibitory effect on colorectal motility. In aged humans, fMRI studies have shown reduced activity in the PMC during bladder filling (Griffiths et al., 2007; Griffiths and Fowler, 2013), which suggests that inhibitory influence over the PMC, or inhibitory receptor density, is increased with age. As previously mentioned, this was not the case regarding ENK density within the region of the PMC, which was maintained in aged mice. However, ENK inputs onto PMC soma and neurites was not presently observed and thus this parameter may show age-associated changes. Furthermore, the PMC receives inhibitory inputs from GABA and glycine which decrease neuronal activity (Guo et al., 2013). Thus, increased age may impact the distribution of GABAergic and glycinergic density within the PMC. Alternatively, there may be an ag-associated change in the receptor density that inhibitory neurons input onto. Additionally, age-associated changes may result within PMC neurons themselves. For example,

neuron morphology or number may change which could impact neuron projection pathways to spinal LUT-innervating neurons, and these parameters were not presently observed.

As presently reported, ENK presumed synapses appose LC neurons, and this has been previously observed, as well as the presence of opioid receptors on LC neurons (Drolet et al., 1992; Guyenet and Aghajanian, 1979; Uhl et al., 1979). Opiate inputs cause prolonged depression of spontaneous LC neuronal activity (Bird and Kuhar, 1977). Additionally, ENK activation of LC MORS in cats results in reduced bladder contractility and increased bladder capacity (Guyenet and Aghajanian, 1979; Matsuzaki, 1990), and thus ENK inputs in the LC have a similar function to ENK inputs in the PMC. In addition, ENK injected into the cat LC results in decreased EAS contractility and therefore likely partially functions in control of voluntary defaecation. Within the present study, no changes were observed that may impact the function of the LC. However, extensive age-associated changes have previously been observed in the LC (see section 1.9.4). Synpatic vesicle protein, involved in regulation of neurotransmitter release, is increased within synapses onto LC neurons in aged humans (Iwanaga et al., 1996). If this is also the case in mice, then it likely impacts non-ENK synapses as these were maintained in the present study. Noradrenergic innervation of spinal pathways that control the LUT and terminal bowel (including the SPN and DLN) that are likely derived from the LC, are decreased with age in rats (Ko et al., 1997; Lyons et al., 1989; Ranson et al., 2003a). This indicates decreased excitatory innervation of the LC or age-associated decline in LC neuron function potentially resulting in neuron loss. In mice, age-associated neuron loss has been observed in the LC which contrasts with the maintenance presently observed (Sturrock and Rao, 1985). This may be due to the use of a different strain of mice i.e. male ASH / TO strain as opposed the presently used male C57BL / 6J mice. Comparable age groups and counting techniques were applied across studies; however, differing methodology in tissue fixation (use of Bouin’s solution and parrafin wax) and staining (use of Lapham’s stain) may have also contributed to disparity between results.

LDTg neurons are DOR$^+$ and ENK input reduces neuron activity (Arvidsson et al., 1995; Capece et al., 1998). The effects of ENK-LDTg inputs in bladder control are unknown, however they are likely to have a similar effect to the LC and PMC since the LDTg directly innervates to the SPN (Hamilton et al., 2009; Hida and Shimizu, 1982). Studies of age-associated change in ENK or general synaptic inputs onto LDTg neurons have not previously been reported. However, the effects of age on neuron number and morphology have been noted (see section 1.9.4 for reports across species). In aged mice, neuron number has been observed to be maintained, emulating present results. However, soma size has been reported to decrease in aged mice which opposes the maintenance in size presently observed. This may be attributable to the use of a different strain of mice i.e. male DDD mice compared to present male C57BL / 6J mice since analysis and age groups were comparable between studies.

3.4.4 Ageing in lumbosacral spinal AOIs

The present study observed that neuron number and soma size are maintained in the lumbosacral SPN, DLN, and SNB. Furthermore, the number of ENK and VGAT inputs that oppose SPN, DLN, and SNB soma did not change with age. The density of ENK and VGAT immunoreactivity remained unchanged in all lumbosacral AOIs with the exception of the SPN, whereby a significant age-associated decrease in VGAT and ENK density was reported. This may be reflective of fewer dendritic inputs since no age-associated changes were observed with the number of VGAT or ENK inputs that apposed SPN soma. However, GABA inputs onto SPN soma and dendrites are unchanged in aged rats at ultrastructural level (Santer et al., 2002). This difference between studies may be attributable to interspecies variability. The effects of ageing on the distribution ENK fibres within the SPN have not previously been observed. However, unlabelled synaptic inputs onto SPN neurons remains unchanged with increased age in rats (Santer et al., 2002). Again, this may be attributable to interspecies variability, or may simply not be reflective of a change that is specific to ENK$^+$ synapses.

The age-associated changes reported at spinal level likely impact bladder and terminal bowel function of C57BL / 6J male mice used presently. Aged C57BL / 6J mice have weaker detrusor contractile and relaxant responses in the bladder, that is more pronounced in males (Kamei et al., 2018). SPN stimulation results in reflex bladder contractions (Ni et al., 2018), whilst ENK and GABA at lumbosacral level inhibits bladder detrusor activity (Dray and Metsch, 1984; Hisamitsu and de Groat, 1984; Sugaya et al., 2019). A decline in inhibitory ENK and GABAergic inputs may result in decreased relaxant responses in the bladder.

Additionally, aged male C57BL / 6J mice suffer from decreased colonic motility and faecal impaction (Patel et al., 2014). Stimulation of the SPN evokes colorectal and IAS contractions (Dorofeeva and Panteleev, 2007; Tai et al., 2001), whilst ENK and GABA at lumbosacral level inhibits DC contractions (Kennedy and Krier, 1987; Nakamori et al., 2018). A decrease in inhibitory SPN inputs with age would likely result in increased DC contractile responses which would oppose age-associated changes in colonic motility observed previously in aged male C57BL / 6J mice (Patel et al., 2014). However, decreased spinal inhibition of DC contractility may be a compensatory mechanism as a result of the potential increase in DC rigidity and DC smooth muscle deterioration with age discussed in section 5.4.

GABAergic innervation of the SPN is derived from spinal interneurons projecting from the DGC and DH, and descending neurons from the rostal ventromedial medulla (Antal et al., 1996; Blok et al., 1997a; Holstege, 1991; Polgar et al., 2003). To our best knowledge, age-associated changes in GABAergic descending rostal ventromedial medulla and spinal interneurons have not been reported. Therefore, it is difficult to ascribe a potential cause for decreased VGAT density observed in the SPN.

ENK innervation to the SPN likely originates from spinal afferents and interneurons since mid-thoracic spinal transection produces no change in lumbosacral ENK density (Micevych et al., 1986; Romagnano et al., 1987). Spinal afferents are thought to supply lesser amounts of ENK to the SPN, since few bladder, DC, and penis afferents are ENK^+

(Keast and de Groat, 1992). ENK soma observed in the thoracic and lumbar spinal DH and DGC likely innervate SPN neurons (Huang et al., 2010; Nicholas et al., 1999; Sasek and Elde, 1986; Seybold and Elde, 1980). Furthermore, the SPN itself contains ENK$^+$ neurons and this may provide short local projections to ChAT$^+$ neurons presently observed (Shimosegawa et al., 1987). However, due to partially masked antigen loci, ENK$^+$ SPN soma were not observed in the present study as ENK$^+$ soma often go undetected with standard immunohistochemical techniques (Huang et al., 2010; Todd et al., 1992). If this was the case, these neurons likely project rostrally or caudally since punctate ENK$^+$ fibres were observed presently with no evidence of lateral projections. ENK immunoreactivity change with age was measured in the rat spinal cord using radioimmunoassay. Within the lumbar cord, ENK$^+$ content was observed to be unchanged with age. However, it was decreased at thoracic level (Missale et al., 1983). Therefore, loss of thoracic ENK$^+$ neurons that may project to the SPN (as described above) may result in the age-associated decline in ENK SPN density presently reported.

Studies in rats showed maintenance of SPN neuron numbers and soma with age and agree with present study results (Dering et al., 1998; Dering et al., 1996; Santer et al., 2002). Studies of the sexually dimorphic DLN and SNB showed age-associated changes in neuron numbers and morphology in male Fischer 344 rats, with a study reporting a decline in neuron numbers. Soma size were observed to be increased (with evident lipofuscin build-up) in one study and decreased in the other study with age (Fargo et al., 2007; Jacob, 1998). Results were likely attributed to decline in circulating testosterone since acute and chronic testosterone treatment reversed age-related DLN and SNB number and morphological changes (Fargo et al., 2007). However, plasma testosterone levels are not significantly decreased in male C57BL / 6J mice (of up to 31 months) with age (Nelson et al., 1975; Svare et al., 1983), and thus may potentially explain maintenance of neuron number and soma size presently observed in aged SNB / DLN neurons. Furthermore, age-associated decline of unlabelled synaptic inputs onto SNB soma have been reported in rats with castration and therefore decreased plasma testosterone being observed to result in significantly reduced SNB synaptic input

(Matsumoto, 1998). Thus, age-associated maintenance of GABA and ENK SNB (and likely DLN) soma inputs is likely attributed to the fact that plasma testosterone does not decrease in aged male C57BL / 6J mice (Nelson et al., 1975; Svare et al., 1983).

3.4.5 Study Limitations

The main limitation of the present study was the inability to count inputs onto dendrites as few labelled dendrites visibly extended from labelled soma. This resulted in a loss of potential information that could have added further insight to age-associated dysfunction; particularly since dendrites and axons have previously been reported to be subject to age-associated loss within the SNB and DLN (Fargo et al., 2007). This could have been improved by the use of transneuronal tracing techniques, which provide better labelling of neuritic structures than standard immunocytochemical methods (Ugolini, 2010). Furthermore, VGAT and ENK punctate structures that apposed soma were presumed to be synapses inputting onto neurons. The clarification of synaptic input onto neurons at ultrastructural level would have improved study validity.

Due to limited availabilty of samples, there was an uneven number of replicates for brainstem sections with n=3 for 12-14 and 24-26 months and n=4 for 3-5 and 29-31 months. Thus, lower replicate numbers potentially reduced the reliability of results. In addition, spinal cord analyses was only undertaken within the two extreme young and aged groups (3-5 and 29-31 months) due to lack of sample availability.

The PMC was unstained in the present study. Thus, ENK input counts onto soma could not be undertaken. Additionally, precise location of the nucleus was predicated based on LC and LDTg location and therefore is subject to error. Staining of the PMC with atriopeptin, as done previously, would likely have proved beneficial (Holets et al., 1988).

3.5 Conclusion

In conclusion, the selected nuclei within the brainstem and lumbosacral spinal cord observed in this study were largely unaffected by ageing in terms of soma size, cell count and, ENK and VGAT appositions onto soma and thus unlikely to influence bladder and terminal bowel dysfunction with increased age. However, the SPN was reported to have a significant decline in inhibitory ENK and VGAT immunoreactivity with age. This may result in reduced relaxant responses in bladder detrusor muscle and increased contractility of DC muscle. The increased DC contractility may be a compensatory mechanism as a result of potential age-associated increased DC wall rigidity as reported in Chapter 5. The decrease in ENK^+ SPN density may be due to a decrease in thoracic ENK^+ neurons potentially projecting to the SPN.

4 EFFECTS OF AGEING ON GABA AND GLUTAMATE INPUTS ONTO SUBNUCLEI WITHIN THE HYPOTHALAMIC PARAVENTRICULAR NUCLEUS

4.1 INTRODUCTION

The prevalence of LUT and terminal bowel dysfunction increases with age resulting in UI, FI and / or constipation (as discussed in section 1.2). The hypothalamic PVN is involved in the control of LUT and terminal bowel function and may be subject to age-associated change. The PVN is active during colonic distension (Martínez et al., 2006; Wang et al., 2009), while neuronal tracing studies consistently show projections from the PVN parvocellular neurons to the LUT (Grill et al., 1999; Marson, 1997; Rouzade-Dominguez et al., 2003a; Sugaya et al., 1997). Hypothalamic lesioning in humans (following surgery to remove hypothalamic-extending pituitary adenomas) resulted in detrusor overactivity during urine storage phase and detrusor underactivity during voiding (Yamamoto et al., 2005). This is similar to age-associated weakening of detrusor contractile and relaxant responses observed in C57BL / 6J mice, which is more pronounced in males (Kamei et al., 2018). The present study aim was to immunohistochemically label OXY and VP PVN neurons and GABA and glutamate synaptic structures in male C57BL / 6J mice and analyse structural changes with increased age that may result in dysfunctional voiding.

As described in section 1.6.3.2, the PVN is a complex nucleus that is involved in the control of multiple neuroendocrine and autonomic functions via pituitary and CNS projections respectively (Qin et al., 2018). The PVN contains OXY and VP posterior pituitary-projecting magnocellular neurons and these comprise 10 % of mouse PVN neurons (Qin et al., 2018; Sturrock, 1992). The remainder of the PVN is made up of parvocellular neurons that are immunopositive for a variety of hormones and neuroactive substances, including OXY and VP, and these project to both the anterior pituitary and various regions of the CNS (Biag et al., 2012; Qin et al., 2018; Swanson and Kuypers,

1980). The PVN in the rat was originally categorised into eight subnuclei based upon location and cell type, and was generally observed to have a magnocellular core with a parvocellular surround (Swanson and Kuypers, 1980). A more recent study shows that the PVN in mice is more heterogeneously organised as magnocellular and parvocellular neurons are interspersed throughout the rostral to caudal and dorsal to ventral extent of the nucleus. Subsequently, the mouse PVN is divided into ten subnuclei based on predominant cell type and location (Biag et al., 2012). These subnuclei divisions were used in the present study and are depicted in Figure 4.2. Additionally, the location of the PVN is depicted in Figure 4.1.

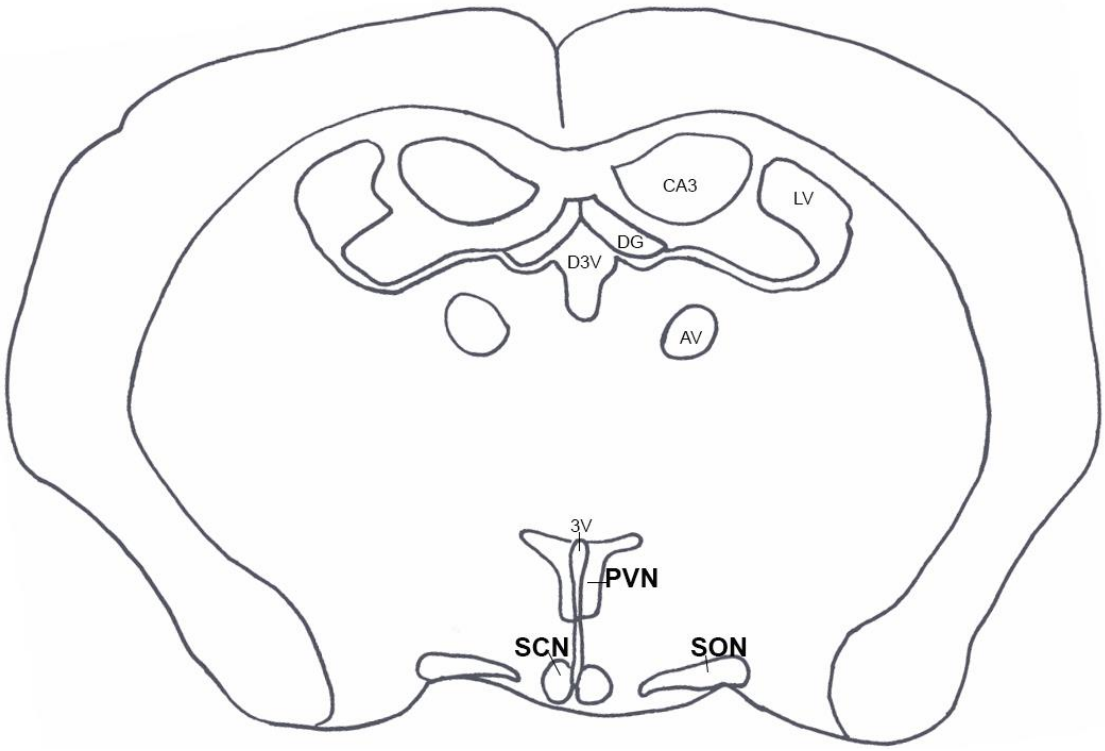

Figure 4.1: Schematic drawing of mouse hypothalamic brain transverse section at Bregma -0.82 mm showing location of PVN, SON and SCN. 3V, Third ventricle; AV, Anteroventral thalamic nucleus; CA3, CA3 region of the hippocampus; D3V, Dorsal third ventricle; DG, Dentate gyrus; LV, Lateral ventricle; PVN, Paraventricular nucleus; SCN, Suprachiasmatic nucleus; SON, supraoptic nucleus. Nuclei labels derived from Paxinos and Franklin (2007).

The PVN sends efferents and receives afferents from various CNS regions involved in LUT and terminal bowel control, which are discussed in section 1.6.3.2 and

1.7.5.2. The PVN sends OXY projections directly to the lumbosacral SPN (Puder and Papka, 2001b; Swanson and McKellar, 1979), and intrathecal administration of OXY causes increases in non-voiding detrusor contractions, which results in increased bladder pressure (Pandita et al., 1998; Puder and Papka, 2001b). VP^+ neurons have been observed to project to the spinal cord (Cechetto and Saper, 1988), and may terminate within the lumbosacral DLN (Nadelhaft and Vera, 1996; Swanson and McKellar, 1979). This potential pathway may partially control EUS function since activation of DLN VP receptors results in EUS closure (Ueno et al., 2011). Furthermore, CRH-containing neurons of the PVN have been observed to project to the lumbosacral spinal cord (Puder and Papka, 2001a) and intrathecal injection of CRH at this level results in decreased detrusor contractions (Pavcovich and Valentino, 1995; Wood et al., 2013). The PVN may also control EUS closure via circulatory release at the pituitary, since circulating VP dose-dependently increases EUS contractility (Ito et al., 2018).

During colonic distension, 81 % of OXY, 18 % of VP, and 16 % of CRH PVN neurons are active (Wang et al., 2009). Studies so far suggest that PVN control over the terminal bowel is mainly via circulatory hormone release as opposed to CNS projections, and is discussed below. OXY released from the PVN into the circulation causes increased colonic motility via activation of myenteric neurons (Xi et al., 2019). Additionally, VP injected into the inferior mesenteric artery inhibits phasic contractions of the colon at low doses and causes giant migratory contractions at high doses (Zhu et al., 1992). Furthermore, CRH delivered intraperitoneally and into the inferior mesenteric artery inputs onto myenteric neurons and increases colonic motility (Maillot et al., 2000; Maillot et al., 2003; Million et al., 2000). There is some evidence, discussed below, that suggests PVN CNS projections are involved in terminal bowel control. The PVN is known to project directly to the LC (Schwarz et al., 2015), and these projections may contain CRH that is known to input onto LC neurons and increase colonic motility (Lechner et al., 1997). Furthermore, OXY^+ PVN neurons innervate lumbosacral spinal motor neurons that project to the pubococcygeus muscle (Perez et al., 2005). The pubococcygeus muscle is a

striated muscular structure connected to the EAS and thus, the PVN may function in control of EAS closure (Garavoglia et al., 1993).

GABA and glutamate are the main neurotransmitters involved in the control of PVN neurons (Herman et al., 2002; Hermes et al., 1996; Womack et al., 2007). GABA inhibits PVN neurons whilst glutamate excites them as discussed in sections 1.8.2 and 1.8.3. Vesicular transporters VGAT and VGLUT2, employed in the present study are ubiquitous throughout the PVN. Both neurotransmitters label at least 85 % of synaptophysin-containing (pre-synaptic) terminals in the mouse and rat PVNmpd (Johnson et al., 2018). Therefore, GABA and glutamate are the most abundant neurotransmitters that influence PVN post-synaptic activity. Thus, increased age may impact GABA or glutamate PVN synapses and may result in voiding dysfunctions.

Age-associated decreases have been observed in unlabelled synapses inputting onto rat PVN neurons (Itzev et al., 2003), and this may be associated with GABA and glutamate synaptic changes with age. Morphological changes within PVN neurons have been reported with age and are detailed in section 1.9.5.

The main hypothesis is that LUT and terminal bowel-controlling PVN neurons may be subject to age-associated changes in GABA and glutamatergic innervation that results in voiding disorders. In order to establish any age-associated changes, OXY and VP PVN neurons and VGAT and VGLUT2 (representing GABA and glutamate terminals respectively) were immunohistochemically labelled. Percentage area measurements of VGAT and VGLUT2-immunolabelling were analysed within individual subnuclei. Additionally, the number of $VGAT^+$ and $VGLUT2^+$ inputs onto PVN parvocellular and magnocellular OXY^+ and VP^+ soma was counted within individual subnuclei. Results were then compared across age groups to determine any age-associated changes.

4.2 MATERIALS AND METHODS

4.2.1 Identification of PVN subnuclei

Biag et al., (2012) mapped out the mouse PVN and created appropriate subnuclei nomenclature (for mouse brains) that was utilised in the present study (see Figure 4.3) (Biag et al., 2012). In order to identify the most rostral and caudal ends of the PVN, the Mouse Brain Atlas was employed (Paxinos and Franklin, 2007). Sections were compared to the Atlas under a light microscope.

4.2.2 Differentiating between parvocellular and magnocellular OXY and VP-immunopositive PVN neurons

To differentiate between parvocellular and magnocellular neurons, soma diameter measurements were used based on previous studies in mice. A separate study measured TRH^+ soma diameter (known to be parvocellular) and VP^+ soma diameter (known to be predominantly magnocellular) in 100 randomly selected PVN neurons and observed that magnocellular (VP^+) soma were ≥ 14 µm. One study measured the diameter of OXY / VP labelled soma in the SON (shown in Figure 4.1), since virtually all SON OXY / VP neurons are magnocellular. The smallest diameter measurement observed was 12.5 µm (Castel and Morris, 1988). The same approach was used in the present study and the diameter of 50 randomly selected OXY^+ and VP^+ SON soma were 12.6 µm in diameter at their smallest. Consequently, a mean of 13 µm was calculated from all three measurements. Therefore, cells were categorised as parvocellular if soma diameter was < 13 µm and magnocellular if soma diameter ≥ 13 µm.

4.2.3 PVN measurement parameters

Analyses of sections focused on age-associated structural change in VGAT and VGLUT2 labelling within the PVN. Analyses was undertaken using captured overlay images of sections (see Chapter 2). Over 5,500 images were analysed.

4.2.3.1 Percentage area coverage of VGLUT2 and VGAT within each subnucleus

Image-pro Plus 7.0 (Media Cybernetics, Inc., Rockville, USA) was used to determine the percentage area coverage for VGAT and VGLUT2 immunoreactivity within each PVN subnucleus. This was then compared across four age ranges; 3-4, 12-14, 24-25, and 30 months (n=4 for all age groups except 24-25 months in which n=2, due to lack of tissue availability). Thresholds for fluorescent intensity were applied to reduce aberrant signalling. These were set manually by the same experimenter, so only fluorescently labelled terminals were included. The percentage area coverage was determined in all sections containing set AOIs and the average per section was calculated in each animal.

In order to maintain consistency, shapes of a set size were placed over subnuclei for measurement of VGAT and VGLUT2 coverage within each shape's boundaries (see Figure 4.2). The boundaries of each shape were mapped using the smallest region of each subnucleus. For example, the PVNmpd appeared smallest when it emerged at Bregma -0.58 mm and therefore a shape was chosen to fit within the PVNmpd at this transverse plane. During measurement, shapes were placed in the most central region of subnuclei. This lessened the chance of shape boundaries overlapping into other PVN subnuclei.

Images of GABA and glutamate presumed terminals were taken at x40 magnification (see section 2.3.3.2 for imaging methodology) and analysed. Every section containing PVN subnuclei was measured using the corresponding shapes as boundaries. This resulted in roughly four measurements taken for each subnucleus per labelling regime per animal. The mean percentage area coverage of VGAT and VGLUT2 within each subnucleus was then calculated per animal.

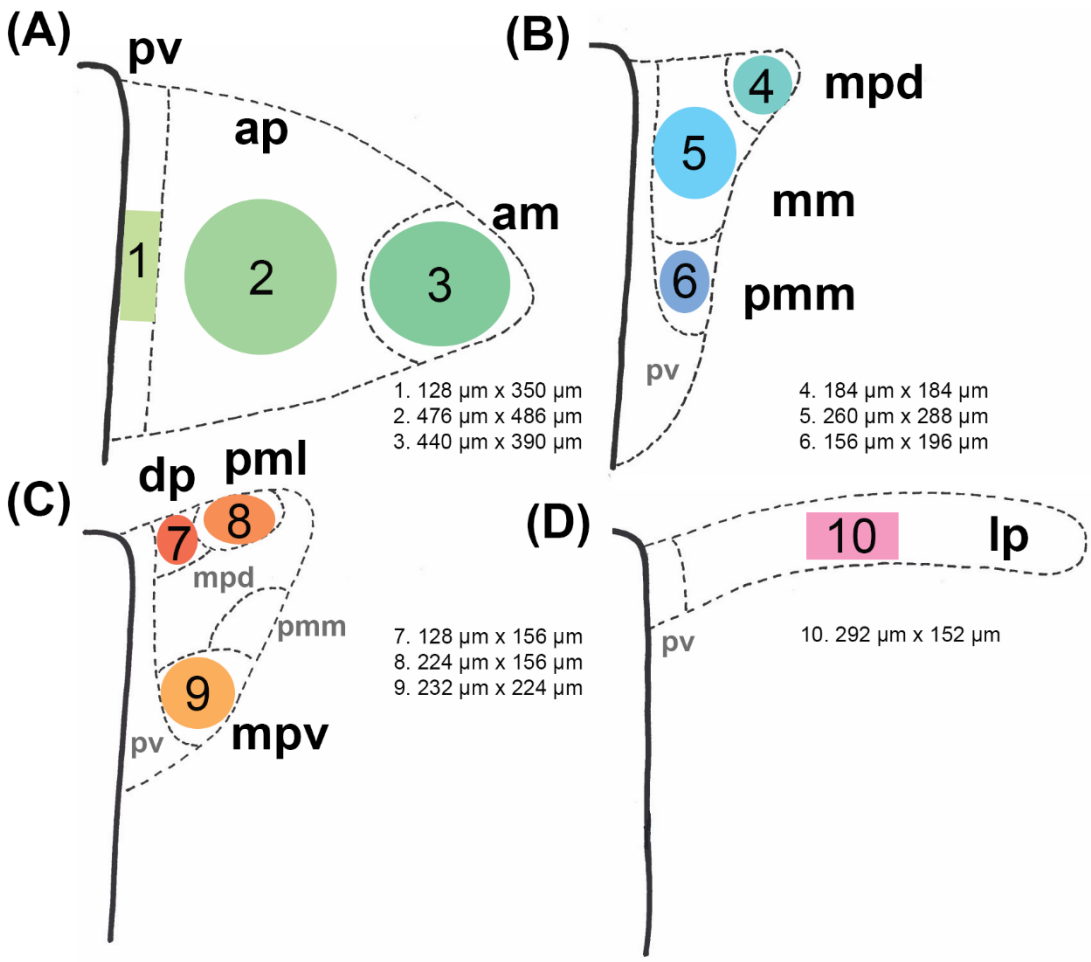

Figure 4.2: Shapes applied to PVN subnuclei for per area measurement within AOI boundaries. A-D shows the varying heights, widths or diameters (µm), and types of shapes (rectangular or ellipses) applied to each subnucleus. Ellipses were applied to more rounded subnuclei (PVNap, PVNam, PVNmm, PVNmpd, PVNpmm, PVNdp, PVNpml and PVNmpv). Rectangles were applied to more elongated subnuclei (PVNpv and PVNlp). AOI, Area of interest; PVNam, Paraventricular nucleus, anterior magnocellular; ap, anterior parvocellular; pv, periventricular part; mpd, medial parvocellular, dorsal zone; mm, medial magnocellular; pmm, posterior magnocellular, medial zone; pml, posterior magnocellular, lateral zone; dp, dorsal parvocellular; mpv, medial parvocellular, ventral zone; lp, lateral parvocellular.

4.2.3.2 Quantifying VGAT and VGLUT2 terminal inputs in apposition to OXY and VP-immunopositive cells within each subnucleus

Overlay images showed VGAT and VGLUT2 synaptic terminal inputs making contact with OXY and VP labelled neurons. Using overlay images at x63 magnification the number of presumed GABA or glutamate inputs in apposition with soma were counted. Soma input counts were calculated separately for each subnucleus and each cell type (parvocellular or magnocellular). Although a worthwhile measurement parameter, input counts onto neurites could not be reliably quantified. This is due to few neurites extending visibly from immunolabelled soma (see Figure 4.3). Therefore, conditions would not be replicable.

Prior to counting inputs, soma diameters of labelled OXY and VP neurons were measured using Image-pro Plus 2.0 to determine whether cells were parvocellular or magnocellular. Double labelling regimes of antibodies for synaptic terminals and antibodies for neuron types were used. Therefore, as two synaptic terminal types (GABA and glutamate) and two neuron types (OXY and VP) were labelled this gave rise to four antibody labelling regimes (see section 2.3.2.3). Thus, each labelling regime was applied to one in every four sections, with a distance of 180 µm (45 µm per section) between regimes. Consequently, incidences occurred in which soma of a subnucleus did not fall under a set neuron type. For example, in the PVNam of one mouse there may have been no visible VP-immunopositive parvocellular soma labelled alongside presumed glutamate terminals. These soma may have not been present at all [as few VP soma are known to reside within the PVNam (Biag et al., 2012)] or may simply have been overlooked and were present in sections in which a separate labelling regime was used.

4.2.4 Tabulation, graphical representation, and statistical analyses

Means of each parameter analysed were calculated per animal. Animals were then grouped into four age groups: 3-4, 12-14, 24-25, and 30 months. For each parameter, the mean of each sample group was calculated ± standard error of the mean (SEM).

Data distribution and variance were determined using Anderson-Darling and Bartlett's tests, respectively. All data was observed to have normal distribution and equal variances. As data met the test assumptions, a one-way ANOVA was applied to test for statistically significant differences between the four age groups. Any data that had p- or f-values observed to be significant were subject to post-hoc tests. A Tukey-Kramer test was applied to determine where significant differences lay between pairs of data.

As mentioned in section 4.2.3.2, not all cell types (i.e. OXY, VP, parvocellular and magnocellular) were present or visible within each PVN subnucleus in any given mouse for GABA and glutamate input quantification. Therefore, some replicates within an age group did not produce data. If less than two replicates within an age group produced data, then statistical tests were not applied to that parameter. For example, in the 24-25-month age group there were two replicates. If OXY-immunopositive parvocellular cells were only observed in one 24-25-month animal in the PVNmpv alongside glutamate terminal inputs, then a one-way ANOVA was not applied to this parameter (i.e. number of glutamate inputs in apposition with OXY parvocellular cells within the PVNmpv).

4.3 RESULTS

4.3.1 Organisation of the mouse PVN based on OXY and VP-immunolabelling

Neurons labelled with OXY and VP were observed to be oval or triangular in shape (see Figure 4.5-4.6). Labelled neurites projected ventro-laterally outwards from the third ventricle, with scattered punctate fibres visible (see Figure 4.3.I-J). Control sections, where primary antibodies had been omitted, showed no specific fluorescent labelling (see Appendix C, Figure 8.4). The PVN as a whole changed shape over its rostral to caudal extent. It sat bilaterally next to the third ventricle, matching ipsilateral/contralateral subnuclei (see Figure 4.3). The rostral tip of the PVN emerged at Bregma -0.34 mm extending laterally from the upper quarter of the third ventricle. Just caudal to this area was a cell sparse region with little OXY or VP immunolabelling. At around Bregma -0.58 mm the PVN took the form of a slim, vertically orientated cylinder encompassing the upper half of the third ventricle. Between Bregma -0.7 to -1.06 mm the dorso-ventral span of the PVN decreased and took on a triangular shape encompassing the upper quarter of the third ventricle. At Bregma -1.22 mm the nucleus became slimmer and extended further in length horizontally after which the PVN terminated.

4.3.1.1 Rostral Subnuclei: emergence at Bregma -0.34 mm

Figure 4.3 depicts the overall organisation of the PVN subnuclei. The rostral end of the nucleus at Bregma -0.34 mm, consisting of the PVNam, the PVNap and the rostral end of the PVNpv (see Figure 4.3.A, B & I), contained mainly OXY-immunopositive neurons, with only 1-2 VP soma visible per animal at this transverse plane. The PVNpv differed from all other subnuclei as it spanned the entire length of the nucleus. It consisted of a band of cells (around 3-4 cells thick) sitting immediately bilateral to the third ventricle. OXY and VP cells were dispersed evenly, but sparsely throughout this subnucleus. It had a low OXY and VP cell packing density compared to other PVN subnuclei, with the exception of the PVNlp. Caudal to the PVNam, a cell-sparse region was observed with a

small number of OXY neurons located within the PVNpv and the PVNap (see Figure 4.3.B).

4.3.1.2 Medial Subnuclei: emergence at Bregma -0.58 mm

At Bregma -0.58 mm OXY and VP neurons were observed to be more evenly distributed compared to rostral sections. At this point of the PVN, the PVNmpd, the PVNmm and the PVNpmm subnuclei emerged (see Figure 4.3.C). All three subnuclei contained a relatively even dispersal of OXY and VP soma. The PVNmm made contact with the dorsal half of the PVNpv; it terminated at Bregma -0.7 mm. The PVNmm consisted of both OXY and VP-immunopositive cells dispersed throughout the subnucleus. The PVNpmm lay ventral to the PVNmm and lateral to the ventral half of the PVNpv. It was present until Bregma -0.82 mm in which it decreased in size and was positioned on the lateral edge of the nucleus, medial to the ventral half of the PVNmpd and the rostral tip of the PVNmpv (see Figure 4.3.E).

The PVNmpd began as a small subnucleus (diameter = around 190 µm) at Bregma -0.58 mm and was located at the dorsolateral tip of the nucleus (see Figure 4.3.C). Caudal to this at Bregma -0.7 to -0.82 mm, it increased in size (diameter = around 248 µm). At this region it was located immediately lateral to the PVNpv and medial to the ventral region of the PVNpml / PVNdp and the dorsal region of the PVNpmm / PVNmpv (see Figure 4.3.D-E). At Bregma -0.94 mm the PVNmpd marginally decreased in size (diameter = around 230 µm) and sat at the dorsolateral edge of the PVN, lateral to the PVNdp and dorsal to the PVNmpv (see Figure 4.3.F). The PVNmpd was observed to contain the greatest number of OXY and VP-immunopositive cells within the PVN. This was largely attributed to it spanning across multiple transverse sections between Bregma -0.58 to -0.94 mm. Thus, it had the largest surface area, as cell packing density within the PVNmpd was similar to other subnuclei (with the exception of the PVNpml that had a higher cell packing density).

4.3.1.3 Caudal Subnuclei: emergence at Bregma -0.7 mm and further caudal

The PVNpml emerged at more caudal levels at Bregma -0.7 mm and was a smaller subnucleus (maximum diameter = around 117 µm) that sat at the most dorsal region of the PVN above the PVNmpd (see Figure 4.3.D-E). It was observed to be a VP-predominant nucleus with a dense sphere of VP-immunopositive neurons; this was the region of the nucleus that had the highest cell packing density. A small number of OXY-immunopositive neurons also sat either side of this VP-immunopositive neuron-dense sphere. This subnucleus remained in the same position throughout sections and was present until Bregma -0.82 mm.

The PVNdp emerged at Bregma -0.82 mm and terminated at Bregma -1.06 mm. It was located medial to the PVNpml / PVNmpd / PVNlp and the top portion of the PVNpv (see Figure 4.3.E-G). It was a small subnucleus (maximum diameter = around 140 µm) and had the lowest OXY and VP-immunopositive cell count. Within the PVNdp, there was an OXY-immunopositive cell predominance, with only 1-2 VP cells visible per mouse. Inferior to the PVNdp, the PVNmpv was situated immediately lateral to the ventral half of the PVNpv. It spanned between Bregma -0.82 mm and Bregma -1.06 mm.

The most caudal subnucleus, the PVNlp, emerged at Bregma -1.06 mm as a small subnucleus mediolateral to the PVNdp and the PVNmpv (see Figure 4.3.G). Further caudal, at Bregma -1.22 mm, it increased in size extending laterally as a thin cylinder (see Figure 4.3.J). OXY and VP neurons were observed to have a low cell packing density. They were sparsely dispersed extending bilaterally from the dorsal end of the third ventricle; both cell types were relatively evenly scattered.

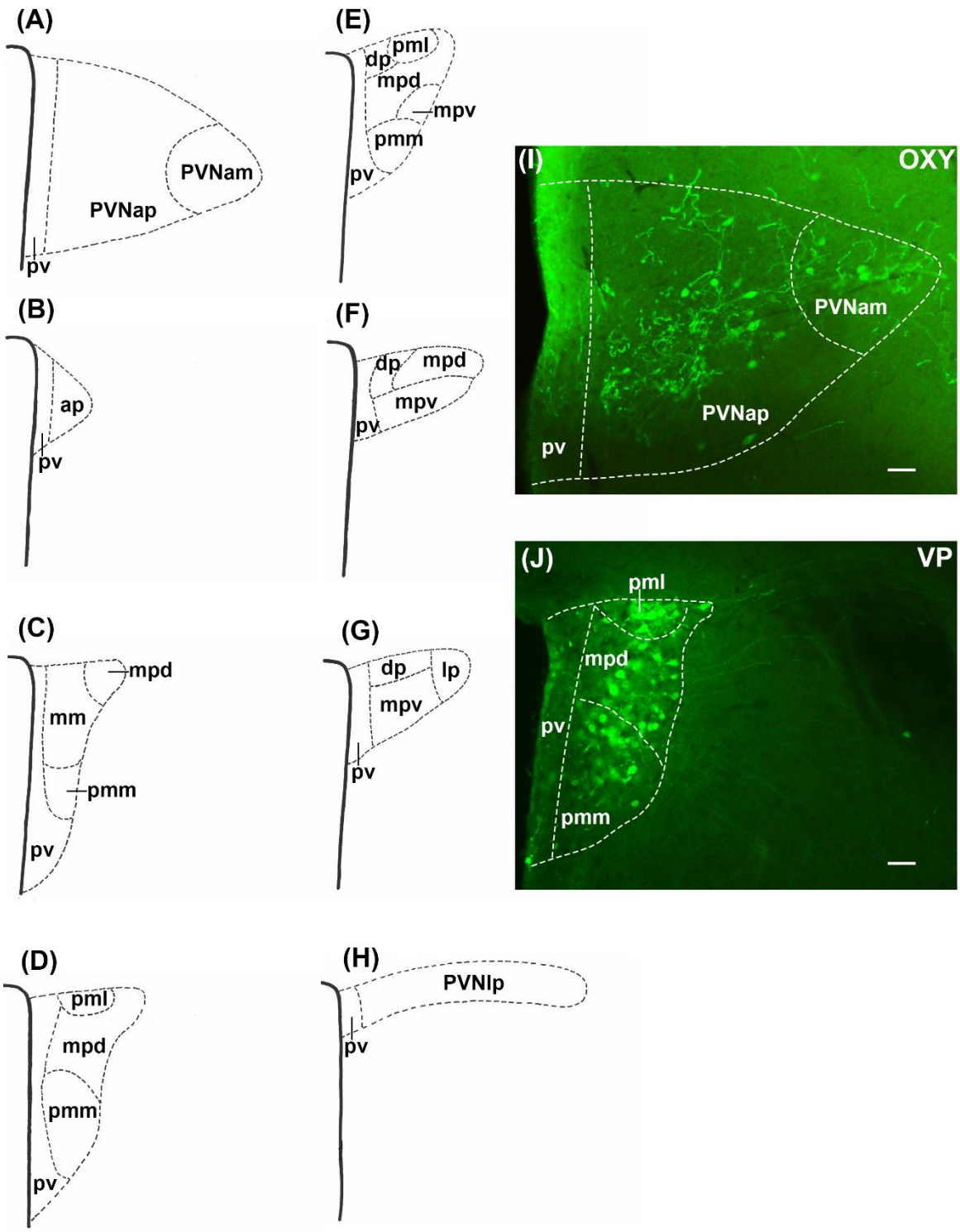

Figure 4.3 A-J: Organisation of the mouse paraventricular nucleus. A-H are schematic drawings, from coronal sections, illustrating the shape and distribution of the PVN subnuclei. Figures are ordered rostral (A) to caudal (H). I and J show Oxytocin (OXY) and Vasopressin (VP) immunolabelled cells in regions equivalent to A (I) and D (J). Scale bars = 20 µm. PVNam, Paraventricular nucleus, anterior magnocellular; ap, anterior parvocellular; pv, periventricular part; mpd, medial parvocellular, dorsal zone; mm, medial magnocellular;

pmm, posterior magnocellular, medial zone; pml, posterior magnocellular, lateral zone; dp, dorsal parvocellular; mpv, medial parvocellular, ventral zone; lp, lateral parvocellular.

4.3.2 Age-associated change in VGAT and VGLUT2 inputs onto OXY and VP-immunopositive soma within PVN subnuclei

Input appositions were counted on parvocellular (diameter ≤ 13 μm) and magnocellular (diameter > 13 μm) perikarya for comparison between age groups. Inputs were also evident along neuritic extensions. However, input counts onto neurites could not be reliably quantified (see section 4.2.3.2 for explanation). Table 4.1-4.2 summarise the number of VGAT, and Table 4.3-4.4 summarise the number of VGLUT2 presumed inputs onto OXY and VP-immunopositive soma compared across different age groups.

4.3.2.1 Age-associated change in number of VGAT inputs onto OXY-immunopositive soma within PVN subnuclei

Table 4.1 shows age-associated changes in the number of GABA inputs onto OXY magnocellular and parvocellular soma. Compared across age groups, nine out of ten subnuclei showed no age-associated change in number of VGAT inputs in apposition to parvocellular or magnocellular OXY-immunopositive soma. However, the number of VGAT inputs in apposition with PVNmpd OXY-immunopositive parvocellular soma showed significant age-associated changes (see Table 4.1 and Figure 4.4). A significant increase (with 95 % confidence) of 8.2 and 6.6 VGAT inputs was observed between 3-4 / 12-14 and 24-25 months respectively. A decline of 5.1 VGAT inputs was reported between the 24-25- and 30-31-month tissue. However, this was only observed to be significant with 90 % confidence.

*Table 4.1. Age-associated change in the number of VGAT synaptic inputs onto OXY-immunopositive magnocellular and parvocellular soma within separate PVN subnuclei. Number of VGAT inputs onto OXY immunolabelled soma ± SEM; *p ≤ 0.05.*

Subnucleus	**3-4 months (n=4)**	**12-14 months (n=4)**	**24-25 months (n=2)**	**30 months (n=4)**
Magnocellular neurons				
PVNap	6 ± 1.2	4 ± 0	-[9]	7.1 ± 3.5
PVNam	4.7 ± 2.1	5.1 ± 1.3	3 ± 3	6.2 ± 3.3
PVNpv	5.5 ± 3.6	4.9 ± 0.1	3.5 ± 3.5	5.7 ± 1.7
PVNmpd	2.3 ± 1.1	-	-	4.5 ± 1.8
PVNmm	3.6 ± 0.9	2.5 ± 1	3.3 ± 0.3	5.8 ± 2.7
PVNpmm	5.1 ± 1.7	3.4 ± 1	7 ± 0.5	7.2 ± 3.3
PVNpml	3.6 ± 1.2	3.5 ± 0.5	-	6.4 ± 1.6
PVNdp	3.9 ± 2	3.5 ± 1.4	-	3.6 ± 3
PVNmpv	4.3 ± 3	3.8 ± 1.3	-	1.7 ± 0.4
PVNlp	3.2 ± 1.7	2.3 ± 0.6	-	6.7 ± 2.3
Parvocellular neurons				
PVNap	3.3 ± 0.9	3.2 ± 0.6	-	3.2 ± 0.9
PVNam	3.5 ± 0.5	-	0.8 ± 0.3	6.7 ± 4.7
PVNpv	-	1.8 ± 0.9	-	6.6 ± 2.1
PVNmpd *	0.8 ± 0.8	2.4 ± 0.5	9 ± 1	3.9 ±1.4
PVNmm	1 ± 0.6	-	-	2 ± 2
PVNpmm	7 ± 2.4	2 ± 1	4.8 ± 0.8	8.3 ± 4.4
PVNpml	2 ± 0.6	5.3 ± 0.4	3 ± 3	6.5 ± 1.6
PVNdp	1.5 ± 1.5	2.5 ± 0.9	-	3.7 ± 1.1
PVNmpv	2.3 ± 1.2	2.5 ± 1	4.3 ± 1.3	3.2 ± 1.4
PVNlp	4.9 ± 4.1	3.1 ± 1	2.8 ± 0.8	6.3 ± 2.7

Abbreviations: OXY, Oxytocin; PVNam, Paraventricular nucleus, anterior magnocellular; ap, anterior parvocellular; pv, periventricular part; mpd, medial parvocellular, dorsal zone; mm, medial magnocellular; pmm, posterior magnocellular, medial zone; pml, posterior magnocellular, lateral zone; dp, dorsal parvocellular; mpv, medial parvocellular, ventral zone; lp, lateral parvocellular; SEM, Standard error of the mean; VGAT, Vesicular GABA transporter.

[9] Null values are due to ≤ 1 replicates within an age group containing immunolabelled soma that met set requirements (see section 4.2.3.2 for further description).

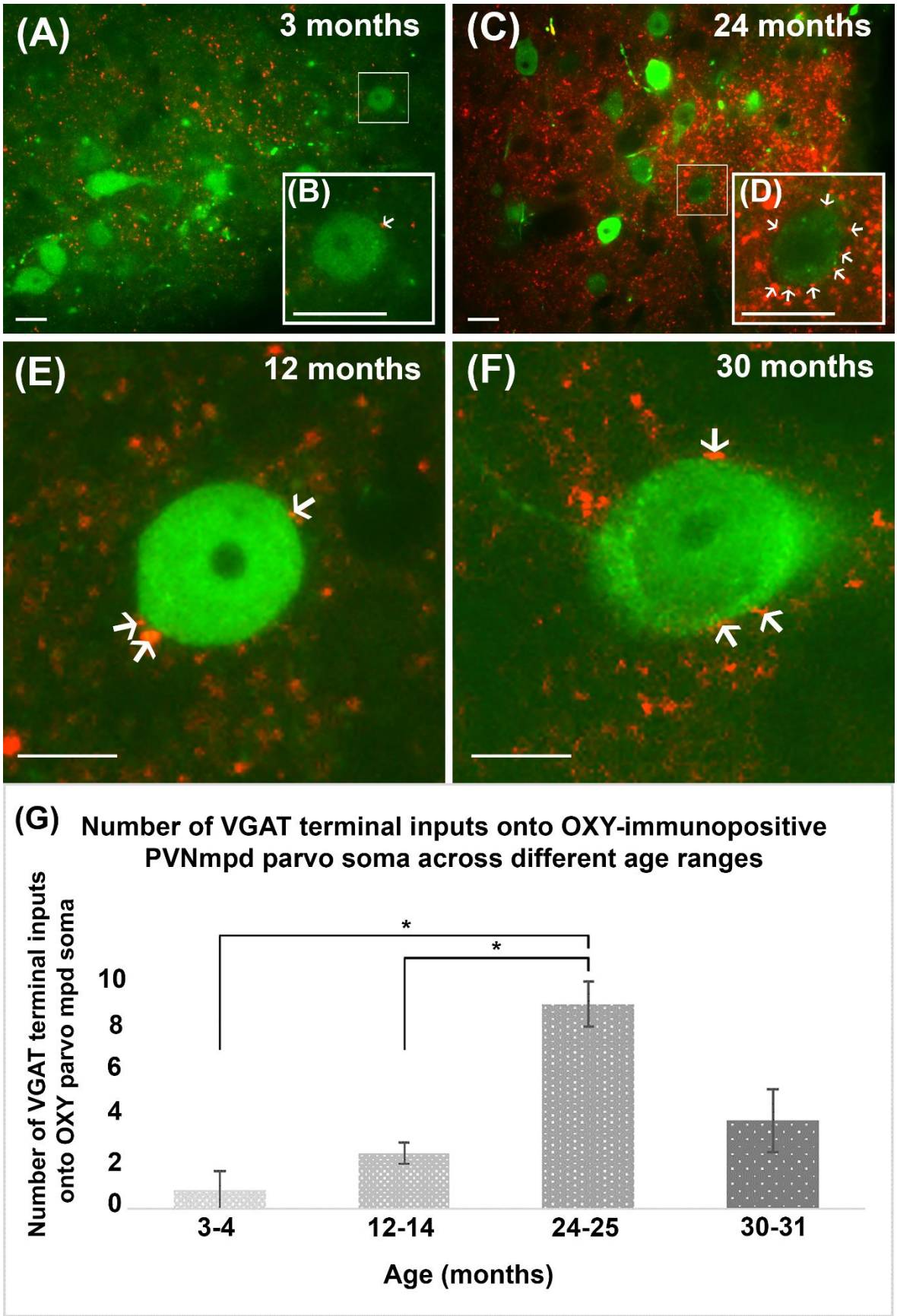

Figure 4.4 A-G: Age-associated changes in number of VGAT presumed terminal inputs in apposition to OXY parvocellular soma within the PVNmpd. A-F are images of fluorescently

*labelled VGAT boutons (red – CY3) in apposition to OXY-immunopositive soma (green - FITC) in the PVNmpd. A-B show 3-4-month and 24-25-month tissue respectively. 24-25-month tissue has a greater number of VGAT inputs onto soma. C-D are increased magnification images of soma in images A and B, respectively. E-F show presumed inputs onto soma of 12- and 30-month-old mice. Boutons of varying sizes were noted. White arrows depict VGAT inputs. G is a graph displaying mean number of VGAT inputs onto OXY parvocellular soma within the PVNmpd across all age groups ± SEM; *p ≤ 0.05. All data had normal distribution and equal variance which was determined by application of the Anderson Darling and Bartlett's tests, respectively. A one-way ANOVA was applied, and data was subject to a Tukey-Kramer post-hoc test where p- or f-values were significant to test for significant differences between age group pairs. Scale bars = 10 µm. OXY, Oxytocin; Parvo, Parvocellular; PVNmpd, Paraventricular nucleus, medial parvocellular, dorsal zone; VGAT, Vesicular GABA transporter.*

4.3.2.2 Age-associated change in number of VGAT inputs onto VP-immunopositive soma within PVN subnuclei

Nine out of ten subnuclei showed no consistent age-associated change in number of VGAT inputs onto VP magnocellular and parvocellular soma (see Table 4.2). A significant age-associated trend was noted within the PVNmpd. A significant increase (with 95 % confidence) of (4.7, 5.4, and 7.5) VGAT inputs onto VP parvocellular PVNmpd soma was reported between the 3-4 / 12-14 / 24-25 and 30-31 month tissue respectively (see Table 4.2 and Figure 4.5).

Table 4.2. Age-associated change in number of VGAT inputs onto VP-immunopositive magnocellular and parvocellular soma within separate PVN subnuclei.

*Number of VGAT input counts onto VP immunolabelled soma ± SEM; *p ≤ 0.05.*

Subnucleus	**3-4 months (n=4)**	**12-14 months (n=4)**	**24-25 months (n=2)**	**30 months (n=4)**
Magnocellular neurons				
PVNap	-[10]	-	-	-
PVNam	-	-	-	-
PVNpv	4.3 ± 1.3	4.2 ± 0.7	2.3 ± 0.3	3.1 ± 0.8
PVNmpd	4.2 ± 1.3	5.4 ±1.6	1.4 ± 0.6	7.9 ± 2
PVNmm	5.6 ± 1.5	3.8 ± 0.8	1 ± 0.2	5.1 ± 1.8
PVNpmm	5.2 ± 0.8	3.8 ± 1.1	1.4 ± 0.1	7.7 ± 3.5
PVNpml	3.3 ± 1	5.3 ± 1.9	-	5.9 ± 2.8
PVNdp	-	-	-	-
PVNmpv	-	-	-	-
PVNlp	3.3 ± 1.8	5 ± 1	-	6.3 ± 3.4
Parvocellular neurons				
PVNap	-	-	-	-
PVNam	-	-	-	-
PVNpv	4.3 ± 2.8	3.9 ± 1.1	0.9 ± 0.4	2.1 ± 1.1
PVNmpd *	4.5 ± 0.3	3.8 ± 0.8	1.7 ± 1.4	9.2 ± 1.4
PVNmm	7.3 ± 5.7	-	0.8 ± 0.8	3.1 ± 1.9
PVNpmm	4.7 ± 2	3.4 ± 1.4	-	6.8 ± 2.9
PVNpml	3.8 ± 0.8	2.8 ± 0.3	1.3 ± 1.3	2.9 ± 0.6
PVNdp	-	-	-	-
PVNmpv	-	-	-	-
PVNlp	3 ± 1.6	2.4 ± 0.6	3.5 ± 3.5	4.4 ± 1.5

Abbreviations: PVNam, Paraventricular nucleus, anterior magnocellular; ap, anterior parvocellular; pv, periventricular part; mpd, medial parvocellular, dorsal zone; mm, medial magnocellular; pmm, posterior magnocellular, medial zone; pml, posterior magnocellular, lateral zone; dp, dorsal parvocellular; mpv, medial parvocellular, ventral zone; lp, lateral parvocellular; SEM, Standard error of the mean; VGAT, Vesicular GABA transporter; VP, Vasopressin.

[10] Null values are due to ≤ 1 replicates within an age group containing immunolabelled soma that met set requirements (see section 4.2.3.2 for further description).

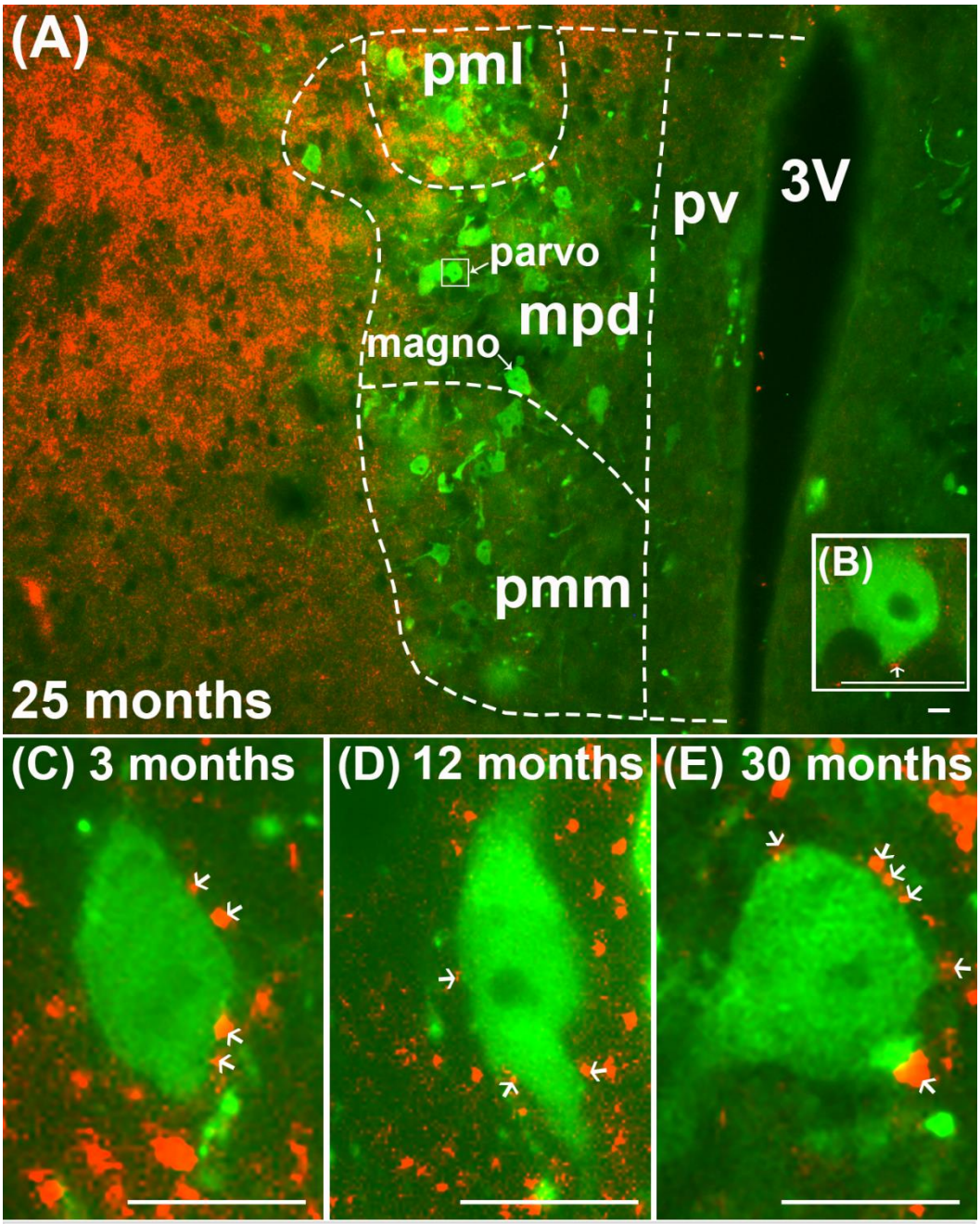
(A)
pml
pv
3V
parvo
mpd
magno
pmm
(B)
25 months
(C) 3 months
(D) 12 months
(E) 30 months

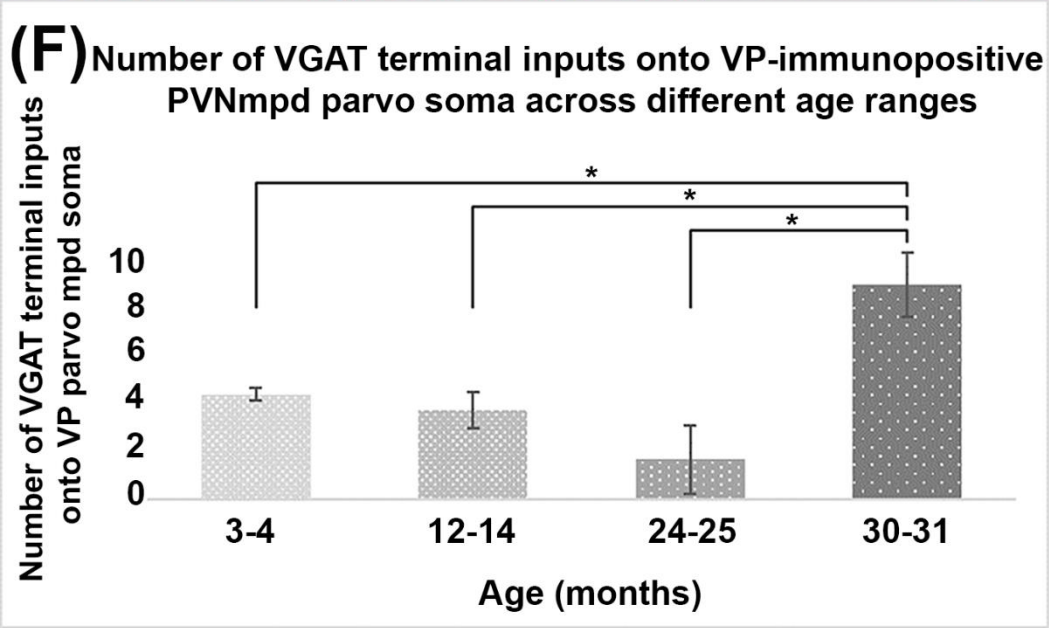
(F) Number of VGAT terminal inputs onto VP-immunopositive PVNmpd parvo soma across different age ranges
Number of VGAT terminal inputs onto VP parvo mpd soma
10
8
6
4
2
0
*
*
*
3-4
12-14
24-25
30-31
Age (months)

*Figure 4.5 A-F: Age-associated changes in the number of VGAT inputs in apposition to VP parvocellular soma within the PVNmpd. A-E are images of fluorescently labelled presumed GABA terminals (red - CY3) in apposition to VP-immunopositive soma (green - FITC) in the PVNmpd. A shows the PVN subnuclei of a 24-month-old mouse at Bregma -0.7 mm. Note that there is an increase in peri-PVN concentration of presumed GABA terminals compared to concentration of terminals within the PVN itself. B is an increased magnification image of a soma and input in image A. Measurements of soma diameter display the difference between parvocellular (11.1 µm) and magnocellular (19.7 µm) soma. C-E show inputs onto soma of 3-, 12-, and 30-month-old mice. White arrows depict VGAT inputs. E is a graph displaying mean number of VGAT inputs onto VP parvocellular soma within the PVNmpd across all age groups ± SEM; *p ≤ 0.05. All data had normal distribution and equal variance which was determined by application of the Anderson Darling and Bartlett's tests, respectively. A one-way ANOVA was applied, and data was subject to a Tukey-Kramer post-hoc test where p- or f-values were significant to test for significant differences between age group pairs. Scale bars = 10 µm. 3V, Third ventricle; Magno, Magnocellular; Parvo, Parvocellular; PVNmpd, Paraventricular nucleus, medial parvocellular, dorsal zone; pml, posterior magnocellular, lateral zone; pmm, posterior magnocellular, medial zone; pv, periventricular part; VGAT, Vesicular GABA transporter; VP, Vasopressin.*

4.3.2.3 Number of VGLUT2 inputs onto OXY-immunopositive soma within PVN subnuclei

There were no significant age-associated changes in the number of VGLUT2 inputs in apposition with OXY soma within all PVN subnuclei (see Table 4.3).

Table 4.3. Age-associated change in number of VGLUT2 inputs onto OXY-immunopositive magnocellular and parvocellular soma within separate PVN subnuclei.

Number of VGLUT2 input counts onto OXY immunolabelled soma ± SEM.

Subnucleus	**3-4 months (n=4)**	**12-14 months (n=4)**	**24-25 months (n=2)**	**30 months (n=4)**
Magnocellular neurons				
PVNap	5 ± 2.3	-[11]	-	2 ± 0.3
PVNam	4 ± 1.4	3.1 ± 1.7	3.5 ± 0.5	5.7 ± 2.1
PVNpv	1.4 ± 0.7	2.3 ± 0.3	-	2.2 ± 0.5
PVNmpd	3.7 ± 2.3	1.9 ± 0.8	-	4.1 ± 2.6
PVNmm	3.5 ± 1.1	3.1 ± 1.1	3.5 ± 0.5	3.5 ±1.5
PVNpmm	3.5 ± 1.5	4.9 ± 2.1	3.2 ± 0.2	5.5 ± 1.1
PVNpml	2.5 ± 1.2	1.4 ± 0.7	4.8 ± 1.2	4.3 ± 1.5
PVNdp	3.7 ± 1.8	1.5 ± 1.5	-	3.2 ± 2.7
PVNmpv	1 ± 1	1.9 ± 1.1	-	3.9 ± 1.9
PVNlp	3.3 ± 3.3	2.5 ± 0.8	-	2.7 ± 1.2
Parvocellular neurons				
PVNap	2 ± 1.2	2.3 ± 0.7	-	4.1 ± 1.4
PVNam	-	3.5 ± 0.5	-	1.8 ± 0.2
PVNpv	1.6 ± 0.7	1.5 ± 0.4	-	3.8 ± 1.8
PVNmpd	3.4 ± 2.3	3.7 ± 0.7	-	4.4 ± 1.3
PVNmm	2.3 ± 0.9	-	-	2.8 ± 1.5
PVNpmm	5.5 ± 2.5	5.3 ± 3.8	-	5.6 ± 2.9
PVNpml	5 ± 4	1.8 ± 0.3	-	1 ± 0
PVNdp	1.7 ± 1.2	1.7 ± 0.3	-	2.4 ± 0.8
PVNmpv	2.7 ± 1.1	4.8 ± 0.6	-	3.5 ± 1.5
PVNlp	3.6 ± 1.7	3.1 ± 0.7	6 ± 2	2.7 ± 1.3

Abbreviations: OXY, Oxytocin; PVNam, Paraventricular nucleus, anterior magnocellular; ap, anterior parvocellular; pv, periventricular part; mpd, medial parvocellular, dorsal zone; mm, medial magnocellular; pmm, posterior magnocellular, medial zone; pml, posterior magnocellular, lateral zone; dp, dorsal parvocellular; mpv, medial parvocellular, ventral zone; lp, lateral parvocellular; SEM, Standard error of the mean; VGLUT2, Vesicular glutamate transporter 2.

[11] Null values are due to ≤ 1 replicates within an age group containing immunolabelled soma that met set requirements (see section 4.2.3.2 for further description).

4.3.2.4 *Age-associated change in number of VGLUT2 inputs onto VP-immunopositive soma within PVN subnuclei*

There were no significant age-associated changes in the number of presumed VGLUT2 inputs in apposition with VP soma across all PVN subnuclei (see Table 4.4).

Table 4.4. Age-associated change in number of VGLUT2 inputs onto VP-immunopositive magnocellular and parvocellular soma within separate PVN subnuclei.

Number of VGLUT2 input counts onto VP immunolabelled soma ± SEM.

Subnucleus	**3-4 months**	**12-14 months**	**24-25 months**	**30 months**
Magnocellular neurons				
PVNap	-[12]	-	-	-
PVNam	7.5 ± 0.5	-	-	-
PVNpv	2.8 ± 0.8	1.3 ± 0.3	2 ± 1.7	3.1 ± 1.7
PVNmpd	2 ± 0.6	1.3 ± 0.3	3.6 ± 1.2	3.8 ± 1.2
PVNmm	5.2 ± 3.6	3.5 ± 2.2	2.4 ± 0.9	4.9 ± 1.9
PVNpmm	1.9 ± 0.7	3.7 ± 1.6	0.9 ± 0.9	3.1 ± 0.8
PVNpml	2 ± 0.6	2.3 ± 0.5	3.4 ± 3.4	2.8 ± 0.3
PVNdp	-	-	-	-
PVNmpv	-	-	-	-
PVNlp	4.5 ± 1.3	3.7 ± 2.1	-	4.7
Parvoocellular neurons				
PVNap	0.5 ± 0.5	-	-	-
PVNam	-	-	-	-
PVNpv	0.9 ± 0.6	2 ± 0.6	-	1.6 ± 1.6
PVNmpd	2.2 ± 0.6	3 ± 1.3	-	3 ± 1.5
PVNmm	1.1 ± 0.8	4.1 ± 1.7	2 ± 1	6 ± 3
PVNpmm	1.8 ± 0.9	3.2 ± 0.9	2.3 ± 1.7	2.4 ± 0.3
PVNpml	1.2 ± 0.8	1.8 ± 0.5	-	1.7 ± 0.2
PVNdp	-	-	-	-
PVNmpv	-	-	-	-
PVNlp	2.7 ± 0.4	2.8 ± 1.4	1.2 ± 0.2	2.8 ± 1.2

Abbreviations: PVNam, Paraventricular nucleus, anterior magnocellular; ap, anterior parvocellular; pv, periventricular part; mpd, medial parvocellular, dorsal zone; mm, medial magnocellular; pmm, posterior magnocellular, medial zone; pml, posterior magnocellular, lateral zone; dp, dorsal parvocellular; mpv, medial parvocellular, ventral zone; lp, lateral parvocellular; SEM, Standard error of the mean; VGLUT2, Vesicular glutamate transporter 2; VP, Vasopressin.

[12] Null values are due to ≤ 1 replicates within an age group containing immunolabelled soma that met set requirements (see section 4.2.3.2 for further description).

4.3.3 Age-associated change in VGAT and VGLUT2 immunolabelling and distribution within PVN subnuclei

VGAT and VGLUT2 primary antibodies showed presumed GABA / glutamate terminals to be ubiquitously distributed throughout the PVN. VGLUT2 abundance was similar to that of VGAT. Peri-PVN regions had significantly higher levels of VGAT and VGLUT2 immunolabelling compared to the PVN itself (see Figure 4.5.A). Immunolabelled boutons appeared as small, punctate structures often present as rings surrounding soma (see Figure 4.4-4.5). Control sections (omission of primary antibodies) showed no fluorescent labelling (see Appendix C, Figure 8.4). Table 4.5 summarises the percentage area coverage of VGAT and VGLUT2 bouton labelling within subnuclei across age groups. VGAT labelling appeared as the most concentrated in the PVNpv compared to other PVN subnuclei. There appeared to be a dense clustering of VGAT terminals on the innermost edge of the PVNpv, adjacent to the outer edge of the third ventricle. There was no significant age-associated change in VGAT or VGLUT2 percentage area coverage within the PVNam, ap, mm, mpd, pmm, pml, mpv, dp or lp.

However, the VGLUT2 immunolabelling within the PVNpv showed significant age-associated changes in percentage area coverage. This subnucleus showed a statistically significant decrease in VGLUT2 immunolabelled structures between the 3-4-month samples and 12-14- / 24-25-month tissues. Furthermore, there were statistically significant increases between 12-14- / 24-25- and 30-month tissue (see Table 4.5 and Figure 4.6).

Table 4.5. Age-related changes in percentage area coverage of VGAT and VGLUT2 within separate PVN subnuclei.

*Mean percentage area coverage of immunolabelled presumed terminals ± SEM; **p ≤ 0.01.*

Subnucleus	3-4 months (n=4)	12-14 months (n=4)	24-25 months (n=2)	30 months (n=4)
VGAT percentage area coverage				
PVNap	29.6 ± 4.4	29.5 ± 11.4	19.2 ± 11.2	18.1 ± 2.9
PVNam	24.9 ± 9.4	31.7 ± 16	10.6 ± 5.7	32.8 ± 2.4
PVNpv	30.2 ± 4.1	30.7 ± 2.7	18 ± 0.3	30.7 ± 5
PVNmpd	20.1 ± 2.9	27.3 ± 8.4	13.2 ± 3.9	25.7 ± 6.8
PVNmm	31.2 ± 10.6	22.5 ± 7	3.7 ± 1.5	20 ± 3.4
PVNpmm	24.2 ± 7.7	23.4 ± 8.1	25 ± 11.7	24 ± 6.2
PVNpml	22.3 ± 2.7	23.9 ± 10.3	11.3 ± 2.4	30.3 ± 6.4
PVNdp	14.6 ± 4.8	14.7 ± 8.1	7.9 ± 7.6	28.7 ± 8.6
PVNmpv	25.9 ± 2.2	27.2 ± 9.8	5.1 ± 0.2	26.6 ± 6.8
PVNlp	32.3 ± 3.6	26.7 ± 9.8	19.2 ± 0.6	30.4 ± 7.7
VGLUT2 percentage area coverage				
PVNap	42.4 ± 12.3	21.9 ± 8.8	12.5 ± 8	17.5 ± 7.7
PVNam	33.6 ± 12.3	17.6 ± 5.4	4.4 ± 3.3	21.5 ± 9.3
PVNpv **	31.6 ± 3.4	12.5 ± 3.9	4.5 ± 2.4	30.1 ± 2.8
PVNmpd	24.2 ± 5.3	16 ± 0.8	12.1 ± 3.8	23.7 ± 2.3
PVNmm	23.5 ± 8.7	8.8 ± 2.6	16.1 ± 0.9	21.9 ± 3.5
PVNpmm	26 ± 5.4	19.6 ± 2.6	11.5 ± 2.2	27.4 ± 5.6
PVNpml	17.3 ± 7.5	15.7 ± 3	6.8 ± 6.4	20.9 ± 5.8
PVNdp	17.7 ± 7.5	4.5 ± 2.2	5.5 ± 4.5	18.3 ± 6.4
PVNmpv	19.8 ± 3.5	15.4 ± 4.5	21.4 ± 1.3	23.5 ± 5.1
PVNlp	21.4 ± 3.4	28.2 ± 10.8	18.7 ± 2.2	26.4 ± 5.1

Abbreviations: PVNam, Paraventricular nucleus, anterior magnocellular; ap, anterior parvocellular; pv, periventricular part; mpd, medial parvocellular, dorsal zone; mm, medial magnocellular; pmm, posterior magnocellular, medial zone; pml, posterior magnocellular, lateral zone; dp, dorsal parvocellular; mpv, medial parvocellular, ventral zone; lp, lateral parvocellular; SEM, Standard error of the mean; VGAT, Vesicular GABA transporter; VGLUT2, Vesicular glutamate transporter 2.

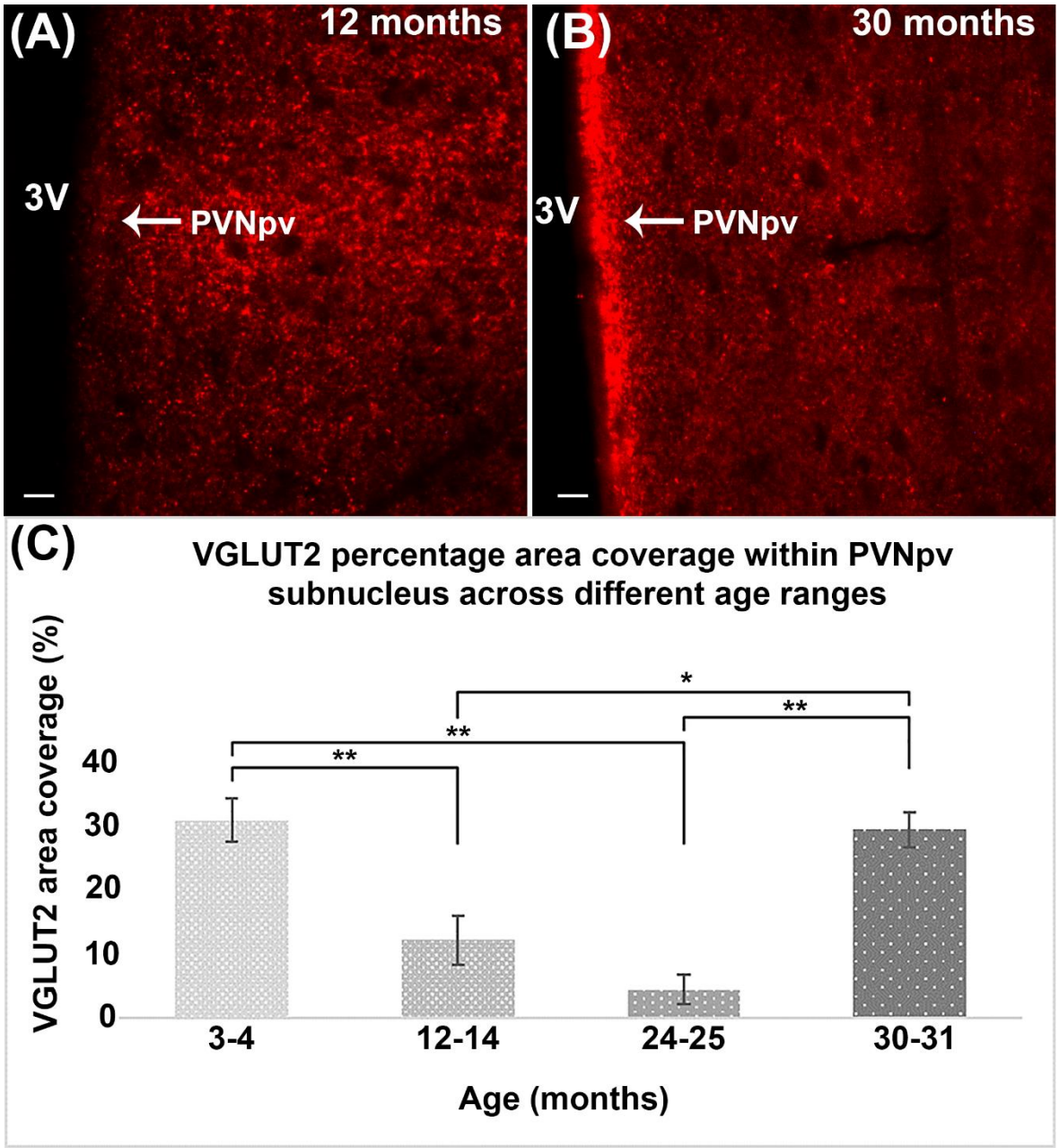

*Figure 4.6 A-D: Age-associated changes in density of VGLUT2 terminals within the PVNpv. A-B are images of fluorescently labelled VGLUT2 terminal boutons (red - CY3) within the PVNpv of the 24-25- and 30-month tissue. A marked increase in the number of VGLUT2 terminals of the PVNpv is evident between the 12-14- / 24-25-month and 30-month tissue. D is a graph depicting the mean VGLUT2 percentage area coverage within the PVNpv across different age groups ± SEM; *p ≤ 0.05; **p ≤ 0.01. All data had normal distribution and equal variance which was determined by application of the Anderson Darling and Bartlett's tests, respectively. A one-way ANOVA was applied, and data was subject to a Tukey-Kramer post-hoc test where p- or f-values were significant to test for*

significant differences between age group pairs. Scale bars = 10 µm. 3V, Third ventricle; PVNpv, paraventricular nucleus, periventricular region; VGLUT2, Vesicular glutamate transporter 2.

4.4 DISCUSSION

4.4.1 Summary of main findings

In this chapter, application of immunohistochemistry allowed for the identification of age-associated changes in VGAT and VGLUT2 density within the mouse PVN. An age-associated increase in the number of VGAT inputs onto OXY (up to 91.1%) and VP (up to 81.5%) parvocellular soma of the PVNmpd was noted. Additionally, there was a significant age-associated increase in the density of VGLUT2 immunoreactivity of up to 85% in the PVNpv. In all other PVN subnuclei the density and number of VGAT and VGLUT2 inputs onto soma remained unchanged with age.

4.4.2 PVN cyto- and chemoarchitecture

Previous studies of the mouse PVN cytoarchitecture, from rostral to caudal extent, exhibit a comparable organisation to that described in the present study. (Biag et al., 2012; Broadwell and Bleier, 1976; Castel and Morris, 1988; Kadar et al., 2010; Rood and De Vries, 2011). The nucleus location, shape, and size as a whole was similar to that observed in rats. However, rats' chemoarchitecture, parvocellular, and magnocellular arrangement differ throughout, as described below (Armstrong et al., 1980; Hou-Yu et al., 1986; Sawchenko and Swanson, 1982a; Swanson and Kuypers, 1980; van den Pol et al., 1984). This must be noted, as the majority of PVN studies, including tracing studies for determination of efferent and afferent connections, have been undertaken in rats. Therefore, known interspecies variability should be taken into account.

Previous immunohistochemical studies of OXY and VP neurons in the mouse PVN showed analogous soma arrangement across subnuclei. For example, the PVNmpd had an even distribution of OXY and VP-immunoreactive soma with moderate cell packing density and was consistent with other mouse studies (Biag et al., 2012; Castel and Morris,

1988; Kadar et al., 2010). In rat homologues of the PVNmpd, OXY and VP soma are the predominant cell type which have a higher cell packing density than mice (Armstrong et al., 1980). Lower cell packing density in mouse PVNmpd is due to an overall CRH-immunoreactive cell predominance (CRH neuron labelling was not presently observed) (Biag et al., 2012). A further example of interspecies variability between the mouse and rat PVN is the organisation of magnocellular and parvocellular cells. In the present study, magnocellular and parvocellular soma were distributed heterogeneously throughout mouse PVN subnuclei, consistent with other studies (Biag et al., 2012; Castel and Morris, 1988; Kadar et al., 2010). Whereas, the rat PVN appears to have a magnocellular-pituitary projecting core surrounded by parvocellular neurons (Swanson and Kuypers, 1980). See discussion by Biag et al., (2012) for further description of cyto- and chemoarchitectural interspecies variability between mice and rats (Biag et al., 2012).

4.4.3 PVN OXY and VP neuron morphometry

OXY and VP-immunoreactive soma were observed to be oval or triangular in shape, consistent with previous studies in mice and rats (Biag et al., 2012; Castel and Morris, 1988; Lolova et al., 1996a; Rood and De Vries, 2011). Immunohistochemical studies in mice show comparable OXY and VP neurite labelling (Castel and Morris, 1988; Rood and De Vries, 2011). OXY and VP-immunoreactive PVN axons projected ventro-laterally from the third ventricle and merged to form part of the hypothalamo-neurohypophysial tract (HNT) for circulatory hormone release at the pituitary (Swaab and Lucassen, 2009). Subsets of OXY and VP neurons project to forebrain, brainstem and spinal regions for cognitive and autonomic control (Cechetto and Saper, 1988; Cui et al., 2013; Knobloch et al., 2012; Moga et al., 1990; Sawchenko, 1987; Swanson et al., 1980; Zheng et al., 1995). Scattered punctate OXY and VP fibres presently observed (in transverse sections) amongst PVN neurons likely represent these rostro-caudal projection pathways.

4.4.4 VGAT and VGLUT2 immunoreactivity

VGAT and VGLUT2 presumed terminals immunolabelled as punctate structures and were ubiquitous throughout the PVN. Peri-PVN regions (in the immediate surround) showed greater abundance of both transporters. This immunolabelling was consistent with previous studies in mice (Inoue et al., 2013; Johnson et al., 2018). Interspecies variability also exists between mice and rats regarding VGAT and VGLUT2 immunolabelling. Johnson et al. (2018) observed that mice had similar VGAT and VGLUT2 density throughout the PVN, consistent with present results. In rats, there was a significant 10 % decrease in VGLUT2 PVN density compared to VGAT, further highlighting the difference between the two species.

4.4.5 Effects of ageing on number VGAT and VGLUT2 inputs in apposition to PVN OXY and VP soma

A significant age-associated increase in the number of VGAT inputs in apposition to OXY and VP parvocellular soma of the PVNmpd was observed. For OXY parvocellular soma, VGAT inputs significantly increased between 3-4- / 12-14- and 24-25-month-old mice. For VP parvocellular soma, VGAT inputs significantly increased between 3-4- / 12-14- / 24-25- and 30-31-month-old mice. This likely results in increased inhibition of OXY and VP parvocellular PVNmpd neurons since GABA is the main inhibitory neurotransmitter in the PVN (Johnson et al., 2018). In the remaining PVN subnuclei, VGAT and VGLUT2 inputs in apposition to OXY and VP parvocellular and magnocellular soma were unchanged with age.

The cellular composition of the mouse PVNmpd is reported by Biag et al., (2012). Double-labelling of OXY / VP neurons with fluorogold (injected intravenously) was observed depicting OXY / VP neurons that project to pituitary. Single-labelled OXY / VP neurons were also observed that likely project to CNS regions. Single-labelling of spinally-projecting neurons (in the PVNmpd) were observed in separate mice and thus spinally-projecting PVNmpd may be OXY^+ and / or VP^+ (Biag et al., 2012). Therefore, results

observed have the potential to impact various autonomic and neuroendocrine functions. However, emphasis here will be placed upon how age-associated changes may result in dysfunctional voiding as the main focus of research.

Increased inhibition of OXY and VP parvocellular soma may result in decreased controlled release of OXY from the hypophysis (Swanson and Kuypers, 1980). Decreased circulating OXY would likely result in decreased colonic contractions (Xi et al., 2019), which may be a precursor to the decreased colonic motility and faecal output observed in aged male C57BL / 6J mice (Patel et al., 2014). Furthermore, decreased circulating VP would likely result in a decrease in colonic giant migratory contractions (Zhu et al., 1992), and this likely prevents colonic faecal 'mass movement' that is necessary for the effective initiation of the RAIR (Bajwa and Emmanuel, 2009; Sarna, 1991). Decreased circulatory VP would also potentially cause decreased EUS contractility (Ito et al., 2018), that may result in urine leakage.

Increased GABA input onto OXY and VP neurons may impact spinally-projecting neurons. This could potentially result in decreased non-voiding contractions due to a decrease in OXY SPN input (Pandita et al., 1998; Puder and Papka, 2001b; Swanson and McKellar, 1979) and may be a precursor to weaker detrusor contractile responses observed in aged C57BL / 6J mice (Kamei et al., 2018). Furthermore, VP projections to the spinal cord may result in further inhibition of EUS contractility (Cechetto and Saper, 1988; Nadelhaft and Vera, 1996; Swanson and McKellar, 1979; Ueno et al., 2011).

To the best of our knowledge, age-associated changes in the number of GABA inputs in apposition to PVN neurons has not previously been reported. HPLC measurement of PVN GABA concentration showed no age-associated change, reflective of the maintenance of VGAT density presently observed (Banay-Schwartz et al., 1989). Other nuclei in the hypothalamus report dissimilar age-associated changes in GABAergic inputs onto neurons. GABA inputs are declined with age (between 2-3 and 9-11 months) in apposition to MPO GnRH neurons in rats (Khan et al., 2010) and declined between 2-3

and 18-20 months in the SCN in mice (labelled in Figure 4.1) (Palomba et al., 2008). However, this may simply be attributed to location-specific age-associated changes.

Ageing may impact the neuronal structures that provide GABAergic input onto PVNmpd neurons. GABAergic structures observed to project to the PVN parvocellular neurons (in rats) include rostral end of the PVN, the anterior hypothalamic area, perinuclear zone of the SON, perifornical region, and SCN (shown in Figure 4.1), and these structures were specifically observed to input onto the rat equivalent (in location) of the PVNmpd (Hermes et al., 1996; Roland and Sawchenko, 1993). An age-associated increase in the number of neurons within aforementioned nuclei may partially explain the increased number of VGAT inputs. Neuron number change with age has been observed in mice in the PVN and SON; however, neuron number remain unchanged or decreased with age (Sturrock, 1992; Yaghmaie et al., 2006). Additionally, in rats, other GABAergic PVN-projecting regions show neuronal maintenance or loss with increased age (Chee et al., 1988; Hsu and Peng, 1978; Kessler et al., 2011; Madeira et al., 1995; Peng and Hsü, 1982; Roozendaal et al., 1987; Tsukahara et al., 2005). Furthermore, specific GABAergic PVN neurons have been observed to be declined in aged rats (Li et al., 2017). Therefore, a change in PVN-projecting neuron number is unlikely the cause of age-related increased VGAT inputs presently reported.

Age-associated increase in VGAT inputs is thus potentially due to intracellular changes within pre-synaptic neurons. This may include endocannabinoid (EC) signalling which is known to deteriorate in the ageing hypothalamus and brain as a whole (Di Marzo et al., 2015). EC Cannabinoid receptor 1 (CB1) receptors are present on pre-synaptic terminals and their activation results initiation of a retrograde signalling pathway that causes transient reduction of GABA and glutamate release within the PVN (Iremonger et al., 2011; Kola et al., 2008; Mazier et al., 2019). Therefore, a decline in this pathway would result in increased GABA and glutamate release. However, age-associated changes in EC signalling specific to the PVN have not yet been observed and thus is a topic that requires further research.

4.4.6 Effects of ageing on VGAT and VGLUT2 percentage area coverage

A significant age-associated change in VGLUT2 percentage area coverage within the PVNpv was observed. These included decreases immunoreactivity between 3-4- and 12-14- / 24-25-month tissue and increases between 12-14- / 24-25- and 30-31-month tissue. In the remaining PVN subnuclei, VGAT and VGLUT2 percentage area was unchanged with age. The PVNpv is a complex subnucleus with the greatest heterogeneity in immunocytochemical labelling of neurons (Biag et al., 2012). Results observed have the potential to impact various autonomic and neuroendocrine functions. However, emphasis will be placed upon how present study age-associated changes may result in dysfunctional voiding.

Increased VGLUT2 density with age likely results in increased post-synaptic neuron firing since glutamate is excitatory (Brann, 1995; Platt, 2007). In order to decipher how age-associated increased VGLUT2 may impact PVNpv functional output it is important to know the cellular composition of this subnucleus. The mouse PVNpv contains neurons immunopositive for somatostatin, OXY, TRH, CRH, and VP. Furthermore, a small proportion of neurons at the caudal end of the subnucleus project to the dorsal vagal complex (DVC) and the spinal cord (Biag et al., 2012). Somatostatin neurons are the pre-dominant cell type in the PVNpv and are mainly implicated in the inhibition of growth hormone (GH) release into the circulation via projections to the median eminence (Fodor et al., 2006; Larsen et al., 2003). They may also be implicated in LUT / terminal bowel control since somatostatin PVN neurons project to the LC (Viollet et al., 2008). However, to our best knowledge, the impact of somatostatin inputs onto LC neurons and its effects on LUT and terminal bowel control have not previously been reported.

Although presently observed age-associated increase in VGLUT2 density did not impact the number of VGLUT2 OXY / VP soma inputs within the PVNpv, they may still impact the number of inputs onto OXY^+ and VP^+ neurites (which was not presently reported). Particularly since approximately 90 % of GABA and glutamate appositions to PVN CRH^+ neurons are non-somatic, and this is likely similar with OXY and VP neurons

(Johnson et al., 2018). Most OXY and VP neurons within the mouse PVNpv are pituitary-projecting, since neurons double-labelled with OXY / VP and intravenously-injected fluorogold have been reported by Biag at al., (2012). Some scattered OXY and VP neurons were also single-labelled suggesting CNS projections. Single-labelled DVC and spinal-projecting neurons were labelled with neuronal tracer in separate mice, and these may be OXY^+ and VP^+ (Biag et al., 2012).

Age-related potential increase in VGLUT2 boutons inputting onto OXY and VP neurites (of pituitary-projecting and spinally-projecting neurons) would likely have the opposite effect on bladder, colonic and EUS contractions to those mentioned in section 4.4.5. This includes an overall increase in colonic motility, bladder contractions and EUS closure. Furthermore CRH neurons (not presently labelled) exist within the PVNpv and may be affected by the age-associated increase in VGLUT2 density. CRH^+ neurons in the PVNpv are unlikely to be spinally or DVC-projecting since they are located at the rostral end of the PVN[13] and thus are expected to be pituitary-projecting (Biag et al., 2012). Age-associated increased excitation of CRH projections to the pituitary and accompanying CRH circulatory release would likely cause an increase in colonic motility (Maillot et al., 2000; Maillot et al., 2003; Million et al., 2000).

However, age-related increased glutamatergic neuronal excitation may result in cellular excitotoxicity that may deplete neuron function. This is particularly associated with excessive activation of NMDA receptors (which are abundant in the PVN) (Eyigor et al., 2001; Herman et al., 2000). Excessive iGluR activation causes ion influx accompanied by water entry and dendritic swelling (Rothman and Olney, 1986). The PVN may be subject to age-associated excitotoxic effects since swelling of dendritic spines has been reported with increased age in rat PVN neurons (Itzev et al., 2003). The process of excitotoxicity also includes cellular entrance of Ca^{2+} ions (via activation of NMDA receptors) with prolonged elevation in cytosolic Ca^{2+} triggering events including activation of intracellular

[13] Where neuronal tracing from the spinal cord and DVC was not observed in mouse study by Biag et al., (2012), as previously mentioned.

lipases and proteases resulting in free radical generation. Additionally, activation of Ca^{2+} ATPase results in depletion of energy reserves and impairment of mitochondrial oxidative phosphorylation (Dykens, 1994). Therefore, excessive VGLUT2 labelling with age may be a precursor of PVN neuronal damage and may ultimately result in the overall decline of projection pathways discussed above.

To the best of our knowledge, the effects of ageing on glutamate terminal density in the PVN has not been previously described. However, age-associated glutamatergic changes in the hypothalamus of female mice and rats have been documented and are detailed as follows. In mouse hypothalamus, effects of ageing on glutamate transporter mRNA expression was measured for VGLUT1, VGLUT3, glutamate transporter-1 (GLT-1) and glutamate aspartate transporter (GLAST). No age-associated changes were observed reflective of results for VGLUT2 density in nine subnuclei observed in the present study (Hascup et al., 2016). With one subnucleus showing change in VGLUT2 density, it is likely that ageing affects glutamate density / expression in specific regions of the hypothalamus.

Indeed, in the median eminence, VGLUT2 density was significantly declined between young (4-5 months) and middle aged (11-12 months) female rats reflective of present study results between 3-4- and 12-14-month material (Yin et al., 2015). In the preoptic area, at the anterior end of the hypothalamus, the number of VGLUT2 inputs in apposition to gonadotrophin releasing hormone (GnRH)-immunopositive neurons was increased between young (2-3 month) and middle aged (9-11 month) female rats, opposing present study results in the PVNpv (Khan et al., 2010). GnRH neurons control diestrus and proestrus cycling which is one of the first systems to show age-related dysfunction in females (Wise, 1982). Therefore, ageing of this pathway takes place earlier in lifespan. Increased number of VGLUT2 inputs may emulate presently observed increases in PVNpv VGLUT2 density in older (30-31 month) mice whose majority functional pathways show age-associated decline later in lifespan (Gupta and Morley, 2014; Ishunina and Swaab, 2002; Qin et al., 2018; Zhou and Swaab, 1999).

CNS sources of PVN glutamate terminals were identified in rats via neuronal tracing, immunohistochemical labelling, electrophysiology studies and application of glutamate receptor (ant)agonists (Chitravanshi et al., 2016; Csáki et al., 2000; Cservenak et al., 2017; Cui et al., 2001; Larsen and Vrang, 1995; Llewellyn et al., 2012; Ulrich-Lai et al., 2011; Ziegler et al., 2012). The majority of these regions have been reported to project near to PVNpv (and closely apposed subnuclei) as discussed below.

Studies so far have not reported specific neuronal sources of glutamate terminals in the PVNpv. However, Csáki et al., (2000) injected [^{3}H]D-aspartate tracer[14] into two tracer sites– the border of medial PVNpv and the PVNmpd, and the border of the caudal PVNpv and the PVNdp / PVNmpv. This labelled glutamatergic PVN interneurons in structures homologous to the mouse PVNpv, PVNmpd, PVNmpv, PVNdp, and PVNlp. Extra-PVN sites that project to the PVNpv are summarised in Table 4.6. Glutamatergic brainstem regions that project to the PVN were not reported (Csáki et al., 2000). Therefore, brainstem sources of glutamate terminals in the PVNpv remain unknown.

Table 4.6: Summary of known glutamatergic CNS regions that project to the rat PVNpv. Constructed from retrograde tracing study carried out by Csáki et al., (2002).

Nucleus / area	**Region**	**Quantity of labelled neurons (per section)**
Septal complex	Lateral septum, ventral aspect, caudal region	20-63
	Lateral septum, ventral aspect, rostal region	2-6
	Septohypothalamic nucleus	Few scattered neurons
Preoptic area	Medial preoptic nucleus	10-49
	Medial preoptic area, ventral	Few scattered neurons
	Lateral preoptic area	Few scattered neurons
Ventral premammillary nucleus	Rostrocaudal extent	20-38

[14] Tracer that is selectively uptaken by terminals of neurons that are glutamatergic / aspartergic.

Bed nucleus of the stria terminalis	Medio-ventral	8-35
	Latero-ventral	5-16
SCN	Medial	11-28
Ventromedial nucleus	Rostrocaudel extent	6-22
Anterior hypothalamic area	Medial	4-22
	Anterior	0-4
Dorsmedial nucleus	Rostrocaudel extent	8-21
Lateral hypothalamic area	-[15]	5-17
Supramammillary nucleus	Medial and lateral	12
Arcuate nucleus	Posterior	7-11
Thalamic PVN	-	1-7

Abbreviations: CNS, central nervous system; PVNp, Paraventricular nucleus, periventricular region.

Age-associated increased VGLUT2 PVNpv immunoreactivity may have been due to increased neuron number within PVNpv-projecting glutamatergic neurons mentioned above. However, where studies report age-associated changes of neuron number in mice, they are observed to be maintained or decreased in the PVN, arcuate nucleus and bed nucleus of the stria terminalis (Kuwahara et al., 2004a; Kuwahara et al., 2004b; Sturrock, 1993; Sturrock, 1992). To the best of our knowledge, neuron number change across age has not been documented in the septal complex, ventral premammillary nucleus, or thalamic PVN across species. In all other regions mentioned in Table 4.6, neuron numbers were maintained or decreased in aged rats, rhesus monkeys, and humans (Chee et al., 1988; Diene et al., 2019; Funabashi and Kimura, 1995; Hsu and Peng, 1978; Lolova et al., 1996a; Madeira et al., 2000; Madeira et al., 2001; Madeira et al., 1995; Peng and Hsü, 1982; Rance et al., 1993; Roberts et al., 2012; Roozendaal et al., 1987; Sabel and Stein, 1981; Sartin and Lamperti, 1985; Shiromani et al., 2000; Tsukahara et al., 2005; Witkin, 1987; Yang et al., 1993; Zhou and Swaab, 1999). Therefore age-associated increase in VGLUT2 PVNpv immunoreactivity is potentially due to intracellular changes within pre-

[15] Not noted in the study.

synaptic neurons and may be associated with decline in EC signalling, as discussed in section 4.4.5.

4.4.7 Study Limitations

The main limitation of the present study was the inability to determine if reported age-associated changes specifically impacted LUT and terminal bowel-projecting neurons. This is partially due to the complexity of the nucleus. Use of neuronal tracer injected into the bladder, DC, or external sphincter structures alongside immunolabelling of VGAT and VGLUT2 may help overcome this. Furthermore, neuronal tracer injected intravenously, as undertaken by Biag et al. (2012), would help define specific pituitary-projecting structures, whose circulatory hormone release impacts LUT and colonic function (as discussed above). Additional immunostaining of PVN neuron subtypes would be beneficial, particularly for delineating which neuron subsets were affected by the age-associated increase in VGLUT2 immunoreactivity within the PVNpv. Furthermore, the number of inputs in apposition to neurites was not quantified. This was not possible to undertake in the present study (see section 4.2.3.2). A different staining approach, for example the use of tracing techniques [such as that undertaken by Ranson et al. (2007)], may increase the visibility of neurites extending from labelled soma (Ranson et al., 2007).

With regards to terminal labelling, glutamate transporters VGLUT1 and VGLUT2 have been observed in the PVN. VGLUT1 has low abundance in the PVN (Nakamura et al., 2005). Nonetheless, a small proportion of PVN glutamate terminals were unidentified. Additionally, it was assumed that VGAT / VGLUT2 inputs that appeared in apposition to labelled soma were synapsing onto these neurons. For confirmation of inputs making contact with soma, ultrastructural studies, such as electron microscopy would prove beneficial. Furthermore, due to limited availability of samples, there was only n=2 for 24-25-month material. This lower replicate number potentially reduced reliability of results.

4.5 CONCLUSION

Two key age-associated findings were observed in VGAT and VGLUT2 PVN labelling. Increased VGLUT2 immunoreactivity was reported in the PVNpv. This may result in age-associated pathophysiology's including excitotoxity of post-synaptic neurons. PVNpv neurons that were affected by this age-related change remain unknown and thus further research is required. The second key finding was an age-associated increase in VGAT inputs in apposition with OXY and VP parvocellular soma within the PVNmpd. The exact projection pathways of PVNmpd OXY and VP parvocellular neurons in mice remain unknown and require further research. However, specific to the LUT / terminal bowel function, potential age-associated impacts may include decreased colonic motility, bladder contractions, and EUS activity. These potential effects emulate the decreased bowel motility and detrusor contractile response reported in other studies of in aged C57BL / 6J mice.

5 EFFECTS OF AGEING ON PROTEIN EXPRESSION WITHIN THE DISTAL COLON

5.1 INTRODUCTION

The prevalence of terminal bowel dysfunction increases with age resulting in FI and / or constipation. The MP is an intrinsic neuronal structure that is essential for DC motility (Smith and Koh, 2017; Spencer et al., 2016), and is known to be subject to age-associated structural change including changes in cellular morphology, number, and density. Furthermore, a build-up of intracellular aggregates with age including tau, lipofuscin and α-synuclein have been observed in MP neurons that likely results in defective function (Ranson and Saffrey, 2015; Saffrey, 2013). The finer molecular / proteomic changes that occur to cause these structural abnormalities are unclear. To rectify this, methodology development that allows for isolation and extraction of the MP from DC tissue and application of subsequent protein analysis is currently in progress (as described in the present study).

5.1.1 Method Development

The proposed strategy behind the methodology was to first extract MP structures from formalin-fixed paraffin-embedded (FFPE) DC tissue sections using laser capture microdissection (LCMD). Following that, protein was to be extracted and contaminants (wax, lipids etc.) removed. Once protein was extracted in large enough concentrations it was to be applied to in-gel trypsin digestion[16] to prepare it for application to LC / MS / MS and further downstream analysis.

There are a number of complications that must be considered during methodology development including: (1) It must be possible to visualise the MP and distinguish it from surrounding muscular tissue in order for successful application of LCMD; (2) Staining

[16] In-gel trypsin digestion involves denaturing proteins and breaking them into smaller peptide fragments required for application to LC / MS / MS.

techniques that allow for MP visualisation can affect protein analysis (if they are antibody-based) or reduce protein yield; (3) Given the previous point, haematoxylin and eosin (H&E) staining is the most suitable technique for MP visualisation without excessively impacting downstream protein analysis. This staining method is best suited to FFPE tissue sections which makes extracting protein more challenging given the additional contaminants and formation of protein-protein cross-links that occur during fixation; (4) Proteins cannot be amplified (as is the case with genomic analysis) and therefore protein concentration must exceed a minimum threshold (usually around 10 µg); (5) With the previous point in mind, it is potentially time-consuming to laser microdissect large enough areas of MP to reach this protein yield, given its small size.

As a result of the aforementioned complications, FFPE C57BL / 6J male mouse DC tissue was used and stained with H&E. The process of protein extraction and downstream analysis (described in detail in section 5.2) took time to develop. Therefore, this pilot study only got to the stage of protein analysis of whole DC sections. This was applied to young (3 month) and aged (30 month) tissue for age-associated comparison of change in protein regulation. The DC wall is a vastly heterogeneous structure with four main layers composed of various cell types (described in section 1.7.2). Therefore, any age-associated changes observed in protein expression may have been ubiquitous throughout all cells but was more likely to be within specific cell types. Assigning age-associated changes to specific cell types was attempted presently but was not definitive. Therefore, further study development and subsequent use of LCMD for the extraction of specific cell groups e.g. MP, would likely eliminate this obstacle.

Development of protein analysis methodology in FFPE tissue may prove beneficial in subsequent, unrelated research, since retrospective analysis can be undertaken in the vast archive of FFPE hospital samples available. This may aid understanding of disease protein make-up in tissues whose pathological status has already been confirmed.

5.1.2 Molecular ageing in the DC

In the present study, protein analysis was carried out in whole mouse DC sections with the aim of application to extracted MP. Comparative protein analysis studies have not been undertaken in MP or whole colon sections. However, genomic study of young vs aged MP and whole colon tissue have been undertaken in humans and rats, respectively (Hetz et al., 2014; Lee et al., 2001). DC MP genes encoding for Ret receptors, neurotrophin p75 receptors and nitric oxide synthase 1 (NOS1) were significantly decreased between <1 year old and 48-58 / 70-75 year old humans. Furthermore, ChAT was significantly increased between <1 year old and 48-58 / 70-75 year old humans (Hetz et al., 2014). The decline in NOS1[17] and the increase in ChAT[18] suggests increased excitation of the DC smooth muscle since NO input inhibits GIT motility (Pelletier et al., 2010), whilst ACh increases it (Matsuyama et al., 2013; Tanahashi et al., 2013). Ageing in the whole rat colon (between 4 and 24 month animals) revealed upregulation of 51 genes including genes encoding for proteins involved in the cell cycle, nutrient digestion and absorption, signal transduction, intracellular signalling pathways, and metabolism; and downregulation of 5 genes encoding for proteins involved in nutrient absorption and intracellular signalling (Lee et al., 2001).

5.1.3 Main hypothesis and aims

The main hypothesis is that the mouse DC undergoes age-associated changes in protein expression that may contribute to decreased colonic motility and faecal impaction observed in aged male C57BL / 6J mice (Patel et al., 2014). In order to establish if this is the case, methodology involving protein analysis of mouse FFPE DC sections was developed and applied as discussed above.

[17] NOS1 encodes for neuronal nitric oxide synthase which catalyses the production of NO.
[18] ChAT catalyses the production of acetylcholine.

5.2 MATERIALS AND METHODS

5.2.1 Animal housing and tissue preparation

Male C57BL / 6J mice were housed and sacrificed as described in section 2.2. Post-sacrifice the GIT was removed and placed in PBS and the DC was separated using a sterile surgical blade. Tissue was further flushed in PBS and external fat tissue was removed. 0.5 cm long cross-section pieces of DC were fixed for 24 hours in 4 % PFA. Tissues were dehydrated over a 12-hour period using Shandon Hypercenter XP enclosed tissue processor (GMI – Trusted Laboratory Solutions, Minneapolis) and embedded in paraffin wax.

5.2.2 Tissue sectioning

Wax blocks containing FFPE mouse DC tissue sacrificed at 3 and 30 months of age were trimmed to remove excess wax. 12 µm thick transverse sections were cut using the wax microtome (RM2125, Leica Biosystems, Milton Keynes) were collected directly into an Eppendorf.

Sections collected into Eppendorfs were deparaffinized and used for downstream protein analysis as described in subsequent sub-chapters. Prior to collection of sections (for protein analysis), the transverse surface area of DC was determined as 2 mm^2. To make up roughly 100 mm^2 surface area (as recommended for 10-15 µm thick sections for deparaffinization and extraction buffer application), 50 sections were collected per Eppendorf.

5.2.3 Deparaffinization of DC sections

0.5 ml n-Heptane was added per Eppendorf containing 50 FFPE DC sections. The Eppendorf was vortexed and incubated at room temperature for one hour. 25 ml Methanol was then added to sections, vortexed, and centrifuged at 9000 x g for two minutes. Supernatant was removed and tissue pellet was left to air dry for five minutes.

5.2.4 Protein extraction

Post deparaffinization, 94 µl ExB plus Qproteome® FFPE tissue extraction buffer (37623, Qiagen, UK) supplemented with 6 µl β-mercaptoethanol (M3148, Sigma-Aldrich, Suffolk, UK) was added to the Eppendorf containing DC tissue pellet and vortexed. The Eppendorf was sealed using a sealing clip, incubated on ice for 5 minutes, vortexed and then incubated at 100 ^{o}C for 20 minutes. Using a thermomixer (5382000031, Eppendorf, Stevenage), the Eppendorf was incubated at 80 ^{o}C for two hours with 750 rpm agitation. The Eppendorf was then incubated at 4 ^{o}C for one minute and was centrifuged at 14,000 x g at 4 ^{o}C for fifteen minutes. Supernatant containing extracted protein was transferred into a fresh Eppendorf.

5.2.5 Protein quantification

To test in-solution protein concentration post-extraction, Bradford and bicinchoninic acid (BCA) assays were trialled. This was undertaken to find the most reliable methodology for protein quantification to determine the minimum amount of mouse DC tissue required for downstream analysis.

5.2.5.1 Bradford assay

Bovine serum albumin (BSA) was used as the protein standard and added (in triplicates) to a flat-based 96-well plate. The following dilutions (using mqH_2O) were added: 0.1, 0.2, 0.3, 0.4, 0.5, 0.6, 0.7, 0.8, 0.9, 1.0, 1.1, 1.2, 1.3, and 1.4 mg / ml (5 µl per well). Extracted protein sample was diluted with mqH_2O to 1:5 concentration. 5 µl of extracted protein sample (unknown concentration) was added in triplicates. 250 µl Bradford reagent (ab102535, Abcam, Cambridge, UK) was added to wells and incubated at 21 ^{o}C for 10 minutes. 96-well plate absorbance was read at 595 nm and a standard curve was plotted from results to determine protein concentration of extracted mouse DC sample(s).

5.2.5.2 BCA assay

5 µl BSA standards were added to 96-well plate in triplicates in the following concentrations: 200, 40, 20, 10, 5, 1, 0.5, 0 µg / ml diluted with 1:250 extraction buffer ExB plus:dH_2O. Extracted protein sample was diluted to 1:250 using dH_2O and 5 µl was added in triplicates to 96-well plate. 150 µl BCA working reagent was added to wells and incubated at 37 ^oC for 2 hours. 96-well plate absorbance was read at 562 nm and a standard curve was plotted from results to determine protein concentration of extracted mouse DC sample(s).

5.2.6 SDS-PAGE

SDS-gels were used in two forms of methodology. Protein concentration of mouse DC samples were not possible to measure using Bradford or BCA assays (see section 5.3.1). Therefore, SDS-PAGE was initially used to confirm presence of protein in mouse DC extract samples and decide concentration of protein used based on level of band staining. Secondly, SDS-PAGE was used to disrupt tertiary protein structure for in-gel trypsin digestion and downstream protein analyses.

5.2.6.1 Initial run

6x SDS loading buffer (375 mM Tris-HCl, 9 % SDS, 50 % glycerol, and 9 % β-mercaptoethanol) was added to protein extract / BSA solution to give 1x final concentration and was incubated for 10 minutes at 100 ^oC. A 12 % SDS polyacrylamide gel was made and added between glass plates (see Figure 5.1 for SDS gel components). Once set, stacking gel was added with a comb inserted to create wells. The gel tank was filled with 1x running buffer (0.2 M tris, 0.2 M glycine, and 10 % SDS). Protein solution(s) and BSA were pipetted into wells. The gel was then run at 200 volts, until protein samples had reached the end of the gel. Gel was removed and placed in a square petri dish. R250 Coomassie Blue was added to cover gel and was incubated at 21 ^oc for 15 minutes. Coomassie blue was removed and gel was washed with Destain (45 % methanol, 45 %

H_2O, 10 % glacial acetic acid) three times. Gel was then incubated in Destain for 24 hours at 21 ^oC. Destain was removed and gel was imaged on Syngene G-box.

Table 5.1: Buffers and volumes used to make SDS polyacrylamide resolving and stacking gels. Resolving buffer components: 46.75 g tris base, 1 g SDS and 250 mL H_2O; stacking buffer components: 1.125 g tris base, 1 g SDS and 250 mL H_2O.

12 % resolving gel	
30 % Acrylamide	3.0 µl
mqH_2O	4.5 µl
Resolving buffer	2.5 µl
10 % Ammonium persulphate (APS- A3678, Sigma-Aldrich, Suffolk, UK)	100 µl
N,N,N',N'- Tetramethyl ethylenediamine (TEMED-T9281, Sigma-Aldrich, Suffolk, UK)	20 µl
Stacking gel	
30 % Acrylamide	0.5 µl
mqH_2O	2.5 µl
Stacking buffer	1.0 µl
10 % APS	30 µl
TEMED	10 µl

5.2.6.2 SDS-PAGE for in-gel trypsin digestion

Based on initial SDS-PAGE results from mouse DC, 1.6 µl protein extract was diluted with 8.4 µl dH_2O. This concentration was selected based on visibility of protein on SDS-gel at lowest concentration (see Figure 5.1) to avoid blockage of LC / MS / MS trap column due to overloading. Additionally, 10 µl of 10 mg/ml BSA was added as an experimental quality control (QC). All SDS-PAGE set-up was the same as section 5.2.6.1, aside from run time. The gel was run at 200 volts for 15 minutes until protein had migrated 1 cm into resolving gel.

5.2.7 In-gel trypsin digestion

In-gel trypsin digestion methods were applied to break protein samples into peptide fragments for downstream protein analysis. Two experiments utilising this technique were undertaken. Methodology was initially applied to one mouse DC sample (3 months old) to qualitatively analyse mouse DC proteome and confirm experimental reproducibility. Secondly, methodology was applied for downstream quantitative comparison of young (3 months, n = 2) versus old (30 months, n = 2) DC tissue to determine change in protein regulation.

Stained protein bands (sample and QC) were excised and cut into 1 mm^2 cubes and placed in separate Lobind microcentrifuge tubes. Tubes were vortexed with 200 µl 100 mM ammonium bicarbonate (NH_4HCO_3) and 60 µl acetonitrile (ACN) for fifteen minutes at 21 ^oC to remove stain. NH_4HCO_3 / ACN solution was removed and gel pieces were dehydrated with 200 µl ACN. ACN was removed. To break protein disulphide bonds, gel pieces were rehydrated with 100 µl 20 mM Dithiothreitol (DTT) for thirty minutes at 56 ^oC. DTT was removed and gel pieces were dehydrated as above. ACN was then removed. To prevent reformation of protein disulphide bonds (via addition of acetoamide to the sulfhydryl group), gel pieces were rehydrated with 100 µl 56 mM Iodoacetamide (IAA) for twenty minutes at 21 ^oC (in the dark). IAA was removed and gel pieces were vortexed with 100 µl 100 mM NH_4HCO_3 twice at ten-minute intervals. NH_4HCO_3 was removed and gel pieces were dehydrated as above. ACN was then removed and any excess ACN was evaporated by placing tubes in a vacuum centrifuge for five minutes at 30 ^oC. Protein-containing gel pieces were then digested by complete saturation with 30 µl 20 µg / ml Trypsin [reconstituted with acetic acid] for 20 minutes on ice. 50 µl 50 mM NH_4HCO_3 was then added to Trypsin-saturated gel pieces and incubated at 37 ^oC for 18 hours. Trypsin solution (containing some peptide extract) was decanted into new protein Lobind Eppendorfs and stored on ice. To further extract peptides, gel pieces were vortexed with 50 µl 50% ACN and 50 µl 5% Formic acid (FA) for 30 minutes at 21 ^oC. ACN / FA Solution was decanted into corresponding tubes. To extract remaining peptides, gel pieces were vortexed with 50 µl 86% ACN and 50 µl 0.2 % FA for 30 minutes at 21 ^oC.

ACN / FA solution was decanted into corresponding tubes. To facilitate freeze drying, a hole was pierced in LoBind microcentrifuge tube lid. Tubes were then snap frozen in liquid nitrogen and placed in the freeze drier for 18 hours until completely lyophilised. Tubes were stored at -80 ^{o}C until analysis. Once ready for LC / MS / MS, lyophilised samples were resuspended in 20 µl of 5 % ACN and 0.1 % FA.

5.2.8 Liquid chromatography and mass spectrometry

All sample handling and analyses regarding liquid chromatography and mass spectrometry (LC / MS) was undertaken by fellow Post-doctoral researcher William Cheng.

5.2.8.1 System information

Peptide characterisations were performed on Nanoflow Dionex™ 3000 RSLC (Dionex, Sunnyvale, CA) linked to a Q-Exactive Plus (Thermo, Hemel Hempstead, UK). High resolution MS was performed using C18 EasySpray column, in a data dependent acquisition.

5.2.8.2 LC instrument settings

Nanoflow liquid chromatographic separation used a binary buffer system for peptide separation. This involved Buffer A (95 % ultrapure water / 5 % ACN with 0.1 % FA), Buffer B (95 % ACN / 5% ultrapure water with 0.1 % formic acid) and a loading and transport buffer (95 % ultrapure water/ 5 % ACN with 0.1 % Tetrafluoruacetic acid). The sample injection amount was 5 µl; flow rate was set 0.3 µl / minute. The trap column used was Acclaim™ PepMap™ 100 C18 LC column (Thermo Scientific™) (5 µm particle size; pore size 100 Å), maintained at 45 ^{o}c.

5.2.8.3 LC gradient elution

The liquid chromatographic profile was performed using the following gradient. Starting condition (4 % buffer B / 96 % buffer A); 3 minutes with 8 % buffer B / 92 % buffer A; 93 minutes with 30 % buffer B / 70 % buffer A; 98 minutes with 80 % buffer B / 20 % buffer A. This was held for an additional 10 minutes, then returned to starting condition for 20 minutes allowing for column equilibration.

5.2.8.4 MS instrument settings

Full scan MS was performed at 70,000 MS resolution with an automatic gain control of $1e^6$ and injection time of 100 ms. The scan range was set to 375 to 1400 m / z. For data-dependant-MS^2, acquisition was performed at 35,000 MS with an automatic gain control of $1e^5$ with a maximum injection time of 100 ms. The isolation window was set to 1.3 m / z, with an underfilled ratio of 0.4 %. Dynamic exclusion was set to 15 seconds, and the top 10 most abundant ions were selected for MS / MS with a normalized Collison energy level of 10, 30, and 50.

5.2.9 Qualitative proteome analysis

Prior to age comparison, qualitative protein analysis was applied to the DC of one 3-month-old mouse, was subject to in-gel trypsin digestion, and analysed by LC / MS / MS. This allowed for observation of the mouse DC proteome as a whole before analysis of age-associated changes was undertaken. Analysis was undertaken using Mascot™ (Matrix Science, London, UK) by fellow PhD student, Jonathan Thompson.

5.2.9.1 Identification of mouse DC proteome

Thermo RAW files (containing raw uninterpreted mass spectral ion peaks) were converted to mascot generic format (.MGF) using RawConverter. A Mascot™ MS / MS ion search was then performed using the following parameters: (a) database: mus musculus,

(b) enzyme: Trypsin, (c) missed cleavages: allow up to one, (d) fixed modifications: carbamidomethyl (cysteine)[19] (e) variable modifications: oxidative (methionine)[20], (f) peptide tolerance: 25 ppm, (g) MS / MS tolerance: 50 ppm, (h) peptide charge: 2+, 3+ and 4+, (i) monoisotopic, (j) data format: Mascot generic, and (k) instrument: ESI-TRAP. A peptide score[21] for each protein match was generated. Proteins were deemed significant based upon meeting the threshold peptide score ($p \leq 0.05$). Mascot™ produces a threshold score based upon experimental data and thus each score is experiment-specific. All proteins scoring ≥ to the threshold peptide score were included in results.

5.2.10 Quantitative proteome analysis

Quantitative proteome analysis was applied to quantify any age-associated changes in protein expression between 3- and 30-month mouse DC. Analysis was undertaken using Progenesis™ LC-MS data analysis software (Nonlinear Dynamics, Newcastle upon Tyne, UK) and Mascot™ (Matrix Science, London, UK) by fellow PhD student, Jonathan Thompson. See Sitek et al. (2012) for more detailed protocol.

5.2.10.1 Differential proteome analysis

RAW thermo files created from LC / MS / MS analysis were imported onto Progenesis™. Using software, identified peptides were automatically aligned to a reference run (sample run with minimal noise signifying stable LC-MS conditions) represented in a two-dimensional map. Additionally, vectors were manually applied to unaligned regions in each sample. Peptides with charges 2+, 3+ and 4+ were included, all other charges were excluded[22]. Experimental design was created by grouping samples

[19] Carbamidomethyl (cysteine) is a deliberate post-translational modification introduced to cysteine residues by reaction with IAA carbamidomethyl (cysteine).
[20] Addition of IAA to protein solution results in non-specific oxidation of methionine.
[21] The peptide score reflects the combined scores of all amino acids that can be matched to peptide sequences within a protein. A higher score indicates a more confident match.
[22] The charge states of tryptic peptides are between 2+ and 5+. This reduces introduction of contaminations into results, which usually have a charge state of 1+.

into young (3 months, n=2) versus aged (30 months, n=2). Peptides with a fold change of ≥ 2 and a p-value ≤ 0.05 (based on one-way ANOVA) were tagged. With parameters applied, features that were differentially regulated were exported to .MGF file format for protein identification.

5.2.10.2 Identification of differentially regulated proteins

Using the .MGF file created in section 5.2.10.1, a Mascot™ MS / MS ion search was performed. Parameters used were identical to those in section 5.2.9.1. Identification data produced was exported to .XML file format and imported into Progenesis™. To refine identified proteins, parameters were set for peptide scores ≥ 30 and hits ≥ 2. Conflicts (when a peptide sequence is associated with more than one protein) were resolved manually based on number of hits, protein score, and mass error. Post-conflict resolution, peptide counts < 2 were removed from database.

5.2.11 Functional clustering analysis of differentially regulated proteins

After age-associated changes in protein regulation were identified, functional clustering was undertaken to further understand which cellular structures and processes may be impacted by this age-associated change in protein expression. Proteins that were upregulated with age were analysed separately to those that were downregulated. This was undertaken using the g:GOSt function on the g:profiler web server (g:Profiler, 2020) which uses several gene databases to functionally cluster identified genes or proteins in a sample. The gene nomenclature of each protein, that showed an age-associated change in protein regulation, was input into the g:GOSt query. The query was then run with ‘mus musculus (mouse)’ as the selected organism resulting in functional clustering of proteins. Only significantly enriched biological processes, pathways and cellular components were included in results. All ambiguous queries were removed.

5.3 RESULTS

5.3.1 Protein concentration measurement

Post-protein extraction from FFPE mouse DC sections, efforts to measure sample protein concentration were made. Bradford and BCA assays were attempted (see section 5.2.5). However, results run in triplicates were unreliable as they produced vastly differing values when read on the microplate reader. Based on appearance of SDS-gels (see Figure 5.1), a standard protein dilution of 1.6 µl extract (roughly one 12 µm section per 2 µl extraction buffer) added to 8.4 µl mqH_2O was applied to SDS-PAGE and further downstream protein analysis was undertaken.

5.3.2 Application of mouse DC protein extract to SDS-PAGE

Trypsin digestion of individual protein bands separated by SDS-PAGE (known as GeLC-MS / MS) is preferential for LC / MS / MS analysis. This maximises sequence coverage due to the fractionation of a complex sample (Dzieciatkowska et al., 2014). However, gels ran with DC protein extract appeared smeared with few visibly identifiable bands. Thus, whole protein samples were used for trypsin digestion and LC / MS / MS analysis (see section 5.2.6). As it was not possible to ascertain protein concentration (from Bradford / BCA assay) varying concentrations were tested (see Figure 5.1).

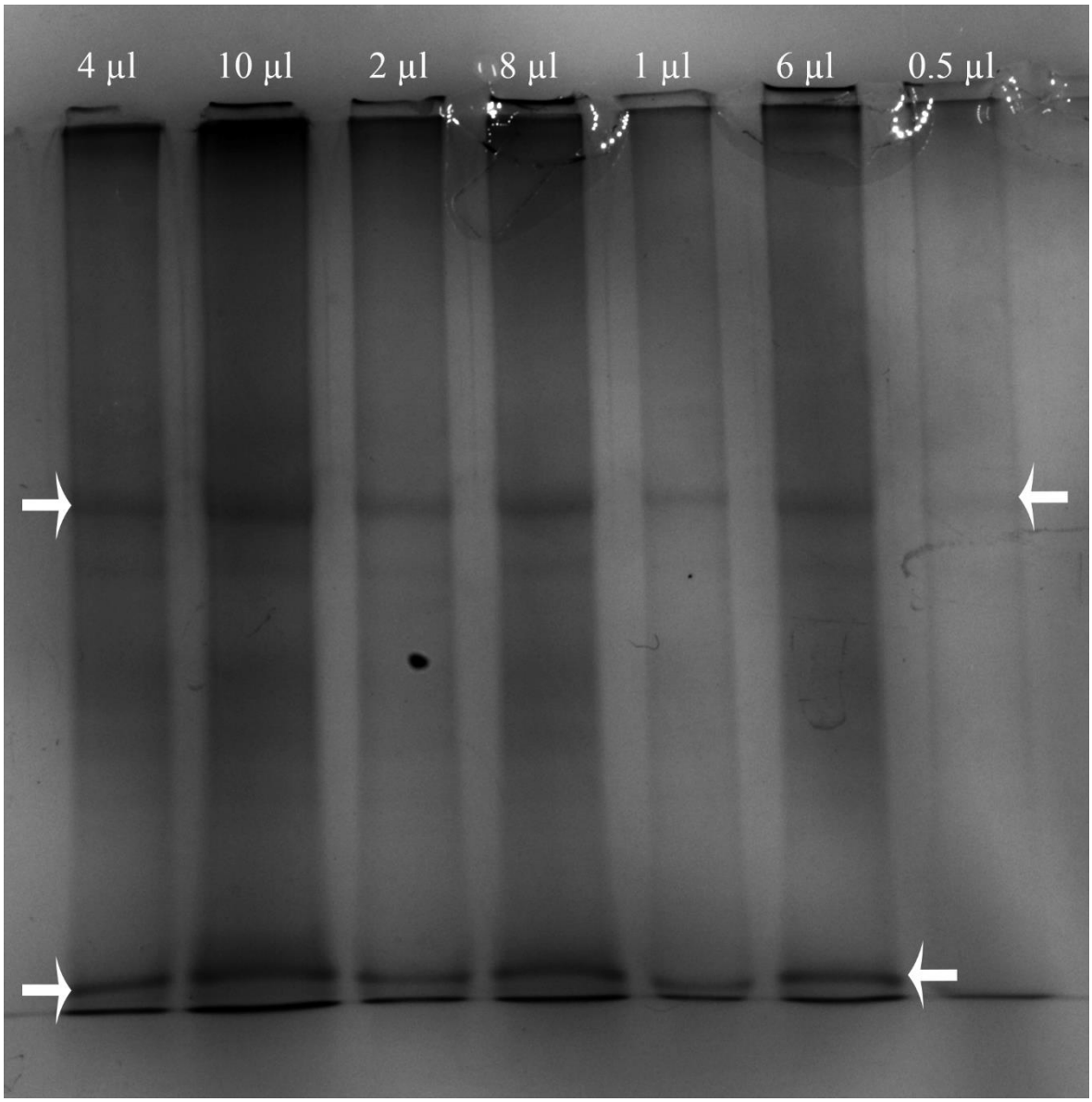

Figure 5.1: Mouse DC (3 months) protein extract on SDS-gel run in varying unknown concentrations and imaged on Syngene G-box. All amounts labelled were made up to 10 µl with mqH_2O (with additional SDS loading buffer– see section 5.2.6). Most obvious bands are depicted with a white arrow. Smearing on gel at all concentrations was evident.

5.3.3 Qualitative analysis (mascot)

The protein composition of a whole 3-month mouse DC was analysed using Mascot software. Output from LC / MS / MS analysis allowed for identification of proteins using Mascot™ database. 330 proteins were reliably identified within set parameters (see Appendix D for list of identified proteins). Due to successful methodology, a subsequent

experiment analysing changes in protein regulation between age groups was undertaken (see section 5.3.4).

5.3.4 Quantitative analysis: changes in protein regulation in 3-month versus 30-month mouse DC

The changes in protein expression between 3- and 30-month mice were analysed using Progenesis™ LC-MS data analysis software (Nonlinear Dynamics, Newcastle upon Tyne, UK) and proteins were identified with Mascot™ (Matrix Science, London, UK). Output LC / MS / MS analyses applied to 3- and 30-month mouse DC samples (n = 2 per age group) allowed for identification of age-associated changes in protein regulation. Parameters set in sections 5.2.10.1–5.2.10.2 were the threshold for protein regulation change that was reliably identified. Additionally, identified proteins with a fold change < 2 were discounted. Within these parameters, 44 proteins were identified to have a significant regulation change with age (see Table 5.2). 41 proteins of these 44 were upregulated with age.

Table 5.2: Mouse DC proteins that were differentially regulated with age. Proteins were categorised by main function based on uniprot search (UniProt, 2020).

For a more extensive tabulation of results, see Appendix E.

Protein	**Gene nomenclature**	**Peptides**	**Score**	**Anova (p)***	**Fold**	**Ageing effect**
Respiratory and metabolic enzymes						
Aspartate aminotransferase, mitochondrial	Got2	2	156.91	2.33E-03	4.14	↑
Dihydrolipoyllysine-residue succinyltransferase component of 2-oxoglutarate	Dlst	2	89.16	6.55E-04	3.79	↑

Protein	Gene nomenclature	Peptides	Score	Anova (p)*	Fold	Ageing effect
dehydrogenase complex, mitochondrial						
Electron transfer flavoprotein subunit alpha	Etfa	2	160.53	2.82E-03	3.4	↑
Isocitrate dehydrogenase [NAD] subunit alpha, mitochondrial	Idh3a	2	123.7	3.63E-03	2.91	↑
Malate dehydrogenase, cytoplasmic	Mdh1	2	101.11	5.72E-04	2.74	↑
Electron transfer flavoprotein subunit beta	Etfb	4	251.06	1.13E-03	2.67	↑
ATP synthase subunit alpha, mitochondrial	Atp5f1a	2	153.5	6.49E-03	2.62	↑
Aldo-keto reductase family 1 member B1	Akr1b1	2	153.13	0.01	2.58	↑
Aconitate hydratase, mitochondrial	Aco2	3	164.03	0.02	2.47	↑
Isocitrate dehydrogenase [NADP], cytoplasmic	Idh3a	2	87.73	8.08E-03	2.41	↑
Malate dehydrogenase, mitochondrial	Mdh2	2	117.37	1.09E-03	2.39	↑
Transketolase	Tkt	3	214.26	1.34E-03	2.28	↑
Pyruvate kinase	Pkm	2	92.9	4.44E-04	2.15	↑
UDP-glucose 6-dehydrogenase	Ugdh	2	98.89	0.02	2.12	↑

Protein	Gene nomenclature	Peptides	Score	Anova (p)*	Fold	Ageing effect
Detoxifying enzymes						
Glutathione S-transferase Mu 1	Gstm1	2	96.81	1.42E-03	2.43	↑
Aldehyde dehydrogenase, mitochondrial	Aldh2	2	125.36	0.02	2.17	↑
Peroxiredoxin-1	Prdx1	3	140.85	3.10E-03	2.1	↑
Protein metabolism						
Protein disulfide-isomerase A3	Pdia3	3	174.16	0.01	2.69	↑
60S ribosomal protein L18	Rpl18	2	171.76	6.95E-03	2.46	↑
Protein-glutamine gamma-glutamyltransferase 2	Tgm2	2	86.03	9.44E-03	2.46	↑
Eukaryotic translation initiation factor 5A-1	Eif5a	2	95.63	2.13E-03	2.39	↑
Cell cycle and nuclear proteins						
Annexin A11	Anxa11	3	144.94	6.77E-03	3.27	↑
Prelamin-A	Lmna	2	169.06	0.02	2.59	↑
Histone H1.2	Hist1h1c	2	114.25	9.10E-04	2.57	↑
Tubulin alpha-1A chain	Tuba1a	2	155.35	0.02	2.27	↑
Histone H3.3C	H3f3c	2	96.39	9.36E-03	2.07	↑
Chaperone proteins						
Heat shock protein HSP 90-beta	Hsp90ab1	3	162.1	0.01	3.22	↑
Heat shock cognate 71 kDa protein	Hspa8	2	166.19	0.03	2.15	↑

Protein	Gene nomenclature	Peptides	Score	Anova (p)*	Fold	Ageing effect
Cytoskeleton proteins						
Profilin-1	Pfn1	2	122.03	0.03	3.11	↑
Keratin, type II cytoskeletal 1	Krt1	2 (1)	204.18	0.03	3.04	↓
Calponin-1	Cnn1	3	231.89	2.02E-03	3.01	↑
Vinculin	Vcl	2	131.62	0.03	2.76	↑
Transgelin	Tagln	4	252.97	6.68E-03	2.47	↑
Filamin-A	Flna	6	480.66	3.56E-03	2.42	↑
Keratin, type II cytoskeletal 79	Krt79	2 (1)	100.32	0.05	2.38	↓
Desmin	Des	2	165.09	1.99E-04	2.15	↑
Vimentin	Vim	3	178.21	0.01	2.13	↑
Keratin, type II cytoskeletal 5	Krt5	4 (3)[23]	268.63	0.03	2.12	↓
Extracellular matrix proteins						
Lumican	Lum	2	84.91	5.25E-03	3.18	↑
Collagen α-1(VI) chain	Col6a1	5	317	2.04E-03	2.46	↑
Collagen α-2(VI) chain	Col6a2	6	351.59	1.74E-03	2.4	↑
Proteins involved in other processes						
Serum albumin	Alb	5	274.24	7.31E-05	3.58	↑
Transgelin-2	Tagln2	2	97.45	1.33E-03	2.43	↑

[23] This protein had 4 distinct identified peptides, but only 3 peptides were used for quantitation.

Protein	Gene nomenclature	Peptides	Score	Anova (p)*	Fold	Ageing effect
Annexin A4	Anxa4	2	172.96	0.02	2.39	↑

5.3.5 Functional clustering of proteins that showed regulation change with age

Appendix F shows the functional clustering of proteins that were upregulated with age. Statistically significant results were identified within the following databases: Gene Ontology: Molecular Function (GO:MF), Gene Ontology: Biological Processes (GO:BP), Gene Ontology: Cellular Component (GO:CC), Kyoto Encyclopedia of Genes and Genomes (KEGG), Reactome Pathways (REAC), WikiPathways (WP), Transcription Factor (TF), and CORUM Protein Complexes.

Of the 41 proteins upregulated with age, the majority of molecular functions and biological processes that were enriched are involved in cellular respiration. Protein binding and tissue growth were also cellular functions that observed to be enriched. In terms of tissue and cellular structure, there were a variety of structures that were upregulated. Some of these structures support cellular respiration e.g. mitochondrion, mitochondrial matrix, and electron transport flavoprotein complex. Other cellular structures that were substantially increased include the myelin sheath and the collagen-containing extracellular matrix.

Appendix G shows the functional clustering of proteins that were downregulated. Statistically significant results were identified in GO:CC and REAC databases. All three proteins that were downregulated are likely structural components of the cytoskeleton. Proteins were also functionally clustered into cellular components of the skin e.g. keratin filament and intermediate filament. However, these results were disregarded as samples did not contain any mouse skin.

5.4 DISCUSSION

5.4.1 Summary if main findings

In this chapter, the application LC / MS / MS identified a significant increase in 41 proteins, and a significant decrease in three proteins in aged (30 months; n = 2) mouse DC compared with young (3 months; n = 2).

5.4.2 Methodology development

Study methodology was successful regarding main aims. This included protein extraction (from FFPE DC tissue) and application to LC / MS / MS producing reliably identified proteins and detection of protein regulation change with age. However, the inability to accurately measure protein extract concentration adds complexity to further method development. Proteins extracted from a sample cannot be amplified, unlike genomic analysis. Therefore, for LCMD of DC MP to be applied, it should be ensured that it would be possible to extract minimum amount of protein required (usually around 10 µg). Protein extracts from whole mouse DC sections supplied sufficient protein concentration. However, MP encompasses a small fraction of tissue amongst the vastly heterogenous cell structure of the colon. Protein extraction is decreased when tissue is H&E stained, adding further complexity (Becker et al., 2008). Recommended kits for protein quantification, to be used alongside extraction buffer ExB plus, included Bio-Rad DC Protein Assay Kit 1 for Lowry method or Pierce Micro BCA Protein Assay Kit (used in the present study) (Geoui et al., 2010). Bradford reagent is known to react with β-mercaptoethanol [added to extraction buffer ExB plus (1:16)] and thus partially explains Bradford failure (Bradford, 1976).

An additional methodological obstacle was the smeared appearance of DC extracted proteins on SDS gels with few visible bands (see Figure 5.1). Although not imperative, tryptic digestion of individual bands maximises sequence coverage (Dzieciatkowska et al., 2014). Furthermore, identification of bands in SDS-gel allows for determination of protein molecular weight (when run alongside a protein standard) which can be compared to LC / MS / MS mass read-out to ensure reliability of results (Wu et al.,

2002). Mouse colon protein extract (from fresh tissue) has previously shown gel smears when applied to SDS-PAGE. Protein bands were more evident than the present study. This may be due to the use of fresh colon with protein extracted immediately after animal sacrifice (Magdeldin et al., 2012). Thus, removing introduction of tissue contaminants during fixation process (see section 5.2.1).

Potential presence of non-protein contaminants such as wax and lipids would likely have been due to sample over-loading. This would reduce efficacy of n-heptane and methanol during deparaffinization, and ExB plus extraction buffer during protein extraction. It was recommended that two sections of 10-15 µm thickness and 100 mm^2 surface area were used for analysis (Geoui et al., 2010). However, since mouse DC sections were around 2 mm^2 in surface area, fifty sections were applied per extraction. Therefore, reducing section number (per extraction) and re-testing protein quantification assays may prove beneficial. An additional sample clean-up step for removal of interfering buffer components as [undertaken by Geoui et al. (2010)] may similarly prove beneficial.

Previous protein extraction from colon of C57BL / 6J mice (2 months old) reliably identified 1,237 proteins using LC / MS / MS. This study was undertaken in fresh colon tissue, with methods applied immediately after animal sacrifice (Magdeldin et al., 2012). In comparison, 330 proteins were reliably identified in the present study. The process of formalin fixation induces protein–protein cross-links (especially between arginine, lysine, serine, and cysteine residues). These cross-links are thought to increase over time as protein identification decreases in tissues stored for longer periods (Nirmalan et al., 2009; Ralton and Murray, 2011; Wolff et al., 2011). For example, Wolff et al. (2011) used the same deparaffinization and protein extraction methodology in the present study (see section 5.2.4) and noted that FFPE tissues stored over a 20 year period had a mean decrease in protein yield of 42 % compared to those stored over a 10 year period. Present study tissue storage time was over a five year period and thus partially explains the decrease in protein yield compared to studies using fresh mouse colon tissue immediately post-surgery (Magdeldin et al., 2012).

Noted experimental defects were also likely attributed to presence of glycosylated proteins within the sample. Many known proteins in the mouse colon undergo post-translational modification, including the addition of oligosaccharide to nitrogen (N-linked) or oxygen (O-linked) atoms (Ruhaak et al., 2018). Furthermore, protein concentration methods have been trialled with glycosylated proteins and have been observed to result in underestimation of protein concentration in Bradford assays and overestimation of protein content in BCA assays (Fountoulakis et al., 1992). Tryptic digestion of glycoproteins is often incomplete due to steric hindrance from the presence of large oligosaccharides (Bernard et al., 1983). Additionally, glycoproteins have been observed to reduce MS protein detection due to unusually high molecular mass and inefficient ionization. This results in loss of spectral data and likely affects protein migration through SDS-gel resulting in gel smearing (Qiao et al., 2014). A future remedy is the treatment of protein extract with glycosidases as undertaken in previous studies (Ostasiewicz et al., 2010; Tarentino and Plummer, 1982).

Furthermore, during data processing and protein identification, Magdeldin et al. (2012) incorporated additional variable modifications to the present study, including glutamine to pyroglutamate (N-terminal), glutamate to pyroglutamate and oxidation of histidine, which likely increased protein identification. On reflection, additional variable modifications should have been applied during present study analysis since post-translational protein processing (in eukaryotic cells), and the application of formalin fixation result in proteins undergoing several modifications as discussed in listed studies (Metz et al., 2006; Perchey et al., 2019; Zhang et al., 2015b).

5.4.3 Age-associated changes in DC protein regulation

The majority of proteins that showed significant age-associated changes in expression, were upregulated with age, with 41 upregulated versus three downregulated. Whole colon proteome / genome expression change with age has not previously been documented in mice. However, Lee et al., (2001) compared regulation change in colon

gene expression in male 4- and 24-month-old rats. Similar to the present study, ageing resulted in increased gene expression, whereby 51 genes were upregulated with age versus five that were downregulated (Lee et al., 2001). Of the genes observed to be upregulated in the rat colon, seven corresponding proteins encoded for by those gene families were observed to be upregulated in the aged mouse colon (see Table 5.3). This upregulation of proteins in aged tissue may indicate reduced cellular clearance of damaged or misfolded proteins that is known to have increased occurrence systemically in aged tissue (Vilchez et al., 2014; Watanabe et al., 2019).

Table 5.3: Proteins presently observed to be upregulated in the aged mouse colon and comparable upregulated genes / gene families in aged rat colon from study by Lee et al. (2001)

Mouse protein upregulated with age	**Corresponding rat gene family member upregulated with age**
ATP synthase subunit alpha, mitochondrial	ATP synthase subunits beta and delta
Aldehyde dehydrogenase, mitochondrial	Aldehyde reductase
60S ribosomal protein L18	60S ribosomal protein L21
Eukaryotic translation initiation factor 5A-1	Eukaryotic translation initiation factor 2A
Annexin A11	Annexin A5
Annexin A4	Annexin A5
Calponin-1	Calponin

When proteins were functionally clustered from the present study results, the proteins that were upregulated with age were heavily involved in cellular respiration. Additionally, an upregulation in structural elements, including the myelin sheath, collagen-containing extracellular matrix (ECM), and ageing markers, peroxisomes, and pigment granules, was observed. The three proteins that were downregulated are all involved in the cytoskeleton. The general increase in protein expression may indicate an increased accumulation of damaged / misfolded proteins, with a decrease in cellular clearance of dysfunctional proteins, two phenomena which are known hallmarks of ageing (Gadecka

and Bielak-Zmijewska, 2019; Vilchez et al., 2014). These processes and implicated functionally enriched proteins are described further in sections 5.4.3.1–5.4.3.4.

5.4.3.1 Ageing mouse DC and upregulation of proteins involved in cellular respiration

Of the 41 proteins upregulated with age, several of them were observed to be functionally enriched in pathways involved in cellular respiration: for example, the TCA cycle, malate dehydrogenase (MDH) activity, isocitrate dehydrogenase (IDH) activity, and NAD and NADH activity etc. The mitochondria is known as the powerhouse for cellular respiration, where the majority of the aforementioned processes occur (Giacomello et al., 2020). In healthy ageing, it is widely accepted that mitochondrial function declines in addition to mitophagy (the cellular removal of dysfunctional mitochondria by autophagy) (Chen et al., 2020; Chistiakov et al., 2014). This may result in accumulation of dysfunctional mitochondrial proteins such as mitochondrial enzymes and elements of the electron transfer chain reflective of the increase in mitochondrial proteins presently observed in the 30-month-old mouse DC. Indeed, markers of oxidative stress, which is strongly associated with cellular damage, were observed to be upregulated and are described in section 5.4.3.4. Furthermore, proteasome and autophagic-lysosomal degradation of damaged / misfolded proteins is susceptible to age-associated functional decline, which may exacerbate the potential cellular accumulation of these proteins (Vilchez et al., 2014).

Mitochondrial dysfunction may also be associated with a change in glucose metabolism in the form of reductive carboxylation coupled with glycolysis. The process of reductive carboxylation is displayed in Figure 5.2 and the proteins upregulated in the 30-month-old mouse involved in this process are depicted in green text. Reductive carboxylation occurs in cells with mitochondrial dysfunction (Gaude et al., 2018; Halbrook et al., 2018), which is thought to affect ageing cells in the GIT (Camilleri et al., 2000). Furthermore, hypoxic cancerous cells have been observed to undergo reductive carboxylation (Filipp et al., 2012; Wise et al., 2011), and hypoxia is observed to impact the

aged rat GIT with up to a 60 % reduction in mucosal blood flow (Tarnawski et al., 2007). Additionally, this may indicate the presence of cancerous cells as the prevalence of colorectal cancer is increased with age in humans (Hamilton et al., 2009; Hoops and Traber, 1997). Additionally, mucosal scrapings from aged C57BL / 6J colon revealed an increased expression of immune-related genes (Steegenga et al., 2012) indicative of increased inflammation and potentially cancerous tissue (Leman et al., 2018).

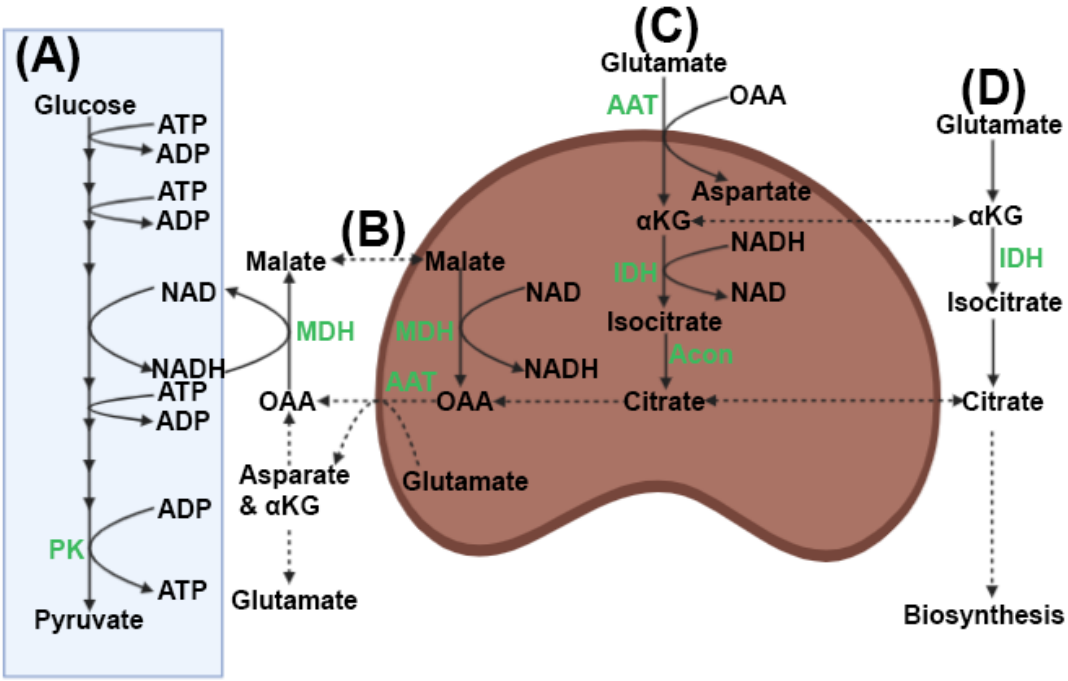

Figure 5.2: Reductive carboxylation coupled with glycolysis proposed to occur in aged mouse colon. Enzymes enhanced with age in the present study mouse DC are coloured green. A) shows the process of glycolysis. B) shows the coupling of reductive carboxylation to glycolysis via MDH redox reaction of OAA and NADH resulting in NAD production for GADPH activity. C) shows reductive carboxylation with the conversion of α-ketoglutarate to citrate, which can be converted to OAA (in the mitochondria) providing fuel for MDH. D) shows that carbon derived from reductive carboxylation can be used for lipid and nucleotide biosynthesis. α-KG, Alpha-ketoglutarate; AAT, Aspartate aminotransferase; Acon, Aconitase; ADP, Adenosine diphosphate; ATP, Adenosine triphosphate; IDH, Isocitrate dehydrogenase; MDH, Malate dehydrogenase; NAD, Nicotinamide adenine dinucleotide;

NADH, Nicotinamide adenine dinucleotide + hydrogen; OAA, Oxaloacetate; PK, Pyruvate kinase.

Reductive carboxylation is the reversal of the TCA cycle, a cellular process presently reported to be functionally enriched in the aged mouse DC. Reductive carboxylation utilises glutamine to produce cytosolic citrate allowing for continued biosynthesis and energy production. One of the key features of reductive carboxylation is the increased activity of isocitrate dehydrogenase (IDH). Cytoplasmic and mitochondrial IDH activity are largely involved in reverse TCA flux. IDH reductively carboxylates glutamine derived α-ketoglutarate to indirectly produce citrate which is utilised in the cytosol for biosynthesis (Filipp et al., 2012; Metallo et al., 2012; Mullen et al., 2012). Additionally, studies undertaken in hypoxic cancerous cells and cells with mitochondrial-induced dysfunction showed that MDH was observed to directly couple reductive carboxylation to glycolysis via nicotinamide adenine dinucleotide (NAD), with glycolysis also presently reported to be functionally enriched in the aged mouse DC. MDH reduces cytosolic OAA to malate and reduces NADH (NAD + hydrogen) to NAD in the process. NAD then functions as an electron acceptor in the reaction catalysed by Glyceraldehyde 3-phosphate dehydrogenase (GADPH) during glycolysis (Gaude et al., 2018; Hanse et al., 2017).

Furthermore, mitochondrial aconitase has been presently reported to be upregulated with age. Aconitase is also involved in the reductive carboxylation pathway, whereby it catalyses the conversion of isocitrate to citrate (Halbrook et al., 2018). Additionally, aspartate aminotransferase (mitochondrial; AAT) was upregulated, and showed the greatest fold-change (4.14) within the present study. Furthermore, upregulated AAT gene expression has previously been observed in colon cancer cell lines (Otsuka et al., 2001). AAT catalyses the reverse transamination of glutamate and oxaloacetate to α-ketoglutarate and aspartate. Thus, AAT is potentially involved in the production of α-ketoglutarate for reductive carboxylation. Aspartate produced during

transamination can be shuttled out of mitochondria and converted to cytosolic OAA for MDH consumption (Lu et al., 2008).

5.4.3.2 Ageing mouse DC and increased myelin sheath

Fifteen of the 41 upregulated proteins in the aged mouse DC were classed as elements that make up the myelin sheath in functional clustering analysis. However, transcriptional profiling of enteric glia shows no evidence of myelination in the mouse ENS (Rao et al., 2015). Therefore, the presence of the myelin sheath is likely from external origin. Extrinsic neurons containing myelin may be partially derived from lumbosacral afferents, in which 5.2% of fibres, that project to the mouse colon, are myelinated (with the remainder being unmyelinated C-fibres) (Christianson et al., 2006). Additionally, the SPN is a potential source of myelinated fibres in the DC since they have been observed in small numbers to project to the colon in cats (de Groat and Krier, 1976). At the level of the DC, myelinated fibres have been observed in dogs, whereby there are roughly three times as many myelinated fibres in the myenteric plexus (1,382 per 40 μm^2) compared to the submucous plexus (348 per 40 μm^2), and the ratio of myelinated nerves was substantially diminished in the mucosa (14.66 per 40 μm^2) versus the submucosa (333.66 per 40 μm^2) (Lee, 1956). This further indicates that myelinated fibres arise externally since MPG fibres, the ganglion which carries SPN fibres, projects to the myenteric plexus in greater abundance compared to the submucous plexus (Brumovsky et al., 2014).

The increased abundance of myelin sheath in the aged mouse DC may indicate a greater extrinsic afferent and / or efferent innervation. This may be a compensatory mechanism since enteric neurons are thought to be more susceptible to age-associated degeneration than other parts of the nervous system (Saffrey, 2013). Myenteric neurons in general have shown no age-associated decline in C57BL / 6J mice of up to 25 months, (Gamage et al., 2013), however cholinergic enteric neurons in the mouse colon are reduced from 20 months onwards (Sun et al., 2018) and cholinergic neurons in the GIT as a whole are more susceptible to age-associated decline than other enteric neuron types

(Saffrey, 2013). Cholinergic innervation plays a major role in colonic motility (Furness et al., 2014) and therefore, an age-associated increase in innervation from the cholinergic SPN may compensate for this acetylcholine loss potentially resulting in an increased distribution of myelinated fibres in the mouse DC.

Regarding DRG afferents projecting to the DC, an age-associated attenuation in mechanosensitvity of high-threshold neurons was observed in 24-month *in vitro* mouse colon tissue (Keating et al., 2016). This likely impairs the relaying of colonic sensory, particularly nociceptive, information, to the spinal cord and brain. As myelin speeds up impulse propagation (Williamson and Lyons, 2018), this impairment of sensory signalling may result in an increase in myelin sheath formation as a compensatory mechanism. Thus, resulting in increased age-associated myelin density overall. Alternatively, myelin sheath aberration may be a contributing factor or a morphological change as a result of neuronal mechanosensory impairment. Indeed, degenerative changes in the morphology of ageing neurons can result in the formation of myelin splits (due to pockets of dense cytoplasm), or myelin balloons (due to excess fluid) (Peters, 2002). These age-associated aberrations may result in myelin debris accumulation as Schwann cell clearance of myelin, and macrophage accumulation, is impaired in aged (24-month-old) mouse sciatic nerve compared to young (2-month) (Painter et al., 2014).

Myelin is an inhibitory substrate for axonal growth and thus myelin debris must be cleared before axonal growth or regeneration can occur (McKerracher et al., 1994). Therefore, unless the presently observed increase in myelin concentration indicates an increase in myelin-containing extrinsic fibres, it is likely that this myelin accumulation is detrimental to neuronal function. This may impact both afferent and efferent extrinsic fibres resulting in impaired conscious processing of DC stretch. Additionally, a reduction in function in efferent cholinergic SPN fibres would result in a further decrease in acetylcholine within the mouse DC (in addition to the age-associated loss of cholinergic ENS neurons) and this is likely associated with decreased DC contractility. Ultimately, the

reduction in function of efferent and / or afferent fibres may be a contributing factor to age-associated constipation that is known to impact this strain of mouse (Patel et al., 2014).

5.4.3.3 Ageing mouse DC and increased collagen-containing extracellular matrix

Proteins that comprise collagen-containing ECM, including lumican, collagen α-1(VI) chain and collagen α-2(VI) were upregulated with age in the mouse DC. Similar to present observations, colonic collagen content has been observed to increase with age in guineapigs (Gabella, 2001). Collagen within the ECM is involved in maintenance of structural integrity. This may result in excessive amounts of collagen cross-linking which potentially contributes to colonic rigidity. Accumulation of advanced glycation end products have been observed in aged tissues, which cause an increase in collagen intra and intermolecular cross-linking (Haus et al., 2007; Zieman and Kass, 2004) and renders collagen less susceptible to degradation (DeGroot et al., 2001). Advanced glycation end products have been observed alongside increased stiffening of the tail tendon in aged mice (Stammers et al., 2020). Advanced glycation end products can form exogenously through the ingestion of processed foods, and these may accumulate over time in the aged DC (Aragno and Mastrocola, 2017). Alternatively, they can be generated in higher rates endogenously due to impaired glucose metabolism (such as that discussed in section 5.4.3.1) with altered glucose metabolism known to increase with age (Kalyani and Egan, 2013). The increased collagen presently observed in the aged mouse DC may be due to this phenomenon. This excess collagen would likely impact the lamina propria, submucosa and the adventitia since these layers are comprised of collagen fibres (Despotovic et al., 2017; Fu and Zhang, 1997; Lord et al., 1977). This likely increased stiffening of the colon may reduce colonic motility and potentially contributes to constipation that has been previously reported in aged C57BL / 6J male mice (Patel et al., 2014).

Furthermore, collagen cross-linking increases with age in humans suffering diverticulitis (Wess et al., 1995), which is a disease whose prevalence is increased with

age that is characterised by colonic inflammation and the formation of abnormal pouches (diverticula). (Soreide et al., 2016). Increased collagen content, cross-linking and intestinal stiffness occur in other colonic pathophysiologies including Crohn's disease, and inflammatory bowel disease (Graham et al., 1988; Johnson et al., 2013; Stewart et al., 2018), and these pathophysiologies often coincide with constipation and FI (Nobrega et al., 2018; Petryszyn and Paradowski, 2018). Therefore, collagen upregulation potentially impacts mammals both at rodent and human level and likely has a direct impact in decreased colonic motility that often coincides with increased age (Fleming and Wade, 2010; Gallegos-Orozco et al., 2012).

5.4.3.4 Ageing mouse DC and markers of oxidative stress

Oxidative stress and the resulting damage to cellular proteins is a process associated with increased age (Gadecka and Bielak-Zmijewska, 2019). Markers of increased oxidative stress have presently been observed in functional clustering analysis of upregulated proteins in 30-month-old mouse DC, including peroxisomes and pigment granules. The upregulation in proteins associated with cellular respiration (discussed in section 5.4.3.1) may result in increased generation of free radicals, particularly as a result of dysfunctioning mitochondria which are more predisposed to O_2^- leakage (Cadenas and Davies, 2000). Peroxodoxin, which was presently upregulated with age, is an enzyme located in peroxisomes which acts as a scavenger for the free radical hydrogen peroxide using cysteine as their primary oxidation site (Nyström et al., 2012). Its inactivation accelerates ageing in mice and causes an increase in reactive oxygen species (ROS) and oxidative DNA damage (Neumann et al., 2003). Therefore, its upregulation is potentially a protective mechanism against increased age-associated oxidative damage (Zhang et al., 2015a).

Increased formation of pigment granules is also associated with ageing. Pigments such as lipofuscin form as a result of residues of lysosomal digestion which is indicative of impaired lysosome function and cellular clearance of damaged / misfolded proteins

(Moreno-García et al., 2018). Increased lysosomal digestion is necessary in aged tissue due to the increased requirement for clearance of oxidatively damaged proteins. However, increased abundance of damaged proteins is likely to put strain on lysosomes and ultimately result in dysfunction (Harman, 1989; Moreno-García et al., 2018). Lipofuscin accumulation has been reported in enteric neurons in aged rats and guineapigs (Saffrey, 2014). Therefore, the presently observed increases in pigment granules may occur in enteric neurons of the aged mouse DC. This potentially implies cellular oxidative damage that could lead to the loss of enteric neurons previously observed in aged C57BL / 6J mice (Sun et al., 2018).

5.4.4 Study Limitations

The majority of study limitations are documented in section 5.4.2, including unsuccessful measurement of protein concentration, SDS-PAGE gel smear formation, and lower protein identification yield in comparison to fresh mouse colon tissue. Additionally, without the use of LCMD, specific tissue regions e.g. MP, could not be isolated. Due to heterogeneity of mouse DC, cell types involved in age-associated change in protein regulation were speculative. Furthermore, only n=2 per age group was applied and thus results may have reduced reliability.

5.5 Conclusion

Methodology development for protein extraction of FFPE mouse DC tissue for downstream protein analysis showed some success. However, methodology had limitations including inability to: accurately quantify protein concentration in extract; isolate protein bands on SDS-gel (due to protein smearing); and qualitatively identify the same number of proteins previously observed from fresh mouse colon samples. Future attempts to resolve these limitations should include decreased sample to deparaffinization buffer / extraction buffer ratio; addition of a sample clean-up step; addition of glycosidases to remove oligosaccharides attached to proteins; and addition of more variable modifications during data processing. These method alterations would likely result in an overall increase

in sequence coverage and protein identification. Additionally, it would allow for knowledge of the minimum amount of MP sample to be micro-dissected from sections to yield enough protein for analysis. However, due to protein–protein cross-links that develop over storage time of FFPE tissue, it is unlikely that protein sample yield will match that of fresh tissue.

Despite methodology limitations, significant age-associated changes in protein composition were observed between 3- and 30-month DC. Proteins in the aged mouse DC were largely upregulated reflecting a previous study in rats (Lee et al., 2001). This is likely indicative of various age-related cellular dysfunctions, which may be contributing factors to the age-associated constipation previously reported in this strain of mouse (Patel et al., 2014). Associated dysfunctions potentially include, but are likely not limited to, accumulation of oxidatively damaged proteins and impaired clearance, mitochondrial dysfunction and altered cellular respiration, decline in function of myelinated extrinsic afferent and / or efferent neurons, and increased collagen cross-linking in the ECM which is likely coupled with colonic rigidity.

6 OVERALL DISCUSSION

6.1 SUMMARY OF MAIN FINDINGS

In Chapters 3 and 4, application of immunohistochemistry allowed for the identification of age-associated changes in the C57BL / 6J male mouse CNS at a cellular level. In the lumbosacral spinal cord, there was a significant decrease (66.5 %) in ENK and VGAT (57.5 %) immunoreactivity in the aged (29–31 months) SPN compared with young (3–5 months). In the PVN of the hypothalamus, there was a significant age-associated increase in the number of VGAT inputs onto OXY (up to 91.1%) and VP (up to 81.5%) parvocellular soma of the PVNmpd. Additionally, there was a significant age-associated increase in the density of VGLUT2 immunoreactivity of up to 85% in the PVNpv.

In Chapter 5, application of protein analysis coupled with functional clustering analysis allowed for the identification of age-associated changes in the C57BL / 6J male mouse DC at a subcellular level. There was a significant upregulation in 41 proteins, with a large proportion of them involved in cellular respiration. Additionally, there was an increase in proteins that form the myelin sheath, the collagen-containing ECM, and the oxidative stress markers, peroxisomes and pigment granules. Additionally, there was a significant downregulation in proteins involved in cytoskeletal structure. Figure 6.1 summarizes the main findings of this thesis.

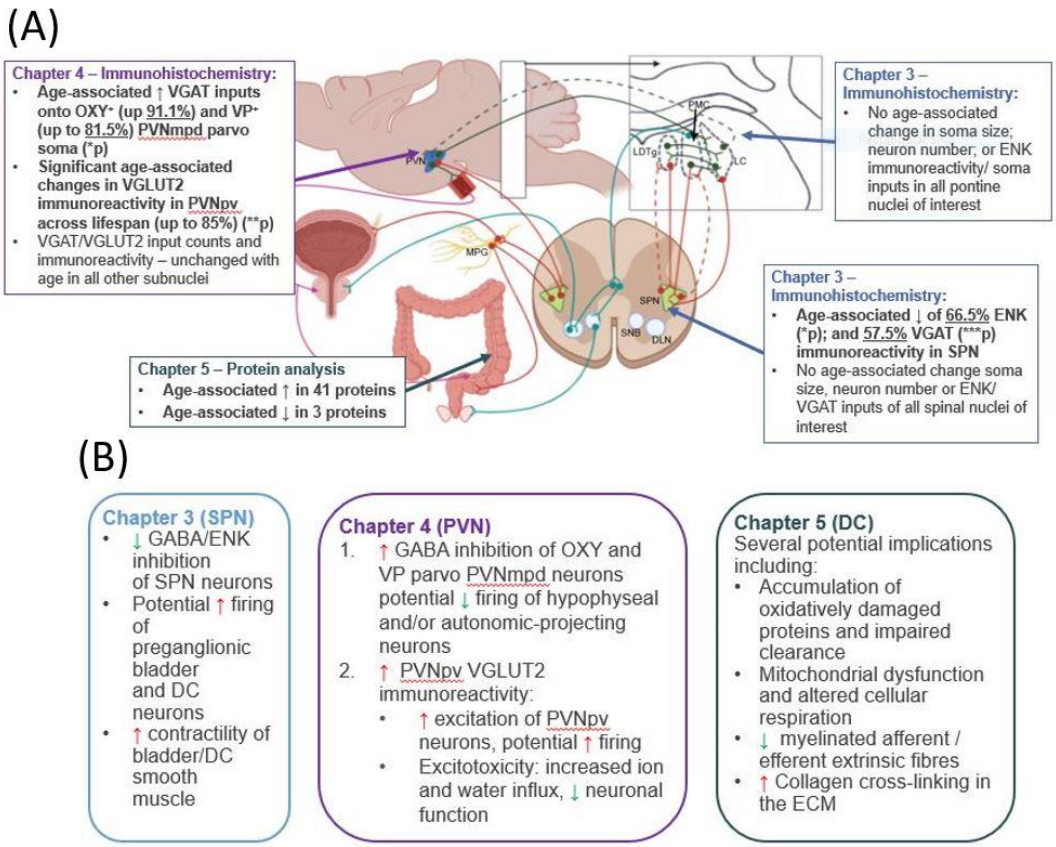

Figure 6.1: Summary of main findings of this PhD thesis. (A) Depicts the age-associated changes that were noted with each technique (immunohistochemistry or protein analysis), and the location of each age-associated change. (B) Depicts the potential implications of each age-associated change. DC, Distal colon; DLN, Dorsolateral nucleus; ECM, Extracellular matrix; ENK, Enkephalin; LC, Locus coeruleus; LDTg, Laterodorsal tegmental nucleus; MPG, Major pelvic ganglion; OXY, Oxytocin; PMC, Pontine micturition centre; PVNmpd: Paraventricular nucleus, medial parvocellular, dorsal zone; PVNpv, Paraventricular nucleus, periventricular part; SNB, Spinal nucleus of the bulbospongiosus; SPN, Sacral parasympathetic nucleus; VGAT, Vesicular GABA transporter; VGLUT2, Vesicular glutamate transporter 2; VP, Vasopressin.

6.2 COLLECTIVE IMPLICATIONS OF FINDINGS

Overall findings within this thesis indicate that age-associated changes occur at all levels of nervous and non-nervous structures that may contribute to age-related voiding dysfunctions. The structures analysed in Chapters 3–5 are all directly and

indirectly linked to one another and ultimately contribute to the function of the LUT and terminal bowel. Therefore, the age-related changes observed in each chapter may influence one another and likely collectively result in the age-associated functional changes that cause impaired voiding and defaecation. At each structural level, the age-related changes observed, and their potential influence on one another are discussed in sections 6.2.1–6.2.3 beginning at the highest level (the PVN) and working down.

6.2.1 Age-related changes in the PVN and its association with age-related changes presently reported in lower level structures

The age-associated changes observed in the subnuclei of the PVN in Chapter 4 are thought to result in decreased neuronal activity overall. The increase in inhibitory VGAT inputs onto OXY and VP parvocellular neurons of the PVNmpd would likely result in decreased neuronal firing and therefore a decrease in the release of OXY and VP at the various possible sites that these neurons project to. Additionally, an increase in VGLUT2 in the PVNpv may result in neuronal excitotoxicity and therefore a decline in neuronal function overall (described in-depth in section 4.4.6). The specific neurons that potentially suffer from glutamate-induced cytotoxicity are unknown and therefore it is not possible to speculate the downstream effects of this event. However, the increase in VGAT inputs specially impacts VP and OXY neurons of the PVNmpd which allows for further speculation of the potential impact this has within the body. OXY and VP neurons within this region project to the pituitary for OXY and VP release into the bloodstream. Additionally, some of these neurons are project to regions within the CNS (Biag et al., 2012).

In terms of CNS-projecting neurons, some PVN OXY neurons are known to project to the SPN and result in non-voiding contrations of the bladder smooth muscle (Pandita et al., 1998; Puder and Papka, 2001b; Swanson and McKellar, 1979). Alongside a potential decrease in OXY inputs onto SPN neurons, there was a decrease in inhibitory ENK and VGAT as reported in Chapter 3. As both ENK and VGAT inputs onto the SPN are

associated with decreased bladder contraction (Dray and Metsch, 1984; Hisamitsu and de Groat, 1984; Kennedy and Krier, 1987; Sugaya et al., 2019; Vaidyanathan et al., 1989), a decrease in inhibitory input would likely be associated with an increase in bladder activity. Therefore, combined results from Chapter 3 and 4 would imply a decrease in OXY-induced non-voiding contractions and an increase in voiding-related contractions. Non-voiding contractions occur with increased bladder volume and are thought to be involved with communication of micturition urgency for increased awareness of bladder filling (Heppner et al., 2016). Whilst general contractions enable sufficient bladder emptying after initiation of micturition (Fowler et al., 2008). The potential combination of decreased non-voiding contractions and increased general contractions may be reflective of the weakened detrusor contractile and relaxant responses, respectively, that were reported in this in C57BL / 6J mice (Kamei et al., 2018). Additionally EUS tone may be reduced due to possible loss of VP DLN projections and circulatory release (Cechetto and Saper, 1988; Nadelhaft and Vera, 1996; Swanson and Kuypers, 1980; Swanson and McKellar, 1979), since VP results in EUS contraction at both these levels (Ito et al., 2018; Ueno et al., 2011). As an age-related increase in voiding frequency is observed in this strain of mouse (Kamei et al., 2018), a decrease in VP-induced EUS tone may be a contributing factor.

A further impact of decreased firing of PVNmpd VP and OXY may be a decrease in the circulatory release of the two hormones at the neurohypophysis (Swanson and Kuypers, 1980). The decrease in concentrations of circulatory VP may result in a decline in EUS tone, as circulatory VP is known to cause EUS contraction (Ito et al., 2018). Additionally, a decrease in the circulation of both hormones may result in decreased DC contractility. This is because VP causes giant migratory contractions associated with mass faecal movement (Zhu et al., 1992) and OXY causes contractions at the level of the ENS (Xi et al., 2019). Age-related changes in DC protein structure (reported in Chapter 5) indicate that the DC is modified in a variety of ways at a subcellular level that are likely associated with impaired overall function. These changes include, but are not limited to, an increase in ECM collagen that is likely associated with increased stiffening of the DC wall (Stammers et al., 2020); and an increase in myelin sheath which is potentially

connected to impaired functioning of extrinsic afferent and / or efferent fibres that partially control DC contractility (McKerracher et al., 1994; Painter et al., 2014). Therefore, a decrease in contraction-inducing OXY and VP, coupled with a impaired spinal control of the DC, and collagen-induced stiffening of the DC wall are all likely contributing factors to the impaired colonic motility and increased faecal impaction reported in this strain of mouse (Patel et al., 2014).

6.2.2 Age-related changes in the SPN and its association with age-related changes presently reported in other structures

The age-associated changes observed in the lumbosacral SPN in Chapter 3 are thought to result in increased neuronal activity overall. This is because a decline in inhibitory GABA and ENK likely results in decreased inhibition of SPN neurons (Dray and Metsch, 1984; Hisamitsu and de Groat, 1984; Kennedy and Krier, 1987; Nakamori et al., 2018; Sugaya et al., 2019). As stimulation of the SPN causes reflex bladder, colorectal and, IAS contractions (Dorofeeva and Panteleev, 2007; Ni et al., 2018; Tai et al., 2001), this potential increase in SPN activity may indicate increased contractility within these pelvic organs, and may reflect the decreased bladder relaxant response and more frequent urination reported in CB57BL / 6J mice (Kamei et al., 2018). However, a general decrease in motility in the CB57BL / 6J mouse colon is reported (Patel et al., 2014). In Chapter 5, protein analysis of the DC showed an increase in collagen-containing ECM, which likely contributes to rigidity of the DC wall (Stammers et al., 2020). Therefore, increased activity of extrinsic SPN fibres inputting onto the DC may be a compensatory mechanism to bolster contractions in a stiffened DC. Alternatively, an age-associated increase in proteins that comprise the myelin sheath may indicate dysfunction of extrinsic fibres in the DC (as described in-depth in section 5.4.3.2). Therefore, there may be a decline in the function of colon-projecting SPN neurons that further amplifies the effects of collagen-induced stiffening, which results in decreased faecal movement through the DC.

In terms of the SPN's potential impact on PVN function, there is indirect afferent connections between the SPN and PVN. The SPN projects to the PMC, which then projects to the PVN via the LC (Ding et al., 1997; Yao et al., 2018). These connections likely form part of the pathway that induces awareness of bladder / rectal fullness. However, because pathways are indirect and the PVN is such a complex nucleus involved in a vast array autonomic and neuroendocrine processes, it is difficult to speculate whether the age-related change in SPN ENK / VGAT density has an association with the age-related changes in PVN VGAT / VGLUT2 density reported in Chapter 4.

6.2.3 Age-related changes in the DC and its association with age-related changes presently reported in higher-level CNS structures

Protein analysis of the mouse DC in Chapter 5 allowed for determination of sub-cellular changes that occur with age in mice. After functional clustering analysis, the main changes reported with age were an increase in the following: proteins involved in various aspects of cellular respiration, myelin sheath, collagen-containing ECM, and markers of oxidative stress (peroxisomes and pigments granules). These changes may all contribute to the decreased colonic motility and faecal impaction that occurs with age in this strain of mouse (Patel et al., 2014). The exact cellular location of these changes in the wall of the mouse DC is unknown, and since the GIT wall is a vastly heterogenous structure, it is difficult to determine exactly what cellular structures these changes impact. However, the age-associated increase in myelin sheath can be attributable solely to extrinsic fibres, as myelination does not occur in the mouse ENS (Rao et al., 2015). This increase in myelin sheath may indicate an accumulation of myelin (as described in-depth in section 5.4.3.2). This may be associated with an impairment in extrinsic afferent communications from the ENS to the CNS. Indeed, an age-associated attenuation in mechanosensitivity of high-threshold neurons was observed in 24-month mice (Keating et al., 2016).

The SPN receives afferents from the DC wall (Harrington et al., 2019), and thus a deleterious change in fibre morphology at the level of the DC may impact the SPN. This

may result in a decrease in the number of inputs to the SPN from DC afferent neurons. Lumbosacral ENK and GABA inputs are thought to derive partially from afferent sources (Blok et al., 1997a; Polgar et al., 2003). More specifically, a retrograde tracing study has shown that DRG ENK afferents are mainly derived from the colon (Keast and de Groat, 1992). As a result, a decline in DC afferent function may result in decreased SPN input from ENK and GABA (and potentially other neuroactive substances). This potential reduction in afferent feedback from the DC to the SPN may further exacerbate, or indeed be a precursor, to the decrease in colonic motility reported with age in mice (Patel et al., 2014). In terms of the PVN, the afferent connection pathway from the DC, and the structure of the PVN itself are both highly complex. Therefore, it is difficult to speculate whether the age-related changes in the DC have an association with the age-related changes in PVN VGAT / VGLUT2 density reported in Chapter 4.

6.3 STUDY LIMITATIONS AND FUTURE WORK

Further work is required to make proposed implications of results more robust and less speculative. A limitation in Chapter 3, was the use of only two age group for lumbosacral spinal work (based on sample availability). The work in the lumbosacral spinal cord would benefit from additional age groups such as the 12-14- and 24-25-month mice (applied in the brainstem and PVN work) to determine if ageing affects groups in between young (3-5 month) and aged (30-31 month) mice. Another limitation applies to IHC labelling techniques whereby there is no certainty which projection pathways are impacted by age-associated changes. In order to determine exactly which projection pathways were affected by age-related changes presently observed, the use of neuronal tracing techniques would be beneficial. For example, transneuronal retrograde tracer injected into the bladder and DC separately with the same counting techniques applied across age groups would have two beneficial effects at spinal level: (1) it would allow for better visualisation of SPN neurites and hence it would clarify whether age-associated decrease in GABA / ENK results in a decreased number of inputs onto neuritic structures;

and (2) it would help elucidate if the decrease in GABA / ENK density impacts bladder, DC-projecting neurons, or both, considering bladder and DC efferent SPN projections are independent of one another (Rouzade-Dominguez et al., 2003a).

Neuronal tracing techniques would be particularly beneficial within the PVN, since the PVN is involved in multiple projection pathways that control various autonomic and neuroendocrine functions (Swanson and Sawchenko, 1980). In the case of the PVN, transneuronal retrograde tracer injected into the bladder / DC would label CNS pathways. Additionally, it would be necessary to inject tracer intravenously to label pituitary-projecting neurons, such as that undertaken by Biag et al. (2012). Double labelling could be applied using OXY and VP to confirm which projection pathways are impacted by the the age-associated increase in GABAergic soma inputs. Furthermore, immunolabelling of CRH neurons would be advantageous since CRH functions in circulatory and CNS control of micturition / defaecation (Lechner et al., 1997; Maillot et al., 2000; Maillot et al., 2003; Million et al., 2000; Monnikes et al., 1994; Pavcovich and Valentino, 1995; Puder and Papka, 2001a; Valentino et al., 1999; Wood et al., 2013). The use of transneuronal tracing techniques would have the added benefit of improved neurite labelling. Therefore, it could aid determination of which neurons are impacted by the increase in VGLUT2. Additionally, clearly labelled neurites could be measured for age-related swelling or loss (as observed in rats) that may be indicative of glutamate-induced excitotoxity (Itzev et al., 2003). Further beneficial methodology, that should be applied to both the lumbosacral spinal cord and the PVN, is the use of ultrastructural analysis. This would confirm that presumed soma (and potentially neuritic) inputs are making synaptic contact with neurons.

As extensively discussed in Chapter 5, there are a number of improvements that could be incorporated into the experimental design with regards to protein analyses of the mouse DC. These include reducing the sample to extraction buffer ratio to reduce any contaminants; the application of glycosidases to breakdown glycoproteins attached to proteins; the addition of variable modifications during Mascot™ MS / MS ion search and Progenesis™ LC-MS data analysis. These changes may result in successful application of

protein quantification assays (e.g. BCA assay). Additionally, there may be reduced gel ‘smearing’ during SDS-PAGE which would allow for the identification and excision of gel bands to maximise sequence coverage and increase overall protein yield. This improvement in methodology must be achieved before attempting to excise MP via LCMD for downstream protein analysis. This is necessary since successful protein quantification assay will help determine if a high enough concentration of protein can be extracted from microscopic MP sections for downstream analysis. Furthermore, with smaller quantities of protein being extracted, protein analysis needs to be refined to detect age associated changes in protein expression.

6.4 CONCLUSION

In conclusion, age-associated changes were reported that occur at all levels of nervous and non-nervous structures, and these changes may contribute to age-related voiding dysfunctions. At the level of the lumbosacral spinal cord, there was a significant age-related decrease in inhibitory VGAT and ENK immunoreactivity. Within the PVN there was an age-related increase in inhibitory VGAT terminals inputting onto PVNmpd OXY and VP soma, and an increase in VGLUT2 density within the PVNpv. Lastly, at the level of the DC, there was an age-associated upregulation in 41 proteins and a downregulation in three. These changes likely, at least in-part, contribute to impairments in the LUT and terminal bowel that result in dysfunctions of micturition and defaecation that occur within the elderly population.

7 REFERENCES

ABCAM. 2020. *How we validate our antibodies* [Online]. Available: https://www.abcam.com/primary-antibodies/how-we-validate-our-antibodies#KO [Accessed].

ABERCROMBIE, M. 1946. Estimation of nuclear population from microtome sections. *Anat Rec,* 94**,** 239-47.

ABRAMS, P., CARDOZO, L., FALL, M., GRIFFITHS, D., ROSIER, P., ULMSTEN, U., VAN KERREBROECK, P., VICTOR, A. & WEIN, A. 2002. The standardisation of terminology of lower urinary tract function: Report from the standardisation sub-committee of the International Continence Society. *Neurourology and Urodynamics,* 21**,** 167-178.

ABYSIQUE, A., ORSONI, P. & BOUVIER, M. 1998. Evidence for supraspinal nervous control of external anal sphincter motility in the cat. *Brain research,* 795**,** 147-156.

AKIGUCHI, I., PALLAS, M., BUDKA, H., AKIYAMA, H., UENO, M., HAN, J., YAGI, H., NISHIKAWA, T., CHIBA, Y., SUGIYAMA, H., TAKAHASHI, R., UNNO, K., HIGUCHI, K. & HOSOKAWA, M. 2017. SAMP8 mice as a neuropathological model of accelerated brain aging and dementia: Toshio Takeda's legacy and future directions. *Neuropathology,* 37**,** 293-305.

ALBERS, H. E., WALTON, J. C., GAMBLE, K. L., MCNEILL, J. K. T. & HUMMER, D. L. 2017. The dynamics of GABA signaling: Revelations from the circadian pacemaker in the suprachiasmatic nucleus. *Front Neuroendocrinol,* 44**,** 35-82.

ANDERS, K. 2000. Coping strategies for women with urinary incontinence. *Baillieres Best Pract Res Clin Obstet Gynaecol,* 14**,** 355-61.

ANDERSSON, K. E. & ARNER, A. 2004. Urinary bladder contraction and relaxation: physiology and pathophysiology. *Physiol Rev,* 84**,** 935-86.

ANDY, U. U., EJIKE, N., KHANIJOW, K. D., FLICK, L. C., MARKLAND, A. D., ARYA, L. A. & FRASSO, R. 2019. Diet Modifications in Older Women With Fecal Incontinence: A Qualitative Study. *Female Pelvic Med Reconstr Surg*.

ANGER, J. T., NISSIM, H. A., LE, T. X., SMITH, A. L., LEE, U., SARKISIAN, C., LITWIN, M. S., RAZ, S., RODRIGUEZ, L. V. &

MALISKI, S. L. 2011. Women's experience with severe overactive bladder symptoms and treatment: insight revealed from patient focus groups. *Neurourol Urodyn,* 30**,** 1295-9.

ANTAL, M., PETKO, M., POLGAR, E., HEIZMANN, C. W. & STORM-MATHISEN, J. 1996. Direct evidence of an extensive GABAergic innervation of the spinal dorsal horn by fibres descending from the rostral ventromedial medulla. *Neuroscience,* 73**,** 509-18.

ARAGNO, M. & MASTROCOLA, R. 2017. Dietary Sugars and Endogenous Formation of Advanced Glycation Endproducts: Emerging Mechanisms of Disease. *Nutrients,* 9**,** 385.

ARMSTRONG, D. M., SAPER, C. B., LEVEY, A. I., WAINER, B. H. & TERRY, R. D. 1983. Distribution of cholinergic neurons in rat brain: Demonstrated by the immunocytochemical localization of choline acetyltransferase. *Journal of Comparative Neurology,* 216**,** 53-68.

ARMSTRONG, W. E., WARACH, S., HATTON, G. I. & MCNEILL, T. H. 1980. Subnuclei in the rat hypothalamic paraventricular nucleus: a cytoarchitectural, horseradish peroxidase and immunocytochemical analysis. *Neuroscience,* 5**,** 1931-58.

ARVIDSSON, U., DADO, R. J., RIEDL, M., LEE, J. H., LAW, P. Y., LOH, H. H., ELDE, R. & WESSENDORF, M. W. 1995. delta-Opioid receptor immunoreactivity: distribution in brainstem and spinal cord, and relationship to biogenic amines and enkephalin. *The Journal of Neuroscience,* 15**,** 1215.

BAFFY, N., FOXX-ORENSTEIN, A. E., HARRIS, L. A. & STERLER, S. 2017. Intractable Constipation in the Elderly. *Curr Treat Options Gastroenterol,* 15**,** 363-381.

BAJWA, A. & EMMANUEL, A. 2009. The physiology of continence and evacuation. *Best Pract Res Clin Gastroenterol,* 23**,** 477-85.

BANAY-SCHWARTZ, M., LAJTHA, A. & PALKOVITS, M. 1989. Changes with aging in the levels of amino acids in rat CNS structural elements. I. Glutamate and related amino acids. *Neurochem Res,* 14**,** 555-62.

BANREZES, B., ANDREY, P., MASCHINO, E., SCHIRAR, A., PEYTEVIN, J., RAMPIN, O. & MAURIN, Y. 2002. Spatial segregation within the sacral parasympathetic nucleus of neurons innervating the

bladder or the penis of the rat as revealed by three-dimensional reconstruction. *Neuroscience,* 115, 97-109.
BARI, B. A., CHOKSHI, V. & SCHMIDT, K. 2020. Locus coeruleus-norepinephrine: basic functions and insights into Parkinson's disease. *Neural Regen Res,* 15, 1006-1013.
BARRINGTON, F. J. F. 1925. THE EFFECT OF LESIONS OF THE HIND- AND MID-BRAIN ON MICTURITION IN THE CAT. *Quarterly Journal of Experimental Physiology,* 15, 81-102.
BARTLETT, L., NOWAK, M. & HO, Y.-H. 2009. Impact of fecal incontinence on quality of life. *World journal of gastroenterology,* 15, 3276-3282.
BAYLISS, W. M. & STARLING, E. H. 1901. The movements and innervation of the small intestine. *J Physiol,* 26, 125-38.
BECKER, K. F., SCHOTT, C., BECKER, I. & HOFLER, H. 2008. Guided protein extraction from formalin-fixed tissues for quantitative multiplex analysis avoids detrimental effects of histological stains. *Proteomics Clin Appl,* 2, 737-43.
BELSEY, J., GREENFIELD, S., CANDY, D. & GERAINT, M. 2010. Systematic review: impact of constipation on quality of life in adults and children. *Aliment Pharmacol Ther,* 31, 938-49.
BENNETT, B. C., KRUSE, M. N., ROPPOLO, J. R., FLOOD, H. D., FRASER, M. & DE GROAT, W. C. 1995. Neural control of urethral outlet activity in vivo: role of nitric oxide. *J Urol,* 153, 2004-9.
BERNARD, B. A., NEWTON, S. A. & OLDEN, K. 1983. Effect of size and location of the oligosaccharide chain on protease degradation of bovine pancreatic ribonuclease. *J Biol Chem,* 258, 12198-202.
BERRIDGE, C. W. & FOOTE, S. L. 1991. Effects of locus coeruleus activation on electroencephalographic activity in neocortex and hippocampus. *J Neurosci,* 11, 3135-45.
BERTHOUD, H. R., JEDRZEJEWSKA, A. & POWLEY, T. L. 1990. Simultaneous labeling of vagal innervation of the gut and afferent projections from the visceral forebrain with dil injected into the dorsal vagal complex in the rat. *J Comp Neurol,* 301, 65-79.

BERTHOUD, H. R., PATTERSON, L. M., NEUMANN, F. & NEUHUBER, W. L. 1997. Distribution and structure of vagal afferent intraganglionic laminar endings (IGLEs) in the rat gastrointestinal tract. *Anat Embryol (Berl),* 195**,** 183-91.

BERTRAND, P. P., KUNZE, W. A., BORNSTEIN, J. C. & FURNESS, J. B. 1998. Electrical mapping of the projections of intrinsic primary afferent neurones to the mucosa of the guinea-pig small intestine. *Neurogastroenterol Motil,* 10**,** 533-41.

BERTRAND, P. P., KUNZE, W. A., BORNSTEIN, J. C., FURNESS, J. B. & SMITH, M. L. 1997. Analysis of the responses of myenteric neurons in the small intestine to chemical stimulation of the mucosa. *Am J Physiol,* 273**,** G422-35.

BHARUCHA, A. E. 2008. Lower gastrointestinal functions. *Neurogastroenterol Motil,* 20 Suppl 1**,** 103-13.

BHARUCHA, A. E., WALD, A., ENCK, P. & RAO, S. 2006. Functional anorectal disorders. *Gastroenterology,* 130**,** 1510-8.

BIAG, J., HUANG, Y., GOU, L., HINTIRYAN, H., ASKARINAM, A., HAHN, J. D., TOGA, A. W. & DONG, H. W. 2012. Cyto- and chemoarchitecture of the hypothalamic paraventricular nucleus in the C57BL/6J male mouse: a study of immunostaining and multiple fluorescent tract tracing. *J Comp Neurol,* 520**,** 6-33.

BIERINX, A. S. & SEBILLE, A. 2006. The urethral striated sphincter in adult male rat. *Anat Embryol (Berl),* 211**,** 435-41.

BIRD, S. J. & KUHAR, M. J. 1977. Iontophoretic application of opiates to the locus coeruleus. *Brain Research,* 122**,** 523-533.

BIRDER, L. A., KULLMANN, A. F. & CHAPPLE, C. R. 2018. The aging bladder insights from animal models. *Asian journal of urology,* 5**,** 135-140.

BIRDER, L. A., NAKAMURA, Y., KISS, S., NEALEN, M. L., BARRICK, S., KANAI, A. J., WANG, E., RUIZ, G., DE GROAT, W. C., APODACA, G., WATKINS, S. & CATERINA, M. J. 2002. Altered urinary bladder function in mice lacking the vanilloid receptor TRPV1. *Nat Neurosci,* 5**,** 856-60.

BLAIR, P. J., BAYGUINOV, Y., SANDERS, K. M. & WARD, S. M. 2012. Relationship between enteric neurons and interstitial cells in

the primate gastrointestinal tract. *Neurogastroenterol Motil,* 24, e437-49.

BLANCO, L., ROS, C. M., TARRAGÓN, E., FERNÁNDEZ-VILLALBA, E. & HERRERO, M. T. 2014. Functional role of Barrington's nucleus in the micturition reflex: Relevance in the surgical treatment of Parkinson's disease. *Neuroscience,* 266, 150-161.

BLISS, D. Z., GURVICH, O. V., EBERLY, L. E. & HARMS, S. 2018. Time to and predictors of dual incontinence in older nursing home admissions. *Neurourol Urodyn,* 37, 229-236.

BLOK, B. F., DE WEERD, H. & HOLSTEGE, G. 1997a. The pontine micturition center projects to sacral cord GABA immunoreactive neurons in the cat. *Neurosci Lett,* 233, 109-12.

BLOK, B. F. & HOLSTEGE, G. 1997. Ultrastructural evidence for a direct pathway from the pontine micturition center to the parasympathetic preganglionic motoneurons of the bladder of the cat. *Neurosci Lett,* 222, 195-8.

BLOK, B. F., WILLEMSEN, A. T. & HOLSTEGE, G. 1997b. A PET study on brain control of micturition in humans. *Brain,* 120 (Pt 1), 111-21.

BLOK, B. F. M. & HOLSTEGE, G. 1994. Direct projections from the periaqueductal gray to the pontine micturition center (M-region). An anterograde and retrograde tracing study in the cat. *Neuroscience Letters,* 166, 93-96.

BOHORQUEZ, D. V., SAMSA, L. A., ROHOLT, A., MEDICETTY, S., CHANDRA, R. & LIDDLE, R. A. 2014. An enteroendocrine cell-enteric glia connection revealed by 3D electron microscopy. *PLoS One,* 9, e89881.

BOHORQUEZ, D. V., SHAHID, R. A., ERDMANN, A., KREGER, A. M., WANG, Y., CALAKOS, N., WANG, F. & LIDDLE, R. A. 2015. Neuroepithelial circuit formed by innervation of sensory enteroendocrine cells. *J Clin Invest,* 125, 782-6.

BOTTING, J. H. & TURMER, A. D. 1966. Mode of action of vasopressin on isolated proximal colon of the guinea-pig. *British journal of pharmacology and chemotherapy,* 28, 197-206.

BRADFORD, M. M. 1976. A rapid and sensitive method for the quantitation of microgram quantities of protein utilizing the principle of protein-dye binding. *Anal Biochem,* 72**,** 248-54.

BRADING, A. F. & RAMALINGAM, T. 2006. Mechanisms controlling normal defecation and the potential effects of spinal cord injury. *Prog Brain Res,* 152**,** 345-58.

BRADLEY, R. M. 2007. Frontiers in Neuroscience

rNST Circuits. *In:* BRADLEY, R. M. (ed.) *The Role of the Nucleus of the Solitary Tract in Gustatory Processing.* Boca Raton (FL): CRC Press/Taylor & Francis

Taylor & Francis Group, LLC.

BRANN, D. W. 1995. Glutamate: a major excitatory transmitter in neuroendocrine regulation. *Neuroendocrinology,* 61**,** 213-25.

BREEDLOVE, S. M. & ARNOLD, A. P. 1981. Sexually dimorphic motor nucleus in the rat lumbar spinal cord: response to adult hormone manipulation, absence in androgen-insensitive rats. *Brain Res,* 225**,** 297-307.

BREHMER, A., RUPPRECHT, H. & NEUHUBER, W. 2010. Two submucosal nerve plexus in human intestines. *Histochem Cell Biol,* 133**,** 149-61.

BRIERLEY, S. M., HIBBERD, T. J. & SPENCER, N. J. 2018. Spinal Afferent Innervation of the Colon and Rectum. *Frontiers in cellular neuroscience,* 12**,** 467-467.

BROADWELL, R. D. & BLEIER, R. 1976. A cytoarchitectonic atlas of the mouse hypothalamus. *Journal of Comparative Neurology,* 167**,** 315-339.

BROOKES, S. J., SONG, Z. M., RAMSAY, G. A. & COSTA, M. 1995. Long aboral projections of Dogiel type II, AH neurons within the myenteric plexus of the guinea pig small intestine. *J Neurosci,* 15**,** 4013-22.

BROWNING, K. N. & TRAVAGLI, R. A. 2014. Central nervous system control of gastrointestinal motility and secretion and modulation of gastrointestinal functions. *Comprehensive Physiology,* 4**,** 1339-1368.

BRUHN, T. O., ANTHONY, E. L. P., WU, P. & JACKSON, I. M. D. 1987. GRF immunoreactive neurons in the paraventricular nucleus

of the rat: an immunohistochemical study with monoclonal and polyclonal antibodies. *Brain Research,* 424**,** 290-298.
BRUMOVSKY, P. R., LA, J.-H. & GEBHART, G. F. 2014. Distribution across tissue layers of extrinsic nerves innervating the mouse colorectum - an in vitro anterograde tracing study. *Neurogastroenterology and motility : the official journal of the European Gastrointestinal Motility Society,* 26**,** 1494-1507.
BRUMOVSKY, P. R., LA, J. H., MCCARTHY, C. J., HÖKFELT, T. & GEBHART, G. F. 2012. Dorsal root ganglion neurons innervating pelvic organs in the mouse express tyrosine hydroxylase. *Neuroscience,* 223**,** 77-91.
BURNSTOCK, G. 2009. Purinergic mechanosensory transduction and visceral pain. *Mol Pain,* 5**,** 69.
CADENAS, E. & DAVIES, K. J. A. 2000. Mitochondrial free radical generation, oxidative stress, and aging11This article is dedicated to the memory of our dear friend, colleague, and mentor Lars Ernster (1920–1998), in gratitude for all he gave to us. *Free Radical Biology and Medicine,* 29**,** 222-230.
CALZA, L., GIARDINO, L., VELARDO, A., BATTISTINI, N. & MARRAMA, P. 1990. Influence of aging on the neurochemical organization of the rat paraventricular nucleus. *J Chem Neuroanat,* 3**,** 215-31.
CAMILLERI, M., LEE, J. S., VIRAMONTES, B., BHARUCHA, A. E. & TANGALOS, E. G. 2000. Insights into the pathophysiology and mechanisms of constipation, irritable bowel syndrome, and diverticulosis in older people. *J Am Geriatr Soc,* 48**,** 1142-50.
CAMPBELL, A. J., REINKEN, J. & MCCOSH, L. 1985. Incontinence in the elderly: prevalence and prognosis. *Age Ageing,* 14**,** 65-70.
CAPECE, M. L., BAGHDOYAN, H. A. & LYDIC, R. 1998. Opioids activate G proteins in REM sleep-related brain stem nuclei of rat. *Neuroreport,* 9**,** 3025-8.
CARLSTEDT, A., NORDGREN, S., FASTH, S., APPELGREN, L. & HULTEN, L. 1988. Sympathetic nervous influence on the internal anal sphincter and rectum in man. *Int J Colorectal Dis,* 3**,** 90-5.
CARTER, M. E., YIZHAR, O., CHIKAHISA, S., NGUYEN, H., ADAMANTIDIS, A., NISHINO, S., DEISSEROTH, K. & DE LECEA, L.

2010. Tuning arousal with optogenetic modulation of locus coeruleus neurons. *Nat Neurosci,* 13**,** 1526-33.

CASTEL, M. & MORRIS, J. F. 1988. The neurophysin-containing innervation of the forebrain of the mouse. *Neuroscience,* 24**,** 937-66.

CAULEY, C. E., SAVITT, L. R., WEINSTEIN, M., WAKAMATSU, M. M., KUNITAKE, H., RICCIARDI, R., STALLER, K. & BORDEIANOU, L. 2019. A Quality-of-Life Comparison of Two Fecal Incontinence Phenotypes: Isolated Fecal Incontinence Versus Concurrent Fecal Incontinence With Constipation. *Dis Colon Rectum,* 62**,** 63-70.

CECHETTO, D. F. & SAPER, C. B. 1988. Neurochemical organization of the hypothalamic projection to the spinal cord in the rat. *J Comp Neurol,* 272**,** 579-604.

CHANCELLOR, M. B. & YOSHIMURA, N. 2004. Neurophysiology of stress urinary incontinence. *Reviews in urology,* 6 Suppl 3**,** S19-S28.

CHASSAGNE, P., JEGO, A., GLOC, P., CAPET, C., TRIVALLE, C., DOUCET, J., DENIS, P. & BERCOFF, E. 2000. Does treatment of constipation improve faecal incontinence in institutionalized elderly patients? *Age Ageing,* 29**,** 159-64.

CHASSAGNE, P., LANDRIN, I., NEVEU, C., CZERNICHOW, P., BOUANICHE, M., DOUCET, J., DENIS, P. & BERCOFF, E. 1999. Fecal incontinence in the institutionalized elderly: incidence, risk factors, and prognosis. *Am J Med,* 106**,** 185-90.

CHEE, C. A., ROOZENDAAL, B., SWAAB, D. F., GOUDSMIT, E. & MIRMIRAN, M. 1988. Vasoactive intestinal polypeptide neuron changes in the senile rat suprachiasmatic nucleus. *Neurobiol Aging,* 9**,** 307-12.

CHEENEY, G., NGUYEN, M., VALESTIN, J. & RAO, S. S. 2012. Topographic and manometric characterization of the recto-anal inhibitory reflex. *Neurogastroenterol Motil,* 24**,** e147-54.

CHEN, G., KROEMER, G. & KEPP, O. 2020. Mitophagy: An Emerging Role in Aging and Age-Associated Diseases. *Frontiers in cell and developmental biology,* 8**,** 200-200.

CHEN, Q. & PAN, H. L. 2006. Regulation of synaptic input to hypothalamic presympathetic neurons by GABA(B) receptors. *Neuroscience,* 142**,** 595-606.

CHENG, L. K., O'GRADY, G., DU, P., EGBUJI, J. U., WINDSOR, J. A. & PULLAN, A. J. 2010. Gastrointestinal system. *Wiley interdisciplinary reviews. Systems biology and medicine,* 2**,** 65-79.

CHISTIAKOV, D. A., SOBENIN, I. A., REVIN, V. V., OREKHOV, A. N. & BOBRYSHEV, Y. V. 2014. Mitochondrial Aging and Age-Related Dysfunction of Mitochondria. *BioMed Research International,* 2014**,** 238463.

CHITRAVANSHI, V. C., KAWABE, K. & SAPRU, H. N. 2016. Stimulation of the hypothalamic arcuate nucleus increases brown adipose tissue nerve activity via hypothalamic paraventricular and dorsomedial nuclei. *Am J Physiol Heart Circ Physiol,* 311**,** H433-44.

CHOI, E. P. H., WAN, E. Y. F., CHIN, W. Y. & LAM, C. L. K. 2020. Lower urinary tract symptoms and health-related quality of life in Hong Kong primary care: a cross-sectional study. *Qual Life Res*.

CHRISTIANSON, J. A., LIANG, R., USTINOVA, E. E., DAVIS, B. M., FRASER, M. O. & PEZZONE, M. A. 2007. Convergence of bladder and colon sensory innervation occurs at the primary afferent level. *Pain,* 128**,** 235-243.

CHRISTIANSON, J. A., TRAUB, R. J. & DAVIS, B. M. 2006. Differences in spinal distribution and neurochemical phenotype of colonic afferents in mouse and rat. *J Comp Neurol,* 494**,** 246-59.

CHUGHTAI, B., THOMAS, D., RUSSELL, D., PHONGTANKUEL, V., BOWLES, K. & PRIGERSON, H. 2019. Prevalence and Risk Factors for Fecal Incontinence in Home Hospice. *Am J Hosp Palliat Care,* 36**,** 33-37.

CHUN, A. L., WALLACE, L. J., GERALD, M. C., LEVIN, R. M. & WEIN, A. J. 1988. Effect of age on in vivo urinary bladder function in the rat. *J Urol,* 139**,** 625-7.

CHUN, A. L., WALLACE, L. J., GERALD, M. C., WEIN, A. J. & LEVIN, R. M. 1989. Effects of age on urinary bladder function in the male rat. *J Urol,* 141**,** 170-3.

CHUN, A. L., WEIN, A. J., HARKAWAY, R. & LEVIN, R. M. 1990. Comparison of urinary bladder function in sexually mature and immature male and female rats. *J Urol,* 143**,** 1267-71.

COBINE, C. A., FONG, M., HAMILTON, R. & KEEF, K. D. 2007. Species dependent differences in the actions of sympathetic nerves and noradrenaline in the internal anal sphincter. *Neurogastroenterol Motil,* 19**,** 937-45.

COBINE, C. A., HANNAH, E. E., ZHU, M. H., LYLE, H. E., ROCK, J. R., SANDERS, K. M., WARD, S. M. & KEEF, K. D. 2017. ANO1 in intramuscular interstitial cells of Cajal plays a key role in the generation of slow waves and tone in the internal anal sphincter. *The Journal of physiology,* 595**,** 2021-2041.

COCKAYNE, D. A., HAMILTON, S. G., ZHU, Q. M., DUNN, P. M., ZHONG, Y., NOVAKOVIC, S., MALMBERG, A. B., CAIN, G., BERSON, A., KASSOTAKIS, L., HEDLEY, L., LACHNIT, W. G., BURNSTOCK, G., MCMAHON, S. B. & FORD, A. P. 2000. Urinary bladder hyporeflexia and reduced pain-related behaviour in P2X3-deficient mice. *Nature,* 407**,** 1011-5.

COLLERTON, J., DAVIES, K., JAGGER, C., KINGSTON, A., BOND, J., ECCLES, M. P., ROBINSON, L. A., MARTIN-RUIZ, C., VON ZGLINICKI, T., JAMES, O. F. W. & KIRKWOOD, T. B. L. 2009. Health and disease in 85 year olds: baseline findings from the Newcastle 85+ cohort study. *BMJ,* 339**,** b4904.

COLOPLAST. 2016. *The cost of constipation report* [Online]. Available: https://www.coloplast.co.uk/Global/UK/Continence/Cost_of_Constipation_Report_FINAL.pdf [Accessed].

CONDON, M., MANNION, E., MOLLOY, D. W. & O'CAOIMH, R. 2019. Urinary and Faecal Incontinence: Point Prevalence and Predictors in a University Hospital. *Int J Environ Res Public Health,* 16.

CORNWALL, J., COOPER, J. D. & PHILLIPSON, O. T. 1990. Afferent and efferent connections of the laterodorsal tegmental nucleus in the rat. *Brain Res Bull,* 25**,** 271-84.

COSTA, M., KEIGHTLEY, L. J., WIKLENDT, L., HIBBERD, T. J., ARKWRIGHT, J. W., OMARI, T., WATTCHOW, D. A., BROOKES, S. J. H., DINNING, P. G. & SPENCER, N. J. 2019. Identification of

multiple distinct neurogenic motor patterns that can occur simultaneously in the guinea pig distal colon. *Am J Physiol Gastrointest Liver Physiol,* 316, G32-g44.

COYNE, K. S., KVASZ, M., IRELAND, A. M., MILSOM, I., KOPP, Z. S. & CHAPPLE, C. R. 2012. Urinary incontinence and its relationship to mental health and health-related quality of life in men and women in Sweden, the United Kingdom, and the United States. *Eur Urol,* 61, 88-95.

CSÁKI, Á., KOCSIS, K., HALÁSZ, B. & KISS, J. 2000. Localization of glutamatergic/aspartatergic neurons projecting to the hypothalamic paraventricular nucleus studied by retrograde transport of [3H]d-aspartate autoradiography. *Neuroscience,* 101, 637-655.

CSERVENAK, M., KELLER, D., KIS, V., FAZEKAS, E. A., OLLOS, H., LEKO, A. H., SZABO, E. R., RENNER, E., USDIN, T. B., PALKOVITS, M. & DOBOLYI, A. 2017. A Thalamo-Hypothalamic Pathway That Activates Oxytocin Neurons in Social Contexts in Female Rats. *Endocrinology,* 158, 335-348.

CUI, L. N., CODERRE, E. & RENAUD, L. P. 2001. Glutamate and GABA mediate suprachiasmatic nucleus inputs to spinal-projecting paraventricular neurons. *Am J Physiol Regul Integr Comp Physiol,* 281, R1283-9.

CUI, Z., GERFEN, C. R. & YOUNG, W. S., 3RD 2013. Hypothalamic and other connections with dorsal CA2 area of the mouse hippocampus. *The Journal of comparative neurology,* 521, 1844-1866.

DE GROAT, W. C. 1998. Anatomy of the Central Neural Pathways Controlling the Lower Urinary Tract. *European Urology,* 34(suppl 1), 2-5.

DE GROAT, W. C., GRIFFITHS, D. & YOSHIMURA, N. 2015. Neural control of the lower urinary tract. *Comprehensive Physiology,* 5, 327-396.

DE GROAT, W. C. & KRIER, J. 1976. An electrophysiological study of the sacral parasympathetic pathway to the colon of the cat. *The Journal of Physiology,* 260, 425-445.

DE GROAT, W. C. & KRIER, J. 1978. The sacral parasympathetic reflex pathway regulating colonic motility and defaecation in the cat. *The Journal of physiology,* 276**,** 481-500.

DE GROAT, W. C. & WICKENS, C. 2013. Organization of the neural switching circuitry underlying reflex micturition. *Acta Physiol (Oxf),* 207**,** 66-84.

DE GROAT, W. C. & YOSHIMURA, N. 2001. Pharmacology of the lower urinary tract. *Annu Rev Pharmacol Toxicol,* 41**,** 691-721.

DE GROAT, W. C. & YOSHIMURA, N. 2009. Afferent nerve regulation of bladder function in health and disease. *Handbook of experimental pharmacology*, 91-138.

DEGROOT, J., VERZIJL, N., WENTING-VAN WIJK, M. J., BANK, R. A., LAFEBER, F. P., BIJLSMA, J. W. & TEKOPPELE, J. M. 2001. Age-related decrease in susceptibility of human articular cartilage to matrix metalloproteinase-mediated degradation: the role of advanced glycation end products. *Arthritis Rheum,* 44**,** 2562-71.

DENNISON, C., PRASAD, M., LLOYD, A., BHATTACHARYYA, S. K., DHAWAN, R. & COYNE, K. 2005. The health-related quality of life and economic burden of constipation. *PharmacoEconomics,* 23**,** 461-476.

DERING, M. A., SANTER, R. M. & WATSON, A. H. 1996. Age-related changes in the morphology of preganglionic neurons projecting to the rat hypogastric ganglion. *J Neurocytol,* 25**,** 555-63.

DERING, M. A., SANTER, R. M. & WATSON, A. H. 1998. Age-related changes in the morphology of preganglionic neurons projecting to the paracervical ganglion of nulliparous and multiparous rats. *Brain Res,* 780**,** 245-52.

DESPOTOVIC, S. Z., MILICEVIC, N. M., MILOSEVIC, D. P., DESPOTOVIC, N., ERCEG, P., SVORCAN, P., SCHUMACHER, U., ULLRICH, S., MIHAJLOVIC, G., KALEM, D., MARKOVIC, S., LALIC, I. M., KRMPOT, A. J., RABASOVIC, M. D., PANTELIC, D. V., JOVANIC, S. Z., ROSCH, T. & MILICEVIC, Z. 2017. Remodeling of extracellular matrix of the lamina propria in the uninvolved human rectal mucosa 10 and 20 cm away from the malignant tumor. *Tumour Biol,* 39**,** 1010428317711654.

DI MARZO, V., STELLA, N. & ZIMMER, A. 2015. Endocannabinoid signalling and the deteriorating brain. *Nature reviews. Neuroscience,* 16, 30-42.

DIENE, L. D., COSTA-FERRO, Z. S. M., BARBOSA, S., MILANESI, B. B., LAZZARI, G. Z., NEVES, L. T., PAZ, L. V., NEVES, P. F. R., BATTISTI, V., MARTINS, L. A., GEHLEN, G., MESTRINER, R. G., DA COSTA, J. C. & XAVIER, L. L. 2019. Selective brain neuronal and glial losses without changes in GFAP immunoreactivity: Young versus mature adult Wistar rats. *Mechanisms of Ageing and Development,* 182, 111128.

DING, Y.-Q., WANG, D., XU, J.-Q. & JU, G. 1999. Direct projections from the medial preoptic area to spinally-projecting neurons in Barrington's nucleus: an electron microscope study in the rat. *Neuroscience Letters,* 271, 175-178.

DING, Y.-Q., ZHENG, H.-X., GONG, L.-W., LU, Y., ZHAO, H. & QIN, B.-Z. 1997. Direct projections from the lumbosacral spinal cord to Barrington's nucleus in the rat: A special reference to micturition reflex. *Journal of Comparative Neurology,* 389, 149-160.

DIXON, J. S., GILPIN, S. A., GILPIN, C. J. & GOSLING, J. A. 1983. Intramural ganglia of the human urinary bladder. *Br J Urol,* 55, 195-8.

DOBBERFUHL, A. D., OTI, T., SAKAMOTO, H. & MARSON, L. 2014. Identification of CNS Neurons Innervating the Levator Ani and Ventral Bulbospongiosus Muscles in Male Rats. *The Journal of Sexual Medicine,* 11, 664-677.

DOCKRAY, G. J. 2013. Enteroendocrine cell signalling via the vagus nerve. *Curr Opin Pharmacol,* 13, 954-8.

DORFMAN, V. B., VEGA, M. C. & COIRINI, H. 2006. Age-related changes of the GABA-B receptor in the lumbar spinal cord of male rats and penile erection. *Life Sci,* 78, 1529-34.

DOROFEEVA, A. A. & PANTELEEV, S. S. 2007. [Motor responses of the colon to stimulation of the sacral parasympathetic nucleus neurons]. *Ross Fiziol Zh Im I M Sechenova,* 93, 1188-95.

DOROFEEVA, A. A., PANTELEEV, S. S. & MAKAROV, F. N. 2009. Involvement of the sacral parasympathetic nucleus in the

innervation of the descending colon and rectum in cats. *Neuroscience and Behavioral Physiology,* 39**,** 207-210.
DOU, X. L., QIN, R. L., QU, J., LIAO, Y. H., LU, Y. C., ZHANG, T., SHAO, C. & LI, Y. Q. 2013. Synaptic connections between endomorphin 2-immunoreactive terminals and μ-opioid receptor-expressing neurons in the sacral parasympathetic nucleus of the rat. *PloS one,* 8**,** e62028-e62028.
DOUGHERTY, J. M. & AEDDULA, N. R. 2019. Male Urinary Retention. *StatPearls.* Treasure Island (FL): StatPearls Publishing

StatPearls Publishing LLC.
DRAKE, M. J., FOWLER, C. J., GRIFFITHS, D., MAYER, E., PATON, J. F. & BIRDER, L. 2010. Neural control of the lower urinary and gastrointestinal tracts: supraspinal CNS mechanisms. *Neurourol Urodyn,* 29**,** 119-27.
DRAY, A. & METSCH, R. 1984. Inhibition of urinary bladder contractions by a spinal action of morphine and other opioids. *The Journal of pharmacology and experimental therapeutics,* 231**,** 254-260.
DROLET, G., VAN BOCKSTAELE, E. J. & ASTON-JONES, G. 1992. Robust enkephalin innervation of the locus coeruleus from the rostral medulla. *J Neurosci,* 12**,** 3162-74.
DROSSAERTS, J., VRIJENS, D., LEUE, C., SCHILDERS, I., VAN KERREBROECK, P. & VAN KOEVERINGE, G. 2016. Screening for depression and anxiety in patients with storage or voiding dysfunction: A retrospective cohort study predicting outcome of sacral neuromodulation. *Neurourol Urodyn,* 35**,** 1011-1016.
DRUMM, B. T., HWANG, S. J., BAKER, S. A., WARD, S. M. & SANDERS, K. M. 2019. Ca2+ signalling behaviours of intramuscular interstitial cells of Cajal in the murine colon. *The Journal of Physiology,* 597**,** 3587-3617.
DUONG, M., DOWNIE, J. W. & DU, H. J. 1999. Transmission of afferent information from urinary bladder, urethra and perineum to periaqueductal gray of cat. *Brain Res,* 819**,** 108-19.
DURNIN, L., LEES, A., MANZOOR, S., SASSE, K. C., SANDERS, K. M. & MUTAFOVA-YAMBOLIEVA, V. N. 2017. Loss of nitric oxide-mediated inhibition of purine neurotransmitter release in the

colon in the absence of interstitial cells of Cajal. *Am J Physiol Gastrointest Liver Physiol,* 313**,** G419-g433.
DYKENS, J. A. 1994. Isolated Cerebral and Cerebellar Mitochondria Produce Free Radicals when Exposed to Elevated Ca2+ and Na+: Implications for Neurodegeneration. *Journal of Neurochemistry,* 63**,** 584-591.
DZIECIATKOWSKA, M., HILL, R. & HANSEN, K. C. 2014. GeLC-MS/MS analysis of complex protein mixtures. *Methods in molecular biology (Clifton, N.J.),* 1156**,** 53-66.
ELAM, M., THORÉN, P. & SVENSSON, T. H. 1986. Locus coeruleus neurons and sympathetic nerves: Activation by visceral afferents. *Brain Research,* 375**,** 117-125.
EMBERTON, M. & ANSON, K. 1999. Acute urinary retention in men: an age old problem. *Bmj,* 318**,** 921-5.
EMMANUEL, A. 2019. Neurogenic bowel dysfunction. *F1000Res,* 8.
ENGELSTOFT, M. S., EGEROD, K. L., HOLST, B. & SCHWARTZ, T. W. 2008. A gut feeling for obesity: 7TM sensors on enteroendocrine cells. *Cell Metab,* 8**,** 447-9.
EYIGOR, O., CENTERS, A. & JENNES, L. 2001. Distribution of ionotropic glutamate receptor subunit mRNAs in the rat hypothalamus. *Journal of Comparative Neurology,* 434**,** 101-124.
FARAGE, M. A., MILLER, K. W., BERARDESCA, E. & MAIBACH, H. I. 2008. Psychosocial and societal burden of incontinence in the aged population: a review. *Arch Gynecol Obstet,* 277**,** 285-90.
FARGO, K. N., IWEMA, C. L., CLARK-PHELPS, M. C. & SENGELAUB, D. R. 2007. Exogenous testosterone reverses age-related atrophy in a spinal neuromuscular system. *Horm Behav,* 51**,** 20-30.
FILIPP, F. V., SCOTT, D. A., RONAI, Z. E. A., OSTERMAN, A. L. & SMITH, J. W. 2012. Reverse TCA cycle flux through isocitrate dehydrogenases 1 and 2 is required for lipogenesis in hypoxic melanoma cells. *Pigment cell & melanoma research,* 25**,** 375-383.
FINKBEINER, A. E. 1993. The aging bladder. *International Urogynecology Journal,* 4**,** 168-174.

FLEMING, V. & WADE, W. E. 2010. A review of laxative therapies for treatment of chronic constipation in older adults. *Am J Geriatr Pharmacother,* 8**,** 514-50.

FODOR, M., KORDON, C. & EPELBAUM, J. 2006. Anatomy of the hypophysiotropic somatostatinergic and growth hormone-releasing hormone system minireview. *Neurochem Res,* 31**,** 137-43.

FOUNTOULAKIS, M., JURANVILLE, J. F. & MANNEBERG, M. 1992. Comparison of the Coomassie brilliant blue, bicinchoninic acid and Lowry quantitation assays, using non-glycosylated and glycosylated proteins. *J Biochem Biophys Methods,* 24**,** 265-74.

FOWLER, C. J., GRIFFITHS, D. & DE GROAT, W. C. 2008. The neural control of micturition. *Nature reviews. Neuroscience,* 9**,** 453-466.

FRENCKNER, B. 1975. Function of the anal sphincters in spinal man. *Gut,* 16**,** 638-44.

FRITSCH, H., BRENNER, E., LIENEMANN, A. & LUDWIKOWSKI, B. 2002. Anal sphincter complex: reinterpreted morphology and its clinical relevance. *Dis Colon Rectum,* 45**,** 188-94.

FU, M. & ZHANG, J. 1997. The discovery and a study of the adventitia rectalis, a fibrous layer of the rectal wall. *J Pediatr Surg,* 32**,** 7-11.

FUNABASHI, T. & KIMURA, F. 1995. The number of luteinizing hormone-releasing hormone immunoreactive neurons is significantly decreased in the forebrain of old-aged female rats. *Neurosci Lett,* 189**,** 85-8.

FURNESS, J. B., CALLAGHAN, B. P., RIVERA, L. R. & CHO, H.-J. 2014. The Enteric Nervous System and Gastrointestinal Innervation: Integrated Local and Central Control. *In:* LYTE, M. & CRYAN, J. F. (eds.) *Microbial Endocrinology: The Microbiota-Gut-Brain Axis in Health and Disease.* New York, NY: Springer New York.

FURNESS, J. B., KUNZE, W. A., BERTRAND, P. P., CLERC, N. & BORNSTEIN, J. C. 1998. Intrinsic primary afferent neurons of the intestine. *Prog Neurobiol,* 54**,** 1-18.

FURNESS, J. B., LLOYD, K. C., STERNINI, C. & WALSH, J. H. 1990. Projections of substance P, vasoactive intestinal peptide and tyrosine hydroxylase immunoreactive nerve fibres in the

canine intestine, with special reference to the innervation of the circular muscle. *Arch Histol Cytol,* 53**,** 129-40.

FURUTA, A., ASANO, K., EGAWA, S., DE GROAT, W. C., CHANCELLOR, M. B. & YOSHIMURA, N. 2009. Role of alpha2-adrenoceptors and glutamate mechanisms in the external urethral sphincter continence reflex in rats. *The Journal of urology,* 181**,** 1467-1473.

G:PROFILER. 2020. *g:GOSt* [Online]. Available: https://biit.cs.ut.ee/gprofiler/gost [Accessed].

GABELLA, G. 2001. Development and ageing of intestinal musculature and nerves: the guinea-pig taenia coli. *J Neurocytol,* 30**,** 733-66.

GADECKA, A. & BIELAK-ZMIJEWSKA, A. 2019. Slowing Down Ageing: The Role of Nutrients and Microbiota in Modulation of the Epigenome. *Nutrients,* 11**,** 1251.

GALLEGOS-OROZCO, J. F., FOXX-ORENSTEIN, A. E., STERLER, S. M. & STOA, J. M. 2012. Chronic constipation in the elderly. *Am J Gastroenterol,* 107**,** 18-25; quiz 26.

GAMAGE, P. P., RANSON, R. N., PATEL, B. A., YEOMAN, M. S. & SAFFREY, M. J. 2013. Myenteric neuron numbers are maintained in aging mouse distal colon. *Neurogastroenterol Motil,* 25**,** e495-e505.

GARAVOGLIA, M., BORGHI, F. & LEVI, A. C. 1993. Arrangement of the anal striated musculature. *Dis Colon Rectum,* 36**,** 10-5.

GAUDE, E., SCHMIDT, C., GAMMAGE, P. A., DUGOURD, A., BLACKER, T., CHEW, S. P., SAEZ-RODRIGUEZ, J., O'NEILL, J. S., SZABADKAI, G., MINCZUK, M. & FREZZA, C. 2018. NADH Shuttling Couples Cytosolic Reductive Carboxylation of Glutamine with Glycolysis in Cells with Mitochondrial Dysfunction. *Mol Cell,* 69**,** 581-593.e7.

GEERLING, J. C., SHIN, J.-W., CHIMENTI, P. C. & LOEWY, A. D. 2010. Paraventricular hypothalamic nucleus: axonal projections to the brainstem. *The Journal of comparative neurology,* 518**,** 1460-1499.

GEOUI, T., URLAUB, H., PLESSMANN, U. & PORSCHEWSKI, P. 2010. Extraction of proteins from formalin-fixed, paraffin-embedded tissue using the Qproteome extraction technique and

preparation of tryptic peptides for liquid chromatography/mass spectrometry analysis. *Curr Protoc Mol Biol,* Chapter 10**,** Unit 10.27.1-12.

GERAEDTS, M. C., TAKAHASHI, T., VIGUES, S., MARKWARDT, M. L., NKOBENA, A., COCKERHAM, R. E., HAJNAL, A., DOTSON, C. D., RIZZO, M. A. & MUNGER, S. D. 2012. Transformation of postingestive glucose responses after deletion of sweet taste receptor subunits or gastric bypass surgery. *Am J Physiol Endocrinol Metab,* 303**,** E464-74.

GERENDAI, I., TOTH, I. E., KOCSIS, K., BOLDOGKOI, Z., RUSVAI, M. & HALASZ, B. 2001. Identification of CNS neurons involved in the innervation of the epididymis: a viral transneuronal tracing study. *Auton Neurosci,* 92**,** 1-10.

GERENDAI, I., WIESEL, O., TOTH, I. E., BOLDOGKOI, Z. S., RUSVAI, M. & HALASZ, B. 2003. Identification of neurones of the brain and spinal cord involved in the innervation of the ductus deferens using the viral tracing method. *Int J Androl,* 26**,** 91-100.

GIACOMELLO, M., PYAKUREL, A., GLYTSOU, C. & SCORRANO, L. 2020. The cell biology of mitochondrial membrane dynamics. *Nature Reviews Molecular Cell Biology,* 21**,** 204-224.

GIBBONS, C. P., TROWBRIDGE, E. A., BANNISTER, J. J. & READ, N. W. 1988. The mechanics of the anal sphincter complex. *Journal of Biomechanics,* 21**,** 601-604.

GIBSON, S. J., POLAK, J. M., BLOOM, S. R. & WALL, P. D. 1981. The distribution of nine peptides in rat spinal cord with special emphasis on the substantia gelatinosa and on the area around the central canal (lamina X). *J Comp Neurol,* 201**,** 65-79.

GILPIN, C. J., DIXON, J. S., GILPIN, S. A. & GOSLING, J. A. 1983. The fine structure of autonomic neurons in the wall of the human urinary bladder. *Journal of anatomy,* 137 (Pt 4)**,** 705-713.

GIULIANO, F., BERNABE, J., MCKENNA, K., LONGUEVILLE, F. & RAMPIN, O. 2001. Spinal proerectile effect of oxytocin in anesthetized rats. *Am J Physiol Regul Integr Comp Physiol,* 280**,** R1870-7.

GOLDMAN, G. & COLEMAN, P. D. 1981. Neuron numbers in locus coeruleus do not change with age in fisher 344 rat. *Neurobiology of Aging,* 2**,** 33-36.

GRAHAM, M. F., DIEGELMANN, R. F., ELSON, C. O., LINDBLAD, W. J., GOTSCHALK, N., GAY, S. & GAY, R. 1988. Collagen content and types in the intestinal strictures of Crohn's disease. *Gastroenterology,* 94**,** 257-65.

GREENWOOD-VAN MEERVELD, B., JOHNSON, A. C. & GRUNDY, D. 2017. Gastrointestinal Physiology and Function. *Handb Exp Pharmacol,* 239**,** 1-16.

GRIFFITHS, D., TADIC, S. D., SCHAEFER, W. & RESNICK, N. M. 2007. Cerebral control of the bladder in normal and urge-incontinent women. *NeuroImage,* 37**,** 1-7.

GRIFFITHS, D. J. & FOWLER, C. J. 2013. The micturition switch and its forebrain influences. *Acta Physiol (Oxf),* 207**,** 93-109.

GRIFFITHS, D. J., TADIC, S. D., SCHAEFER, W. & RESNICK, N. M. 2009. Cerebral control of the lower urinary tract: how age-related changes might predispose to urge incontinence. *NeuroImage,* 47**,** 981-986.

GRILL, W. M., EROKWU, B. O., HADZIEFENDIC, S. & HAXHIU, M. A. 1999. Extended survival time following pseudorabies virus injection labels the suprapontine neural network controlling the bladder and urethra in the rat. *Neurosci Lett,* 270**,** 63-6.

GRONEBERG, D., LIES, B., KONIG, P., JAGER, R., SEIDLER, B., KLEIN, S., SAUR, D. & FRIEBE, A. 2013. Cell-specific deletion of nitric oxide-sensitive guanylyl cyclase reveals a dual pathway for nitrergic neuromuscular transmission in the murine fundus. *Gastroenterology,* 145**,** 188-196.

GUO, Y. X., LI, D. P., CHEN, S. R. & PAN, H. L. 2013. Distinct intrinsic and synaptic properties of pre-sympathetic and pre-parasympathetic output neurons in Barrington's nucleus. *J Neurochem,* 126**,** 338-48.

GUPTA, D. & MORLEY, J. E. 2014. Hypothalamic-pituitary-adrenal (HPA) axis and aging. *Compr Physiol,* 4**,** 1495-510.

GUYENET, P. G. & AGHAJANIAN, G. K. 1979. ACh, substance P and met-enkephalin in the locus coeruleus: Pharmacological evidence for independent sites of action. *European Journal of Pharmacology,* 53**,** 319-328.

HABIB, A. M., RICHARDS, P., CAIRNS, L. S., ROGERS, G. J., BANNON, C. A., PARKER, H. E., MORLEY, T. C., YEO, G. S., REIMANN, F. &

GRIBBLE, F. M. 2012. Overlap of endocrine hormone expression in the mouse intestine revealed by transcriptional profiling and flow cytometry. *Endocrinology,* 153**,** 3054-65.

HALBROOK, C. J., NWOSU, Z. C. & LYSSIOTIS, C. A. 2018. Fine-Tuning Mitochondrial Dysfunction and Reductive Carboxylation. *Trends in Endocrinology & Metabolism,* 29**,** 599-602.

HAMILTON, M. O., PAPKA, R. E., O'DONOGHUE, D. L., VAIDYA, A. M., WILLIAMS, S. J., POFF, C. R. & MCNEILL, D. L. 1995. Spinal projection neurons to the laterodorsal pontine tegmental nucleus: relationship to preganglionic neurons and nitric oxide synthase. *J Comp Neurol,* 353**,** 1-8.

HAMILTON, W., LANCASHIRE, R., SHARP, D., PETERS, T. J., CHENG, K. K. & MARSHALL, T. 2009. The risk of colorectal cancer with symptoms at different ages and between the sexes: a case-control study. *BMC Medicine,* 7**,** 17.

HANSE, E. A., RUAN, C., KACHMAN, M., WANG, D., LOWMAN, X. H. & KELEKAR, A. 2017. Cytosolic malate dehydrogenase activity helps support glycolysis in actively proliferating cells and cancer. *Oncogene,* 36**,** 3915-3924.

HANSEN, J. L., BLISS, D. Z. & PEDEN-MCALPINE, C. 2006. Diet strategies used by women to manage fecal incontinence. *J Wound Ostomy Continence Nurs,* 33**,** 52-61; discussion 61-2.

HARDCASTLE, J. D. & MANN, C. V. 1968. Study of large bowel peristalsis. *Gut,* 9**,** 512-20.

HARMAN, D. 1989. Lipofuscin and ceroid formation: the cellular recycling system. *Advances in experimental medicine and biology,* 266**,** 3-15.

HARRINGTON, A. M., CARABALLO, S. G., MADDERN, J. E., GRUNDY, L., CASTRO, J. & BRIERLEY, S. M. 2019. Colonic afferent input and dorsal horn neuron activation differs between the thoracolumbar and lumbosacral spinal cord. *Am J Physiol Gastrointest Liver Physiol,* 317**,** G285-g303.

HASCUP, E. R., WANG, F., KOPCHICK, J. J. & BARTKE, A. 2016. Inflammatory and Glutamatergic Homeostasis Are Involved in Successful Aging. *The journals of gerontology. Series A, Biological sciences and medical sciences,* 71**,** 281-289.

HAUS, J. M., CARRITHERS, J. A., TRAPPE, S. W. & TRAPPE, T. A. 2007. Collagen, cross-linking, and advanced glycation end products in aging human skeletal muscle. *J Appl Physiol (1985),* 103**,** 2068-76.

HE, Z.-G., WANG, Q., XIE, R.-S., LI, Y.-S., HONG, Q.-X. & XIANG, H.-B. 2018. Neuroanatomical autonomic substrates of brainstem-gut circuitry identified using transsynaptic tract-tracing with pseudorabies virus recombinants. *American journal of clinical and experimental immunology,* 7**,** 16-24.

HEPPNER, T. J., TYKOCKI, N. R., HILL-EUBANKS, D. & NELSON, M. T. 2016. Transient contractions of urinary bladder smooth muscle are drivers of afferent nerve activity during filling. *The Journal of general physiology,* 147**,** 323-335.

HERMAN, J. P., EYIGOR, O., ZIEGLER, D. R. & JENNES, L. 2000. Expression of ionotropic glutamate receptor subunit mRNAs in the hypothalamic paraventricular nucleus of the rat. *Journal of Comparative Neurology,* 422**,** 352-362.

HERMAN, J. P., MUELLER, N. K. & FIGUEIREDO, H. 2004. Role of GABA and glutamate circuitry in hypothalamo-pituitary-adrenocortical stress integration. *Ann N Y Acad Sci,* 1018**,** 35-45.

HERMAN, J. P., TASKER, J. G., ZIEGLER, D. R. & CULLINAN, W. E. 2002. Local circuit regulation of paraventricular nucleus stress integration: glutamate-GABA connections. *Pharmacol Biochem Behav,* 71**,** 457-68.

HERMES, M. L., CODERRE, E. M., BUIJS, R. M. & RENAUD, L. P. 1996. GABA and glutamate mediate rapid neurotransmission from suprachiasmatic nucleus to hypothalamic paraventricular nucleus in rat. *The Journal of Physiology,* 496**,** 749-757.

HERRITY, A. N., RAU, K. K., PETRUSKA, J. C., STIRLING, D. P. & HUBSCHER, C. H. 2014. Identification of bladder and colon afferents in the nodose ganglia of male rats. *J Comp Neurol,* 522**,** 3667-82.

HETZ, S., ACIKGOEZ, A., MOLL, C., JAHNKE, H. G., ROBITZKI, A. A., METZGER, R. & METZGER, M. 2014. Age-related gene expression analysis in enteric ganglia of human colon after laser microdissection. *Front Aging Neurosci,* 6**,** 276.

HIDA, T. & SHIMIZU, N. 1982. The interrelation between the latero-dorsal tegmental area and lumbosacral segments of rats as studied by HRP method. *Arch Histol Jpn,* 45**,** 495-504.

HISAMITSU, T. & DE GROAT, W. C. 1984. The inhibitory effect of opioid peptides and morphine applied intrathecally and intracerebroventricularly on the micturition reflex in the cat. *Brain Research,* 298**,** 51-65.

HOLETS, V. R., HÖKFELT, T., RÖKAEUS, Å., TERENIUS, L. & GOLDSTEIN, M. 1988. Locus coeruleus neurons in the rat containing neuropeptide Y, tyrosine hydroxylase or galanin and their efferent projections to the spinal cord, cerebral cortex and hypothalamus. *Neuroscience,* 24**,** 893-906.

HOLSTEGE, J. 1991. Ultrastructural evidence for GABAergic brain stem projections to spinal motoneurons in the rat. *The Journal of Neuroscience,* 11**,** 159-167.

HOOPS, T. C. & TRABER, P. G. 1997. Molecular pathogenesis of colorectal cancer. *Hematol Oncol Clin North Am,* 11**,** 609-33.

HORROCKS, S., SOMERSET, M., STODDART, H. & PETERS, T. J. 2004. What prevents older people from seeking treatment for urinary incontinence? A qualitative exploration of barriers to the use of community continence services. *Family Practice,* 21**,** 689-696.

HOTTA, H., MORRISON, J. F., SATO, A. & UCHIDA, S. 1995. The effects of aging on the rat bladder and its innervation. *Jpn J Physiol,* 45**,** 823-36.

HOU-YU, A., LAMME, A. T., ZIMMERMAN, E. A. & SILVERMAN, A. J. 1986. Comparative Distribution of Vasopressin and Oxytocin Neurons in the Rat Brain Using a Double-Label Procedure. *Neuroendocrinology,* 44**,** 235-246.

HOU, X. H., HYUN, M., TARANDA, J., HUANG, K. W., TODD, E., FENG, D., ATWATER, E., CRONEY, D., ZEIDEL, M. L., OSTEN, P. & SABATINI, B. L. 2016. Central Control Circuit for Context-Dependent Micturition. *Cell,* 167**,** 73-86.e12.

HSU, H. K. & PENG, M. T. 1978. Hypothalamic neuron number of old female rats. *Gerontology,* 24**,** 434-40.

HUANG, J., CHEN, J., WANG, W., WANG, W., KOSHIMIZU, Y., WEI, Y.-Y., KANEKO, T., LI, Y.-Q. & WU, S.-X. 2010. Neurochemical

properties of enkephalinergic neurons in lumbar spinal dorsal horn revealed by preproenkephalin-green fluorescent protein transgenic mice. *Journal of neurochemistry,* 113, 1555-1564.
HUIZINGA, J. D., THUNEBERG, L., KLUPPEL, M., MALYSZ, J., MIKKELSEN, H. B. & BERNSTEIN, A. 1995. W/kit gene required for interstitial cells of Cajal and for intestinal pacemaker activity. *Nature,* 373, 347-9.
HUNSKAAR, S. & SANDVIK, H. 1993. One hundred and fifty men with urinary incontinence: III. Psychosocial consequences. *Scandinavian Journal of Primary Health Care,* 11, 193-196.
INOUE, W., BAIMOUKHAMETOVA, D. V., FUZESI, T., WAMSTEEKER CUSULIN, J. I., KOBLINGER, K., WHELAN, P. J., PITTMAN, Q. J. & BAINS, J. S. 2013. Noradrenaline is a stress-associated metaplastic signal at GABA synapses. *Nat Neurosci,* 16, 605-12.
IREMONGER, K. J., KUZMISKI, J. B., BAIMOUKHAMETOVA, D. V. & BAINS, J. S. 2011. Dual regulation of anterograde and retrograde transmission by endocannabinoids. *J Neurosci,* 31, 12011-20.
IRWIN, D. E., MUNGAPEN, L., MILSOM, I., KOPP, Z., REEVES, P. & KELLEHER, C. 2009. The economic impact of overactive bladder syndrome in six Western countries. *BJU Int,* 103, 202-9.
ISHIDA, Y., SHIROKAWA, T., KOMATSU, Y. & ISOBE, K. 2001a. Changes in cortical noradrenergic axon terminals of locus coeruleus neurons in aged F344 rats. *Neurosci Lett,* 307, 197-9.
ISHIDA, Y., SHIROKAWA, T., MIYAISHI, O., KOMATSU, Y. & ISOBE, K. 2001b. Age-dependent changes in noradrenergic innervations of the frontal cortex in F344 rats. *Neurobiol Aging,* 22, 283-6.
ISHUNINA, T. A. & SWAAB, D. F. 2002. Neurohypophyseal peptides in aging and Alzheimer's disease. *Ageing Res Rev,* 1, 537-58.
ITO, H., DRAKE, M. J., FRY, C. H., KANAI, A. J. & PICKERING, A. E. 2018. Characterization of mouse neuro-urological dynamics in a novel decerebrate arterially perfused mouse (DAPM) preparation. *Neurourology and urodynamics,* 37, 1302-1312.

ITZEV, D. E., LOLOV, S. R. & USUNOFF, K. G. 2003. Aging and synaptic changes in the paraventricular hypothalamic nucleus of the rat. *Acta Physiol Pharmacol Bulg,* 27**,** 75-82.

IWANAGA, K., YAMADA, M., WAKABAYASHI, K., IKUTA, F. & TAKAHASHI, H. 1996. A newly discovered age-related synaptic change in the human locus ceruleus: morphometric and ultrastructural studies. *Acta Neuropathol,* 91**,** 337-42.

JACOB, J. M. 1998. Lumbar motor neuron size and number is affected by age in male F344 rats. *Mechanisms of Ageing and Development,* 106**,** 205-216.

JAIRAM, R., DROSSAERTS, J., VRIJENS, D., LEUE, C., VAN KERREBROECK, P. & VAN KOEVERINGE, G. 2018. Affective symptoms and quality of life in patients with voiding or storage dysfunction: Results before and after sacral neuromodulation: A prospective follow-up study. *Neurourology and Urodynamics,* 37**,** 1801-1808.

JAMIESON, H. A., SCHLUTER, P. J., PYUN, J., ARNOLD, T., SCRASE, R., NISBET-ABEY, R., MOR, V., DEELY, J. M. & GRAY, L. 2017. Fecal Incontinence Is Associated With Mortality Among Older Adults With Complex Needs: An Observational Cohort Study. *Am J Gastroenterol,* 112**,** 1431-1437.

JANIG, W. & MCLACHLAN, E. M. 1987. Organization of lumbar spinal outflow to distal colon and pelvic organs. *Physiological Reviews,* 67**,** 1332-1404.

JEMBREK, M. J. & VLAINIC, J. 2015. GABA Receptors: Pharmacological Potential and Pitfalls. *Curr Pharm Des,* 21**,** 4943-59.

JEREZ-ROIG, J., SANTOS, M. M., SOUZA, D. L. B., AMARAL, F. L. J. S. & LIMA, K. C. 2016. Prevalence of urinary incontinence and associated factors in nursing home residents. *Neurourology and Urodynamics,* 35**,** 102-107.

JIANG, H.-H., PAN, H. Q., GUSTILO-ASHBY, M. A., GILL, B., GLAAB, J., ZASZCZURYNSKI, P. & DAMASER, M. 2009. Dual Simulated Childbirth Injuries Result in Slowed Recovery of Pudendal Nerve and Urethral Function. *Neurourology and Urodynamics,* 28**,** 229-235.

JOHN, G., GERSTEL, E., JUNG, M., DALLENBACH, P., FALTIN, D., PETOUD, V., ZUMWALD, C. & RUTSCHMANN, O. T. 2014. Urinary incontinence as a marker of higher mortality in patients receiving home care services. *BJU Int,* 113**,** 113-9.

JOHNSON, C. S., BAINS, J. S. & WATTS, A. G. 2018. Neurotransmitter diversity in pre-synaptic terminals located in the parvicellular neuroendocrine paraventricular nucleus of the rat and mouse hypothalamus. *J Comp Neurol,* 526**,** 1287-1306.

JOHNSON, L. A., RODANSKY, E. S., SAUDER, K. L., HOROWITZ, J. C., MIH, J. D., TSCHUMPERLIN, D. J. & HIGGINS, P. D. 2013. Matrix stiffness corresponding to strictured bowel induces a fibrogenic response in human colonic fibroblasts. *Inflammatory bowel diseases,* 19**,** 891-903.

JONES, B. E. & YANG, T. Z. 1985. The efferent projections from the reticular formation and the locus coeruleus studied by anterograde and retrograde axonal transport in the rat. *J Comp Neurol,* 242**,** 56-92.

JONES, M. P., DILLEY, J. B., DROSSMAN, D. & CROWELL, M. D. 2006. Brain–gut connections in functional GI disorders: anatomic and physiologic relationships. *Neurogastroenterology & Motility,* 18**,** 91-103.

JORDAN, C. L., BREEDLOVE, S. M. & ARNOLD, A. P. 1982. Sexual dimorphism and the influence of neonatal androgen in the dorsolateral motor nucleus of the rat lumbar spinal cord. *Brain Research,* 249**,** 309-314.

JUBELIN, B., GALEANO, C., LADOUCEUR, D., LEMAIRE, S. & ELHILALI, M. M. 1984. Effect of enkephalin on the micturition cycle of the cat. *Life Sciences,* 34**,** 2015-2027.

KADAR, A., SANCHEZ, E., WITTMANN, G., SINGRU, P. S., FUZESI, T., MARSILI, A., LARSEN, P. R., LIPOSITS, Z., LECHAN, R. M. & FEKETE, C. 2010. Distribution of hypophysiotropic thyrotropin-releasing hormone (TRH)-synthesizing neurons in the hypothalamic paraventricular nucleus of the mouse. *J Comp Neurol,* 518**,** 3948-61.

KADEKAWA, K., SUGAYA, K., NISHIJIMA, S., ASHITOMI, K., MIYAZATO, M., UEDA, T. & YAMAMOTO, H. 2013. Effect of naftopidil, an alpha1D/A-adrenoceptor antagonist, on the

urinary bladder in rats with spinal cord injury. *Life Sci,* 92, 1024-8.
KALYANI, R. R. & EGAN, J. M. 2013. Diabetes and altered glucose metabolism with aging. *Endocrinology and metabolism clinics of North America,* 42, 333-347.
KAMEI, J., ITO, H., AIZAWA, N., HOTTA, H., KOJIMA, T., FUJITA, Y., ITO, M., HOMMA, Y. & IGAWA, Y. 2018. Age-related changes in function and gene expression of the male and female mouse bladder. *Sci Rep,* 8, 2089.
KARICHETI, V. & CHRIST, G. J. 2001. Physiological roles for K+ channels and gap junctions in urogenital smooth muscle: implications for improved understanding of urogenital function, disease and therapy. *Curr Drug Targets,* 2, 1-20.
KATAGIRI, T., GIBSON, S. J., SU, H. C. & POLAK, J. M. 1986. Composition and central projections of the pudendal nerve in the rat investigated by combined peptide immunocytochemistry and retrograde fluorescent labelling. *Brain research,* 372, 313-322.
KAWAMATA, T., NAKAMURA, S., AKIGUCHI, I., KIMURA, J., KAMEYAMA, M., KIMURA, H. & TAKEDA, T. 1990. Effect of aging on NADPH-diaphorase neurons in laterodorsal tegmental nucleus and striatum of mice. *Neurobiol Aging,* 11, 185-92.
KEAST, J. R. & DE GROAT, W. C. 1992. Segmental distribution and peptide content of primary afferent neurons innervating the urogenital organs and colon of male rats. *Journal of Comparative Neurology,* 319, 615-623.
KEATING, C., NOCCHI, L., YU, Y., DONOVAN, J. & GRUNDY, D. 2016. Ageing and gastrointestinal sensory function: altered colonic mechanosensory and chemosensory function in the aged mouse. *The Journal of Physiology,* 594, 4549-4564.
KEEF, K. D. & COBINE, C. A. 2019. Control of Motility in the Internal Anal Sphincter. *Journal of neurogastroenterology and motility,* 25, 189-204.
KELLER, J. A., CHEN, J., SIMPSON, S., WANG, E. H.-J., LILASCHAROEN, V., GEORGE, O., LIM, B. K. & STOWERS, L. 2018. Voluntary

urination control by brainstem neurons that relax the urethral sphincter. *Nature neuroscience,* 21, 1229-1238.
KENNEDY, C. & KRIER, J. 1987. [Met5]enkephalin acts via delta-opioid receptors to inhibit pelvic nerve-evoked contractions of cat distal colon. *British journal of pharmacology,* 92, 291-298.
KESSLER, B. A., STANLEY, E. M., FREDERICK-DUUS, D. & FADEL, J. 2011. Age-related loss of orexin/hypocretin neurons. *Neuroscience,* 178, 82-88.
KHAN, M., DE SEVILLA, L., MAHESH, V. B. & BRANN, D. W. 2010. Enhanced glutamatergic and decreased GABAergic synaptic appositions to GnRH neurons on proestrus in the rat: modulatory effect of aging. *PLoS One,* 5, e10172.
KINUGASA, Y., ARAKAWA, T., MURAKAMI, G., FUJIMIYA, M. & SUGIHARA, K. 2014. Nerve supply to the internal anal sphincter differs from that to the distal rectum: an immunohistochemical study of cadavers. *Int J Colorectal Dis,* 29, 429-36.
KIRCHGESSNER, A. L., TAMIR, H. & GERSHON, M. D. 1992. Identification and stimulation by serotonin of intrinsic sensory neurons of the submucosal plexus of the guinea pig gut: activity-induced expression of Fos immunoreactivity. *J Neurosci,* 12, 235-48.
KNOBLOCH, H. S., CHARLET, A., HOFFMANN, L. C., ELIAVA, M., KHRULEV, S., CETIN, A. H., OSTEN, P., SCHWARZ, M. K., SEEBURG, P. H., STOOP, R. & GRINEVICH, V. 2012. Evoked axonal oxytocin release in the central amygdala attenuates fear response. *Neuron,* 73, 553-66.
KNOWLES, C. H. 2018. Human studies of anorectal sensory function. *Irish journal of medical science,* 187, 1143-1147.
KO, M. L., KING, M. A., GORDON, T. L. & CRISP, T. 1997. The effects of aging on spinal neurochemistry in the rat. *Brain Res Bull,* 42, 95-8.
KO, Y., LIN, S. J., SALMON, J. W. & BRON, M. S. 2005. The impact of urinary incontinence on quality of life of the elderly. *Am J Manag Care,* 11, S103-11.
KOH, B. H., ROY, R., HOLLYWOOD, M. A., THORNBURY, K. D., MCHALE, N. G., SERGEANT, G. P., HATTON, W. J., WARD, S. M.,

SANDERS, K. M. & KOH, S. D. 2012. Platelet-derived growth factor receptor-alpha cells in mouse urinary bladder: a new class of interstitial cells. *J Cell Mol Med,* 16**,** 691-700.

KOH, S. D., LEE, H., WARD, S. M. & SANDERS, K. M. 2018. The Mystery of the Interstitial Cells in the Urinary Bladder. *Annu Rev Pharmacol Toxicol,* 58**,** 603-623.

KOHNO, J., SHINODA, K., KAWAI, Y., PENG, Y., ONO, K. & SHIOTANI, Y. 1989. Enkephalin fibers synapse on cholinergic neurons in the rat sacral intermediolateral nucleus: A double-immunostaining at the light and electron microscopic levels. *Neuroscience,* 28**,** 487-494.

KOK, A. L., VOORHORST, F. J., BURGER, C. W., VAN HOUTEN, P., KENEMANS, P. & JANSSENS, J. 1992. Urinary and faecal incontinence in community-residing elderly women. *Age Ageing,* 21**,** 211-5.

KOLA, B., FARKAS, I., CHRIST-CRAIN, M., WITTMANN, G., LOLLI, F., AMIN, F., HARVEY-WHITE, J., LIPOSITS, Z., KUNOS, G., GROSSMAN, A. B., FEKETE, C. & KORBONITS, M. 2008. The orexigenic effect of ghrelin is mediated through central activation of the endogenous cannabinoid system. *PLoS One,* 3**,** e1797.

KOSOYAN, H. P., GRIGORIADIS, D. E. & TACHE, Y. 2005. The CRF(1) receptor antagonist, NBI-35965, abolished the activation of locus coeruleus neurons induced by colorectal distension and intracisternal CRF in rats. *Brain Res,* 1056**,** 85-96.

KROGH, K. & CHRISTENSEN, P. 2009. Neurogenic colorectal and pelvic floor dysfunction. *Best Pract Res Clin Gastroenterol,* 23**,** 531-43.

KRUSE, M. N., MALLORY, B. S., NOTO, H., ROPPOLO, J. R. & DE GROAT, W. C. 1991. Properties of the descending limb of the spinobulbospinal micturition reflex pathway in the cat. *Brain Res,* 556**,** 6-12.

KUHN, A., VITS, K., KUHN, P. & MONGA, A. 2006. Do women with urinary incontinence really know where all the toilets are?: The toilet paper. *European Journal of Obstetrics & Gynecology and Reproductive Biology,* 129**,** 65-68.

KUIPERS, R., EGGENS-MEIJER, E. & MCMURRAY, G. 2007. Barrington's nucleus in the guinea pig (Cavia porcellus): location in relation to noradrenergic cell groups and connections to the lumbosacral spinal cord. *Brain Res Bull,* 72**,** 49-56.

KUIPERS, R., MOUTON, L. J. & HOLSTEGE, G. 2006. Afferent projections to the pontine micturition center in the cat. *Journal of Comparative Neurology,* 494**,** 36-53.

KUMAR, D., WALDRON, D., WILLIAMS, N. S., BROWNING, C., HUTTON, M. R. & WINGATE, D. L. 1990. Prolonged anorectal manometry and external anal sphincter electromyography in ambulant human subjects. *Dig Dis Sci,* 35**,** 641-8.

KUNZE, W. A., FURNESS, J. B., BERTRAND, P. P. & BORNSTEIN, J. C. 1998. Intracellular recording from myenteric neurons of the guinea-pig ileum that respond to stretch. *J Physiol,* 506 (Pt 3)**,** 827-42.

KURZ, E. M., BREWER, R. G. & SENGELAUB, D. R. 1991. Hormonally mediated plasticity of motoneuron morphology in the adult rat spinal cord: A cholera toxin-HRP study. *Journal of Neurobiology,* 22**,** 976-988.

KUWAHARA, S., KESUMA SARI, D., TSUKAMOTO, Y., TANAKA, S. & SASAKI, F. 2004a. Age-related changes in growth hormone (GH)-releasing hormone and somatostatin neurons in the hypothalamus and in GH cells in the anterior pituitary of female mice. *Brain Res,* 1025**,** 113-22.

KUWAHARA, S., SARI, D. K., TSUKAMOTO, Y., TANAKA, S. & SASAKI, F. 2004b. Age-related changes in growth hormone (GH) cells in the pituitary gland of male mice are mediated by GH-releasing hormone but not by somatostatin in the hypothalamus. *Brain Res,* 998**,** 164-73.

LANZOTTI, N. J. & BOLLA, S. R. 2019. Physiology, Bladder. *StatPearls.* Treasure Island (FL): StatPearls Publishing

StatPearls Publishing LLC.

LARSEN, P. J., SEIER, V., FINK-JENSEN, A., HOLST, J. J., WARBERG, J. & VRANG, N. 2003. Cocaine- and amphetamine-regulated transcript is present in hypothalamic neuroendocrine

neurones and is released to the hypothalamic-pituitary portal circuit. *J Neuroendocrinol,* 15, 219-26.

LARSEN, P. J. & VRANG, N. 1995. Neurones projecting to the hypothalamus from the brainstem A1 catecholaminergic cell group express glutamate-R2,3 receptor immunoreactivity. *Brain Res,* 705, 209-15.

LASSERRE, A., PELAT, C., GUEROULT, V., HANSLIK, T., CHARTIER-KASTLER, E., BLANCHON, T., CIOFU, C., MONTEFIORE, E. D., ALVAREZ, F. P. & BLOCH, J. 2009. Urinary incontinence in French women: prevalence, risk factors, and impact on quality of life. *Eur Urol,* 56, 177-83.

LATORRE, R., STERNINI, C., DE GIORGIO, R. & GREENWOOD-VAN MEERVELD, B. 2016. Enteroendocrine cells: a review of their role in brain-gut communication. *Neurogastroenterology and motility : the official journal of the European Gastrointestinal Motility Society,* 28, 620-630.

LAW, N. M., BHARUCHA, A. E. & ZINSMEISTER, A. R. 2002. Rectal and colonic distension elicit viscerovisceral reflexes in humans. *Am J Physiol Gastrointest Liver Physiol,* 283, G384-9.

LECHNER, S. M., CURTIS, A. L., BRONS, R. & VALENTINO, R. J. 1997. Locus coeruleus activation by colon distention: role of corticotropin-releasing factor and excitatory amino acids. *Brain Res,* 756, 114-24.

LEE, H.-M., GREELEY, G. H. & ENGLANDER, E. W. 2001. Age-associated changes in gene expression patterns in the duodenum and colon of rats. *Mechanisms of Ageing and Development,* 122, 355-371.

LEE, I. M. 1956. The distribution of the myelinated nerves in the colon

of the dog. *Arch Jap Chir,* 25, 263-9.

LEMAN, J. K., SANDFORD, S. K., RHODES, J. L. & KEMP, R. A. 2018. Multiparametric analysis of colorectal cancer immune responses. *World journal of gastroenterology,* 24, 2995-3005.

LESLIE, M., FORGER, N. G. & MARC BREEDLOVE, S. 1991. Sexual dimorphism and androgen effects on spinal motoneurons innervating the rat flexor digitorum brevis. *Brain Research,* 561, 269-273.

LESTAR, B., PENNINCKX, F. & KERREMANS, R. 1989. The composition of anal basal pressure. An in vivo and in vitro study in man. *Int J Colorectal Dis,* 4**,** 118-22.

LI, Y., ZHAO, Z., CAI, J., GU, B., LV, Y. & ZHAO, L. 2017. The Frequency-Dependent Aerobic Exercise Effects of Hypothalamic GABAergic Expression and Cardiovascular Functions in Aged Rats. *Frontiers in aging neuroscience,* 9**,** 212-212.

LIGUZ-LECZNAR, M. & SKANGIEL-KRAMSKA, J. 2007. Vesicular glutamate transporters (VGLUTs): the three musketeers of glutamatergic system. *Acta Neurobiol Exp (Wars),* 67**,** 207-18.

LLEWELLYN, T., ZHENG, H., LIU, X., XU, B. & PATEL, K. P. 2012. Median preoptic nucleus and subfornical organ drive renal sympathetic nerve activity via a glutamatergic mechanism within the paraventricular nucleus. *Am J Physiol Regul Integr Comp Physiol,* 302**,** R424-32.

LOHR, J. B. & JESTE, D. V. 1988. Locus ceruleus morphometry in aging and schizophrenia. *Acta Psychiatr Scand,* 77**,** 689-97.

LOLOVA, I. S., DAVIDOFF, M. S. & YAKIMOFF, N. A. 1996a. Vasopressin- and oxytocin-immunoreactive nerve cells in the aging rat hypothalamus. *Acta Physiol Pharmacol Bulg,* 22**,** 7-16.

LOLOVA, I. S., LOLOV, S. R. & ITZEV, D. E. 1996b. Changes in NADPH-diaphorase neurons of the rat laterodorsal and pedunculopontine tegmental nuclei in aging. *Mechanisms of Ageing and Development,* 90**,** 111-128.

LORD, M. G., VALIES, P. & BROUGHTON, A. C. 1977. A morphologic study of the submucosa of the large intestine. *Surg Gynecol Obstet,* 145**,** 55-60.

LU, M., ZHOU, L., STANLEY, W. C., CABRERA, M. E., SAIDEL, G. M. & YU, X. 2008. Role of the malate-aspartate shuttle on the metabolic response to myocardial ischemia. *Journal of theoretical biology,* 254**,** 466-475.

LUCKENSMEYER, G. B. & KEAST, J. R. 1994. Projections from the prevertebral and major pelvic ganglia to the ileum and large intestine of the male rat. *J Auton Nerv Syst,* 49**,** 247-59.

LUPPI, P. H., ASTON-JONES, G., AKAOKA, H., CHOUVET, G. & JOUVET, M. 1995. Afferent projections to the rat locus coeruleus demonstrated by retrograde and anterograde tracing with cholera-toxin B subunit and Phaseolus vulgaris leucoagglutinin. *Neuroscience,* 65**,** 119-60.

LYONS, W., FRITSCHY, J. & GRZANNA, R. 1989. The noradrenergic neurotoxin DSP-4 eliminates the coeruleospinal projection but spares projections of the A5 and A7 groups to the ventral horn of the rat spinal cord. *The Journal of Neuroscience,* 9**,** 1481-1489.

MACDONAGH, R., SUN, W., THOMAS, D., SMALLWOOD, R. & READ, N. 1992. Anorectal function in patients with complete supraconal spinal cord lesions. *Gut,* 33**,** 1532-8.

MADEIRA, M. D., ANDRADE, J. P. & PAULA-BARBOSA, M. M. 2000. Hypertrophy of the ageing rat medial preoptic nucleus. *J Neurocytol,* 29**,** 173-97.

MADEIRA, M. D., FERREIRA-SILVA, L., RUELA, C. & PAULA-BARBOSA, M. M. 2001. Differential effects of the aging process on the morphology of the hypothalamic ventromedial nucleus of male and female rats. *Neurosci Lett,* 314**,** 73-6.

MADEIRA, M. D., SOUSA, N., SANTER, R. M., PAULA-BARBOSA, M. M. & GUNDERSEN, H. J. 1995. Age and sex do not affect the volume, cell numbers, or cell size of the suprachiasmatic nucleus of the rat: an unbiased stereological study. *J Comp Neurol,* 361**,** 585-601.

MADEO, M., KOVÁCS, A. D. & PEARCE, D. A. 2014. The human synaptic vesicle protein, SV2A, functions as a galactose transporter in Saccharomyces cerevisiae. *The Journal of biological chemistry,* 289**,** 33066-33071.

MAGDELDIN, S., YOSHIDA, Y., LI, H., MAEDA, Y., YOKOYAMA, M., ENANY, S., ZHANG, Y., XU, B., FUJINAKA, H., YAOITA, E., SASAKI, S. & YAMAMOTO, T. 2012. Murine colon proteome and characterization of the protein pathways. *BioData Mining,* 5**,** 11.

MAGOUL, R., ONTENIENTE, B., GEFFARD, M. & CALAS, A. 1987. Anatomical distribution and ultrastructural organization of the GABAergic system in the rat spinal cord. An

immunocytochemical study using anti-GABA antibodies. *Neuroscience,* 20, 1001-9.
MAHATO, P. K., RAMSAKHA, N., OJHA, P., GULIA, R., SHARMA, R. & BHATTACHARYYA, S. 2018. Group I Metabotropic Glutamate Receptors (mGluRs): Ins and Outs. *Adv Exp Med Biol,* 1112, 163-175.
MAILLOT, C., MILLION, M., WEI, J. Y., GAUTHIER, A. & TACHE, Y. 2000. Peripheral corticotropin-releasing factor and stress-stimulated colonic motor activity involve type 1 receptor in rats. *Gastroenterology,* 119, 1569-79.
MAILLOT, C., WANG, L., MILLION, M. & TACHÉ, Y. 2003. Intraperitoneal corticotropin-releasing factor and urocortin induce Fos expression in brain and spinal autonomic nuclei and long lasting stimulation of colonic motility in rats. *Brain research,* 974, 70-81.
MALLORY, B., STEERS, W. D. & DE GROAT, W. C. 1989. Electrophysiological study of micturition reflexes in rats. *Am J Physiol,* 257, R410-21.
MALLORY, B. S., ROPPOLO, J. R. & DE GROAT, W. C. 1991. Pharmacological modulation of the pontine micturition center. *Brain Res,* 546, 310-20.
MALYKHINA, A. P. 2017. How the brain controls urination. *eLife,* 6, e33219.
MANAYE, K. F., MCINTIRE, D. D., MANN, D. M. & GERMAN, D. C. 1995. Locus coeruleus cell loss in the aging human brain: a non-random process. *J Comp Neurol,* 358, 79-87.
MANNEN, T. 2000. Neuropathological findings of Onuf's nucleus and its significance. *Neuropathology,* 20 Suppl, S30-3.
MANOHAR, A., CURTIS, A. L., ZDERIC, S. A. & VALENTINO, R. J. 2017. Brainstem network dynamics underlying the encoding of bladder information. *eLife,* 6, e29917.
MARFIL, C., DAVIES, G. J. & DETTMAR, P. W. 2005. Laxative use and its relationship with straining in a London elderly population: free-living versus institutionalised. *J Nutr Health Aging,* 9, 185-7.
MARKLAND, A. D., GREER, W. J., VOGT, A., REDDEN, D. T., GOODE, P. S., BURGIO, K. L. & RICHTER, H. E. 2010. Factors impacting

quality of life in women with fecal incontinence. *Dis Colon Rectum,* 53**,** 1148-54.
MARSON, L. 1997. Identification of central nervous system neurons that innervate the bladder body, bladder base, or external urethral sphincter of female rats: a transneuronal tracing study using pseudorabies virus. *J Comp Neurol,* 389**,** 584-602.
MARTÍNEZ, V., WANG, L. & TACHÉ, Y. 2006. Proximal colon distension induces Fos expression in the brain and inhibits gastric emptying through capsaicin-sensitive pathways in conscious rats. *Brain research,* 1086**,** 168-180.
MARVIZON, J. C., CHEN, W. & MURPHY, N. 2009. Enkephalins, dynorphins, and beta-endorphin in the rat dorsal horn: an immunofluorescence colocalization study. *J Comp Neurol,* 517**,** 51-68.
MATSUMOTO, A. 1997. Hormonally Induced Neuronal Plasticity in the Adult Motoneurons. *Brain Research Bulletin,* 44**,** 539-547.
MATSUMOTO, A. 1998. Synaptic changes in the perineal motoneurons of aged male rats. *Journal of Comparative Neurology,* 400**,** 103-109.
MATSUMOTO, A. 2001. Androgen stimulates neuronal plasticity in the perineal motoneurons of aged male rats. *Journal of Comparative Neurology,* 430**,** 389-395.
MATSUMOTO, A., MICEVYCH, P. E. & ARNOLD, A. P. 1988. Androgen regulates synaptic input to motoneurons of the adult rat spinal cord. *The Journal of Neuroscience,* 8**,** 4168.
MATSUMOTO, S., LEVENDUSKY, M. C., LONGHURST, P. A., LEVIN, R. M. & MILLINGTON, W. R. 2004. Activation of mu opioid receptors in the ventrolateral periaqueductal gray inhibits reflex micturition in anesthetized rats. *Neurosci Lett,* 363**,** 116-9.
MATSUURA, S., DOWNIE, J. W. & ALLEN, G. V. 2000. Micturition evoked by glutamate microinjection in the ventrolateral periaqueductal gray is mediated through Barrington's nucleus in the rat. *Neuroscience,* 101**,** 1053-1061.
MATSUYAMA, H., TANAHASHI, Y., KITAZAWA, T., YAMADA, M., KOMORI, S. & UNNO, T. 2013. Evidence for M2 and M3 muscarinic receptor involvement in cholinergic excitatory

junction potentials through synergistic activation of cation channels in the longitudinal muscle of mouse ileum. *J Pharmacol Sci,* 121**,** 227-36.

MATSUZAKI, A. 1990. [A study of the pontine urine storage center in decerebrate cats]. *Nihon Hinyokika Gakkai Zasshi,* 81**,** 672-9.

MAYER, E. A., AZIZ, Q., COEN, S., KERN, M., LABUS, J. S., LANE, R., KUO, B., NALIBOFF, B. & TRACEY, I. 2009. Brain imaging approaches to the study of functional GI disorders: A Rome Working Team Report. *Neurogastroenterology & Motility,* 21**,** 579-596.

MAZIER, W., SAUCISSE, N., SIMON, V., CANNICH, A., MARSICANO, G., MASSA, F. & COTA, D. 2019. mTORC1 and CB1 receptor signaling regulate excitatory glutamatergic inputs onto the hypothalamic paraventricular nucleus in response to energy availability. *Mol Metab,* 28**,** 151-159.

MCKELLAR, S. & LOEWY, A. D. 1981. Organization of some brain stem afferents to the paraventricular nucleus of the hypothalamus in the rat. *Brain Research,* 217**,** 351-357.

MCKENNA, K. E. & NADELHAFT, I. 1986. The organization of the pudendal nerve in the male and female rat. *J Comp Neurol,* 248**,** 532-49.

MCKERRACHER, L., DAVID, S., JACKSON, D. L., KOTTIS, V., DUNN, R. J. & BRAUN, P. E. 1994. Identification of myelin-associated glycoprotein as a major myelin-derived inhibitor of neurite growth. *Neuron,* 13**,** 805-11.

MERCHANT, H. A., LIU, F., ORLU GUL, M. & BASIT, A. W. 2016. Age-mediated changes in the gastrointestinal tract. *Int J Pharm,* 512**,** 382-395.

MERCK. 2020. *Antibody Development, Validation and Guarantee* [Online]. Available: https://www.merckmillipore.com/GB/en/life-science-research/antibodies-assays/antibodies-overview/Antibody-Development-and-Validation/cFOb.qB.8McAAAFOb64qQvSS,nav?ReferrerURL=https%3A%2F%2Fwww.google.com%2F [Accessed].

MERRILL, L., GONZALEZ, E. J., GIRARD, B. M. & VIZZARD, M. A. 2016. Receptors, channels, and signalling in the urothelial sensory system in the bladder. *Nature reviews. Urology,* 13**,** 193-204.

MERSDORF, A., SCHMIDT, R. A., KAULA, N. & TANAGHO, E. A. 1992. Intrathecal administration of substance P in the rat: the effect on bladder and urethral sphincteric activity. *Urology,* 40**,** 87-96.

METALLO, C. M., GAMEIRO, P. A., BELL, E. L., MATTAINI, K. R., YANG, J., HILLER, K., JEWELL, C. M., JOHNSON, Z. R., IRVINE, D. J., GUARENTE, L., KELLEHER, J. K., VANDER HEIDEN, M. G., ILIOPOULOS, O. & STEPHANOPOULOS, G. 2012. Reductive glutamine metabolism by IDH1 mediates lipogenesis under hypoxia. *Nature,* 481**,** 380-384.

METZ, B., KERSTEN, G. F., BAART, G. J., DE JONG, A., MEIRING, H., TEN HOVE, J., VAN STEENBERGEN, M. J., HENNINK, W. E., CROMMELIN, D. J. & JISKOOT, W. 2006. Identification of formaldehyde-induced modifications in proteins: reactions with insulin. *Bioconjug Chem,* 17**,** 815-22.

MEYER, I., BLANCHARD, C. T., MARKLAND, A. D., GIBSON, E. G. & RICHTER, H. E. 2019. Fecal Incontinence Symptoms and Impact in Older Versus Younger Women Seeking Care. *Dis Colon Rectum,* 62**,** 733-738.

MICEVYCH, P. E., COQUELIN, A. & ARNOLD, A. P. 1986. Immunohistochemical distribution of substance P, serotonin, and methionine enkephalin in sexually dimorphic nuclei of the rat lumbar spinal cord. *The Journal of comparative neurology,* 248**,** 235-244.

MILLION, M., WANG, L., MARTINEZ, V. & TACHÉ, Y. 2000. Differential Fos expression in the paraventricular nucleus of the hypothalamus, sacral parasympathetic nucleus and colonic motor response to water avoidance stress in Fischer and Lewis rats. *Brain research,* 877**,** 345-353.

MISSALE, C., GOVONI, S., CASTELLETTI, L., SPANO, P. F. & TRABUCCHI, M. 1983. Age related changes of enkephalin in rat spinal cord. *Brain Res,* 262**,** 160-2.

MOGA, M. M., SAPER, C. B. & GRAY, T. S. 1990. Neuropeptide organization of the hypothalamic projection to the

parabrachial nucleus in the rat. *Journal of Comparative Neurology,* 295, 662-682.
MOISSET, X., BOUHASSIRA, D., DENIS, D., DOMINIQUE, G., BENOIT, C. & SABATE, J. M. 2010. Anatomical connections between brain areas activated during rectal distension in healthy volunteers: a visceral pain network. *Eur J Pain,* 14, 142-8.
MOLINUEVO, B. & BATISTA-MIRANDA, J. E. 2012. Under the tip of the iceberg: Psychological factors in incontinence. *Neurourology and Urodynamics,* 31, 669-671.
MONNIKES, H., SCHMIDT, B. G., TEBBE, J., BAUER, C. & TACHE, Y. 1994. Microinfusion of corticotropin releasing factor into the locus coeruleus/subcoeruleus nuclei stimulates colonic motor function in rats. *Brain Res,* 644, 101-8.
MORENO-GARCÍA, A., KUN, A., CALERO, O., MEDINA, M. & CALERO, M. 2018. An Overview of the Role of Lipofuscin in Age-Related Neurodegeneration. *Frontiers in Neuroscience,* 12.
MORITA, Y., ZHANG, J. H., HIRONAKA, T., TATENO, E., NOGUCHI, K., SATO, M., KIYAMA, H. & TOHYAMA, M. 1990. Postnatal development of preproenkephalin mRNA containing neurons in the rat lower brainstem. *J Comp Neurol,* 292, 193-213.
MOSS, M. S., GLAZER, E. J. & BASBAUM, A. I. 1983. The peptidergic organization of the cat periaqueductal gray. I. The distribution of immunoreactive enkephalin-containing neurons and terminals. *J Neurosci,* 3, 603-16.
MOUNSEY, A., RALEIGH, M. & WILSON, A. 2015. Management of Constipation in Older Adults. *Am Fam Physician,* 92, 500-4.
MOUTON, P. R., PAKKENBERG, B., GUNDERSEN, H. J. & PRICE, D. L. 1994. Absolute number and size of pigmented locus coeruleus neurons in young and aged individuals. *J Chem Neuroanat,* 7, 185-90.
MUGIE, S. M., KOPPEN, I. J. N., VAN DEN BERG, M. M., GROOT, P. F. C., RENEMAN, L., DE RUITER, M. B. & BENNINGA, M. A. 2018. Brain processing of rectal sensation in adolescents with functional defecation disorders and healthy controls. *Neurogastroenterology & Motility,* 30, e13228.
MULLEN, A. R., WHEATON, W. W., JIN, E. S., CHEN, P.-H., SULLIVAN, L. B., CHENG, T., YANG, Y., LINEHAN, W. M., CHANDEL, N. S. &

DEBERARDINIS, R. J. 2012. Reductive carboxylation supports growth in tumour cells with defective mitochondria. *Nature,* 481, 385-388.

NADELHAFT, I. & VERA, P. L. 1996. Neurons in the rat brain and spinal cord labeled after pseudorabies virus injected into the external urethral sphincter. *J Comp Neurol,* 375, 502-17.

NAGANUMA, S., SHIINA, T., YASUDA, S., SUZUKI, Y. & SHIMIZU, Y. 2018. Histamine-enhanced contractile responses of gastric smooth muscle via interstitial cells of Cajal in the Syrian hamster. *Neurogastroenterol Motil,* 30, e13255.

NAKAMORI, H., NAITOU, K., HORII, Y., SHIMAOKA, H., HORII, K., SAKAI, H., YAMADA, A., FURUE, H., SHIINA, T. & SHIMIZU, Y. 2018. Medullary raphe nuclei activate the lumbosacral defecation center through the descending serotonergic pathway to regulate colorectal motility in rats. *Am J Physiol Gastrointest Liver Physiol,* 314, G341-g348.

NAKAMURA, K., HIOKI, H., FUJIYAMA, F. & KANEKO, T. 2005. Postnatal changes of vesicular glutamate transporter (VGluT)1 and VGluT2 immunoreactivities and their colocalization in the mouse forebrain. *Journal of Comparative Neurology,* 492, 263-288.

NAKANISHI, N., TATARA, K., NARAMURA, H., FUJIWARA, H., TAKASHIMA, Y. & FUKUDA, H. 1997. Urinary and fecal incontinence in a community-residing older population in Japan. *J Am Geriatr Soc,* 45, 215-9.

NELSON, J. F., LATHAM, K. R. & FINCH, C. E. 1975. Plasma testosterone levels in C57BL/6J male mice: effects of age and disease. *Acta Endocrinol (Copenh),* 80, 744-52.

NEUMANN, C. A., KRAUSE, D. S., CARMAN, C. V., DAS, S., DUBEY, D. P., ABRAHAM, J. L., BRONSON, R. T., FUJIWARA, Y., ORKIN, S. H. & VAN ETTEN, R. A. 2003. Essential role for the peroxiredoxin Prdx1 in erythrocyte antioxidant defence and tumour suppression. *Nature,* 424, 561-5.

NEUNLIST, M., DOBREVA, G. & SCHEMANN, M. 1999. Characteristics of mucosally projecting myenteric neurones in the guinea-pig proximal colon. *The Journal of physiology,* 517 (Pt 2), 533-546.

NHS ENGLAND. 2016. *Prescriptions dispensed in the community* [Online]. Available: https://files.digital.nhs.uk/publicationimport/pub20xxx/pub20664/pres-disp-com-eng-2005-15-rep.pdf [Accessed].

NHS ENGLAND. 2017. *Falls and fracture consensus statement: supporting commissioning for prevention* [Online]. Available: https://www.england.nhs.uk/south/wp-content/uploads/sites/6/2017/03/falls-fracture.pdf [Accessed].

NHS ENGLAND. 2018. *Excellence in continence care: practical guidance for commissioners, and leaders in health and social care* [Online]. Available: https://www.england.nhs.uk/wp-content/uploads/2018/07/excellence-in-continence-care.pdf [Accessed].

NI, J., WANG, X., CAO, N., SI, J. & GU, B. 2018. Efficacy of different spinal nerve roots for neuromodulation of micturition reflex in rats. *Oncotarget,* 9**,** 13382-13389.

NICHOLAS, A. P., ZHANG, X. & HÖKFELT, T. 1999. An immunohistochemical investigation of the opioid cell column in lamina X of the male rat lumbosacral spinal cord. *Neuroscience letters,* 270**,** 9-12.

NICOLOPOULOS-STOURNARAS, S. & ILES, J. F. 1983. Motor neuron columns in the lumbar spinal cord of the rat. *Journal of Comparative Neurology,* 217**,** 75-85.

NIELSEN, S. D., FAABORG, P. M., FINNERUP, N. B., CHRISTENSEN, P. & KROGH, K. 2017. Ageing with neurogenic bowel dysfunction. *Spinal Cord,* 55**,** 769-773.

NIRMALAN, N. J., HARNDEN, P., SELBY, P. J. & BANKS, R. E. 2009. Development and validation of a novel protein extraction methodology for quantitation of protein expression in formalin-fixed paraffin-embedded tissues using western blotting. *J Pathol,* 217**,** 497-506.

NISHIZAWA, O., SUGAYA, K., NOTO, H., HARADA, T. & TSUCHIDA, S. 1988. Pontine micturition center in the dog. *J Urol,* 140**,** 872-4.

NOBREGA, V. G., SILVA, I. N. N., BRITO, B. S., SILVA, J., SILVA, M. & SANTANA, G. O. 2018. THE ONSET OF CLINICAL

MANIFESTATIONS IN INFLAMMATORY BOWEL DISEASE PATIENTS. *Arq Gastroenterol,* 55**,** 290-295.

NOMIYA, M. & YAMAGUCHI, O. 2003. A quantitative analysis of mRNA expression of alpha 1 and beta-adrenoceptor subtypes and their functional roles in human normal and obstructed bladders. *J Urol,* 170**,** 649-53.

NOTO, H., ROPPOLO, J. R., STEERS, W. D. & DE GROAT, W. C. 1989. Excitatory and inhibitory influences on bladder activity elicited by electrical stimulation in the pontine micturition center in the rat. *Brain Research,* 492**,** 99-115.

NOUR, S., SVARER, C., KRISTENSEN, J. K., PAULSON, O. B. & LAW, I. 2000. Cerebral activation during micturition in normal men. *Brain,* 123 (Pt 4)**,** 781-9.

NOZAWA, K., KAWABATA-SHODA, E., DOIHARA, H., KOJIMA, R., OKADA, H., MOCHIZUKI, S., SANO, Y., INAMURA, K., MATSUSHIME, H., KOIZUMI, T., YOKOYAMA, T. & ITO, H. 2009. TRPA1 regulates gastrointestinal motility through serotonin release from enterochromaffin cells. *Proc Natl Acad Sci U S A,* 106**,** 3408-13.

NUDING, S. C. & NADELHAFT, I. 1998. Bilateral projections of the pontine micturition center to the sacral parasympathetic nucleus in the rat. *Brain Res,* 785**,** 185-94.

NYGREN, L. G. & OLSON, L. 1977. A new major projection from locus coeruleus: the main source of noradrenergic nerve terminals in the ventral and dorsal columns of the spinal cord. *Brain Res,* 132**,** 85-93.

NYSTRÖM, T., YANG, J. & MOLIN, M. 2012. Peroxiredoxins, gerontogenes linking aging to genome instability and cancer. *Genes & development,* 26**,** 2001-2008.

OBOKHARE, I. 2012. Fecal impaction: a cause for concern? *Clin Colon Rectal Surg,* 25**,** 53-8.

OFFICE FOR NATIONAL STATISTICS. 2019. *Overview of the UK population: August 2019* [Online]. Available: https://backup.ons.gov.uk/wp-content/uploads/sites/3/2019/08/Overview-of-the-UK-population-August-2019.pdf [Accessed].

OHM, T. G., BUSCH, C. & BOHL, J. 1997. Unbiased estimation of neuronal numbers in the human nucleus coeruleus during aging. *Neurobiol Aging,* 18**,** 393-9.

OLSSON, C., CHEN, B. N., JONES, S., CHATAWAY, T. K., COSTA, M. & BROOKES, S. J. 2006. Comparison of extrinsic efferent innervation of guinea pig distal colon and rectum. *J Comp Neurol,* 496**,** 787-801.

OSTASIEWICZ, P., ZIELINSKA, D. F., MANN, M. & WISNIEWSKI, J. R. 2010. Proteome, phosphoproteome, and N-glycoproteome are quantitatively preserved in formalin-fixed paraffin-embedded tissue and analyzable by high-resolution mass spectrometry. *J Proteome Res,* 9**,** 3688-700.

OTSUKA, M., KATO, M., YOSHIKAWA, T., CHEN, H., BROWN, E. J., MASUHO, Y., OMATA, M. & SEKI, N. 2001. Differential Expression of the L-Plastin Gene in Human Colorectal Cancer Progression and Metastasis. *Biochemical and Biophysical Research Communications,* 289**,** 876-881.

PAGE, M. E., AKAOKA, H., ASTON-JONES, G. & VALENTINO, R. J. 1992. Bladder distention activates noradrenergic locus coeruleus neurons by an excitatory amino acid mechanism. *Neuroscience,* 51**,** 555-63.

PAINTER, M. W., BROSIUS LUTZ, A., CHENG, Y.-C., LATREMOLIERE, A., DUONG, K., MILLER, C. M., POSADA, S., COBOS, E. J., ZHANG, A. X., WAGERS, A. J., HAVTON, L. A., BARRES, B., OMURA, T. & WOOLF, C. J. 2014. Diminished Schwann cell repair responses underlie age-associated impaired axonal regeneration. *Neuron,* 83**,** 331-343.

PALIT, S., LUNNISS, P. J. & SCOTT, S. M. 2012. The Physiology of Human Defecation. *Digestive Diseases and Sciences,* 57**,** 1445-1464.

PALOMBA, M., NYGÅRD, M., FLORENZANO, F., BERTINI, G., KRISTENSSON, K. & BENTIVOGLIO, M. 2008. Decline of the Presynaptic Network, Including GABAergic Terminals, in the Aging Suprachiasmatic Nucleus of the Mouse. *Journal of Biological Rhythms,* 23**,** 220-231.

PANDITA, R. K., NYLÉN, A. & ANDERSSON, K. E. 1998. Oxytocin-induced stimulation and inhibition of bladder activity in

normal, conscious rats—Influence of nitric oxide synthase inhibition. *Neuroscience,* 85**,** 1113-1119.

PAPKA, R. E., MCCURDY, J. R., WILLIAMS, S. J., MAYER, B., MARSON, L. & PLATT, K. B. 1995. Parasympathetic preganglionic neurons in the spinal cord involved in uterine innervation are cholinergic and nitric oxide-containing. *Anat Rec,* 241**,** 554-62.

PARK, J. B., SKALSKA, S., SON, S. & STERN, J. E. 2007. Dual GABAA receptor-mediated inhibition in rat presympathetic paraventricular nucleus neurons. *J Physiol,* 582**,** 539-51.

PATEL, B. A., PATEL, N., FIDALGO, S., WANG, C., RANSON, R. N., SAFFREY, M. J. & YEOMAN, M. S. 2014. Impaired colonic motility and reduction in tachykinin signalling in the aged mouse. *Exp Gerontol,* 53**,** 24-30.

PAVCOVICH, L. A. & VALENTINO, R. J. 1995. Central regulation of micturition in the rat the corticotropin-releasing hormone from Barrington's nucleus. *Neurosci Lett,* 196**,** 185-8.

PAVCOVICH, L. A., YANG, M., MISELIS, R. R. & VALENTINO, R. J. 1998. Novel role for the pontine micturition center, Barrington's nucleus: evidence for coordination of colonic and forebrain activity. *Brain Research,* 784**,** 355-361.

PAXINOS, G. & FRANKLIN, K. B. J. 2007. *The Mouse Brain in Stereotaxic Coordinates*, Elsevier Science.

PAYETTE, R. F., TENNYSON, V. M., PHAM, T. D., MAWE, G. M., POMERANZ, H. D., ROTHMAN, T. P. & GERSHON, M. D. 1987. Origin and morphology of nerve fibers in the aganglionic colon of the lethal spotted (ls/ls) mutant mouse. *J Comp Neurol,* 257**,** 237-52.

PELLETIER, A. M., VENKATARAMANA, S., MILLER, K. G., BENNETT, B. M., NAIR, D. G., LOURENSSEN, S. & BLENNERHASSETT, M. G. 2010. Neuronal nitric oxide inhibits intestinal smooth muscle growth. *Am J Physiol Gastrointest Liver Physiol,* 298**,** G896-907.

PENG, M. T. & HSÜ, H. K. 1982. No Neuron Loss from Hypothalamic Nuclei of Old Male Rats. *Gerontology,* 28**,** 19-22.

PERCHEY, R. T., TONINI, L., TOSOLINI, M., FOURNIÉ, J.-J., LOPEZ, F., BESSON, A. & PONT, F. 2019. PTMselect: optimization of protein modifications discovery by mass spectrometry. *Scientific Reports,* 9**,** 4181.

PEREZ, C. A., CONCHA, A., HERNANDEZ, M. E. & MANZO, J. 2005. Influence of the paraventricular nucleus and oxytocin on the retrograde stain of pubococcygeus muscle motoneurons in male rats. *Brain Res,* 1041, 11-8.

PETERS, A. 2002. The effects of normal aging on myelin and nerve fibers: a review. *J Neurocytol,* 31, 581-93.

PETROV, T., KRUKOFF, T. L. & JHAMANDAS, J. H. 1994. Chemically defined collateral projections from the pons to the central nucleus of the amygdala and hypothalamic paraventricular nucleus in the rat. *Cell and Tissue Research,* 277, 289-295.

PETRYSZYN, P. W. & PARADOWSKI, L. 2018. Stool patterns and symptoms of disordered anorectal function in patients with inflammatory bowel diseases. *Adv Clin Exp Med,* 27, 813-818.

PICKEL, V. M., JOH, T. H. & REIS, D. J. 1977. A serotonergic innervation of noradrenergic neurons in nucleus locus coeruleus: Demonstration by immunocytochemical localization of the transmitter specific enzymes tyrosine and tryptophan hydroxylase. *Brain Research,* 131, 197-214.

PLATT, S. R. 2007. The role of glutamate in central nervous system health and disease – A review. *The Veterinary Journal,* 173, 278-286.

POLGAR, E., HUGHES, D. I., RIDDELL, J. S., MAXWELL, D. J., PUSKAR, Z. & TODD, A. J. 2003. Selective loss of spinal GABAergic or glycinergic neurons is not necessary for development of thermal hyperalgesia in the chronic constriction injury model of neuropathic pain. *Pain,* 104, 229-39.

POMPOLO, S. & FURNESS, J. B. 1993. Origins of synaptic inputs to calretinin immunoreactive neurons in the guinea-pig small intestine. *J Neurocytol,* 22, 531-46.

PORTBURY, A. L., POMPOLO, S., FURNESS, J. B., STEBBING, M. J., KUNZE, W. A., BORNSTEIN, J. C. & HUGHES, S. 1995. Cholinergic, somatostatin-immunoreactive interneurons in the guinea pig intestine: morphology, ultrastructure, connections and projections. *J Anat,* 187 (Pt 2), 303-21.

PORTILLO, F., CARRASCO, M. & JUAN VALLO, J. 1998. Separate populations of neurons within the paraventricular hypothalamic nucleus of the rat project to vagal and thoracic

autonomic preganglionic levels and express c-Fos protein induced by lithium chloride. *Journal of Chemical Neuroanatomy,* 14**,** 95-102.

PROANO, M., CAMILLERI, M., PHILLIPS, S. F., BROWN, M. L. & THOMFORDE, G. M. 1990. Transit of solids through the human colon: regional quantification in the unprepared bowel. *Am J Physiol,* 258**,** G856-62.

PSICHAS, A., SLEETH, M. L., MURPHY, K. G., BROOKS, L., BEWICK, G. A., HANYALOGLU, A. C., GHATEI, M. A., BLOOM, S. R. & FROST, G. 2015. The short chain fatty acid propionate stimulates GLP-1 and PYY secretion via free fatty acid receptor 2 in rodents. *Int J Obes (Lond),* 39**,** 424-9.

PUDER, B. A. & PAPKA, R. E. 2001a. Distribution and origin of corticotropin-releasing factor-immunoreactive axons in the female rat lumbosacral spinal cord. *J Neurosci Res,* 66**,** 1217-25.

PUDER, B. A. & PAPKA, R. E. 2001b. Hypothalamic paraventricular axons projecting to the female rat lumbosacral spinal cord contain oxytocin immunoreactivity. *Journal of Neuroscience Research,* 64**,** 53-60.

QIAO, X., QIN, X., SHE, D., WANG, R., ZHANG, X., ZHANG, L. & ZHANG, Y. 2014. Mass spectrometry-based tag and its application to high efficient peptide analysis - A review. *Talanta,* 126**,** 91-102.

QIN, C., LI, J. & TANG, K. 2018. The Paraventricular Nucleus of the Hypothalamus: Development, Function, and Human Diseases. *Endocrinology,* 159**,** 3458-3472.

RALTON, L. D. & MURRAY, G. I. 2011. The use of formalin fixed wax embedded tissue for proteomic analysis. *J Clin Pathol,* 64**,** 297-302.

RANCE, N. E., USWANDI, S. V. & MCMULLEN, N. T. 1993. Neuronal hypertrophy in the hypothalamus of older men. *Neurobiol Aging,* 14**,** 337-42.

RANSON, R. N., DODDS, A. L., SMITH, M. J., SANTER, R. M. & WATSON, A. H. 2003a. Age-associated changes in the monoaminergic innervation of rat lumbosacral spinal cord. *Brain Res,* 972**,** 149-58.

RANSON, R. N., GAUNT, K., SANTER, R. M. & WATSON, A. H. D. 2003b. The effects of ageing and of DSP-4 administration on the micturition characteristics of male Wistar rats. *Brain research,* 988**,** 130-138.

RANSON, R. N., PRIESTLEY, D. J., SANTER, R. M. & WATSON, A. H. 2005. Changes in the substance P-containing innervation of the lumbosacral spinal cord in male Wistar rats as a consequence of ageing. *Brain Res,* 1036**,** 139-44.

RANSON, R. N. & SAFFREY, M. J. 2015. Neurogenic mechanisms in bladder and bowel ageing. *Biogerontology,* 16**,** 265-84.

RANSON, R. N., SANTER, R. M. & WATSON, A. H. 2006. The relationship between serotonin, dopamine beta hydroxylase and GABA immunoreactive inputs and spinal preganglionic neurones projecting to the major pelvic ganglion of Wistar rats. *Neuroscience,* 141**,** 1935-49.

RANSON, R. N., SANTER, R. M. & WATSON, A. H. 2007. Ageing reduces the number of vesicular glutamate transporter 2 containing immunoreactive inputs to identified rat pelvic motoneurons. *Exp Gerontol,* 42**,** 506-16.

RAO, M., NELMS, B. D., DONG, L., SALINAS-RIOS, V., RUTLIN, M., GERSHON, M. D. & CORFAS, G. 2015. Enteric glia express proteolipid protein 1 and are a transcriptionally unique population of glia in the mammalian nervous system. *Glia,* 63**,** 2040-2057.

RAO, S. S. & WELCHER, K. 1996. Periodic rectal motor activity: the intrinsic colonic gatekeeper? *Am J Gastroenterol,* 91**,** 890-7.

RAO, S. S. C. 2004. Pathophysiology of adult fecal incontinence. *Gastroenterology,* 126**,** S14-S22.

RASMUSSEN, M. M., KROGH, K., CLEMMENSEN, D., BLUHME, H., RAWASHDEH, Y. & CHRISTENSEN, P. 2013. Colorectal transport during defecation in subjects with supraconal spinal cord injury. *Spinal Cord,* 51**,** 683-687.

READ, N. W. & ABOUZEKRY, L. 1986. Why do patients with faecal impaction have faecal incontinence. *Gut,* 27**,** 283-287.

REINER, A. & LEVITZ, J. 2018. Glutamatergic Signaling in the Central Nervous System: Ionotropic and Metabotropic Receptors in Concert. *Neuron,* 98**,** 1080-1098.

ROBERTS, D. E., KILLIANY, R. J. & ROSENE, D. L. 2012. Neuron numbers in the hypothalamus of the normal aging rhesus monkey: stability across the adult lifespan and between the sexes. *The Journal of comparative neurology,* 520**,** 1181-1197.

ROBINSON, D. R., MCNAUGHTON, P. A., EVANS, M. L. & HICKS, G. A. 2004. Characterization of the primary spinal afferent innervation of the mouse colon using retrograde labelling. *Neurogastroenterol Motil,* 16**,** 113-24.

ROLAND, B. L. & SAWCHENKO, P. E. 1993. Local origins of some GABAergic projections to the paraventricular and supraoptic nuclei of the hypothalamus in the rat. *Journal of Comparative Neurology,* 332**,** 123-143.

ROMAGNANO, M. A., BRAIMAN, J., LOOMIS, M. & HAMILL, R. W. 1987. Enkephalin fibers in autonomic nuclear regions: Intraspinal vs. supraspinal origin. *Journal of Comparative Neurology,* 266**,** 319-331.

ROMAGNANO, M. A. & HAMILL, R. W. 1985. Spinal parasympathetic enkephalin fibers: patterns and projections. *Brain research,* 335**,** 174-181.

ROOD, B. D. & DE VRIES, G. J. 2011. Vasopressin innervation of the mouse (Mus musculus) brain and spinal cord. *The Journal of comparative neurology,* 519**,** 2434-2474.

ROOZENDAAL, B., VAN GOOL, W. A., SWAAB, D. F., HOOGENDIJK, J. E. & MIRMIRAN, M. 1987. Changes in vasopressin cells of the rat suprachiasmatic nucleus with aging. *Brain Res,* 409**,** 259-64.

ROTHMAN, S. M. & OLNEY, J. W. 1986. Glutamate and the pathophysiology of hypoxic--ischemic brain damage. *Ann Neurol,* 19**,** 105-11.

ROUZADE-DOMINGUEZ, M. L., CURTIS, A. L. & VALENTINO, R. J. 2001. Role of Barrington's nucleus in the activation of rat locus coeruleus neurons by colonic distension. *Brain Res,* 917**,** 206-18.

ROUZADE-DOMINGUEZ, M. L., MISELIS, R. & VALENTINO, R. J. 2003a. Central representation of bladder and colon revealed by dual transsynaptic tracing in the rat: substrates for pelvic visceral coordination. *Eur J Neurosci,* 18**,** 3311-24.

ROUZADE-DOMINGUEZ, M. L., PERNAR, L., BECK, S. & VALENTINO, R. J. 2003b. Convergent responses of Barrington's nucleus neurons to pelvic visceral stimuli in the rat: a juxtacellular labelling study. *Eur J Neurosci,* 18**,** 3325-34.

ROY, H. A. & GREEN, A. L. 2019. The Central Autonomic Network and Regulation of Bladder Function. *Frontiers in neuroscience,* 13**,** 535-535.

RUHAAK, L. R., XU, G., LI, Q., GOONATILLEKE, E. & LEBRILLA, C. B. 2018. Mass Spectrometry Approaches to Glycomic and Glycoproteomic Analyses. *Chem Rev,* 118**,** 7886-7930.

SABEL, B. A. & STEIN, D. G. 1981. Extensive loss of subcortical neurons in the aging rat brain. *Exp Neurol,* 73**,** 507-16.

SADEGHI, M., ERICKSON, A., CASTRO, J., DEITEREN, A., HARRINGTON, A. M., GRUNDY, L., ADAMS, D. J. & BRIERLEY, S. M. 2018. Contribution of membrane receptor signalling to chronic visceral pain. *The International Journal of Biochemistry & Cell Biology,* 98**,** 10-23.

SAFFREY, M. J. 2013. Cellular changes in the enteric nervous system during ageing. *Developmental Biology,* 382**,** 344-355.

SAFFREY, M. J. 2014. Aging of the mammalian gastrointestinal tract: a complex organ system. *Age (Dordrecht, Netherlands),* 36**,** 9603-9603.

SAGA, S., VINSNES, A. G., MORKVED, S., NORTON, C. & SEIM, A. 2013. Prevalence and correlates of fecal incontinence among nursing home residents: a population-based cross-sectional study. *BMC Geriatr,* 13**,** 87.

SAMUELS, E. R. & SZABADI, E. 2008. Functional neuroanatomy of the noradrenergic locus coeruleus: its roles in the regulation of arousal and autonomic function part I: principles of functional organisation. *Current neuropharmacology,* 6**,** 235-253.

SAMUELSSON, E., ODEBERG, J., STENZELIUS, K., MOLANDER, U., HAMMARSTRÖM, M., FRANZEN, K., ANDERSSON, G. & MIDLÖV, P. 2015. Effect of pharmacological treatment for urinary incontinence in the elderly and frail elderly: A systematic review. *Geriatrics & Gerontology International,* 15**,** 521-534.

SANDERS, K. M., WARD, S. M. & KOH, S. D. 2014. Interstitial cells: regulators of smooth muscle function. *Physiol Rev,* 94**,** 859-907.

SANTER, R. M., DERING, M. A., RANSON, R. N., WABOSO, H. N. & WATSON, A. H. D. 2002. Differential susceptibility to ageing of rat preganglionic neurones projecting to the major pelvic ganglion and of their afferent inputs. *Autonomic Neuroscience,* 96**,** 73-81.

SARNA, S. K. 1991. Physiology and pathophysiology of colonic motor activity (2). *Dig Dis Sci,* 36**,** 998-1018.

SARTIN, J. L. & LAMPERTI, A. A. 1985. Neuron numbers in hypothalamic nuclei of young, middle-aged and aged male rats. *Experientia,* 41**,** 109-11.

SASEK, C. A. & ELDE, R. P. 1986. Coexistence of enkephalin and dynorphin immunoreactivities in neurons in the dorsal gray commissure of the sixth lumbar and first sacral spinal cord segments in rat. *Brain research,* 381**,** 8-14.

SAWCHENKO, P. E. 1987. Evidence for differential regulation of corticotropin-releasing factor and vasopressin immunoreactivities in parvocellular neurosecretory and autonomic-related projections of the paraventricular nucleus. *Brain Res,* 437**,** 253-63.

SAWCHENKO, P. E. & SWANSON, L. W. 1982a. Immunohistochemical identification of neurons in the paraventricular nucleus of the hypothalamus that project to the medulla or to the spinal cord in the rat. *J Comp Neurol,* 205**,** 260-72.

SAWCHENKO, P. E. & SWANSON, L. W. 1982b. The organization of noradrenergic pathways from the brainstem to the paraventricular and supraoptic nuclei in the rat. *Brain Research Reviews,* 4**,** 275-325.

SCHLUTER, P. J., WARD, C., ARNOLD, E. P., SCRASE, R. & JAMIESON, H. A. 2017. Urinary incontinence, but not fecal incontinence, is a risk factor for admission to aged residential care of older persons in New Zealand. *Neurourol Urodyn,* 36**,** 1588-1595.

SCHNELLE, J. F., SIMMONS, S. F., BEUSCHER, L., PETERSON, E. N., HABERMANN, R. & LEUNG, F. 2009. Prevalence of constipation

symptoms in fecally incontinent nursing home residents. *J Am Geriatr Soc,* 57, 647-52.
SCHRØDER, H. D. 1980. Organization of the motoneurons innervating the pelvic muscles of the male rat. *Journal of Comparative Neurology,* 192, 567-587.
SCHWARZ, L. A., MIYAMICHI, K., GAO, X. J., BEIER, K. T., WEISSBOURD, B., DELOACH, K. E., REN, J., IBANES, S., MALENKA, R. C., KREMER, E. J. & LUO, L. 2015. Viral-genetic tracing of the input–output organization of a central noradrenaline circuit. *Nature,* 524, 88-92.
SEARCY, J. A. R. 2017. Geriatric Urinary Incontinence. *Nurs Clin North Am,* 52, 447-455.
SEYBOLD, V. & ELDE, R. 1980. Immunohistochemical studies of peptidergic neurons in the dorsal horn of the spinal cord. *J Histochem Cytochem,* 28, 367-70.
SHAH, B. J., CHOKHAVATIA, S. & ROSE, S. 2012. Fecal incontinence in the elderly: FAQ. *Am J Gastroenterol,* 107, 1635-46.
SHAMLIYAN, T., WYMAN, J., BLISS, D. Z., KANE, R. L. & WILT, T. J. 2007. Prevention of urinary and fecal incontinence in adults. *Evid Rep Technol Assess (Full Rep)*, 1-379.
SHAW, C., GUPTA, R. D., BUSHNELL, D. M., ASSASSA, R. P., ABRAMS, P., WAGG, A., MAYNE, C., HARDWICK, C. & MARTIN, M. 2006. The extent and severity of urinary incontinence amongst women in UK GP waiting rooms. *Family Practice,* 23, 497-506.
SHEFCHYK, S. J. 2002. Chapter 6 Spinal cord neural organization controlling the urinary bladder and striated sphincter. *In:* MCKERRACHER, L., DOUCET, G. & ROSSIGNOL, S. (eds.) *Progress in Brain Research.* Elsevier.
SHIMADA, S., INAGAKI, S., KUBOTA, Y., KITO, S., SHIOTANI, Y. & TOHYAMA, M. 1987. Coexistence of substance P- and enkephalin-like peptides in single neurons of the rat hypothalamus. *Brain Res,* 425, 256-62.
SHIMOSEGAWA, T., KOIZUMI, M., TOYOTA, T., GOTO, Y., YANAIHARA, C. & YANAIHARA, N. 1987. An immunohistochemical study of methionine-enkephalin-Arg6-Gly7-Leu8-like immunoreactivity-containing neurons in the

parasympathetic preganglionic regions of the rat spinal cord. *Brain research,* 406, 341-347.
SHIROKAWA, T., ISHIDA, Y. & ISOBE, K. 2000. Changes in electrophysiological properties of axon terminals of locus coeruleus neurons with age in F344 rat. *Neurosci Lett,* 289, 69-71.
SHIROMANI, P. J., LU, J., WAGNER, D., THAKKAR, J., GRECO, M. A., BASHEER, R. & THAKKAR, M. 2000. Compensatory sleep response to 12 h wakefulness in young and old rats. *Am J Physiol Regul Integr Comp Physiol,* 278, R125-33.
SIE, J. A., BLOK, B. F., DE WEERD, H. & HOLSTEGE, G. 2001. Ultrastructural evidence for direct projections from the pontine micturition center to glycine-immunoreactive neurons in the sacral dorsal gray commissure in the cat. *J Comp Neurol,* 429, 631-7.
SILVERMAN, A. J., HOFFMAN, D. L. & ZIMMERMAN, E. A. 1981. The descending afferent connections of the paraventricular nucleus of the hypothalamus (PVN). *Brain Research Bulletin,* 6, 47-61.
SILVERMAN, D. H., MUNAKATA, J. A., ENNES, H., MANDELKERN, M. A., HOH, C. K. & MAYER, E. A. 1997. Regional cerebral activity in normal and pathological perception of visceral pain. *Gastroenterology,* 112, 64-72.
SITEK, B., WALDERA-LUPA, D., POSCHMANN, G., MEYER, H. & STUEHLER, K. 2012. Application of Label-Free Proteomics for Differential Analysis of Lung Carcinoma Cell Line A549. *Methods in molecular biology (Clifton, N.J.),* 893, 241-8.
SMITH, T. K. & KOH, S. D. 2017. A model of the enteric neural circuitry underlying the generation of rhythmic motor patterns in the colon: the role of serotonin. *American journal of physiology. Gastrointestinal and liver physiology,* 312, G1-G14.
SMITH, T. K., SPENCER, N. J., HENNIG, G. W. & DICKSON, E. J. 2007. Recent advances in enteric neurobiology: mechanosensitive interneurons. *Neurogastroenterol Motil,* 19, 869-78.
SMOLILO, D., HIBBERD, T., COSTA, M., WATTCHOW, D., DE FONTGALLAND, D. & SPENCER, N. J. 2020. Intrinsic sensory neurons provide direct input to motor neurons and

interneurons in mouse distal colon via varicose baskets. *J Comp Neurol*.

SMOLILO, D. J., COSTA, M., HIBBERD, T. J., BROOKES, S. J. H., WATTCHOW, D. A. & SPENCER, N. J. 2019. Distribution, projections, and association with calbindin baskets of motor neurons, interneurons, and sensory neurons in guinea-pig distal colon. *J Comp Neurol,* 527**,** 1140-1158.

SNOOKS, S. J., HENRY, M. M. & SWASH, M. 1985. Faecal incontinence due to external anal sphincter division in childbirth is associated with damage to the innervation of the pelvic floor musculature: a double pathology. *BJOG: An International Journal of Obstetrics & Gynaecology,* 92**,** 824-828.

SNOW, P. J., RENSHAW, G. M. & HAMLIN, K. E. 1996. Localization of enkephalin immunoreactivity in the spinal cord of the long-tailed ray Himantura fai. *J Comp Neurol,* 367**,** 264-73.

SOENEN, S., RAYNER, C. K., JONES, K. L. & HOROWITZ, M. 2016. The ageing gastrointestinal tract. *Curr Opin Clin Nutr Metab Care,* 19**,** 12-8.

SOLIMAN, Y., MEYER, R. & BAUM, N. 2016. Falls in the Elderly Secondary to Urinary Symptoms. *Rev Urol,* 18**,** 28-32.

SOMOGYI, G. T. & DE GROAT, W. C. 1993. Modulation of release of [3H]acetylcholine in the major pelvic ganglion of the rat. *Am J Physiol,* 264**,** R1084-8.

SONG, H. J. & BAE, J. M. 2007. Prevalence of urinary incontinence and lower urinary tract symptoms for community-dwelling elderly 85 years of age and older. *J Wound Ostomy Continence Nurs,* 34**,** 535-41.

SONG, S., WANG, Q., JIANG, L., OYARZABAL, E., RIDDICK, N. V., WILSON, B., MOY, S. S., SHIH, Y. I. & HONG, J. S. 2019. Noradrenergic dysfunction accelerates LPS-elicited inflammation-related ascending sequential neurodegeneration and deficits in non-motor/motor functions. *Brain Behav Immun,* 81**,** 374-387.

SONG, Z. M., BROOKES, S. J. & COSTA, M. 1991. Identification of myenteric neurons which project to the mucosa of the guinea-pig small intestine. *Neurosci Lett,* 129**,** 294-8.

SONG, Z. M., BROOKES, S. J. H., RAMSAY, G. A. & COSTA, M. 1997. Characterization of myenteric interneurons with somatostatin immunoreactivity in the guinea-pig small intestine. *Neuroscience,* 80**,** 907-923.

SOREIDE, K., BOERMEESTER, M. A., HUMES, D. J. & VELMAHOS, G. C. 2016. Acute colonic diverticulitis: modern understanding of pathomechanisms, risk factors, disease burden and severity. *Scand J Gastroenterol,* 51**,** 1416-1422.

SPENCER, N. J., DINNING, P. G., BROOKES, S. J. & COSTA, M. 2016. Insights into the mechanisms underlying colonic motor patterns. *J Physiol,* 594**,** 4099-116.

SPENCER, S. J., BULLER, K. M. & DAY, T. A. 2005. Medial prefrontal cortex control of the paraventricular hypothalamic nucleus response to psychological stress: possible role of the bed nucleus of the stria terminalis. *J Comp Neurol,* 481**,** 363-76.

STAMMERS, M., IVANOVA, I. M., NIEWCZAS, I. S., SEGONDS-PICHON, A., STREETER, M., SPIEGEL, D. A. & CLARK, J. 2020. Age-related changes in the physical properties, cross-linking, and glycation of collagen from mouse tail tendon. *J Biol Chem,* 295**,** 10562-10571.

STANDAERT, D. G., SAPER, C. B., RYE, D. B. & WAINER, B. H. 1986. Colocalization of atriopeptin-like immunoreactivity with choline acetyltransferase- and substance P-like immunoreactivity in the pedunculopontine and laterodorsal tegmental nuclei in the rat. *Brain Res,* 382**,** 163-8.

STEEGENGA, W. T., DE WIT, N. J., BOEKSCHOTEN, M. V., IJSSENNAGGER, N., LUTE, C., KESHTKAR, S., BROMHAAR, M. M. G., KAMPMAN, E., DE GROOT, L. C. & MULLER, M. 2012. Structural, functional and molecular analysis of the effects of aging in the small intestine and colon of C57BL/6J mice. *BMC medical genomics,* 5**,** 38-38.

STEELE, P. A., BROOKES, S. J. & COSTA, M. 1991. Immunohistochemical identification of cholinergic neurons in the myenteric plexus of guinea-pig small intestine. *Neuroscience,* 45**,** 227-39.

STEPHENS, M. A. 1979. Tests of fit for the logistic distribution based on the empirical distribution function. *Biometrika,* 66**,** 591-595.

STEWART, D. C., BERRIE, D., LI, J., LIU, X., RICKERSON, C., MKOJI, D., IQBAL, A., TAN, S., DOTY, A. L., GLOVER, S. C. & SIMMONS, C. S. 2018. Quantitative assessment of intestinal stiffness and associations with fibrosis in human inflammatory bowel disease. *PloS one,* 13**,** e0200377-e0200377.

STICKLEY, A., SANTINI, Z. I. & KOYANAGI, A. 2017. Urinary incontinence, mental health and loneliness among community-dwelling older adults in Ireland. *BMC Urol,* 17**,** 29.

STURROCK, R. R. 1992. Stability of neuron number in the ageing mouse para-ventricular nucleus. *Annals of Anatomy - Anatomischer Anzeiger,* 174**,** 337-340.

STURROCK, R. R. 1993. The effect of ageing on the posterior medial and posterior lateral subnuclei of the bed nucleus of the stria terminalis in the mouse. *Ann Anat,* 175**,** 189-93.

STURROCK, R. R. & RAO, K. A. 1985. A quantitative histological study of neuronal loss from the locus coeruleus of ageing mice. *Neuropathol Appl Neurobiol,* 11**,** 55-60.

SUGAYA, K., MATSUYAMA, K., TAKAKUSAKI, K. & MORI, S. 1987. Electrical and chemical stimulations of the pontine micturition center. *Neurosci Lett,* 80**,** 197-201.

SUGAYA, K., NISHIJIMA, S., KADEKAWA, K., NOGUCHI, K., UEDA, T. & YAMAMOTO, H. 2019. Spinal glycinergic and gamma-aminobutyric acid-ergic neurons inhibit the micturition reflex after electrical stimulation of the perineum in rats with pelvic venous congestion. *Int J Urol,* 26**,** 1149-1155.

SUGAYA, K., NISHIJIMA, S., MIYAZATO, M., ASHITOMI, K., HATANO, T. & OGAWA, Y. 2002. Effects of intrathecal injection of tamsulosin and naftopidil, alpha-1A and -1D adrenergic receptor antagonists, on bladder activity in rats. *Neurosci Lett,* 328**,** 74-6.

SUGAYA, K., ROPPOLO, J. R., YOSHIMURA, N., CARD, J. P. & DE GROAT, W. C. 1997. The central neural pathways involved in micturition in the neonatal rat as revealed by the injection of

pseudorabies virus into the urinary bladder. *Neurosci Lett,* 223**,** 197-200.

SUN, T., LI, D., HU, S., HUANG, L., SUN, H., YANG, S., WU, B., JI, F. & ZHOU, D. 2018. Aging-dependent decrease in the numbers of enteric neurons, interstitial cells of Cajal and expression of connexin43 in various regions of gastrointestinal tract. *Aging,* 10**,** 3851-3865.

SUNG, T. S., HWANG, S. J., KOH, S. D., BAYGUINOV, Y., PERI, L. E., BLAIR, P. J., WEBB, T. I., PARDO, D. M., ROCK, J. R., SANDERS, K. M. & WARD, S. M. 2018. The cells and conductance mediating cholinergic neurotransmission in the murine proximal stomach. *J Physiol,* 596**,** 1549-1574.

SVARE, B., MANN, M., BROIDA, J., KINSLEY, C., GHIRALDI, L., MIELE, J. & KONEN, C. 1983. Intermale aggression and infanticide in aged C57BL/6J male mice: behavioral deficits are not related to serum testosterone (T) levels and are not recovered by supplemental T. *Neurobiol Aging,* 4**,** 305-12.

SWAAB, D. F. & LUCASSEN, P. J. 2009. Hypothalamo-neurohypophysial System. *In:* BINDER, M. D., HIROKAWA, N. & WINDHORST, U. (eds.) *Encyclopedia of Neuroscience.* Berlin, Heidelberg: Springer Berlin Heidelberg.

SWANSON, L. W. & KUYPERS, H. G. 1980. The paraventricular nucleus of the hypothalamus: cytoarchitectonic subdivisions and organization of projections to the pituitary, dorsal vagal complex, and spinal cord as demonstrated by retrograde fluorescence double-labeling methods. *J Comp Neurol,* 194**,** 555-70.

SWANSON, L. W. & MCKELLAR, S. 1979. The distribution of oxytocin- and neurophysin-stained fibers in the spinal cord of the rat and monkey. *J Comp Neurol,* 188**,** 87-106.

SWANSON, L. W. & SAWCHENKO, P. E. 1980. Paraventricular nucleus: a site for the integration of neuroendocrine and autonomic mechanisms. *Neuroendocrinology,* 31**,** 410-7.

SWANSON, L. W., SAWCHENKO, P. E., BEROD, A., HARTMAN, B. K., HELLE, K. B. & VANORDEN, D. E. 1981. An immunohistochemical study of the organization of catecholaminergic cells and terminal fields in the

paraventricular and supraoptic nuclei of the hypothalamus. *J Comp Neurol,* 196**,** 271-85.
SWANSON, L. W., SAWCHENKO, P. E., WIEGAND, S. J. & PRICE, J. L. 1980. Separate neurons in the paraventricular nucleus project to the median eminence and to the medulla or spinal cord. *Brain Res,* 198**,** 190-5.
SYNAPTIC-SYSTEMS 2020. Antibody Validation.
SZABO, S. M., GOOCH, K. L., WALKER, D. R., JOHNSTON, K. M. & WAGG, A. S. 2018. The Association Between Overactive Bladder and Falls and Fractures: A Systematic Review. *Adv Ther,* 35**,** 1831-1841.
TAI, C., BOOTH, A. M., DE GROAT, W. C. & ROPPOLO, J. R. 2001. Colon and anal sphincter contractions evoked by microstimulation of the sacral spinal cord in cats. *Brain Res,* 889**,** 38-48.
TAI, C., WANG, J., JIN, T., WANG, P., KIM, S. G., ROPPOLO, J. R. & DE GROAT, W. C. 2009. Brain switch for reflex micturition control detected by FMRI in rats. *J Neurophysiol,* 102**,** 2719-30.
TAKAHASHI, A. 2016. Subchapter 7A - Enkephalin. *In:* TAKEI, Y., ANDO, H. & TSUTSUI, K. (eds.) *Handbook of Hormones.* San Diego: Academic Press.
TAKASAKI, A., HUI, M. & SASAKI, M. 2010. Is the periaqueductal gray an essential relay center for the micturition reflex pathway in the cat? *Brain Research,* 1317**,** 108-115.
TANAHASHI, Y., WAKI, N., UNNO, T., MATSUYAMA, H., IINO, S., KITAZAWA, T., YAMADA, M. & KOMORI, S. 2013. Roles of M2 and M3 muscarinic receptors in the generation of rhythmic motor activity in mouse small intestine. *Neurogastroenterol Motil,* 25**,** e687-97.
TANG, Y., RAMPIN, O., CALAS, A., FACCHINETTI, P. & GIULIANO, F. 1998. Oxytocinergic and serotonergic innervation of identified lumbosacral nuclei controlling penile erection in the male rat. *Neuroscience,* 82**,** 241-54.
TANG, Y., RAMPIN, O., GIULIANO, F. & UGOLINI, G. 1999. Spinal and brain circuits to motoneurons of the bulbospongiosus muscle: retrograde transneuronal tracing with rabies virus. *J Comp Neurol,* 414**,** 167-92.

TARENTINO, A. L. & PLUMMER, T. H., JR. 1982. Oligosaccharide accessibility to peptide:N-glycosidase as promoted by protein-unfolding reagents. *J Biol Chem,* 257**,** 10776-80.

TARNAWSKI, A., PAI, R., DENG, X., AHLUWALIA, A., KHOMENKO, T., TANIGAWA, T., AKAHOSHI, T., SANDOR, Z. & SZABO, S. 2007. Aging gastropathy-novel mechanisms: hypoxia, up-regulation of multifunctional phosphatase PTEN, and proapoptotic factors. *Gastroenterology,* 133**,** 1938-47.

TAWEEL, W. A. & SEYAM, R. 2015. Neurogenic bladder in spinal cord injury patients. *Research and reports in urology,* 7**,** 85-99.

TENNYSON, L. E., TAI, C. & CHERMANSKY, C. J. 2016. Using the Native Afferent Nervous System to Sense Bladder Fullness: State of the Art. *Current bladder dysfunction reports,* 11**,** 346-349.

TEUNISSEN, T. A., VAN DEN BOSCH, W. J., VAN DEN HOOGEN, H. J. & LAGRO-JANSSEN, A. L. 2004. Prevalence of urinary, fecal and double incontinence in the elderly living at home. *Int Urogynecol J Pelvic Floor Dysfunct,* 15**,** 10-3; discussion 13.

THOMAS, A. M. & MORSE, J. M. 1991. Managing urinary incontinence with self-care practices. *J Gerontol Nurs,* 17**,** 9-14.

THOMAS, C., GIOIELLO, A., NORIEGA, L., STREHLE, A., OURY, J., RIZZO, G., MACCHIARULO, A., YAMAMOTO, H., MATAKI, C., PRUZANSKI, M., PELLICCIARI, R., AUWERX, J. & SCHOONJANS, K. 2009. TGR5-mediated bile acid sensing controls glucose homeostasis. *Cell metabolism,* 10**,** 167-177.

THOR, K. B. & DE GROAT, W. C. 2010. Neural control of the female urethral and anal rhabdosphincters and pelvic floor muscles. *Am J Physiol Regul Integr Comp Physiol,* 299**,** R416-38.

TIMMERMANS, J.-P., ADRIAENSEN, D., CORNELISSEN, W. & SCHEUERMANN, D. W. 1997. Structural Organization and Neuropeptide Distribution in the Mammalian Enteric Nervous System, with Special Attention to Those Components Involved in Mucosal Reflexes. *Comparative Biochemistry and Physiology Part A: Physiology,* 118**,** 331-340.

TOBIN, G. W. & BROCKLEHURST, J. C. 1986. Faecal incontinence in residential homes for the elderly: prevalence, aetiology and management. *Age Ageing,* 15**,** 41-6.

TODD, A. J., SPIKE, R. C., RUSSELL, G. & JOHNSTON, H. M. 1992. Immunohistochemical evidence that Met-enkephalin and GABA coexist in some neurones in rat dorsal horn. *Brain Res,* 584**,** 149-56.

TONG, W. D., RIDOLFI, T. J., KOSINSKI, L., LUDWIG, K. & TAKAHASHI, T. 2010. Effects of autonomic nerve stimulation on colorectal motility in rats. *Neurogastroenterology and motility : the official journal of the European Gastrointestinal Motility Society,* 22**,** 688-693.

TRUDRUNG, P., FURNESS, J. B., POMPOLO, S. & MESSENGER, J. P. 1994. Locations and chemistries of sympathetic nerve cells that project to the gastrointestinal tract and spleen. *Arch Histol Cytol,* 57**,** 139-50.

TSUKAHARA, S., TANAKA, S., ISHIDA, K., HOSHI, N. & KITAGAWA, H. 2005. Age-related change and its sex differences in histoarchitecture of the hypothalamic suprachiasmatic nucleus of F344/N rats. *Exp Gerontol,* 40**,** 147-55.

TSURUOKA, M., MAEDA, M. & INOUE, T. 2005. Stimulation of the nucleus locus coeruleus/subcoeruleus suppresses visceromotor responses to colorectal distention in the rat. *Neurosci Lett,* 381**,** 97-101.

UENO, H., KUNO, M., SHINTANI, Y. & KAMO, I. 2011. Role of vasopressin V((1)A) receptor in the urethral closure reflex in rats. *Am J Physiol Renal Physiol,* 300**,** F976-82.

UGOLINI, G. 2010. Advances in viral transneuronal tracing. *J Neurosci Methods,* 194**,** 2-20.

UGURLUCAN, F. G., EVRUKE, I., YASA, C., DURAL, O. & YALCIN, O. 2019. Sexual functions and quality of life of women over 50 years with urinary incontinence, lower urinary tract symptoms and/or pelvic organ prolapse. *Int J Impot Res*.

UHL, G. R., GOODMAN, R. R., KUHAR, M. J., CHILDERS, S. R. & SNYDER, S. H. 1979. Immunohistochemical mapping of enkephalin containing cell bodies, fibers and nerve terminals in the brain stem of the rat. *Brain Research,* 166**,** 75-94.

ULRICH-LAI, Y. M., JONES, K. R., ZIEGLER, D. R., CULLINAN, W. E. & HERMAN, J. P. 2011. Forebrain origins of glutamatergic innervation to the rat paraventricular nucleus of the hypothalamus: differential inputs to the anterior versus posterior subregions. *J Comp Neurol,* 519**,** 1301-19.

UNIPROT. 2020. *UniProt* [Online]. Available: https://www.uniprot.org/ [Accessed].

VAIDYANATHAN, S., SANKARANARAYANAN, A., SZEKELY, J. I. & HEMAL, A. K. 1989. Lowering of maximum urethral pressure by (D-Met2, Pro5)-enkephalinamide in patients with neurogenic vesicourethral dysfunction due to spinal cord injury. *International journal of clinical pharmacology, therapy, and toxicology,* 27**,** 92-95.

VALENTINO, R. J., CHEN, S., ZHU, Y. & ASTON-JONES, G. 1996. Evidence for divergent projections to the brain noradrenergic system and the spinal parasympathetic system from Barrington's nucleus. *Brain Res,* 732**,** 1-15.

VALENTINO, R. J., KOSBOTH, M., COLFLESH, M. & MISELIS, R. R. 2000. Transneuronal labeling from the rat distal colon: anatomic evidence for regulation of distal colon function by a pontine corticotropin-releasing factor system. *J Comp Neurol,* 417**,** 399-414.

VALENTINO, R. J., MISELIS, R. R. & PAVCOVICH, L. A. 1999. Pontine regulation of pelvic viscera: pharmacological target for pelvic visceral dysfunctions. *Trends Pharmacol Sci,* 20**,** 253-60.

VALENTINO, R. J., PAGE, M. E., LUPPI, P. H., ZHU, Y., VAN BOCKSTAELE, E. & ASTON-JONES, G. 1994. Evidence for widespread afferents to Barrington's nucleus, a brainstem region rich in corticotropin-releasing hormone neurons. *Neuroscience,* 62**,** 125-43.

VALENTINO, R. J., WOOD, S. K., WEIN, A. J. & ZDERIC, S. A. 2011. The bladder-brain connection: putative role of corticotropin-releasing factor. *Nature reviews. Urology,* 8**,** 19-28.

VAN BOCKSTAELE, E. J., BRANCHEREAU, P. & PICKEL, V. M. 1995. Morphologically heterogeneous met-enkephalin terminals form synapses with tyrosine hydroxylase-containing dendrites

in the rat nucleus locus coeruleus. *Journal of Comparative Neurology,* 363, 423-438.
VAN DEN POL, A. N. 1994. Metabotropic glutamate receptor mGluR1 distribution and ultrastructural localization in hypothalamus. *Journal of Comparative Neurology,* 349, 615-632.
VAN DEN POL, A. N., HERBST, R. S. & POWELL, J. F. 1984. Tyrosine hydroxylase-immunoreactive neurons of the hypothalamus: A light and electron microscopic study. *Neuroscience,* 13, 1117-1156.
VAN DEN POL, A. N., ROMANO, C. & GHOSH, P. 1995. Metabotropic glutamate receptor mGluR5 subcellular distribution and developmental expression in hypothalamus. *Journal of Comparative Neurology,* 362, 134-150.
VAZEY, E. M. & ASTON-JONES, G. 2014. Designer receptor manipulations reveal a role of the locus coeruleus noradrenergic system in isoflurane general anesthesia. *Proc Natl Acad Sci U S A,* 111, 3859-64.
VAZQUEZ ROQUE, M. & BOURAS, E. P. 2015. Epidemiology and management of chronic constipation in elderly patients. *Clin Interv Aging,* 10, 919-30.
VERBITSKAIA, L. B. & BOGOLEPOV, N. N. 1984. [Changes in the hypothalamic ultrastructure during aging]. *Zh Nevropatol Psikhiatr Im S S Korsakova,* 84, 987-93.
VERONNEAU-LONGUEVILLE, F., RAMPIN, O., FREUND-MERCIER, M. J., TANG, Y., CALAS, A., MARSON, L., MCKENNA, K. E., STOECKEL, M. E., BENOIT, G. & GIULIANO, F. 1999. Oxytocinergic innervation of autonomic nuclei controlling penile erection in the rat. *Neuroscience,* 93, 1437-47.
VERSTEGEN, A. M. J., VANDERHORST, V., GRAY, P. A., ZEIDEL, M. L. & GEERLING, J. C. 2017. Barrington's nucleus: Neuroanatomic landscape of the mouse "pontine micturition center". *The Journal of comparative neurology,* 525, 2287-2309.
VIJAYASHANKAR, N. & BRODY, H. 1979. A quantitative study of the pigmented neurons in the nuclei locus coeruleus and subcoeruleus in man as related to aging. *J Neuropathol Exp Neurol,* 38, 490-7.

VILCHEZ, D., SAEZ, I. & DILLIN, A. 2014. The role of protein clearance mechanisms in organismal ageing and age-related diseases. *Nature Communications,* 5**,** 5659.

VIOLLET, C., LEPOUSEZ, G., LOUDES, C., VIDEAU, C., SIMON, A. & EPELBAUM, J. 2008. Somatostatinergic systems in brain: Networks and functions. *Molecular and Cellular Endocrinology,* 286**,** 75-87.

VIZZARD, M. A., ERICKSON, V. L., CARD, J. P., ROPPOLO, J. R. & DE GROAT, W. C. 1995. Transneuronal labeling of neurons in the adult rat brainstem and spinal cord after injection of pseudorabies virus into the urethra. *J Comp Neurol,* 355**,** 629-40.

VON HEYDEN, B., JORDAN, U. & HERTLE, L. 1998. Neurotransmitters in the human urethral sphincter in the absence of voiding dysfunction. *Urol Res,* 26**,** 299-310.

VRIJENS, D., DROSSAERTS, J., VAN KOEVERINGE, G., VAN KERREBROECK, P., VAN OS, J. & LEUE, C. 2015. Affective symptoms and the overactive bladder - a systematic review. *J Psychosom Res,* 78**,** 95-108.

WAGNER, C. K. & CLEMENS, L. G. 1993. Neurophysin-containing pathway from the paraventricular nucleus of the hypothalamus to a sexually dimorphic motor nucleus in lumbar spinal cord. *J Comp Neurol,* 336**,** 106-16.

WALD, A., SCARPIGNATO, C., KAMM, M. A., MUELLER-LISSNER, S., HELFRICH, I., SCHUIJT, C., BUBECK, J., LIMONI, C. & PETRINI, O. 2007. The burden of constipation on quality of life: results of a multinational survey. *Aliment Pharmacol Ther,* 26**,** 227-36.

WALDHOER, M., BARTLETT, S. E. & WHISTLER, J. L. 2004. Opioid receptors. *Annu Rev Biochem,* 73**,** 953-90.

WANG, F. B. & POWLEY, T. L. 2007. Vagal innervation of intestines: afferent pathways mapped with new en bloc horseradish peroxidase adaptation. *Cell Tissue Res,* 329**,** 221-30.

WANG, L., LARAUCHE, M. H. & TACHE, Y. 2010. M1304 Intrathecal Injection of Corticotropin-Releasing Factor (CRF), Unlike Urocortin 2, Increases Distal Colonic Contractions and Neuronal Activation in Lumbosacral Spinal Cord of Rats. *Gastroenterology,* 138**,** S-376.

WANG, L., LIANG, Y., CHEN, Q., AHMED, N., WANG, F., HU, B. & YANG, P. 2018. Identification and Distribution of the Interstitial Cells of Cajal in the Abomasum of Goats. *Cell transplantation,* 27**,** 335-344.

WANG, L., MARTINEZ, V., LARAUCHE, M. & TACHE, Y. 2009. Proximal colon distension induces Fos expression in oxytocin-, vasopressin-, CRF- and catecholamines-containing neurons in rat brain. *Brain Res,* 1247**,** 79-91.

WARD, S. M., BURNS, A. J., TORIHASHI, S. & SANDERS, K. M. 1994. Mutation of the proto-oncogene c-kit blocks development of interstitial cells and electrical rhythmicity in murine intestine. *The Journal of physiology,* 480 (Pt 1)**,** 91-97.

WARD, S. M. & SANDERS, K. M. 2006. Involvement of intramuscular interstitial cells of Cajal in neuroeffector transmission in the gastrointestinal tract. *J Physiol,* 576**,** 675-82.

WATANABE, K., IKUNO, Y., KAKEYA, Y., IKENO, S., TANIURA, H., KURONO, M., MINEMORI, K., KATSUYAMA, Y. & NAKA-KANEDA, H. 2019. Age-related dysfunction of the DNA damage response in intestinal stem cells. *Inflammation and Regeneration,* 39**,** 8.

WEHRBERGER, C., MADERSBACHER, S., JUNGWIRTH, S., FISCHER, P. & TRAGL, K. H. 2012. Lower urinary tract symptoms and urinary incontinence in a geriatric cohort - a population-based analysis. *BJU Int,* 110**,** 1516-21.

WERTH, B. L., WILLIAMS, K. A. & PONT, L. G. 2015. A longitudinal study of constipation and laxative use in a community-dwelling elderly population. *Arch Gerontol Geriatr,* 60**,** 418-24.

WERTH, B. L., WILLIAMS, K. A. & PONT, L. G. 2017. Laxative Use and Self-Reported Constipation in a Community-Dwelling Elderly Population: A Community-Based Survey From Australia. *Gastroenterol Nurs,* 40**,** 134-141.

WESS, L., EASTWOOD, M. A., WESS, T. J., BUSUTTIL, A. & MILLER, A. 1995. Cross linking of collagen is increased in colonic diverticulosis. *Gut,* 37**,** 91-4.

WESTLUND, K. N., BOWKER, R. M., ZIEGLER, M. G. & COULTER, J. D. 1983. Noradrenergic projections to the spinal cord of the rat. *Brain Res,* 263**,** 15-31.

WILLIAMSON, J. M. & LYONS, D. A. 2018. Myelin Dynamics Throughout Life: An Ever-Changing Landscape? *Frontiers in Cellular Neuroscience,* 12.

WINGE, K., RASMUSSEN, D. & WERDELIN, L. M. 2003. Constipation in neurological diseases. *Journal of Neurology, Neurosurgery & Psychiatry,* 74**,** 13.

WISE, D. R., WARD, P. S., SHAY, J. E. S., CROSS, J. R., GRUBER, J. J., SACHDEVA, U. M., PLATT, J. M., DEMATTEO, R. G., SIMON, M. C. & THOMPSON, C. B. 2011. Hypoxia promotes isocitrate dehydrogenase-dependent carboxylation of α-ketoglutarate to citrate to support cell growth and viability. *Proceedings of the National Academy of Sciences of the United States of America,* 108**,** 19611-19616.

WISE, P. M. 1982. Alterations in proestrous LH, FSH, and prolactin surges in middle-aged rats. *Proc Soc Exp Biol Med,* 169**,** 348-54.

WISKUR, B. & GREENWOOD-VAN MEERVELD, B. 2010. The aging colon: the role of enteric neurodegeneration in constipation. *Curr Gastroenterol Rep,* 12**,** 507-12.

WITKIN, J. W. 1987. Aging changes in synaptology of luteinizing hormone-releasing hormone neurons in male rat preoptic area. *Neuroscience,* 22**,** 1003-1013.

WOLFF, C., SCHOTT, C., PORSCHEWSKI, P., REISCHAUER, B. & BECKER, K.-F. 2011. Successful protein extraction from over-fixed and long-term stored formalin-fixed tissues. *PloS one,* 6**,** e16353-e16353.

WOMACK, M. D., MORRIS, R., GENT, T. C. & BARRETT-JOLLEY, R. 2007. Substance P targets sympathetic control neurons in the paraventricular nucleus. *Circ Res,* 100**,** 1650-8.

WOOD, S. K., MCFADDEN, K., GRIFFIN, T., WOLFE, J. H., ZDERIC, S. & VALENTINO, R. J. 2013. A corticotropin-releasing factor receptor antagonist improves urodynamic dysfunction produced by social stress or partial bladder outlet obstruction in male rats. *American journal of physiology. Regulatory, integrative and comparative physiology,* 304**,** R940-R950.

WREE, A., BRAAK, H., SCHLEICHER, A. & ZILLES, K. 1980. Biomathematical analysis of the neuronal loss in the aging

human brain of both sexes, demonstrated in pigment preparations of the pars cerebellaris loci coerulei. *Anat Embryol (Berl),* 160**,** 105-19.

WU, J. M., MATTHEWS, C. A., VAUGHAN, C. P. & MARKLAND, A. D. 2015. Urinary, fecal, and dual incontinence in older U.S. Adults. *J Am Geriatr Soc,* 63**,** 947-53.

WU, S. L., AMATO, H., BIRINGER, R., CHOUDHARY, G., SHIEH, P. & HANCOCK, W. S. 2002. Targeted proteomics of low-level proteins in human plasma by LC/MSn: using human growth hormone as a model system. *J Proteome Res,* 1**,** 459-65.

XI, T.-F., LI, D.-N., LI, Y.-Y., QIN, Y., WANG, H.-H., SONG, N.-N., ZHANG, Q., DING, Y.-Q., SHI, X.-Z. & XIE, D.-P. 2019. Central 5-hydroxytryptamine (5-HT) mediates colonic motility by hypothalamus oxytocin-colonic oxytocin receptor pathway. *Biochemical and Biophysical Research Communications,* 508**,** 959-964.

XU, D. & KANE, R. L. 2013. Effect of urinary incontinence on older nursing home residents' self-reported quality of life. *J Am Geriatr Soc,* 61**,** 1473-81.

YAGHMAIE, F., SAEED, O., GARAN, S. A., VOELKER, M. A., GOUW, A. M., FREITAG, W., STERNBERG, H. & TIMIRAS, P. S. 2006. Age-dependent loss of insulin-like growth factor-1 receptor immunoreactive cells in the supraoptic hypothalamus is reduced in calorically restricted mice. *Int J Dev Neurosci,* 24**,** 431-6.

YAMAGUCHI, N., MIMURA, K. & OKADA, S. 2019. GABAB receptors in the hypothalamic paraventricular nucleus mediate beta-adrenoceptor-induced elevations of plasma noradrenaline in rats. *Eur J Pharmacol,* 848**,** 88-95.

YAMAMOTO, T., SAKAKIBARA, R., UCHIYAMA, T., LIU, Z., ITO, T., YAMANISHI, T. & HATTORI, T. 2005. Lower urinary tract function in patients with pituitary adenoma compressing hypothalamus. *Journal of Neurology, Neurosurgery & Psychiatry,* 76**,** 390-394.

YAMAO, Y., KOYAMA, Y., AKIHIRO, K., YUKIHIKO, K. & TSUNEHARU, M. 2001. Discrete regions in the laterodorsal tegmental area

of the rat regulating the urinary bladder and external urethral sphincter. *Brain Res,* 912**,** 162-70.

YANG, P., WANG, S., GANDAHI, J. A., BIAN, X., WU, L., LIU, Y., ZHANG, L., ZHANG, Q. & CHEN, Q. 2012. Ultrastructural identification of different subtypes of interstitial cells of Cajal in the chicken ileum. *Poult Sci,* 91**,** 1936-40.

YANG, S. L., HSU, C., HSU, H. K., LIU, K. M. & PENG, M. T. 1993. Effects of long-term estradiol exposure on the hypothalamic neuron number. *Acta Endocrinol (Copenh),* 129**,** 543-7.

YAO, J., LI, Q., LI, X., QIN, H., LIANG, S., LIAO, X., CHEN, X., LI, W. & YAN, J. 2019. Simultaneous Measurement of Neuronal Activity in the Pontine Micturition Center and Cystometry in Freely Moving Mice. *Front Neurosci,* 13**,** 663.

YAO, J., ZHANG, Q., LIAO, X., LI, Q., LIANG, S., LI, X., ZHANG, Y., LI, X., WANG, H., QIN, H., WANG, M., LI, J., ZHANG, J., HE, W., ZHANG, W., LI, T., XU, F., GONG, H., JIA, H., XU, X., YAN, J. & CHEN, X. 2018. A corticopontine circuit for initiation of urination. *Nat Neurosci,* 21**,** 1541-1550.

YE, L. & LIDDLE, R. A. 2017. Gastrointestinal hormones and the gut connectome. *Current opinion in endocrinology, diabetes, and obesity,* 24**,** 9-14.

YIN, W., SUN, Z., MENDENHALL, J. M., WALKER, D. M., RIHA, P. D., BEZNER, K. S. & GORE, A. C. 2015. Expression of Vesicular Glutamate Transporter 2 (vGluT2) on Large Dense-Core Vesicles within GnRH Neuroterminals of Aging Female Rats. *PLoS One,* 10**,** e0129633.

YOKOYAMA, O., ITO, H., AOKI, Y., OYAMA, N., MIWA, Y. & AKINO, H. 2010. Selective alpha1A-blocker improves bladder storage function in rats via suppression of C-fiber afferent activity. *World J Urol,* 28**,** 609-14.

YOSHIMURA, N. & DE GROAT, W. C. 1997. Neural control of the lower urinary tract. *Int J Urol,* 4**,** 111-25.

YOSHIMURA, N., SASA, M., YOSHIDA, O. & TAKAORI, S. 1990. Mediation of Micturition Reflex by Central Norepinephrine from the Locus Coeruleus in the Cat. *Journal of Urology,* 143**,** 840-843.

YOUNG, H. M. & FURNESS, J. B. 1995. Ultrastructural examination of the targets of serotonin-immunoreactive descending interneurons in the guinea pig small intestine. *J Comp Neurol,* 356**,** 101-14.

ZHANG, H., DAVIES, K. J. A. & FORMAN, H. J. 2015a. Oxidative stress response and Nrf2 signaling in aging. *Free radical biology & medicine,* 88**,** 314-336.

ZHANG, J.-H., SAMPOGNA, S., MORALES, F. R. & CHASE, M. H. 2005. Age-related changes in cholinergic neurons in the laterodorsal and the pedunculo-pontine tegmental nuclei of cats: A combined light and electron microscopic study. *Brain Research,* 1052**,** 47-55.

ZHANG, Y., MULLER, M., XU, B., YOSHIDA, Y., HORLACHER, O., NIKITIN, F., GARESSUS, S., MAGDELDIN, S., KINOSHITA, N., FUJINAKA, H., YAOITA, E., HASEGAWA, M., LISACEK, F. & YAMAMOTO, T. 2015b. Unrestricted modification search reveals lysine methylation as major modification induced by tissue formalin fixation and paraffin embedding. *PROTEOMICS,* 15**,** 2568-2579.

ZHENG, J. Q., SEKI, M., HAYAKAWA, T., ITO, H. & ZYO, K. 1995. Descending projections from the paraventricular hypothalamic nucleus to the spinal cord: anterograde tracing study in the rat. *Okajimas Folia Anat Jpn,* 72**,** 119-35.

ZHOU, J. N. & SWAAB, D. F. 1999. Activation and degeneration during aging: a morphometric study of the human hypothalamus. *Microsc Res Tech,* 44**,** 36-48.

ZHU, Y. R., COWLES, V. E., HERRANZ, E. S., SCHULTE, W. J. & CONDON, R. E. 1992. Arginine vasopressin inhibits phasic contractions and stimulates giant contractions in monkey colon. *Gastroenterology,* 102**,** 868-74.

ZIEGLER, D. R., EDWARDS, M. R., ULRICH-LAI, Y. M., HERMAN, J. P. & CULLINAN, W. E. 2012. Brainstem origins of glutamatergic innervation of the rat hypothalamic paraventricular nucleus. *The Journal of comparative neurology,* 520**,** 2369-2394.

ZIEMAN, S. & KASS, D. 2004. Advanced glycation end product cross-linking: pathophysiologic role and therapeutic target in

cardiovascular disease. *Congest Heart Fail,* 10**,** 144-9; quiz 150-1.

ZUCCA, F. A., SEGURA-AGUILAR, J., FERRARI, E., MUÑOZ, P., PARIS, I., SULZER, D., SARNA, T., CASELLA, L. & ZECCA, L. 2017. Interactions of iron, dopamine and neuromelanin pathways in brain aging and Parkinson's disease. *Progress in neurobiology,* 155**,** 96-119.

8 APPENDICES

APPENDIX A

Ethical approval letter

Professor Kathleen McCourt, CBE FRCN

This matter is being dealt with by:

Dr R. N. Ranson
Applied Sciences Ethics Lead
Faculty of Health & Life Sciences
Northumberland Building
Newcastle upon Tyne
NE1 8ST

Date: 02/12/2015

Project Ref: BMS36UNNEDRNR2015

Period of Coverage: 3 year from date above unless the study has been significantly changed or completed which will require an amendment to be submitted.

Dear Emily Doogan

Faculty of Health and Life Sciences Research –Biomedical Ethics Review.

Title: Investigation of effects of ageing on cells that mediate bladder, bowel and reproductive function

Following independent peer review of the above proposal I am pleased to inform you that Departmental (and thus) Faculty approval has been granted for this proposal- subject to compliance with the University policies on ethics and consent and any other policies applicable to your individual research.

NB. If your research involves working with children and/or vulnerable adults you should also have recent Disclosure & Barring Service (DBS) and occupational health clearance.

The University's Policies and Procedures are available from the following web link: http://www.northumbria.ac.uk/researchandconsultancy/sa/ethgov/policies/?view=Standard

All researchers must give notice of the following:

- Any significant changes to the study design;
- Any incidents which have an adverse effect on participants, researchers or study outcomes;
- Any suspension or abandonment of the study;

Please keep this letter with your application as proof of ethical clearance and for any future auditing requirements.

Yours sincerely

Dr R. N. Ranson

Applied Science and Biomedical Ethics Faculty Representative.

APPENDIX B

Control images from Chapter 3.

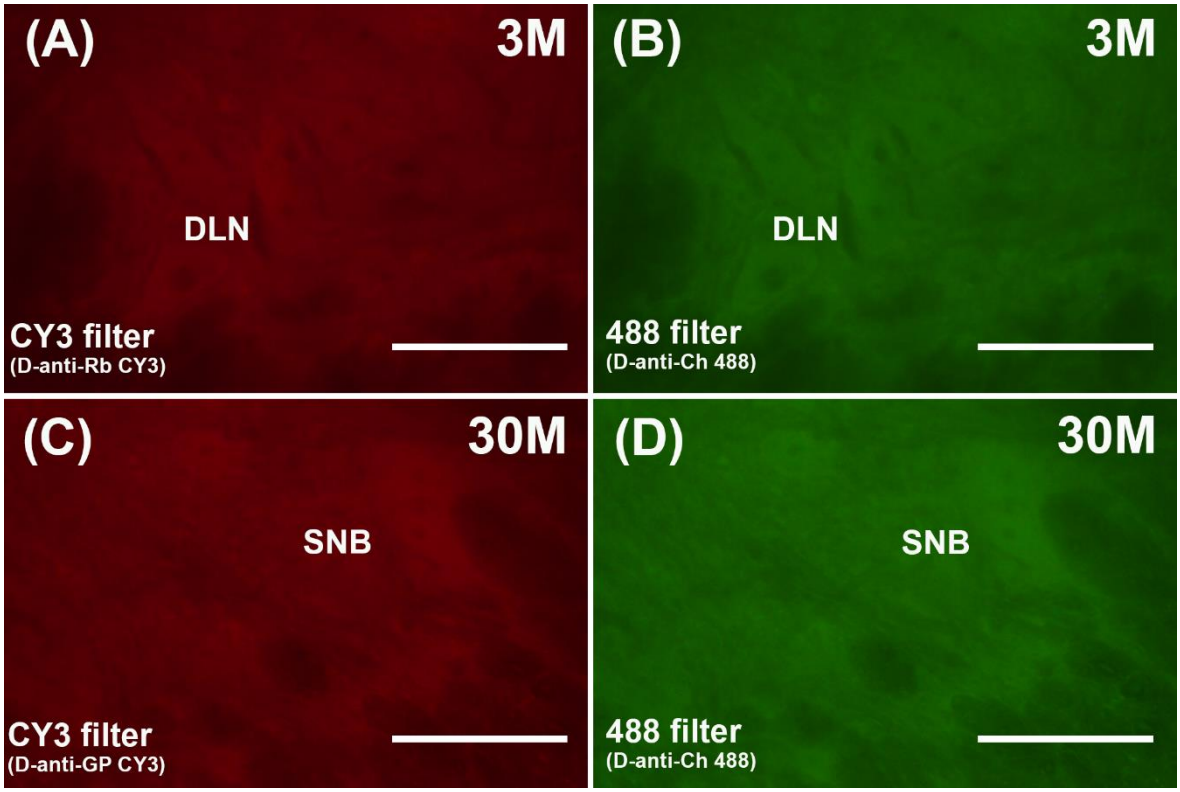

Figure 8.1: Control DLN- and SNB-containing LS spinal sections with primary antibodies omitted. A-B show the unlabelled DLN of 3-month-old mouse taken under both the CY3 (red) and 488 (green) filters. C-D show the unlabelled SNB of 30-month-old mouse taken under both the CY3 (red) and 488 (green) filters. A and C depict lack of terminal labelling with secondary D-anti-Rb CY3 and D-anti-GP CY3 antibodies, respectively. B and D depict lack of neuronal labelling with secondary D-anti-Ch 488 antibodies. Scale bars = 50 µm. D-anti-Ch 488, Donkey-anti-chicken 488; D-anti-GP CY3, Donkey-anti-guineapig CY3; D-anti-Rb CY3, Donkey-anti-rabbit CY3; DLN, Dorsolateral nucleus; LS, Lumbosacral; M, Months; SNB, Spinal nucleus of the bulbospongiosus.

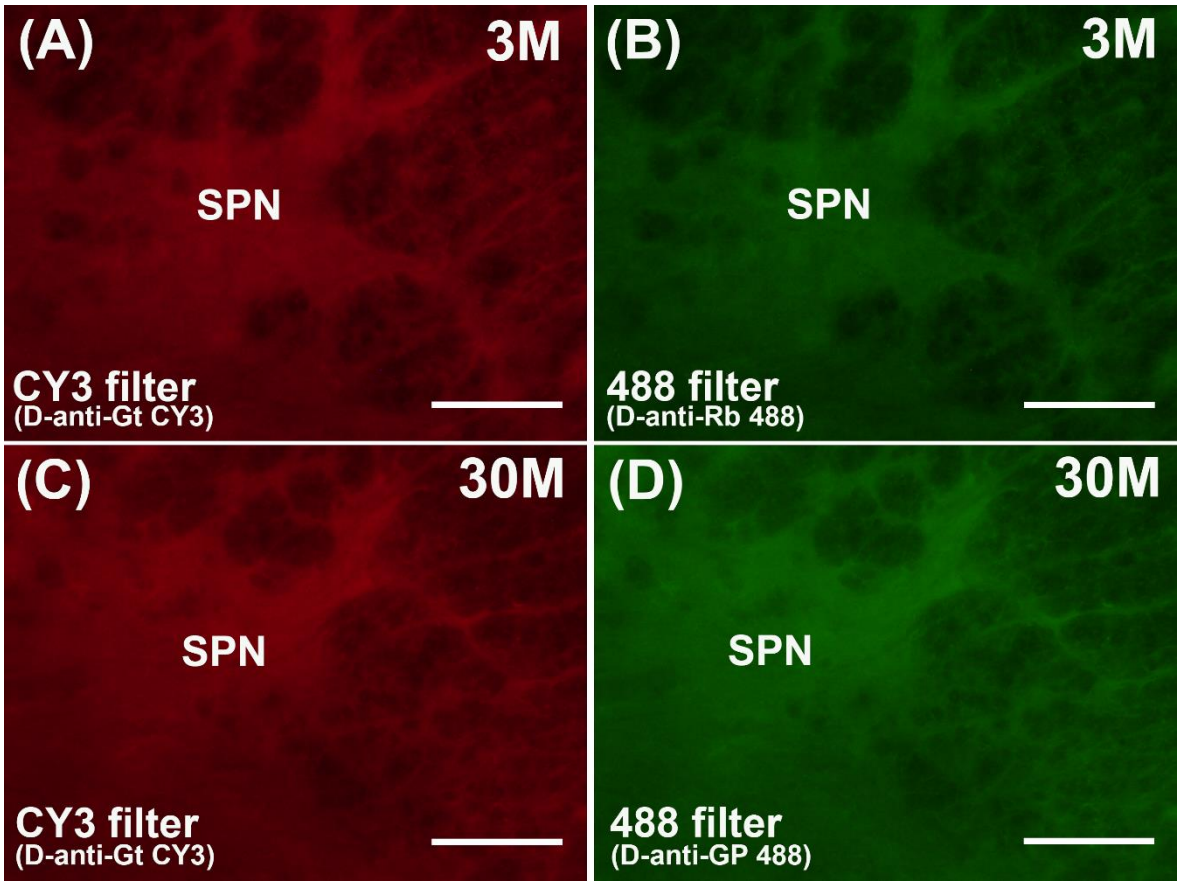

Figure 8.2: Control SPN-containing LS spinal sections with primary antibodies omitted. A-B show the SPN of 3-month-old mouse taken under both the CY3 (red) and 488 (green) filters. C-D show the SPN of 30-month-old mouse taken under both the CY3 (red) and 488 (green) filters. A and C depict lack of neuronal labelling with secondary D-anti-Gt CY3 antibodies. B and D depict lack of terminal labelling with secondary D-anti-Rb 488 and D-anti-GP 488 antibodies, respectively. Scale bars = 50 µm. D-anti-GP 488, Donkey-anti-guineapig 488; D-anti-Gt CY3, Donkey-anti-Gt CY3; D-anti-Rb 488, Donkey-anti-rabbit 488; LS, Lumbosacral; M, Months; SPN, Sacral parasympathetic nucleus.

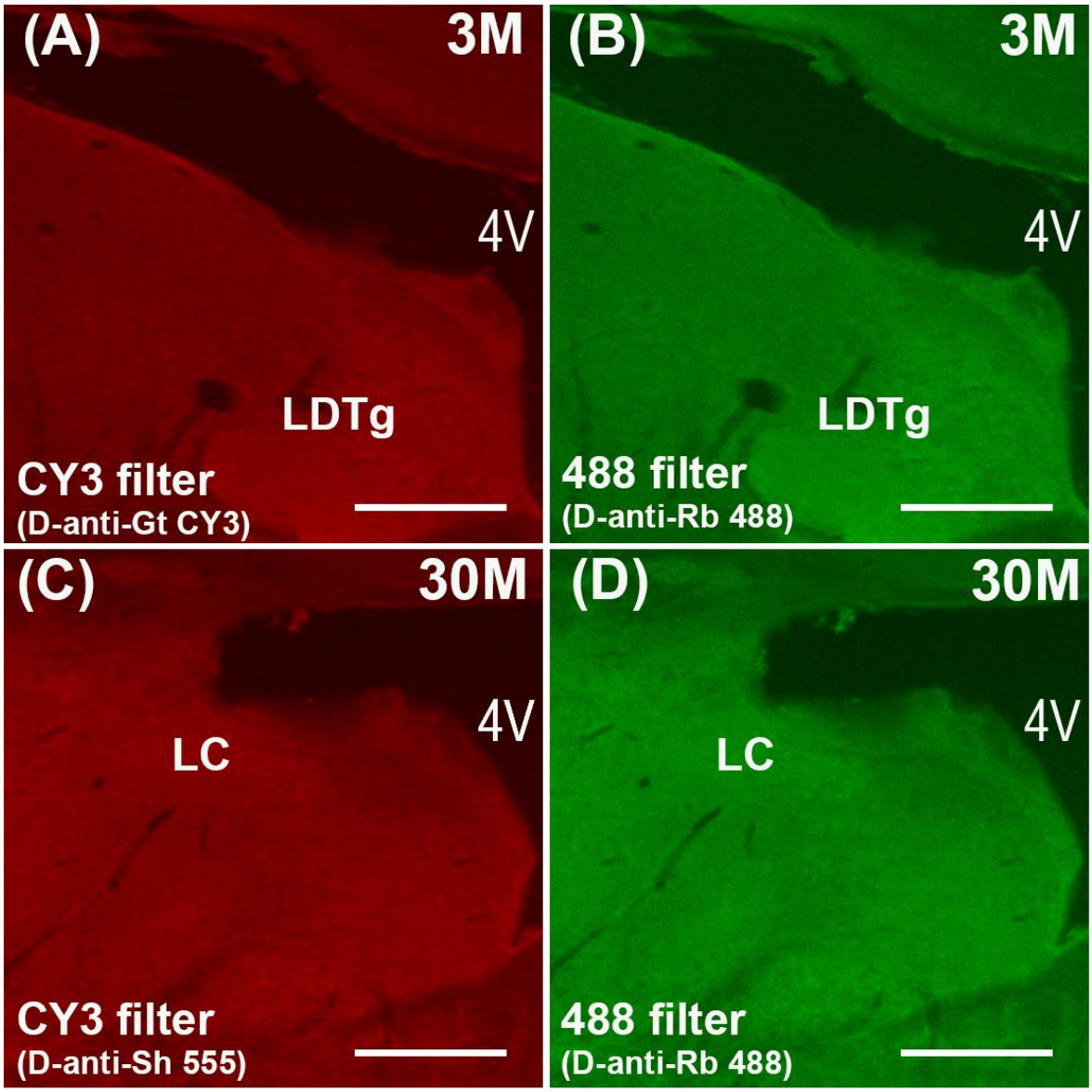

Figure 8.3: Control LDTg- and LC-containing brainstem sections with primary antibodies omitted. A-B show the unlabelled LDTg of 3-month-old mouse taken under both the CY3 (red) and 488 (green) filters. C-D show the unlabelled LC of 30-month-old mouse taken under both the CY3 (red) and 488 (green) filters. A and C depict lack of neuronal labelling with secondary D-anti-Gt CY3 and D-anti-Sh 555 antibodies, respectively. B and D depict lack of terminal labelling with secondary D-anti-Rb 488 antibodies. Scale bars = 100 µm. 4V, Fourth ventricle; D-anti-Gt CY3, Donkey-anti-goat CY3; D-anti-Rb 488, Donkey-anti-rabbit 488; D-anti-Sh 555, Donkey-anti-sheep 555; LC, Locus coeruleus; LDTg, Laterodorsal tegmental nucleus; M, Months.

APPENDIX C

Control images from Chapter 4.

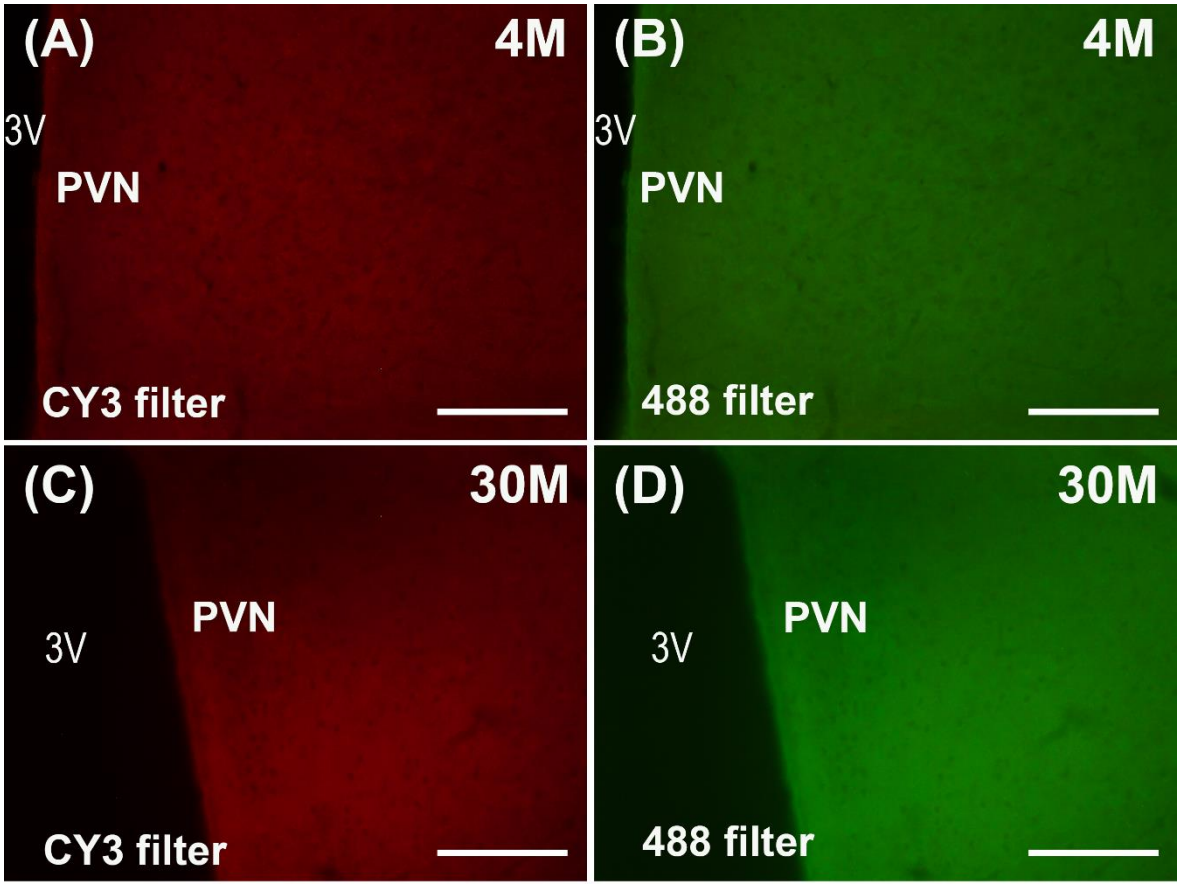

Figure 8.4: Control PVN-containing LS spinal sections with primary antibodies omitted. A-D show the unlabelled PVN of 4-month-old mouse taken under both the CY3 (red) and 488 (green) filters. C-D show the unlabelled PVN of 30-month-old mouse taken under both the CY3 (red) and 488 (green) filters. A and C depict lack of terminal labelling with secondary D-anti-GP CY3 antibodies. B and D depict lack of neuronal labelling with secondary D-anti-Rb 488 antibodies. Scale bars = 100 µm. 3V, Third ventricle; D-anti-GP CY3, Donkey-anti-guineapig CY3; D-anti-Rb 488, Donkey-anti-rabbit 488; M, Months; PVN, Paraventricular nucleus.

APPENDIX D

Qualitative protein analysis from Chapter 5: proteins identified from 3-month-old mouse DC when analysed with LC / MS / MS and tagged on Mascot™ database.

Sequence	Family	Member	Database	Accession	Score	Mass	Num. of m	Num. of si	Num. of s	Num. of s	emPAI	Description
0.63	4	1	SwissProt	TAGL_MO	668	22618	36	30	13	13	26.33	Transgelin OS=Mus musculus OX=10090 GN=Tagln PE=1 SV=3
0.48	18	1	SwissProt	MYL6_MO	311	17090	10	9	7	6	4.14	Myosin light polypeptide 6 OS=Mus musculus OX=10090 GN=Myl6 PE=1 SV=3
0.46	1	1	SwissProt	ACTA_MO	2281	42381	106	88	17	16	7.25	Actin, aortic smooth muscle OS=Mus musculus OX=10090 GN=Acta2 PE=1 SV=1
0.42	3	1	SwissProt	DESM_MC	1109	53522	40	33	20	18	4.34	Desmin OS=Mus musculus OX=10090 GN=Des PE=1 SV=3
0.42	45	1	SwissProt	HBA_MOU	143	15133	7	5	5	3	1.52	Hemoglobin subunit alpha OS=Mus musculus OX=10090 GN=Hba PE=1 SV=2
0.4	5	2	SwissProt	K1C19_MC	408	44515	29	24	17	14	3.4	Keratin, type I cytoskeletal 19 OS=Mus musculus OX=10090 GN=Krt19 PE=1 SV=1
0.39	24	1	SwissProt	H4_MOUS	234	11360	8	7	4	3	2.41	Histone H4 OS=Mus musculus OX=10090 GN=Hist1h4a PE=1 SV=2
0.36	1	2	SwissProt	ACTB_MO	1674	42052	81	67	14	13	4.99	Actin, cytoplasmic 1 OS=Mus musculus OX=10090 GN=Actb PE=1 SV=1
0.35	20	1	SwissProt	CNN1_MC	264	33506	10	10	8	8	2.07	Calponin-1 OS=Mus musculus OX=10090 GN=Cnn1 PE=1 SV=1
0.34	23	1	SwissProt	CSRP1_MC	256	21425	8	7	5	5	1.98	Cysteine and glycine-rich protein 1 OS=Mus musculus OX=10090 GN=Csrp1 PE=1 SV=3
0.33	3	2	SwissProt	VIME_MO	426	53712	19	14	15	12	1.87	Vimentin OS=Mus musculus OX=10090 GN=Vim PE=1 SV=3
0.33	29	1	SwissProt	HSPB1_MC	202	23057	9	7	7	7	3.14	Heat shock protein beta-1 OS=Mus musculus OX=10090 GN=Hspb1 PE=1 SV=3
0.31	14	2	SwissProt	TBB4B_MC	354	50255	13	11	10	9	1.32	Tubulin beta-4B chain OS=Mus musculus OX=10090 GN=Tubb4b PE=1 SV=1
0.3	16	1	SwissProt	TBA1B_MC	343	50804	12	10	10	9	1.3	Tubulin alpha-1B chain OS=Mus musculus OX=10090 GN=Tuba1b PE=1 SV=2
0.3	32	1	SwissProt	MYL9_MO	182	19898	6	6	5	5	2.24	Myosin regulatory light polypeptide 9 OS=Mus musculus OX=10090 GN=Myl9 PE=1 SV=3
0.29	204	1	SwissProt	RLA2_MO	40	11644	1	1	1	1	0.49	60S acidic ribosomal protein P2 OS=Mus musculus OX=10090 GN=Rplp2 PE=1 SV=3
0.28	8	1	SwissProt	LMNA_MC	427	74478	21	16	18	16	1.76	Prelamin-A/C OS=Mus musculus OX=10090 GN=Lmna PE=1 SV=2
0.28	30	1	SwissProt	PRDX6_MC	201	24969	6	6	6	6	2.08	Peroxiredoxin-6 OS=Mus musculus OX=10090 GN=Prdx6 PE=1 SV=3
0.27	35	1	SwissProt	H2A1B_MC	171	14127	10	8	3	3	1.69	Histone H2A type 1-B OS=Mus musculus OX=10090 GN=Hist1h2ab PE=1 SV=1
0.27	38	1	SwissProt	1433Z_MC	160	27925	7	5	7	5	1.31	14-3-3 protein zeta/delta OS=Mus musculus OX=10090 GN=Ywhaz PE=1 SV=1
0.27	51	1	SwissProt	RS3_MOU	127	26828	6	5	6	5	1.39	40S ribosomal protein S3 OS=Mus musculus OX=10090 GN=Rps3 PE=1 SV=1
0.27	74	1	SwissProt	GSTM1_M	99	26067	7	6	7	6	1.94	Glutathione S-transferase Mu 1 OS=Mus musculus OX=10090 GN=Gstm1 PE=1 SV=2
0.26	224	1	SwissProt	QCR8_MO	37	9762	2	2	2	2	1.57	Cytochrome b-c1 complex subunit 8 OS=Mus musculus OX=10090 GN=Uqcrq PE=1 SV=3
0.25	14	1	SwissProt	TBB5_MO	371	50095	12	10	9	8	1.12	Tubulin beta-5 chain OS=Mus musculus OX=10090 GN=Tubb5 PE=1 SV=1
0.25	19	1	SwissProt	G3P_MOU	285	36072	9	9	7	7	1.49	Glyceraldehyde-3-phosphate dehydrogenase OS=Mus musculus OX=10090 GN=Gapdh PE=1 SV=2
0.25	31	1	SwissProt	EF1A1_MC	197	50424	10	9	9	8	1.11	Elongation factor 1-alpha 1 OS=Mus musculus OX=10090 GN=Eef1a1 PE=1 SV=3
0.25	54	1	SwissProt	RS4X_MO	121	29807	8	6	8	6	1.57	40S ribosomal protein S4, X isoform OS=Mus musculus OX=10090 GN=Rps4x PE=1 SV=2
0.25	184	1	SwissProt	CYB5_MO	45	15232	2	2	2	2	0.84	Cytochrome b5 OS=Mus musculus OX=10090 GN=Cyb5a PE=1 SV=2
0.24	2	1	SwissProt	FLNA_MO	1202	283897	55	45	48	38	0.88	Filamin-A OS=Mus musculus OX=10090 GN=Flna PE=1 SV=5
0.24	25	1	SwissProt	PDLI3_MC	233	34734	6	4	5	3	0.5	PDZ and LIM domain protein 3 OS=Mus musculus OX=10090 GN=Pdlim3 PE=1 SV=1
0.24	32	2	SwissProt	ML12B_MC	145	19824	5	5	4	4	1.56	Myosin regulatory light chain 12B OS=Mus musculus OX=10090 GN=Myl12b PE=1 SV=2
0.24	77	1	SwissProt	RL12_MOU	95	17965	3	3	3	3	1.18	60S ribosomal protein L12 OS=Mus musculus OX=10090 GN=Rpl12 PE=1 SV=2
0.23	22	1	SwissProt	ENOA_MC	259	47453	10	8	8	7	1	Alpha-enolase OS=Mus musculus OX=10090 GN=Eno1 PE=1 SV=3
0.22	28	1	SwissProt	ANXA2_M	204	38937	7	5	7	5	0.83	Annexin A2 OS=Mus musculus OX=10090 GN=Anxa2 PE=1 SV=2

0.21	21	1	SwissProt	SBP1_MOI	260	53051	10	9	9	8	1.04	Methanethiol oxidase OS=Mus musculus OX=10090 GN=Selenbp1 PE=1 SV=2
0.21	3	7	SwissProt	K2C8_MOI	244	54531	12	10	12	10	1.38	Keratin, type II cytoskeletal 8 OS=Mus musculus OX=10090 GN=Krt8 PE=1 SV=4
0.21	104	1	SwissProt	RL27A_MC	71	16709	3	2	3	2	0.74	60S ribosomal protein L27a OS=Mus musculus OX=10090 GN=Rpl27a PE=1 SV=5
0.21	143	1	SwissProt	COX6C_M	56	8464	3	3	3	3	4.11	Cytochrome c oxidase subunit 6C OS=Mus musculus OX=10090 GN=Cox6c PE=1 SV=3
0.2	9	1	SwissProt	ATPA_MO	425	59830	13	12	9	9	1.03	ATP synthase subunit alpha, mitochondrial OS=Mus musculus OX=10090 GN=Atp5f1a PE=1 SV=1
0.2	12	1	SwissProt	KCRB_MO	389	42971	9	9	6	6	0.93	Creatine kinase B-type OS=Mus musculus OX=10090 GN=Ckb PE=1 SV=1
0.2	14	3	SwissProt	TBB2A_M	235	50274	10	8	7	6	0.75	Tubulin beta-2A chain OS=Mus musculus OX=10090 GN=Tubb2a PE=1 SV=1
0.2	60	1	SwissProt	RS13_MOI	113	17212	4	2	4	2	0.72	40S ribosomal protein S13 OS=Mus musculus OX=10090 GN=Rps13 PE=1 SV=2
0.2	100	1	SwissProt	AT1B1_M	72	35571	5	3	5	3	0.49	Sodium/potassium-transporting ATPase subunit beta-1 OS=Mus musculus OX=10090 GN=Atp1b1 PE=1 SV=1
0.2	133	1	SwissProt	DEST_MOI	58	18852	3	2	3	2	0.64	Destrin OS=Mus musculus OX=10090 GN=Dstn PE=1 SV=3
0.2	333	1	SwissProt	RS29_MOI	21	6900	1	1	1	1	0.94	40S ribosomal protein S29 OS=Mus musculus OX=10090 GN=Rps29 PE=1 SV=2
0.19	11	1	SwissProt	VINC_MO	402	117215	19	16	19	16	0.91	Vinculin OS=Mus musculus OX=10090 GN=Vcl PE=1 SV=4
0.19	5	4	SwissProt	K1C42_M	332	50444	18	13	9	7	0.92	Keratin, type I cytoskeletal 42 OS=Mus musculus OX=10090 GN=Krt42 PE=1 SV=1
0.19	67	1	SwissProt	H3C_MOU	106	15363	5	5	4	4	2.37	Histone H3.3C OS=Mus musculus OX=10090 GN=H3f3c PE=3 SV=3
0.19	127	1	SwissProt	RS20_MOI	61	13478	2	2	2	2	1	40S ribosomal protein S20 OS=Mus musculus OX=10090 GN=Rps20 PE=1 SV=1
0.18	3	3	SwissProt	K2C6A_M	368	59641	18	14	13	11	1.39	Keratin, type II cytoskeletal 6A OS=Mus musculus OX=10090 GN=Krt6a PE=1 SV=3
0.18	3	4	SwissProt	K2C5_MOI	358	61957	17	15	13	12	1.49	Keratin, type II cytoskeletal 5 OS=Mus musculus OX=10090 GN=Krt5 PE=1 SV=1
0.18	5	5	SwissProt	K1C17_M	279	48417	19	16	9	8	1.18	Keratin, type I cytoskeletal 17 OS=Mus musculus OX=10090 GN=Krt17 PE=1 SV=3
0.18	39	1	SwissProt	ALDOA_M	157	39787	8	6	7	6	1.04	Fructose-bisphosphate aldolase A OS=Mus musculus OX=10090 GN=Aldoa PE=1 SV=2
0.18	49	1	SwissProt	ANXA4_M	135	36178	5	4	5	4	0.68	Annexin A4 OS=Mus musculus OX=10090 GN=Anxa4 PE=1 SV=4
0.18	72	1	SwissProt	RS18_MOI	100	17708	3	3	3	3	1.2	40S ribosomal protein S18 OS=Mus musculus OX=10090 GN=Rps18 PE=1 SV=3
0.18	137	1	SwissProt	CYC_MOU	58	11712	2	2	2	2	1.2	Cytochrome c, somatic OS=Mus musculus OX=10090 GN=Cycs PE=1 SV=2
0.17	6	1	SwissProt	TPM1_MC	509	32718	16	13	8	7	2.15	Tropomyosin alpha-1 chain OS=Mus musculus OX=10090 GN=Tpm1 PE=1 SV=1
0.17	26	1	SwissProt	ATPB_MO	221	56265	10	7	8	6	0.65	ATP synthase subunit beta, mitochondrial OS=Mus musculus OX=10090 GN=Atp5f1b PE=1 SV=2
0.17	38	2	SwissProt	1433T_MC	100	28046	4	4	4	4	0.95	14-3-3 protein theta OS=Mus musculus OX=10090 GN=Ywhaq PE=1 SV=1
0.17	74	2	SwissProt	GSTM2_M	64	25871	4	3	4	3	0.72	Glutathione S-transferase Mu 2 OS=Mus musculus OX=10090 GN=Gstm2 PE=1 SV=2
0.17	120	1	SwissProt	HINT1_M	63	13882	2	2	2	2	0.95	Histidine triad nucleotide-binding protein 1 OS=Mus musculus OX=10090 GN=Hint1 PE=1 SV=3
0.17	168	1	SwissProt	KCY_MOU	48	22379	3	3	3	3	0.87	UMP-CMP kinase OS=Mus musculus OX=10090 GN=Cmpk1 PE=1 SV=1
0.17	227	1	SwissProt	FHL1_MOI	36	33806	4	3	4	3	0.52	Four and a half LIM domains protein 1 OS=Mus musculus OX=10090 GN=Fhl1 PE=1 SV=3
0.17	289	1	SwissProt	ATP5I_MC	27	8230	1	1	1	1	0.75	ATP synthase subunit e, mitochondrial OS=Mus musculus OX=10090 GN=Atp5me PE=1 SV=2
0.17	306	1	SwissProt	BLVRB_M	24	22297	3	2	3	2	0.52	Flavin reductase (NADPH) OS=Mus musculus OX=10090 GN=Blvrb PE=1 SV=3
0.17	324	1	SwissProt	LEG1_MOI	22	15198	2	2	2	2	0.84	Galectin-1 OS=Mus musculus OX=10090 GN=Lgals1 PE=1 SV=3
0.16	13	1	SwissProt	KCRU_MO	379	47373	7	7	6	6	0.82	Creatine kinase U-type, mitochondrial OS=Mus musculus OX=10090 GN=Ckmt1 PE=1 SV=1
0.16	33	2	SwissProt	AL1B1_M	166	58087	9	8	7	7	0.77	Aldehyde dehydrogenase X, mitochondrial OS=Mus musculus OX=10090 GN=Aldh1b1 PE=1 SV=1
0.16	46	1	SwissProt	ETFB_MOI	142	27834	3	3	3	3	0.66	Electron transfer flavoprotein subunit beta OS=Mus musculus OX=10090 GN=Etfb PE=1 SV=3
0.16	47	1	SwissProt	CBR3_MO	142	31333	4	4	4	4	0.82	Carbonyl reductase [NADPH] 3 OS=Mus musculus OX=10090 GN=Cbr3 PE=1 SV=1
0.16	48	1	SwissProt	ADT2_MO	142	33138	7	5	5	5	1.03	ADP/ATP translocase 2 OS=Mus musculus OX=10090 GN=Slc25a5 PE=1 SV=3
0.16	56	1	SwissProt	TPIS_MOU	118	32684	4	4	4	4	0.78	Triosephosphate isomerase OS=Mus musculus OX=10090 GN=Tpi1 PE=1 SV=4
0.16	89	1	SwissProt	RS27A_M	82	18282	3	2	2	2	0.66	Ubiquitin-40S ribosomal protein S27a OS=Mus musculus OX=10090 GN=Rps27a PE=1 SV=2
0.16	90	1	SwissProt	CAH1_MO	82	28370	4	4	4	4	0.94	Carbonic anhydrase 1 OS=Mus musculus OX=10090 GN=Ca1 PE=1 SV=4

0.16	119	1	SwissProt	PPIA_MOU	64	18131	3	2	3	2	0.68	Peptidyl-prolyl cis-trans isomerase A OS=Mus musculus OX=10090 GN=Ppia PE=1 SV=2
0.16	136	1	SwissProt	RS14_MOU	58	16434	2	2	2	2	0.76	40S ribosomal protein S14 OS=Mus musculus OX=10090 GN=Rps14 PE=1 SV=3
0.16	162	1	SwissProt	PRDX1_MO	50	22390	4	3	4	3	0.87	Peroxiredoxin-1 OS=Mus musculus OX=10090 GN=Prdx1 PE=1 SV=1
0.16	192	1	SwissProt	SODC_MO	43	16104	2	1	2	1	0.34	Superoxide dismutase [Cu-Zn] OS=Mus musculus OX=10090 GN=Sod1 PE=1 SV=2
0.16	232	1	SwissProt	GSTO1_MO	36	27708	5	3	4	2	0.4	Glutathione S-transferase omega-1 OS=Mus musculus OX=10090 GN=Gsto1 PE=1 SV=2
0.16	240	1	SwissProt	RL17_MOU	34	21637	2	1	2	1	0.24	60S ribosomal protein L17 OS=Mus musculus OX=10090 GN=Rpl17 PE=1 SV=3
0.16	279	1	SwissProt	FRIH_MOU	28	21224	3	2	3	2	0.55	Ferritin heavy chain OS=Mus musculus OX=10090 GN=Fth1 PE=1 SV=2
0.15	34	1	SwissProt	LDHA_MO	175	36817	5	4	5	4	0.67	L-lactate dehydrogenase A chain OS=Mus musculus OX=10090 GN=Ldha PE=1 SV=3
0.15	116	1	SwissProt	HBB1_MO	65	15944	2	2	2	2	0.79	Hemoglobin subunit beta-1 OS=Mus musculus OX=10090 GN=Hbb-b1 PE=1 SV=2
0.15	124	1	SwissProt	H2B1B_MO	62	13944	4	3	3	3	1.71	Histone H2B type 1-B OS=Mus musculus OX=10090 GN=Hist1h2bb PE=1 SV=3
0.15	144	1	SwissProt	NDKB_MO	56	17466	3	2	2	2	0.71	Nucleoside diphosphate kinase B OS=Mus musculus OX=10090 GN=Nme2 PE=1 SV=1
0.15	307	1	SwissProt	RS11_MOU	24	18590	3	2	3	2	0.65	40S ribosomal protein S11 OS=Mus musculus OX=10090 GN=Rps11 PE=1 SV=3
0.15	328	1	SwissProt	QCR7_MO	21	13519	2	1	2	1	0.41	Cytochrome b-c1 complex subunit 7 OS=Mus musculus OX=10090 GN=Uqcrb PE=1 SV=3
0.14	5	1	SwissProt	K1C10_MO	526	57906	28	20	10	9	1.26	Keratin, type I cytoskeletal 10 OS=Mus musculus OX=10090 GN=Krt10 PE=1 SV=3
0.14	17	1	SwissProt	CO6A1_M	315	109562	16	13	13	11	0.61	Collagen alpha-1(VI) chain OS=Mus musculus OX=10090 GN=Col6a1 PE=1 SV=1
0.14	55	1	SwissProt	H12_MOU	120	21254	4	3	3	2	0.55	Histone H1.2 OS=Mus musculus OX=10090 GN=Hist1h1c PE=1 SV=2
0.14	58	1	SwissProt	ROA2_MO	114	37437	5	5	5	5	0.88	Heterogeneous nuclear ribonucleoproteins A2/B1 OS=Mus musculus OX=10090 GN=Hnrnpa2b1 PE=1 SV=2
0.14	110	1	SwissProt	ATPD_MO	69	17589	2	2	2	2	0.7	ATP synthase subunit delta, mitochondrial OS=Mus musculus OX=10090 GN=Atp5f1d PE=1 SV=1
0.14	146	1	SwissProt	UBE2N_M	55	17184	2	2	2	2	0.72	Ubiquitin-conjugating enzyme E2 N OS=Mus musculus OX=10090 GN=Ube2n PE=1 SV=1
0.14	150	1	SwissProt	ATPK_MO	54	10394	1	1	1	1	0.56	ATP synthase subunit f, mitochondrial OS=Mus musculus OX=10090 GN=Atp5mf PE=1 SV=3
0.14	153	1	SwissProt	PHB_MOU	54	29859	4	3	4	3	0.6	Prohibitin OS=Mus musculus OX=10090 GN=Phb PE=1 SV=1
0.13	5	3	SwissProt	K1C13_MO	334	48066	19	16	8	7	0.99	Keratin, type I cytoskeletal 13 OS=Mus musculus OX=10090 GN=Krt13 PE=1 SV=2
0.13	37	1	SwissProt	RSSA_MO	167	32931	3	3	3	3	0.53	40S ribosomal protein SA OS=Mus musculus OX=10090 GN=Rpsa PE=1 SV=4
0.13	22	2	SwissProt	ENOB_MO	133	47337	4	3	4	3	0.35	Beta-enolase OS=Mus musculus OX=10090 GN=Eno3 PE=1 SV=3
0.13	53	1	SwissProt	LEG4_MOU	123	36405	6	5	4	4	0.68	Galectin-4 OS=Mus musculus OX=10090 GN=Lgals4 PE=1 SV=2
0.13	59	1	SwissProt	MDHC_MO	113	36659	5	4	5	4	0.67	Malate dehydrogenase, cytoplasmic OS=Mus musculus OX=10090 GN=Mdh1 PE=1 SV=3
0.13	63	1	SwissProt	ANXA5_M	112	35787	5	5	5	5	0.93	Annexin A5 OS=Mus musculus OX=10090 GN=Anxa5 PE=1 SV=1
0.13	48	2	SwissProt	ADT1_MO	105	33111	6	4	4	4	0.77	ADP/ATP translocase 1 OS=Mus musculus OX=10090 GN=Slc25a4 PE=1 SV=4
0.13	84	1	SwissProt	CISY_MOU	85	51988	6	5	6	5	0.57	Citrate synthase, mitochondrial OS=Mus musculus OX=10090 GN=Cs PE=1 SV=1
0.13	92	1	SwissProt	ETFA_MO	81	35330	3	2	3	2	0.31	Electron transfer flavoprotein subunit alpha, mitochondrial OS=Mus musculus OX=10090 GN=Etfa PE=1 SV=2
0.13	101	1	SwissProt	MXRA7_M	72	19502	2	1	2	1	0.27	Matrix-remodeling-associated protein 7 OS=Mus musculus OX=10090 GN=Mxra7 PE=1 SV=2
0.13	131	1	SwissProt	GDIR1_MO	59	23450	2	2	2	2	0.49	Rho GDP-dissociation inhibitor 1 OS=Mus musculus OX=10090 GN=Arhgdia PE=1 SV=3
0.13	181	1	SwissProt	RS8_MOU	46	24475	3	2	3	2	0.47	40S ribosomal protein S8 OS=Mus musculus OX=10090 GN=Rps8 PE=1 SV=2
0.13	199	1	SwissProt	RL27_MOU	41	15788	2	1	2	1	0.34	60S ribosomal protein L27 OS=Mus musculus OX=10090 GN=Rpl27 PE=1 SV=2
0.13	223	1	SwissProt	RL7_MOUS	37	31457	3	1	3	1	0.16	60S ribosomal protein L7 OS=Mus musculus OX=10090 GN=Rpl7 PE=1 SV=2
0.13	248	1	SwissProt	RL34_MOU	33	13513	2	1	2	1	0.41	60S ribosomal protein L34 OS=Mus musculus OX=10090 GN=Rpl34 PE=1 SV=2
0.13	381	1	SwissProt	UB2V1_MO	14	16458	2	1	2	1	0.33	Ubiquitin-conjugating enzyme E2 variant 1 OS=Mus musculus OX=10090 GN=Ube2v1 PE=1 SV=1
0.12	6	2	SwissProt	TPM2_MO	390	32931	11	10	5	5	1.04	Tropomyosin beta chain OS=Mus musculus OX=10090 GN=Tpm2 PE=1 SV=1
0.12	40	1	SwissProt	ACON_MO	155	86151	8	6	8	6	0.39	Aconitate hydratase, mitochondrial OS=Mus musculus OX=10090 GN=Aco2 PE=1 SV=1
0.12	44	1	SwissProt	ACTN1_M	145	103631	10	9	10	9	0.51	Alpha-actinin-1 OS=Mus musculus OX=10090 GN=Actn1 PE=1 SV=1

0.12	75	1	SwissProt	MDHM_M	98	36045	5	5	4	4	0.68	Malate dehydrogenase, mitochondrial OS=Mus musculus OX=10090 GN=Mdh2 PE=1 SV=3
0.12	38	3	SwissProt	1433G_MC	95	28456	3	3	3	3	0.64	14-3-3 protein gamma OS=Mus musculus OX=10090 GN=Ywhag PE=1 SV=2
0.12	79	1	SwissProt	ETHE1_MC	89	28234	2	2	2	2	0.4	Persulfide dioxygenase ETHE1, mitochondrial OS=Mus musculus OX=10090 GN=Ethe1 PE=1 SV=2
0.12	85	1	SwissProt	PGK1_MO	85	44921	4	2	4	2	0.23	Phosphoglycerate kinase 1 OS=Mus musculus OX=10090 GN=Pgk1 PE=1 SV=4
0.12	135	1	SwissProt	ATPO_MC	58	23406	2	2	2	2	0.49	ATP synthase subunit O, mitochondrial OS=Mus musculus OX=10090 GN=Atp5po PE=1 SV=1
0.12	152	1	SwissProt	THIO_MO	54	12010	1	1	1	1	0.47	Thioredoxin OS=Mus musculus OX=10090 GN=Txn PE=1 SV=3
0.12	201	1	SwissProt	ILEUA_MC	40	42719	5	2	4	2	0.25	Leukocyte elastase inhibitor A OS=Mus musculus OX=10090 GN=Serpinb1a PE=1 SV=1
0.12	221	1	SwissProt	CAH2_MO	37	29129	3	2	3	2	0.38	Carbonic anhydrase 2 OS=Mus musculus OX=10090 GN=Ca2 PE=1 SV=4
0.11	5	6	SwissProt	K1C16_MC	275	51973	17	12	6	5	0.72	Keratin, type I cytoskeletal 16 OS=Mus musculus OX=10090 GN=Krt16 PE=1 SV=3
0.11	33	1	SwissProt	ALDH2_M	179	57015	8	7	6	5	0.51	Aldehyde dehydrogenase, mitochondrial OS=Mus musculus OX=10090 GN=Aldh2 PE=1 SV=1
0.11	50	1	SwissProt	TKT_MOU	134	68272	6	4	6	4	0.32	Transketolase OS=Mus musculus OX=10090 GN=Tkt PE=1 SV=1
0.11	62	1	SwissProt	ALBU_MO	112	70700	6	5	6	5	0.4	Serum albumin OS=Mus musculus OX=10090 GN=Alb PE=1 SV=3
0.11	70	1	SwissProt	YBOX1_M	102	35709	2	2	2	2	0.3	Nuclease-sensitive element-binding protein 1 OS=Mus musculus OX=10090 GN=Ybx1 PE=1 SV=3
0.11	38	4	SwissProt	1433E_MC	75	29326	3	3	3	3	0.62	14-3-3 protein epsilon OS=Mus musculus OX=10090 GN=Ywhae PE=1 SV=1
0.11	103	1	SwissProt	TAGL2_MC	71	22552	2	2	2	2	0.52	Transgelin-2 OS=Mus musculus OX=10090 GN=Tagln2 PE=1 SV=4
0.11	105	1	SwissProt	THIM_MO	70	42260	3	2	3	2	0.25	3-ketoacyl-CoA thiolase, mitochondrial OS=Mus musculus OX=10090 GN=Acaa2 PE=1 SV=3
0.11	114	1	SwissProt	IDHP_MO	65	51330	5	4	5	4	0.44	Isocitrate dehydrogenase [NADP], mitochondrial OS=Mus musculus OX=10090 GN=Idh2 PE=1 SV=3
0.11	195	1	SwissProt	ZG16_MO	42	18369	1	1	1	1	0.29	Zymogen granule membrane protein 16 OS=Mus musculus OX=10090 GN=Zg16 PE=1 SV=1
0.11	308	1	SwissProt	ATP5H_M	23	18795	2	1	2	1	0.28	ATP synthase subunit d, mitochondrial OS=Mus musculus OX=10090 GN=Atp5pd PE=1 SV=3
0.11	359	1	SwissProt	RS25_MOU	17	13791	2	1	2	1	0.4	40S ribosomal protein S25 OS=Mus musculus OX=10090 GN=Rps25 PE=1 SV=1
0.1	10	1	SwissProt	MYH11_M	410	227743	19	13	19	13	0.31	Myosin-11 OS=Mus musculus OX=10090 GN=Myh11 PE=1 SV=1
0.1	61	1	SwissProt	KPYM_MC	112	58378	5	4	4	4	0.38	Pyruvate kinase PKM OS=Mus musculus OX=10090 GN=Pkm PE=1 SV=4
0.1	64	1	SwissProt	RL4_MOU	110	47409	3	3	3	3	0.35	60S ribosomal protein L4 OS=Mus musculus OX=10090 GN=Rpl4 PE=1 SV=3
0.1	68	1	SwissProt	HSP7C_M	104	71055	6	4	6	4	0.3	Heat shock cognate 71 kDa protein OS=Mus musculus OX=10090 GN=Hspa8 PE=1 SV=1
0.1	71	1	SwissProt	BASI_MOU	101	42874	4	3	4	3	0.39	Basigin OS=Mus musculus OX=10090 GN=Bsg PE=1 SV=2
0.1	96	1	SwissProt	PGM5_MC	77	62751	7	6	6	5	0.46	Phosphoglucomutase-like protein 5 OS=Mus musculus OX=10090 GN=Pgm5 PE=1 SV=2
0.1	129	1	SwissProt	RS5_MOU	60	23046	2	1	2	1	0.22	40S ribosomal protein S5 OS=Mus musculus OX=10090 GN=Rps5 PE=1 SV=3
0.1	185	1	SwissProt	PGS2_MO	45	40126	3	1	3	1	0.12	Decorin OS=Mus musculus OX=10090 GN=Dcn PE=1 SV=1
0.1	252	1	SwissProt	RS27L_MC	32	9813	1	1	1	1	0.6	40S ribosomal protein S27-like OS=Mus musculus OX=10090 GN=Rps27l PE=1 SV=3
0.1	265	1	SwissProt	ALRF2_MC	30	23773	2	1	2	1	0.22	Aly/REF export factor 2 OS=Mus musculus OX=10090 GN=Alyref2 PE=1 SV=1
0.1	274	1	SwissProt	PGAM1_M	29	28928	2	2	2	2	0.38	Phosphoglycerate mutase 1 OS=Mus musculus OX=10090 GN=Pgam1 PE=1 SV=3
0.1	277	1	SwissProt	CX6B1_MC	28	10293	1	1	1	1	0.56	Cytochrome c oxidase subunit 6B1 OS=Mus musculus OX=10090 GN=Cox6b1 PE=1 SV=2
0.1	325	1	SwissProt	RL7A_MO	22	30129	3	2	3	2	0.37	60S ribosomal protein L7a OS=Mus musculus OX=10090 GN=Rpl7a PE=1 SV=2
0.09	2	2	SwissProt	FLNC_MO	419	293560	21	12	21	12	0.21	Filamin-C OS=Mus musculus OX=10090 GN=Flnc PE=1 SV=3
0.09	3	6	SwissProt	K2C73_MC	248	59502	13	13	6	6	0.61	Keratin, type II cytoskeletal 73 OS=Mus musculus OX=10090 GN=Krt73 PE=1 SV=1
0.09	3	10	SwissProt	K2C4_MO	150	56590	8	7	7	6	0.65	Keratin, type II cytoskeletal 4 OS=Mus musculus OX=10090 GN=Krt4 PE=1 SV=2
0.09	52	1	SwissProt	CO6A2_M	125	111406	10	8	9	8	0.4	Collagen alpha-2(VI) chain OS=Mus musculus OX=10090 GN=Col6a2 PE=1 SV=3
0.09	3	12	SwissProt	K2C79_MC	93	57802	6	5	5	4	0.39	Keratin, type II cytoskeletal 79 OS=Mus musculus OX=10090 GN=Krt79 PE=1 SV=2
0.09	83	1	SwissProt	GELS_MOU	86	86287	8	5	8	5	0.32	Gelsolin OS=Mus musculus OX=10090 GN=Gsn PE=1 SV=3
0.09	108	1	SwissProt	ARF4_MO	69	20498	2	2	2	2	0.58	ADP-ribosylation factor 4 OS=Mus musculus OX=10090 GN=Arf4 PE=1 SV=2

0.09	121	1	SwissProt	ECHA_MO	62	83302	5	3	5	3	0.19	Trifunctional enzyme subunit alpha, mitochondrial OS=Mus musculus OX=10090 GN=Hadha PE=1 SV=1
0.09	139	1	SwissProt	SRSF5_MC	57	30987	2	2	2	2	0.35	Serine/arginine-rich splicing factor 5 OS=Mus musculus OX=10090 GN=Srsf5 PE=1 SV=2
0.09	141	1	SwissProt	RL13_MOU	57	24348	3	1	2	1	0.21	60S ribosomal protein L13 OS=Mus musculus OX=10090 GN=Rpl13 PE=1 SV=3
0.09	148	1	SwissProt	COR1C_M	55	53771	4	2	4	2	0.19	Coronin-1C OS=Mus musculus OX=10090 GN=Coro1c PE=1 SV=2
0.09	218	1	SwissProt	S10A6_MC	38	10101	1	1	1	1	0.58	Protein S100-A6 OS=Mus musculus OX=10090 GN=S100a6 PE=1 SV=3
0.09	239	1	SwissProt	STUM_MC	34	15223	1	1	1	1	0.36	Protein stum homolog OS=Mus musculus OX=10090 GN=Stum PE=1 SV=1
0.09	250	1	SwissProt	LEG3_MOU	32	27612	3	2	2	1	0.19	Galectin-3 OS=Mus musculus OX=10090 GN=Lgals3 PE=1 SV=3
0.09	255	1	SwissProt	FRIL1_MO	31	20847	1	1	1	1	0.25	Ferritin light chain 1 OS=Mus musculus OX=10090 GN=Ftl1 PE=1 SV=2
0.09	267	1	SwissProt	RL6_MOUS	30	33546	4	2	4	2	0.32	60S ribosomal protein L6 OS=Mus musculus OX=10090 GN=Rpl6 PE=1 SV=3
0.09	292	1	SwissProt	RRAS2_M	26	23613	3	1	2	1	0.22	Ras-related protein R-Ras2 OS=Mus musculus OX=10090 GN=Rras2 PE=1 SV=1
0.09	321	1	SwissProt	CRIP1_MC	22	8943	1	1	1	1	0.71	Cysteine-rich protein 1 OS=Mus musculus OX=10090 GN=Crip1 PE=1 SV=2
0.09	352	1	SwissProt	SORCN_M	17	21898	2	1	2	1	0.24	Sorcin OS=Mus musculus OX=10090 GN=Sri PE=1 SV=1
0.08	3	8	SwissProt	K22O_MO	195	63319	10	9	7	6	0.56	Keratin, type II cytoskeletal 2 oral OS=Mus musculus OX=10090 GN=Krt76 PE=1 SV=1
0.08	3	9	SwissProt	K22E_MOU	191	71336	12	11	8	7	0.7	Keratin, type II cytoskeletal 2 epidermal OS=Mus musculus OX=10090 GN=Krt2 PE=1 SV=1
0.08	70	2	SwissProt	YBOX3_M	91	38790	2	2	2	2	0.28	Y-box-binding protein 3 OS=Mus musculus OX=10090 GN=Ybx3 PE=1 SV=2
0.08	82	1	SwissProt	ANXA6_M	87	76294	6	4	6	4	0.28	Annexin A6 OS=Mus musculus OX=10090 GN=Anxa6 PE=1 SV=3
0.08	93	1	SwissProt	LYZ1_MOU	78	17240	2	2	1	1	0.31	Lysozyme C-1 OS=Mus musculus OX=10090 GN=Lyz1 PE=1 SV=1
0.08	109	1	SwissProt	RS6_MOU	69	28834	2	2	2	2	0.38	40S ribosomal protein S6 OS=Mus musculus OX=10090 GN=Rps6 PE=1 SV=1
0.08	130	1	SwissProt	CAPZB_M	60	31611	2	1	2	1	0.16	F-actin-capping protein subunit beta OS=Mus musculus OX=10090 GN=Capzb PE=1 SV=3
0.08	156	1	SwissProt	ALDR_MO	52	36052	3	2	3	2	0.3	Aldo-keto reductase family 1 member B1 OS=Mus musculus OX=10090 GN=Akr1b1 PE=1 SV=3
0.08	165	1	SwissProt	RS3A_MO	50	30094	2	1	2	1	0.17	40S ribosomal protein S3a OS=Mus musculus OX=10090 GN=Rps3a PE=1 SV=3
0.08	191	1	SwissProt	LUM_MOU	43	38640	3	2	3	2	0.28	Lumican OS=Mus musculus OX=10090 GN=Lum PE=1 SV=2
0.08	200	1	SwissProt	MIME_MC	41	34333	3	2	3	2	0.32	Mimecan OS=Mus musculus OX=10090 GN=Ogn PE=1 SV=1
0.08	216	1	SwissProt	H2AY_MO	38	39882	2	2	2	2	0.27	Core histone macro-H2A.1 OS=Mus musculus OX=10090 GN=H2afy PE=1 SV=3
0.08	187	2	SwissProt	ROAA_MC	38	30926	2	2	2	2	0.35	Heterogeneous nuclear ribonucleoprotein A/B OS=Mus musculus OX=10090 GN=Hnrnpab PE=1 SV=1
0.08	228	1	SwissProt	CAV1_MO	36	20697	1	1	1	1	0.25	Caveolin-1 OS=Mus musculus OX=10090 GN=Cav1 PE=1 SV=1
0.08	241	1	SwissProt	RL15_MOU	34	24245	2	2	2	2	0.47	60S ribosomal protein L15 OS=Mus musculus OX=10090 GN=Rpl15 PE=1 SV=4
0.08	263	1	SwissProt	PSA1_MO	31	29813	2	2	2	2	0.37	Proteasome subunit alpha type-1 OS=Mus musculus OX=10090 GN=Psma1 PE=1 SV=1
0.08	268	1	SwissProt	PGRC1_M	30	21795	2	1	2	1	0.24	Membrane-associated progesterone receptor component 1 OS=Mus musculus OX=10090 GN=Pgrmc1 PE=1 SV=4
0.08	290	1	SwissProt	RS26_MOU	26	13292	1	1	1	1	0.42	40S ribosomal protein S26 OS=Mus musculus OX=10090 GN=Rps26 PE=1 SV=3
0.08	314	1	SwissProt	RL10L_MC	23	24998	2	1	2	1	0.21	60S ribosomal protein L10-like OS=Mus musculus OX=10090 GN=Rpl10l PE=2 SV=1
0.08	345	1	SwissProt	RS19_MOU	18	16076	1	1	1	1	0.34	40S ribosomal protein S19 OS=Mus musculus OX=10090 GN=Rps19 PE=1 SV=3
0.08	378	1	SwissProt	SET_MOUS	14	33358	2	1	2	1	0.15	Protein SET OS=Mus musculus OX=10090 GN=Set PE=1 SV=1
0.07	7	1	SwissProt	FBN1_MO	485	332668	19	17	17	16	0.26	Fibrillin-1 OS=Mus musculus OX=10090 GN=Fbn1 PE=1 SV=2
0.07	36	1	SwissProt	AOC3_MC	171	85108	6	6	5	5	0.32	Membrane primary amine oxidase OS=Mus musculus OX=10090 GN=Aoc3 PE=1 SV=3
0.07	41	1	SwissProt	AT1A1_M	148	114221	5	4	5	4	0.18	Sodium/potassium-transporting ATPase subunit alpha-1 OS=Mus musculus OX=10090 GN=Atp1a1 PE=1 SV=1
0.07	76	1	SwissProt	NB5R3_M	98	34334	2	2	2	2	0.32	NADH-cytochrome b5 reductase 3 OS=Mus musculus OX=10090 GN=Cyb5r3 PE=1 SV=3
0.07	86	1	SwissProt	PRELP_MC	84	43607	3	2	3	2	0.24	Prolargin OS=Mus musculus OX=10090 GN=Prelp PE=1 SV=2
0.07	91	1	SwissProt	SMTN_MC	81	100798	6	3	6	3	0.15	Smoothelin OS=Mus musculus OX=10090 GN=Smtn PE=1 SV=2
0.07	94	1	SwissProt	SAHH_MC	77	48170	3	3	3	3	0.34	Adenosylhomocysteinase OS=Mus musculus OX=10090 GN=Ahcy PE=1 SV=3

0.07	111	1	SwissProt	NACA_MO	66	23370	1	1	1	1	0.22	Nascent polypeptide-associated complex subunit alpha OS=Mus musculus OX=10090 GN=Naca PE=1 SV=1
0.07	117	1	SwissProt	RL10A_MO	64	25072	3	2	2	2	0.45	60S ribosomal protein L10a OS=Mus musculus OX=10090 GN=Rpl10a PE=1 SV=3
0.07	118	1	SwissProt	QCR1_MO	64	53446	3	3	3	3	0.3	Cytochrome b-c1 complex subunit 1, mitochondrial OS=Mus musculus OX=10090 GN=Uqcrc1 PE=1 SV=2
0.07	122	1	SwissProt	PDIA3_MO	62	57099	3	2	3	2	0.18	Protein disulfide-isomerase A3 OS=Mus musculus OX=10090 GN=Pdia3 PE=1 SV=2
0.07	126	1	SwissProt	GNAI2_MO	61	41033	3	2	2	2	0.26	Guanine nucleotide-binding protein G(i) subunit alpha-2 OS=Mus musculus OX=10090 GN=Gnai2 PE=1 SV=5
0.07	173	1	SwissProt	VDAC2_M	47	32340	2	2	2	2	0.34	Voltage-dependent anion-selective channel protein 2 OS=Mus musculus OX=10090 GN=Vdac2 PE=1 SV=2
0.07	178	1	SwissProt	RL23A_MO	46	17684	2	1	1	1	0.3	60S ribosomal protein L23a OS=Mus musculus OX=10090 GN=Rpl23a PE=1 SV=1
0.07	179	1	SwissProt	FABP5_MO	46	15470	1	1	1	1	0.35	Fatty acid-binding protein 5 OS=Mus musculus OX=10090 GN=Fabp5 PE=1 SV=3
0.07	187	1	SwissProt	HNRPD_M	44	38501	2	2	2	2	0.28	Heterogeneous nuclear ribonucleoprotein D0 OS=Mus musculus OX=10090 GN=Hnrnpd PE=1 SV=2
0.07	207	1	SwissProt	RL3_MOUS	39	46366	3	1	3	1	0.11	60S ribosomal protein L3 OS=Mus musculus OX=10090 GN=Rpl3 PE=1 SV=3
0.07	249	1	SwissProt	HMGB1_M	32	25049	1	1	1	1	0.21	High mobility group protein B1 OS=Mus musculus OX=10090 GN=Hmgb1 PE=1 SV=2
0.07	262	1	SwissProt	CATA_MO	31	60043	3	2	3	2	0.17	Catalase OS=Mus musculus OX=10090 GN=Cat PE=1 SV=4
0.07	264	1	SwissProt	RL31_MOU	31	14454	1	1	1	1	0.38	60S ribosomal protein L31 OS=Mus musculus OX=10090 GN=Rpl31 PE=1 SV=1
0.07	315	1	SwissProt	NDUAD_M	23	16849	1	1	1	1	0.32	NADH dehydrogenase [ubiquinone] 1 alpha subcomplex subunit 13 OS=Mus musculus OX=10090 GN=Ndufa13 PE=1 SV=3
0.07	316	1	SwissProt	RL23_MOU	23	14970	1	1	1	1	0.36	60S ribosomal protein L23 OS=Mus musculus OX=10090 GN=Rpl23 PE=1 SV=1
0.07	323	1	SwissProt	RAC1_MO	22	21835	1	1	1	1	0.24	Ras-related C3 botulinum toxin substrate 1 OS=Mus musculus OX=10090 GN=Rac1 PE=1 SV=1
0.07	340	1	SwissProt	ANXA1_M	19	38995	2	1	2	1	0.13	Annexin A1 OS=Mus musculus OX=10090 GN=Anxa1 PE=1 SV=2
0.07	360	1	SwissProt	CH10_MO	17	10956	1	1	1	1	0.5	10 kDa heat shock protein, mitochondrial OS=Mus musculus OX=10090 GN=Hspe1 PE=1 SV=2
0.06	15	1	SwissProt	SYNEM_M	363	173276	9	7	9	7	0.21	Synemin OS=Mus musculus OX=10090 GN=Synm PE=1 SV=2
0.06	3	5	SwissProt	K2C1_MOU	262	66079	11	11	5	5	0.43	Keratin, type II cytoskeletal 1 OS=Mus musculus OX=10090 GN=Krt1 PE=1 SV=4
0.06	27	1	SwissProt	PGBM_MO	207	407847	18	13	18	13	0.16	Basement membrane-specific heparan sulfate proteoglycan core protein OS=Mus musculus OX=10090 GN=Hspg2 PE=1 SV=1
0.06	42	1	SwissProt	PCBP1_MO	148	37987	2	2	2	2	0.28	Poly(rC)-binding protein 1 OS=Mus musculus OX=10090 GN=Pcbp1 PE=1 SV=1
0.06	65	1	SwissProt	ARP3_MO	109	47783	2	2	2	2	0.22	Actin-related protein 3 OS=Mus musculus OX=10090 GN=Actr3 PE=1 SV=3
0.06	66	1	SwissProt	HS90B_MO	108	83571	4	4	4	4	0.25	Heat shock protein HSP 90-beta OS=Mus musculus OX=10090 GN=Hsp90ab1 PE=1 SV=3
0.06	47	2	SwissProt	CBR1_MO	70	30907	2	2	2	2	0.36	Carbonyl reductase [NADPH] 1 OS=Mus musculus OX=10090 GN=Cbr1 PE=1 SV=3
0.06	112	1	SwissProt	ADH1_MO	66	40601	3	2	3	2	0.26	Alcohol dehydrogenase 1 OS=Mus musculus OX=10090 GN=Adh1 PE=1 SV=2
0.06	113	1	SwissProt	IF4A1_MO	66	46353	2	1	2	1	0.11	Eukaryotic initiation factor 4A-I OS=Mus musculus OX=10090 GN=Eif4a1 PE=1 SV=1
0.06	68	2	SwissProt	HS71A_MO	63	70321	3	3	3	3	0.22	Heat shock 70 kDa protein 1A OS=Mus musculus OX=10090 GN=Hspa1a PE=1 SV=2
0.06	147	1	SwissProt	MPCP_MO	55	40063	2	1	2	1	0.12	Phosphate carrier protein, mitochondrial OS=Mus musculus OX=10090 GN=Slc25a3 PE=1 SV=1
0.06	154	1	SwissProt	GBB1_MO	53	38151	2	2	2	2	0.28	Guanine nucleotide-binding protein G(I)/G(S)/G(T) subunit beta-1 OS=Mus musculus OX=10090 GN=Gnb1 PE=1 SV=3
0.06	159	1	SwissProt	THIL_MOU	51	45129	3	2	3	2	0.23	Acetyl-CoA acetyltransferase, mitochondrial OS=Mus musculus OX=10090 GN=Acat1 PE=1 SV=1
0.06	167	1	SwissProt	ROA3_MO	49	39856	2	2	2	2	0.27	Heterogeneous nuclear ribonucleoprotein A3 OS=Mus musculus OX=10090 GN=Hnrnpa3 PE=1 SV=1
0.06	177	1	SwissProt	THY1_MO	46	18297	1	1	1	1	0.29	Thy-1 membrane glycoprotein OS=Mus musculus OX=10090 GN=Thy1 PE=1 SV=1
0.06	186	1	SwissProt	PRDX2_MO	44	21936	1	1	1	1	0.24	Peroxiredoxin-2 OS=Mus musculus OX=10090 GN=Prdx2 PE=1 SV=3
0.06	226	1	SwissProt	RL26_MOU	37	17248	1	1	1	1	0.31	60S ribosomal protein L26 OS=Mus musculus OX=10090 GN=Rpl26 PE=1 SV=1
0.06	253	1	SwissProt	CAP1_MO	31	51875	2	1	2	1	0.1	Adenylyl cyclase-associated protein 1 OS=Mus musculus OX=10090 GN=Cap1 PE=1 SV=4
0.06	271	1	SwissProt	PIGR_MOU	29	86257	2	1	2	1	0.06	Polymeric immunoglobulin receptor OS=Mus musculus OX=10090 GN=Pigr PE=1 SV=1
0.06	272	1	SwissProt	AGR2_MO	29	19965	1	1	1	1	0.26	Anterior gradient protein 2 homolog OS=Mus musculus OX=10090 GN=Agr2 PE=1 SV=1
0.06	287	1	SwissProt	VASP_MO	27	39813	2	1	2	1	0.13	Vasodilator-stimulated phosphoprotein OS=Mus musculus OX=10090 GN=Vasp PE=1 SV=4
0.06	300	1	SwissProt	GOLM1_M	25	44470	3	1	3	1	0.11	Golgi membrane protein 1 OS=Mus musculus OX=10090 GN=Golm1 PE=1 SV=2

0.06	309	1	SwissProt	RAP1A_M	23	21316	1	1	1	1	0.25	Ras-related protein Rap-1A OS=Mus musculus OX=10090 GN=Rap1a PE=1 SV=1
0.06	311	1	SwissProt	RAB5A_M	23	23812	1	1	1	1	0.22	Ras-related protein Rab-5A OS=Mus musculus OX=10090 GN=Rab5a PE=1 SV=1
0.06	337	1	SwissProt	RL8_MOU	20	28235	2	1	2	1	0.18	60S ribosomal protein L8 OS=Mus musculus OX=10090 GN=Rpl8 PE=1 SV=2
0.06	383	1	SwissProt	VAPA_MC	14	28065	2	1	1	1	0.18	Vesicle-associated membrane protein-associated protein A OS=Mus musculus OX=10090 GN=Vapa PE=1 SV=2
0.05	57	1	SwissProt	POSTN_M	114	93769	4	2	4	2	0.11	Periostin OS=Mus musculus OX=10090 GN=Postn PE=1 SV=2
0.05	69	1	SwissProt	VILI_MOU	104	93230	4	3	4	3	0.16	Villin-1 OS=Mus musculus OX=10090 GN=Vil1 PE=1 SV=3
0.05	106	1	SwissProt	SIAS_MOU	69	40455	1	1	1	1	0.12	Sialic acid synthase OS=Mus musculus OX=10090 GN=Nans PE=1 SV=1
0.05	123	1	SwissProt	TGM2_MC	62	78153	3	2	3	2	0.13	Protein-glutamine gamma-glutamyltransferase 2 OS=Mus musculus OX=10090 GN=Tgm2 PE=1 SV=4
0.05	132	1	SwissProt	EZRI_MOU	59	69478	3	2	3	2	0.15	Ezrin OS=Mus musculus OX=10090 GN=Ezr PE=1 SV=3
0.05	140	1	SwissProt	PDLI7_MC	57	51170	2	2	2	2	0.2	PDZ and LIM domain protein 7 OS=Mus musculus OX=10090 GN=Pdlim7 PE=1 SV=1
0.05	157	1	SwissProt	ROA1_MC	52	34289	1	1	1	1	0.15	Heterogeneous nuclear ribonucleoprotein A1 OS=Mus musculus OX=10090 GN=Hnrnpa1 PE=1 SV=2
0.05	170	1	SwissProt	RACK1_M	48	35511	2	2	2	2	0.3	Receptor of activated protein C kinase 1 OS=Mus musculus OX=10090 GN=Rack1 PE=1 SV=3
0.05	171	1	SwissProt	LAMB2_M	48	203579	6	3	6	3	0.07	Laminin subunit beta-2 OS=Mus musculus OX=10090 GN=Lamb2 PE=1 SV=2
0.05	183	1	SwissProt	H15_MOU	45	22562	1	1	1	1	0.23	Histone H1.5 OS=Mus musculus OX=10090 GN=Hist1h1b PE=1 SV=2
0.05	189	1	SwissProt	IPYR_MOU	44	33102	1	1	1	1	0.15	Inorganic pyrophosphatase OS=Mus musculus OX=10090 GN=Ppa1 PE=1 SV=1
0.05	197	1	SwissProt	KAD2_MO	42	26737	1	1	1	1	0.19	Adenylate kinase 2, mitochondrial OS=Mus musculus OX=10090 GN=Ak2 PE=1 SV=5
0.05	214	1	SwissProt	DERM_MC	38	24549	1	1	1	1	0.21	Dermatopontin OS=Mus musculus OX=10090 GN=Dpt PE=1 SV=1
0.05	217	1	SwissProt	PSB6_MO	38	25591	1	1	1	1	0.2	Proteasome subunit beta type-6 OS=Mus musculus OX=10090 GN=Psmb6 PE=1 SV=3
0.05	231	1	SwissProt	IF5A1_MC	36	17049	1	1	1	1	0.31	Eukaryotic translation initiation factor 5A-1 OS=Mus musculus OX=10090 GN=Eif5a PE=1 SV=2
0.05	235	1	SwissProt	RL11_MOU	35	20468	1	1	1	1	0.26	60S ribosomal protein L11 OS=Mus musculus OX=10090 GN=Rpl11 PE=1 SV=4
0.05	237	1	SwissProt	AMYP_MC	34	57966	4	1	2	1	0.08	Pancreatic alpha-amylase OS=Mus musculus OX=10090 GN=Amy2 PE=1 SV=2
0.05	238	1	SwissProt	SRSF3_MC	34	19546	1	1	1	1	0.27	Serine/arginine-rich splicing factor 3 OS=Mus musculus OX=10090 GN=Srsf3 PE=1 SV=1
0.05	247	1	SwissProt	PLAK_MO	33	82490	3	2	3	2	0.12	Junction plakoglobin OS=Mus musculus OX=10090 GN=Jup PE=1 SV=3
0.05	275	1	SwissProt	UCRI_MOU	29	29634	2	2	2	2	0.37	Cytochrome b-c1 complex subunit Rieske, mitochondrial OS=Mus musculus OX=10090 GN=Uqcrfs1 PE=1 SV=1
0.05	295	1	SwissProt	SCMC1_M	25	53096	2	1	2	1	0.09	Calcium-binding mitochondrial carrier protein SCaMC-1 OS=Mus musculus OX=10090 GN=Slc25a24 PE=1 SV=1
0.05	297	1	SwissProt	CY1_MOU	25	35533	1	1	1	1	0.14	Cytochrome c1, heme protein, mitochondrial OS=Mus musculus OX=10090 GN=Cyc1 PE=1 SV=1
0.05	303	1	SwissProt	DBNL_MO	24	48955	2	1	2	1	0.1	Drebrin-like protein OS=Mus musculus OX=10090 GN=Dbnl PE=1 SV=2
0.05	310	1	SwissProt	CALM1_M	23	16827	1	1	1	1	0.32	Calmodulin-1 OS=Mus musculus OX=10090 GN=Calm1 PE=1 SV=1
0.05	313	1	SwissProt	PARK7_M	23	20236	1	1	1	1	0.26	Protein/nucleic acid deglycase DJ-1 OS=Mus musculus OX=10090 GN=Park7 PE=1 SV=1
0.05	322	1	SwissProt	LSM4_MO	22	15238	1	1	1	1	0.36	U6 snRNA-associated Sm-like protein LSm4 OS=Mus musculus OX=10090 GN=Lsm4 PE=1 SV=1
0.05	326	1	SwissProt	COX5A_M	21	16319	1	1	1	1	0.33	Cytochrome c oxidase subunit 5A, mitochondrial OS=Mus musculus OX=10090 GN=Cox5a PE=1 SV=2
0.05	327	1	SwissProt	GDIB_MO	21	51018	2	1	2	1	0.1	Rab GDP dissociation inhibitor beta OS=Mus musculus OX=10090 GN=Gdi2 PE=1 SV=1
0.05	363	1	SwissProt	RS7_MOU	16	22113	1	1	1	1	0.24	40S ribosomal protein S7 OS=Mus musculus OX=10090 GN=Rps7 PE=2 SV=1
0.05	372	1	SwissProt	MIC19_M	15	26546	1	1	1	1	0.19	MICOS complex subunit Mic19 OS=Mus musculus OX=10090 GN=Chchd3 PE=1 SV=1
0.05	373	1	SwissProt	NUD12_M	15	52162	2	1	2	1	0.09	Peroxisomal NADH pyrophosphatase NUDT12 OS=Mus musculus OX=10090 GN=Nudt12 PE=1 SV=1
0.04	43	1	SwissProt	FINC_MOU	148	276017	9	6	7	5	0.09	Fibronectin OS=Mus musculus OX=10090 GN=Fn1 PE=1 SV=4
0.04	3	11	SwissProt	KRT85_M	134	57377	3	3	2	2	0.18	Keratin, type II cuticular Hb5 OS=Mus musculus OX=10090 GN=Krt85 PE=1 SV=2
0.04	73	1	SwissProt	TLN1_MO	99	271820	11	4	10	4	0.07	Talin-1 OS=Mus musculus OX=10090 GN=Tln1 PE=1 SV=2
0.04	33	3	SwissProt	AL1A1_M	71	55060	3	3	2	2	0.19	Retinal dehydrogenase 1 OS=Mus musculus OX=10090 GN=Aldh1a1 PE=1 SV=5
0.04	128	1	SwissProt	GRP75_M	60	73701	2	2	2	2	0.14	Stress-70 protein, mitochondrial OS=Mus musculus OX=10090 GN=Hspa9 PE=1 SV=3

0.04	142	1	SwissProt	IF2A_MOU	56	36371	1	1	1	1	0.14	Eukaryotic translation initiation factor 2 subunit 1 OS=Mus musculus OX=10090 GN=Eif2s1 PE=1 SV=3
0.04	151	1	SwissProt	PA1B3_MO	54	25951	1	1	1	1	0.2	Platelet-activating factor acetylhydrolase IB subunit gamma OS=Mus musculus OX=10090 GN=Pafah1b3 PE=1 SV=1
0.04	68	3	SwissProt	BIP_MOUS	53	72492	3	2	3	2	0.14	Endoplasmic reticulum chaperone BiP OS=Mus musculus OX=10090 GN=Hspa5 PE=1 SV=3
0.04	172	1	SwissProt	PDIA6_MO	48	48469	1	1	1	1	0.1	Protein disulfide-isomerase A6 OS=Mus musculus OX=10090 GN=Pdia6 PE=1 SV=3
0.04	175	1	SwissProt	ACADM_M	46	46908	1	1	1	1	0.11	Medium-chain specific acyl-CoA dehydrogenase, mitochondrial OS=Mus musculus OX=10090 GN=Acadm PE=1 SV=1
0.04	114	2	SwissProt	IDHC_MOI	44	47044	2	2	2	2	0.22	Isocitrate dehydrogenase [NADP] cytoplasmic OS=Mus musculus OX=10090 GN=Idh1 PE=1 SV=2
0.04	198	1	SwissProt	PRDX5_MI	42	22226	1	1	1	1	0.23	Peroxiredoxin-5, mitochondrial OS=Mus musculus OX=10090 GN=Prdx5 PE=1 SV=2
0.04	202	1	SwissProt	KCRM_MO	40	43246	2	2	2	2	0.24	Creatine kinase M-type OS=Mus musculus OX=10090 GN=Ckm PE=1 SV=1
0.04	205	1	SwissProt	MK03_MO	40	43381	2	1	2	1	0.11	Mitogen-activated protein kinase 3 OS=Mus musculus OX=10090 GN=Mapk3 PE=1 SV=5
0.04	215	1	SwissProt	LASP1_MO	38	30374	1	1	1	1	0.17	LIM and SH3 domain protein 1 OS=Mus musculus OX=10090 GN=Lasp1 PE=1 SV=1
0.04	219	1	SwissProt	EMIL1_MO	38	108830	4	1	4	1	0.04	EMILIN-1 OS=Mus musculus OX=10090 GN=Emilin1 PE=1 SV=1
0.04	225	1	SwissProt	CAVN1_M	37	43927	1	1	1	1	0.11	Caveolae-associated protein 1 OS=Mus musculus OX=10090 GN=Cavin1 PE=1 SV=1
0.04	242	1	SwissProt	PEBP1_MO	34	20988	1	1	1	1	0.25	Phosphatidylethanolamine-binding protein 1 OS=Mus musculus OX=10090 GN=Pebp1 PE=1 SV=3
0.04	245	1	SwissProt	FAM3A_M	33	25605	1	1	1	1	0.2	Protein FAM3A OS=Mus musculus OX=10090 GN=Fam3a PE=2 SV=1
0.04	254	1	SwissProt	AATM_MO	31	47780	2	1	2	1	0.1	Aspartate aminotransferase, mitochondrial OS=Mus musculus OX=10090 GN=Got2 PE=1 SV=1
0.04	266	1	SwissProt	QCR2_MO	30	48262	1	1	1	1	0.1	Cytochrome b-c1 complex subunit 2, mitochondrial OS=Mus musculus OX=10090 GN=Uqcrc2 PE=1 SV=1
0.04	269	1	SwissProt	6PGD_MO	29	53726	2	1	2	1	0.09	6-phosphogluconate dehydrogenase, decarboxylating OS=Mus musculus OX=10090 GN=Pgd PE=1 SV=3
0.04	282	1	SwissProt	ODPA_MO	28	43888	2	1	2	1	0.11	Pyruvate dehydrogenase E1 component subunit alpha, somatic form, mitochondrial OS=Mus musculus OX=10090 GN=Pdha1 PE=1 SV=1
0.04	283	1	SwissProt	EF2_MOUS	27	96222	5	3	5	3	0.16	Elongation factor 2 OS=Mus musculus OX=10090 GN=Eef2 PE=1 SV=2
0.04	285	1	SwissProt	MVP_MOI	27	96150	3	2	3	2	0.1	Major vault protein OS=Mus musculus OX=10090 GN=Mvp PE=1 SV=4
0.04	286	1	SwissProt	CH60_MO	27	61088	2	1	2	1	0.08	60 kDa heat shock protein, mitochondrial OS=Mus musculus OX=10090 GN=Hspd1 PE=1 SV=1
0.04	288	1	SwissProt	PARVA_M	27	42361	2	2	2	2	0.25	Alpha-parvin OS=Mus musculus OX=10090 GN=Parva PE=1 SV=1
0.04	298	1	SwissProt	GSTA1_MO	25	25706	2	2	1	1	0.2	Glutathione S-transferase A1 OS=Mus musculus OX=10090 GN=Gsta1 PE=1 SV=2
0.04	312	1	SwissProt	SDHB_MO	23	32591	1	1	1	1	0.15	Succinate dehydrogenase [ubiquinone] iron-sulfur subunit, mitochondrial OS=Mus musculus OX=10090 GN=Sdhb PE=1 SV=1
0.04	346	1	SwissProt	NHRF1_M	18	38862	1	1	1	1	0.13	Na(+)/H(+) exchange regulatory cofactor NHE-RF1 OS=Mus musculus OX=10090 GN=Slc9a3r1 PE=1 SV=3
0.04	348	1	SwissProt	PLCA_MO	18	32031	2	1	1	1	0.16	1-acyl-sn-glycerol-3-phosphate acyltransferase alpha OS=Mus musculus OX=10090 GN=Agpat1 PE=1 SV=1
0.04	356	1	SwissProt	TES_MOUS	17	49605	2	1	2	1	0.1	Testin OS=Mus musculus OX=10090 GN=Tes PE=1 SV=1
0.04	368	1	SwissProt	AL4A1_MO	16	62258	2	1	2	1	0.08	Delta-1-pyrroline-5-carboxylate dehydrogenase, mitochondrial OS=Mus musculus OX=10090 GN=Aldh4a1 PE=1 SV=3
0.04	380	1	SwissProt	CLCB_MO	14	25270	1	1	1	1	0.2	Clathrin light chain B OS=Mus musculus OX=10090 GN=Cltb PE=1 SV=1
0.03	5	7	SwissProt	KRT35_MO	103	51809	6	5	2	2	0.21	Keratin, type I cuticular Ha5 OS=Mus musculus OX=10090 GN=Krt35 PE=1 SV=1
0.03	80	1	SwissProt	DPYL2_MO	88	62638	1	1	1	1	0.08	Dihydropyrimidinase-related protein 2 OS=Mus musculus OX=10090 GN=Dpysl2 PE=1 SV=2
0.03	87	1	SwissProt	MYLK_MO	83	215415	5	4	5	4	0.09	Myosin light chain kinase, smooth muscle OS=Mus musculus OX=10090 GN=Mylk PE=1 SV=3
0.03	88	1	SwissProt	ODO1_MO	83	117572	3	3	3	3	0.13	2-oxoglutarate dehydrogenase, mitochondrial OS=Mus musculus OX=10090 GN=Ogdh PE=1 SV=3
0.03	99	1	SwissProt	NPTN_MO	75	44688	1	1	1	1	0.11	Neuroplastin OS=Mus musculus OX=10090 GN=Nptn PE=1 SV=3
0.03	102	1	SwissProt	HNRPM_M	71	77940	2	2	2	2	0.13	Heterogeneous nuclear ribonucleoprotein M OS=Mus musculus OX=10090 GN=Hnrnpm PE=1 SV=3
0.03	107	1	SwissProt	NIPS1_MO	69	33570	1	1	1	1	0.15	Protein NipSnap homolog 1 OS=Mus musculus OX=10090 GN=Nipsnap1 PE=1 SV=1
0.03	134	1	SwissProt	CAD17_MI	58	92045	2	2	2	2	0.11	Cadherin-17 OS=Mus musculus OX=10090 GN=Cdh17 PE=1 SV=1
0.03	138	1	SwissProt	NDUS1_M	58	80752	2	2	2	2	0.12	NADH-ubiquinone oxidoreductase 75 kDa subunit, mitochondrial OS=Mus musculus OX=10090 GN=Ndufs1 PE=1 SV=2
0.03	161	1	SwissProt	UD12_MO	51	60987	2	1	2	1	0.08	UDP-glucuronosyltransferase 1-2 OS=Mus musculus OX=10090 GN=Ugt1a2 PE=1 SV=1
0.03	164	1	SwissProt	NID1_MOI	50	139302	4	2	4	2	0.07	Nidogen-1 OS=Mus musculus OX=10090 GN=Nid1 PE=1 SV=2

0.03	169	1	SwissProt	HEM2_MC	48	36456	1	1	1	1	0.14	Delta-aminolevulinic acid dehydratase OS=Mus musculus OX=10090 GN=Alad PE=1 SV=1
0.03	174	1	SwissProt	PDXD1_M	47	88136	2	1	2	1	0.06	Pyridoxal-dependent decarboxylase domain-containing protein 1 OS=Mus musculus OX=10090 GN=Pdxdc1 PE=1 SV=2
0.03	180	1	SwissProt	MYPT2_M	46	109326	2	1	2	1	0.04	Protein phosphatase 1 regulatory subunit 12B OS=Mus musculus OX=10090 GN=Ppp1r12b PE=1 SV=2
0.03	188	1	SwissProt	SQOR_MC	44	50706	1	1	1	1	0.1	Sulfide:quinone oxidoreductase, mitochondrial OS=Mus musculus OX=10090 GN=Sqor PE=1 SV=3
0.03	190	1	SwissProt	HOOK2_M	43	83885	5	2	3	2	0.13	Protein Hook homolog 2 OS=Mus musculus OX=10090 GN=Hook2 PE=1 SV=3
0.03	203	1	SwissProt	WDR1_MC	40	67049	2	1	2	1	0.07	WD repeat-containing protein 1 OS=Mus musculus OX=10090 GN=Wdr1 PE=1 SV=3
0.03	206	1	SwissProt	ACADS_M	40	45146	1	1	1	1	0.11	Short-chain specific acyl-CoA dehydrogenase, mitochondrial OS=Mus musculus OX=10090 GN=Acads PE=1 SV=2
0.03	211	1	SwissProt	RBMX_MC	39	42275	1	1	1	1	0.12	RNA-binding motif protein, X chromosome OS=Mus musculus OX=10090 GN=Rbmx PE=1 SV=1
0.03	213	1	SwissProt	COX2_MO	39	26130	1	1	1	1	0.2	Cytochrome c oxidase subunit 2 OS=Mus musculus OX=10090 GN=Mtco2 PE=1 SV=1
0.03	229	1	SwissProt	TGM3_MC	36	77717	3	3	3	3	0.2	Protein-glutamine gamma-glutamyltransferase E OS=Mus musculus OX=10090 GN=Tgm3 PE=1 SV=2
0.03	233	1	SwissProt	ANXA3_M	35	36533	1	1	1	1	0.14	Annexin A3 OS=Mus musculus OX=10090 GN=Anxa3 PE=1 SV=4
0.03	234	1	SwissProt	LIMA1_MC	35	84635	2	1	2	1	0.06	LIM domain and actin-binding protein 1 OS=Mus musculus OX=10090 GN=Lima1 PE=1 SV=3
0.03	236	1	SwissProt	TALDO_M	35	37534	1	1	1	1	0.13	Transaldolase OS=Mus musculus OX=10090 GN=Taldo1 PE=1 SV=2
0.03	259	1	SwissProt	FUBP2_MC	31	77184	2	1	2	1	0.06	Far upstream element-binding protein 2 OS=Mus musculus OX=10090 GN=Khsrp PE=1 SV=2
0.03	261	1	SwissProt	MUC13_M	31	59805	1	1	1	1	0.08	Mucin-13 OS=Mus musculus OX=10090 GN=Muc13 PE=2 SV=1
0.03	270	1	SwissProt	CLIC1_MO	29	27338	1	1	1	1	0.19	Chloride intracellular channel protein 1 OS=Mus musculus OX=10090 GN=Clic1 PE=1 SV=3
0.03	276	1	SwissProt	ANX11_M	28	54387	1	1	1	1	0.09	Annexin A11 OS=Mus musculus OX=10090 GN=Anxa11 PE=1 SV=2
0.03	280	1	SwissProt	CALX_MO	28	67635	2	1	2	1	0.07	Calnexin OS=Mus musculus OX=10090 GN=Canx PE=1 SV=1
0.03	284	1	SwissProt	SRBS2_MC	27	133464	3	1	3	1	0.04	Sorbin and SH3 domain-containing protein 2 OS=Mus musculus OX=10090 GN=Sorbs2 PE=1 SV=2
0.03	318	1	SwissProt	G3BP1_MC	22	51854	1	1	1	1	0.1	Ras GTPase-activating protein-binding protein 1 OS=Mus musculus OX=10090 GN=G3bp1 PE=1 SV=1
0.03	320	1	SwissProt	DNPEP_M	22	52744	1	1	1	1	0.09	Aspartyl aminopeptidase OS=Mus musculus OX=10090 GN=Dnpep PE=1 SV=2
0.03	329	1	SwissProt	HNRPU_M	21	88661	3	1	3	1	0.05	Heterogeneous nuclear ribonucleoprotein U OS=Mus musculus OX=10090 GN=Hnrnpu PE=1 SV=1
0.03	330	1	SwissProt	EPCAM_M	21	35681	1	1	1	1	0.14	Epithelial cell adhesion molecule OS=Mus musculus OX=10090 GN=Epcam PE=1 SV=1
0.03	336	1	SwissProt	GPD1L_MC	20	38828	1	1	1	1	0.13	Glycerol-3-phosphate dehydrogenase 1-like protein OS=Mus musculus OX=10090 GN=Gpd1l PE=1 SV=2
0.03	341	1	SwissProt	UGDH_MC	19	55482	1	1	1	1	0.09	UDP-glucose 6-dehydrogenase OS=Mus musculus OX=10090 GN=Ugdh PE=1 SV=1
0.03	342	1	SwissProt	ZYX_MOU	19	61818	1	1	1	1	0.08	Zyxin OS=Mus musculus OX=10090 GN=Zyx PE=1 SV=2
0.03	344	1	SwissProt	GSTT1_MC	18	27641	2	1	1	1	0.19	Glutathione S-transferase theta-1 OS=Mus musculus OX=10090 GN=Gstt1 PE=1 SV=4
0.03	349	1	SwissProt	ECHM_MC	18	31853	1	1	1	1	0.16	Enoyl-CoA hydratase, mitochondrial OS=Mus musculus OX=10090 GN=Echs1 PE=1 SV=1
0.03	354	1	SwissProt	PSA7_MO	17	28009	1	1	1	1	0.19	Proteasome subunit alpha type-7 OS=Mus musculus OX=10090 GN=Psma7 PE=1 SV=1
0.03	355	1	SwissProt	5HT1F_MC	17	42520	1	1	1	1	0.12	5-hydroxytryptamine receptor 1F OS=Mus musculus OX=10090 GN=Htr1f PE=2 SV=1
0.03	365	1	SwissProt	ENTP2_MC	16	54912	1	1	1	1	0.09	Ectonucleoside triphosphate diphosphohydrolase 2 OS=Mus musculus OX=10090 GN=Entpd2 PE=1 SV=2
0.03	366	1	SwissProt	RNH1_MC	16	32070	1	1	1	1	0.16	Ribonuclease H1 OS=Mus musculus OX=10090 GN=Rnaseh1 PE=2 SV=1
0.03	369	1	SwissProt	DLDH_MO	16	54751	1	1	1	1	0.09	Dihydrolipoyl dehydrogenase, mitochondrial OS=Mus musculus OX=10090 GN=Dld PE=1 SV=2
0.03	375	1	SwissProt	ADCL3_MC	15	47051	3	1	1	1	0.11	Arylacetamide deacetylase-like 3 OS=Mus musculus OX=10090 GN=Aadacl3 PE=3 SV=1
0.03	377	1	SwissProt	NONO_MC	14	54620	1	1	1	1	0.09	Non-POU domain-containing octamer-binding protein OS=Mus musculus OX=10090 GN=Nono PE=1 SV=3
0.03	382	1	SwissProt	LKHA4_MC	14	69634	2	1	2	1	0.07	Leukotriene A-4 hydrolase OS=Mus musculus OX=10090 GN=Lta4h PE=1 SV=4
0.03	384	1	SwissProt	NOA1_MC	14	78128	2	1	2	1	0.06	Nitric oxide-associated protein 1 OS=Mus musculus OX=10090 GN=Noa1 PE=1 SV=1
0.03	385	1	SwissProt	TCPZ_MO	14	58424	2	1	2	1	0.08	T-complex protein 1 subunit zeta OS=Mus musculus OX=10090 GN=Cct6a PE=1 SV=3
0.03	386	1	SwissProt	COR1A_M	13	51641	1	1	1	1	0.1	Coronin-1A OS=Mus musculus OX=10090 GN=Coro1a PE=1 SV=5
0.02	78	1	SwissProt	CO1A1_M	92	138974	2	2	2	2	0.07	Collagen alpha-1(I) chain OS=Mus musculus OX=10090 GN=Col1a1 PE=1 SV=4

0.02	81	1	SwissProt	LAMC1_M	88	182830	2	1	2	1	0.03	Laminin subunit gamma-1 OS=Mus musculus OX=10090 GN=Lamc1 PE=1 SV=2
0.02	95	1	SwissProt	ITA5_MOU	77	116111	2	2	2	2	0.08	Integrin alpha-5 OS=Mus musculus OX=10090 GN=Itga5 PE=1 SV=3
0.02	97	1	SwissProt	ITB1_MOU	76	91424	2	2	2	2	0.11	Integrin beta-1 OS=Mus musculus OX=10090 GN=Itgb1 PE=1 SV=1
0.02	98	1	SwissProt	HNRPK_M	76	51230	1	1	1	1	0.1	Heterogeneous nuclear ribonucleoprotein K OS=Mus musculus OX=10090 GN=Hnrnpk PE=1 SV=1
0.02	115	1	SwissProt	CO4A2_M	65	168417	3	2	3	2	0.06	Collagen alpha-2(IV) chain OS=Mus musculus OX=10090 GN=Col4a2 PE=1 SV=4
0.02	145	1	SwissProt	ECHB_MO	56	51639	1	1	1	1	0.1	Trifunctional enzyme subunit beta, mitochondrial OS=Mus musculus OX=10090 GN=Hadhb PE=1 SV=1
0.02	149	1	SwissProt	GMDS_MO	54	42300	1	1	1	1	0.12	GDP-mannose 4,6 dehydratase OS=Mus musculus OX=10090 GN=Gmds PE=1 SV=1
0.02	158	1	SwissProt	ACADL_M	51	48277	1	1	1	1	0.1	Long-chain specific acyl-CoA dehydrogenase, mitochondrial OS=Mus musculus OX=10090 GN=Acadl PE=1 SV=2
0.02	166	1	SwissProt	IDH3A_MO	49	40069	1	1	1	1	0.12	Isocitrate dehydrogenase [NAD] subunit alpha, mitochondrial OS=Mus musculus OX=10090 GN=Idh3a PE=1 SV=1
0.02	132	2	SwissProt	CROCC_M	43	227379	7	2	4	2	0.04	Rootletin OS=Mus musculus OX=10090 GN=Crocc PE=1 SV=2
0.02	193	1	SwissProt	SND1_MO	42	102709	2	1	2	1	0.05	Staphylococcal nuclease domain-containing protein 1 OS=Mus musculus OX=10090 GN=Snd1 PE=1 SV=1
0.02	196	1	SwissProt	MECR_MO	42	40545	1	1	1	1	0.12	Enoyl-[acyl-carrier-protein] reductase, mitochondrial OS=Mus musculus OX=10090 GN=Mecr PE=1 SV=2
0.02	209	1	SwissProt	MOCS3_M	39	50313	5	2	1	1	0.1	Adenylyltransferase and sulfurtransferase MOCS3 OS=Mus musculus OX=10090 GN=Mocs3 PE=1 SV=1
0.02	212	1	SwissProt	BGH3_MO	39	75177	2	2	2	2	0.13	Transforming growth factor-beta-induced protein ig-h3 OS=Mus musculus OX=10090 GN=Tgfbi PE=1 SV=1
0.02	220	1	SwissProt	EFTU_MO	37	49876	1	1	1	1	0.1	Elongation factor Tu, mitochondrial OS=Mus musculus OX=10090 GN=Tufm PE=1 SV=1
0.02	230	1	SwissProt	CALU_MO	36	37155	1	1	1	1	0.14	Calumenin OS=Mus musculus OX=10090 GN=Calu PE=1 SV=1
0.02	243	1	SwissProt	AIFM1_MO	33	66952	1	1	1	1	0.07	Apoptosis-inducing factor 1, mitochondrial OS=Mus musculus OX=10090 GN=Aifm1 PE=1 SV=1
0.02	244	1	SwissProt	K1C12_MO	33	52774	1	1	1	1	0.09	Keratin, type I cytoskeletal 12 OS=Mus musculus OX=10090 GN=Krt12 PE=1 SV=2
0.02	258	1	SwissProt	PYGB_MO	31	97353	2	1	2	1	0.05	Glycogen phosphorylase, brain form OS=Mus musculus OX=10090 GN=Pygb PE=1 SV=3
0.02	251	1	SwissProt	GFPT1_MO	31	79287	2	2	2	2	0.13	Glutamine--fructose-6-phosphate aminotransferase [isomerizing] 1 OS=Mus musculus OX=10090 GN=Gfpt1 PE=1 SV=3
0.02	273	1	SwissProt	IVD_MOU	29	46695	1	1	1	1	0.11	Isovaleryl-CoA dehydrogenase, mitochondrial OS=Mus musculus OX=10090 GN=Ivd PE=1 SV=1
0.02	278	1	SwissProt	DX39A_MO	28	49549	1	1	1	1	0.1	ATP-dependent RNA helicase DDX39A OS=Mus musculus OX=10090 GN=Ddx39a PE=1 SV=1
0.02	291	1	SwissProt	SLMAP_M	26	97729	2	1	2	1	0.05	Sarcolemmal membrane-associated protein OS=Mus musculus OX=10090 GN=Slmap PE=1 SV=2
0.02	302	1	SwissProt	TM11E_MO	24	48776	2	1	1	1	0.11	Transmembrane protease serine 11E OS=Mus musculus OX=10090 GN=Tmprss11e PE=1 SV=2
0.02	304	1	SwissProt	AL1L1_MO	24	99502	2	1	2	1	0.05	Cytosolic 10-formyltetrahydrofolate dehydrogenase OS=Mus musculus OX=10090 GN=Aldh1l1 PE=1 SV=1
0.02	305	1	SwissProt	SYSC_MOU	24	58865	1	1	1	1	0.08	Serine--tRNA ligase, cytoplasmic OS=Mus musculus OX=10090 GN=Sars PE=1 SV=3
0.02	331	1	SwissProt	SPAT7_MO	21	66184	2	1	1	1	0.07	Spermatogenesis-associated protein 7 homolog OS=Mus musculus OX=10090 GN=Spata7 PE=1 SV=1
0.02	332	1	SwissProt	RINI_MOU	21	51495	1	1	1	1	0.1	Ribonuclease inhibitor OS=Mus musculus OX=10090 GN=Rnh1 PE=1 SV=1
0.02	338	1	SwissProt	PHB2_MO	20	33276	1	1	1	1	0.15	Prohibitin-2 OS=Mus musculus OX=10090 GN=Phb2 PE=1 SV=1
0.02	343	1	SwissProt	TERA_MO	19	89950	2	1	2	1	0.05	Transitional endoplasmic reticulum ATPase OS=Mus musculus OX=10090 GN=Vcp PE=1 SV=4
0.02	347	1	SwissProt	TCPA_MO	18	60867	1	1	1	1	0.08	T-complex protein 1 subunit alpha OS=Mus musculus OX=10090 GN=Tcp1 PE=1 SV=3
0.02	353	1	SwissProt	PP1R7_MO	17	41380	1	1	1	1	0.12	Protein phosphatase 1 regulatory subunit 7 OS=Mus musculus OX=10090 GN=Ppp1r7 PE=1 SV=2
0.02	364	1	SwissProt	CAVN2_M	16	46792	1	1	1	1	0.11	Caveolae-associated protein 2 OS=Mus musculus OX=10090 GN=Cavin2 PE=1 SV=3
0.02	367	1	SwissProt	SIAT2_MO	16	60496	2	2	1	1	0.08	Beta-galactoside alpha-2,6-sialyltransferase 2 OS=Mus musculus OX=10090 GN=St6gal2 PE=2 SV=2
0.02	371	1	SwissProt	ATPG_MO	16	32979	1	1	1	1	0.15	ATP synthase subunit gamma, mitochondrial OS=Mus musculus OX=10090 GN=Atp5f1c PE=1 SV=1
0.02	374	1	SwissProt	PLSL_MOU	15	70732	1	1	1	1	0.07	Plastin-2 OS=Mus musculus OX=10090 GN=Lcp1 PE=1 SV=4
0.02	376	1	SwissProt	AT2A2_MO	14	116437	2	1	2	1	0.04	Sarcoplasmic/endoplasmic reticulum calcium ATPase 2 OS=Mus musculus OX=10090 GN=Atp2a2 PE=1 SV=2
0.01	125	1	SwissProt	UBA1_MO	62	118931	1	1	1	1	0.04	Ubiquitin-like modifier-activating enzyme 1 OS=Mus musculus OX=10090 GN=Uba1 PE=1 SV=1
0.01	155	1	SwissProt	DSG1A_M	52	115551	1	1	1	1	0.04	Desmoglein-1-alpha OS=Mus musculus OX=10090 GN=Dsg1a PE=2 SV=2
0.01	160	1	SwissProt	CAN2_MO	51	80677	1	1	1	1	0.06	Calpain-2 catalytic subunit OS=Mus musculus OX=10090 GN=Capn2 PE=1 SV=4

0.01	163	1	SwissProt	TRFE_MOU	50	78841	1	1	1	1	0.06	Serotransferrin OS=Mus musculus OX=10090 GN=Tf PE=1 SV=1
0.01	176	1	SwissProt	PALLD_MO	46	153576	1	1	1	1	0.03	Palladin OS=Mus musculus OX=10090 GN=Palld PE=1 SV=2
0.01	182	1	SwissProt	CO4A1_M	46	161719	1	1	1	1	0.03	Collagen alpha-1(IV) chain OS=Mus musculus OX=10090 GN=Col4a1 PE=1 SV=4
0.01	194	1	SwissProt	SFPQ_MO	42	75508	1	1	1	1	0.06	Splicing factor, proline- and glutamine-rich OS=Mus musculus OX=10090 GN=Sfpq PE=1 SV=1
0.01	208	1	SwissProt	ODP2_MO	39	68469	1	1	1	1	0.07	Dihydrolipoyllysine-residue acetyltransferase component of pyruvate dehydrogenase complex, mitochondrial OS=Mus musculus OX=10
0.01	210	1	SwissProt	TENA_MO	39	237304	3	1	2	1	0.02	Tenascin OS=Mus musculus OX=10090 GN=Tnc PE=1 SV=1
0.01	222	1	SwissProt	ACSF2_MO	37	68591	1	1	1	1	0.07	Acyl-CoA synthetase family member 2, mitochondrial OS=Mus musculus OX=10090 GN=Acsf2 PE=1 SV=1
0.01	246	1	SwissProt	RASL2_MO	33	91087	1	1	1	1	0.05	Ras GTPase-activating protein 4 OS=Mus musculus OX=10090 GN=Rasa4 PE=1 SV=1
0.01	256	1	SwissProt	DHE3_MO	31	61640	1	1	1	1	0.08	Glutamate dehydrogenase 1, mitochondrial OS=Mus musculus OX=10090 GN=Glud1 PE=1 SV=1
0.01	260	1	SwissProt	ACLY_MO	31	120564	1	1	1	1	0.04	ATP-citrate synthase OS=Mus musculus OX=10090 GN=Acly PE=1 SV=1
0.01	281	1	SwissProt	PLEC_MOU	28	535800	4	1	3	1	0.01	Plectin OS=Mus musculus OX=10090 GN=Plec PE=1 SV=3
0.01	293	1	SwissProt	MTA70_M	25	65260	1	1	1	1	0.07	N6-adenosine-methyltransferase subunit METTL3 OS=Mus musculus OX=10090 GN=Mettl3 PE=1 SV=2
0.01	294	1	SwissProt	TBC15_MO	25	77447	1	1	1	1	0.06	TBC1 domain family member 15 OS=Mus musculus OX=10090 GN=Tbc1d15 PE=1 SV=1
0.01	296	1	SwissProt	NID2_MO	25	156610	1	1	1	1	0.03	Nidogen-2 OS=Mus musculus OX=10090 GN=Nid2 PE=1 SV=2
0.01	299	1	SwissProt	MUC2_MO	25	305502	2	1	2	1	0.02	Mucin-2 (Fragments) OS=Mus musculus OX=10090 GN=Muc2 PE=1 SV=2
0.01	301	1	SwissProt	TYW4_MO	24	75989	3	2	1	1	0.06	tRNA wybutosine-synthesizing protein 4 OS=Mus musculus OX=10090 GN=Lcmt2 PE=2 SV=4
0.01	317	1	SwissProt	FERM2_M	23	78435	1	1	1	1	0.06	Fermitin family homolog 2 OS=Mus musculus OX=10090 GN=Fermt2 PE=1 SV=1
0.01	319	1	SwissProt	RTN4_MO	22	127048	1	1	1	1	0.04	Reticulon-4 OS=Mus musculus OX=10090 GN=Rtn4 PE=1 SV=2
0.01	334	1	SwissProt	DESP_MO	21	335158	3	1	3	1	0.01	Desmoplakin OS=Mus musculus OX=10090 GN=Dsp PE=1 SV=1
0.01	335	1	SwissProt	TRFL_MOU	21	79670	1	1	1	1	0.06	Lactotransferrin OS=Mus musculus OX=10090 GN=Ltf PE=1 SV=4
0.01	350	1	SwissProt	MTM1_MO	18	70028	1	1	1	1	0.07	Myotubularin OS=Mus musculus OX=10090 GN=Mtm1 PE=1 SV=2
0.01	357	1	SwissProt	LAMA4_M	17	204372	1	1	1	1	0.02	Laminin subunit alpha-4 OS=Mus musculus OX=10090 GN=Lama4 PE=1 SV=2
0.01	361	1	SwissProt	SBNO2_M	16	150455	1	1	1	1	0.03	Protein strawberry notch homolog 2 OS=Mus musculus OX=10090 GN=Sbno2 PE=1 SV=1
0.01	362	1	SwissProt	GANAB_M	16	107300	1	1	1	1	0.05	Neutral alpha-glucosidase AB OS=Mus musculus OX=10090 GN=Ganab PE=1 SV=1
0.01	370	1	SwissProt	CO1A2_M	16	129992	1	1	1	1	0.04	Collagen alpha-2(I) chain OS=Mus musculus OX=10090 GN=Col1a2 PE=1 SV=2
0.01	379	1	SwissProt	GUF1_MO	14	72760	208	1	1	1	0.07	Translation factor Guf1, mitochondrial OS=Mus musculus OX=10090 GN=Guf1 PE=1 SV=1
0	257	1	SwissProt	KIF1B_MO	31	205322	1	1	1	1	0.02	Kinesin-like protein KIF1B OS=Mus musculus OX=10090 GN=Kif1b PE=1 SV=2
0	339	1	SwissProt	KI67_MOU	19	352247	1	1	1	1	0.01	Proliferation marker protein Ki-67 OS=Mus musculus OX=10090 GN=Mki67 PE=1 SV=1
0	351	1	SwissProt	MAST4_M	18	286338	1	1	1	1	0.02	Microtubule-associated serine/threonine-protein kinase 4 OS=Mus musculus OX=10090 GN=Mast4 PE=1 SV=3
0	358	1	SwissProt	IF140_MO	17	167479	1	1	1	1	0.03	Intraflagellar transport protein 140 homolog OS=Mus musculus OX=10090 GN=Ift140 PE=1 SV=1

Figure 8.5: Protein composition of 3-month-old mouse DC identified by proteomic analysis with LC / MS / MS and Mascot™ database.

APPENDIX E

Quantitative protein analysis from Chapter 5: Protein change in regulation between 3-month and 30-month mouse DC when analysed with LC / MS / MS and subsequently analysed using Progenesis™ LC-MS data analysis software.

Accession	Peptides	Score	Anova (p)*	Fold	Description	Average normalised abundance	
						Young	Aged
FLNA_MOUSE	6	480.66	3.56E-03	2.42	Filamin-A OS=Mus musculus OX=10090 GN=Flna PE=1 SV=5	2.27E+05	5.49E+05
CO6A2_MOUSE	6	351.59	1.74E-03	2.4	Collagen alpha-2(VI) chain OS=Mus musculus OX=10090 GN=Col6a2 PE=1 SV=3	1.99E+05	4.77E+05
CO6A1_MOUSE	5	317	2.04E-03	2.46	Collagen alpha-1(VI) chain OS=Mus musculus OX=10090 GN=Col6a1 PE=1 SV=1	1.58E+05	3.88E+05
ALBU_MOUSE	5	274.24	7.31E-05	3.58	Serum albumin OS=Mus musculus OX=10090 GN=Alb PE=1 SV=3	1.58E+05	5.66E+05
K2C5_MOUSE	4 (3)	268.63	0.03	2.12	Keratin, type II cytoskeletal 5 OS=Mus musculus OX=10090 GN=Krt5 PE=1 SV=1	5.90E+05	2.79E+05
TAGL_MOUSE	4	252.97	6.68E-03	2.47	Transgelin OS=Mus musculus OX=10090 GN=Tagln PE=1 SV=3	3.34E+05	8.24E+05
ETFB_MOUSE	4	251.06	1.13E-03	2.67	Electron transfer flavoprotein subunit beta OS=Mus musculus OX=10090 GN=Etfb PE=1 SV=3	8.32E+04	2.23E+05
CNN1_MOUSE	3	231.89	2.02E-03	3.01	Calponin-1 OS=Mus musculus OX=10090 GN=Cnn1 PE=1 SV=1	8.49E+04	2.56E+05
TKT_MOUSE	3	214.26	1.34E-03	2.28	Transketolase OS=Mus musculus OX=10090 GN=Tkt PE=1 SV=1	8.73E+04	2.00E+05
K2C1_MOUSE	2 (1)	204.18	0.03	3.04	Keratin, type II cytoskeletal 1 OS=Mus musculus OX=10090 GN=Krt1 PE=1 SV=4	2.21E+06	7.29E+05
VIME_MOUSE	3	178.21	0.01	2.13	Vimentin OS=Mus musculus OX=10090 GN=Vim PE=1 SV=3	3.57E+05	7.63E+05
PDIA3_MOUSE	3	174.16	0.01	2.69	Protein disulfide-isomerase A3 OS=Mus musculus OX=10090 GN=Pdia3 PE=1 SV=2	6.67E+04	1.80E+05
ANXA4_MOUSE	2	172.96	0.02	2.39	Annexin A4 OS=Mus musculus OX=10090 GN=Anxa4 PE=1 SV=4	1.69E+04	4.03E+04
RL18_MOUSE	2	171.76	6.95E-03	2.46	60S ribosomal protein L18 OS=Mus musculus OX=10090 GN=Rpl18 PE=1 SV=3	4.06E+04	9.98E+04
LMNA_MOUSE	2	169.06	0.02	2.59	Prelamin-A/C OS=Mus musculus OX=10090 GN=Lmna PE=1 SV=2	4.61E+04	1.19E+05
HSP7C_MOUSE	2	166.19	0.03	2.15	Heat shock cognate 71 kDa protein OS=Mus musculus OX=10090 GN=Hspa8 PE=1 SV=1	1.15E+05	2.49E+05
DESM_MOUSE	2	165.09	1.99E-04	2.15	Desmin OS=Mus musculus OX=10090 GN=Des PE=1 SV=3	1.03E+06	2.21E+06
ACON_MOUSE	3	164.03	0.02	2.47	Aconitate hydratase, mitochondrial OS=Mus musculus OX=10090 GN=Aco2 PE=1 SV=1	3.26E+04	8.04E+04
HS90B_MOUSE	3	162.1	0.01	3.22	Heat shock protein HSP 90-beta OS=Mus musculus OX=10090 GN=Hsp90ab1 PE=1 SV=3	5.39E+04	1.74E+05
ETFA_MOUSE	2	160.53	2.82E-03	3.4	Electron transfer flavoprotein subunit alpha, mitochondrial OS=Mus musculus OX=10090 GN=Etfa PE=1 SV=2	2.62E+04	8.90E+04
AATM_MOUSE	2	156.91	2.33E-03	4.14	Aspartate aminotransferase, mitochondrial OS=Mus musculus OX=10090 GN=Got2 PE=1 SV=1	3.00E+04	1.24E+05
TBA1A_MOUSE	2	155.35	0.02	2.27	Tubulin alpha-1A chain OS=Mus musculus OX=10090 GN=Tuba1a PE=1 SV=1	1.11E+05	2.53E+05
ATPA_MOUSE	2	153.5	6.49E-03	2.62	ATP synthase subunit alpha, mitochondrial OS=Mus musculus OX=10090 GN=Atp5f1a PE=1 SV=1	2.49E+04	6.52E+04
ALDR_MOUSE	2	153.13	0.01	2.58	Aldo-keto reductase family 1 member B1 OS=Mus musculus OX=10090 GN=Akr1b1 PE=1 SV=3	2.24E+04	5.79E+04
ANX11_MOUSE	3	144.94	6.77E-03	3.27	Annexin A11 OS=Mus musculus OX=10090 GN=Anxa11 PE=1 SV=2	2.35E+04	7.70E+04
PRDX1_MOUSE	3	140.85	3.10E-03	2.1	Peroxiredoxin-1 OS=Mus musculus OX=10090 GN=Prdx1 PE=1 SV=1	2.33E+05	4.88E+05
VINC_MOUSE	2	131.62	0.03	2.76	Vinculin OS=Mus musculus OX=10090 GN=Vcl PE=1 SV=4	3.54E+04	9.80E+04
ALDH2_MOUSE	2	125.36	0.02	2.17	Aldehyde dehydrogenase, mitochondrial OS=Mus musculus OX=10090 GN=Aldh2 PE=1 SV=1	2.90E+05	6.29E+05

IDH3A_MOUSE	2	123.7	3.63E-03	2.91	Isocitrate dehydrogenase [NAD] subunit alpha, mitochondrial OS=Mus musculus OX=10090 GN=Idh3a PE=1 SV=1	4.17E+04	1.22E+05	
PROF1_MOUSE	2	122.03	0.03	3.11	Profilin-1 OS=Mus musculus OX=10090 GN=Pfn1 PE=1 SV=2	1.15E+04	3.59E+04	
MDHM_MOUSE	2	117.37	1.09E-03	2.39	Malate dehydrogenase, mitochondrial OS=Mus musculus OX=10090 GN=Mdh2 PE=1 SV=3	1.07E+05	2.55E+05	
H12_MOUSE	2	114.25	9.10E-04	2.57	Histone H1.2 OS=Mus musculus OX=10090 GN=Hist1h1c PE=1 SV=2	3.03E+05	7.80E+05	
MDHC_MOUSE	2	101.11	5.72E-04	2.74	Malate dehydrogenase, cytoplasmic OS=Mus musculus OX=10090 GN=Mdh1 PE=1 SV=3	3.58E+04	9.83E+04	
K2C79_MOUSE	2 (1)	100.32	0.05	2.38	Keratin, type II cytoskeletal 79 OS=Mus musculus OX=10090 GN=Krt79 PE=1 SV=2	6.32E+04	2.65E+04	
UGDH_MOUSE	2	98.89	0.02	2.12	UDP-glucose 6-dehydrogenase OS=Mus musculus OX=10090 GN=Ugdh PE=1 SV=1	2.18E+04	4.62E+04	
TAGL2_MOUSE	2	97.45	1.33E-03	2.43	Transgelin-2 OS=Mus musculus OX=10090 GN=Tagln2 PE=1 SV=4	4.09E+04	9.94E+04	
GSTM1_MOUSE	2	96.81	1.42E-03	2.43	Glutathione S-transferase Mu 1 OS=Mus musculus OX=10090 GN=Gstm1 PE=1 SV=2	3.08E+04	7.50E+04	
H3C_MOUSE	2	96.39	9.36E-03	2.07	Histone H3.3C OS=Mus musculus OX=10090 GN=H3f3c PE=3 SV=3	7.34E+05	1.52E+06	
IF5A1_MOUSE	2	95.63	2.13E-03	2.39	Eukaryotic translation initiation factor 5A-1 OS=Mus musculus OX=10090 GN=Eif5a PE=1 SV=2	4.87E+04	1.16E+05	
KPYM_MOUSE	2	92.9	4.44E-04	2.15	Pyruvate kinase PKM OS=Mus musculus OX=10090 GN=Pkm PE=1 SV=4	4.93E+04	1.06E+05	
ODO2_MOUSE	2	89.16	6.55E-04	3.79	Dihydrolipoyllysine-residue succinyltransferase component of 2-oxoglutarate dehydrogenase complex, mitochondrial OS=Mus musculus OX=10090 GN=Dlst PE=1 SV=1	1.42E+04	5.39E+04	
IDHC_MOUSE	2	87.73	8.08E-03	2.41	Isocitrate dehydrogenase [NADP] cytoplasmic OS=Mus musculus OX=10090 GN=Idh1 PE=1 SV=2	6.48E+04	1.56E+05	
TGM2_MOUSE	2	86.03	9.44E-03	2.46	Protein-glutamine gamma-glutamyltransferase 2 OS=Mus musculus OX=10090 GN=Tgm2 PE=1 SV=4	3.34E+04	8.21E+04	
LUM_MOUSE	2	84.91	5.25E-03	3.18	Lumican OS=Mus musculus OX=10090 GN=Lum PE=1 SV=2	2.87E+04	9.14E+04	

Figure 8.6: Change in protein regulation in 3-month versus 30-month mouse DC identified by proteomic analysis with LC / MS / MS and Progenesis™ LC-MS data analysis software.

APPENDIX F

Chapter 5 functional clustering of the 41 proteins that were upregulated with age in the mouse distal colon.

Figure 8.7 to Figure 8.14 display proteins upregulated with age that were functionally clustered by each database. Gene nomenclature is used to label proteins. Proteins that were functionally enriched have a coloured box under gene nomenclature tag. P-values and functionally enriched proteins are colour coded as displayed in Figure 8.7.

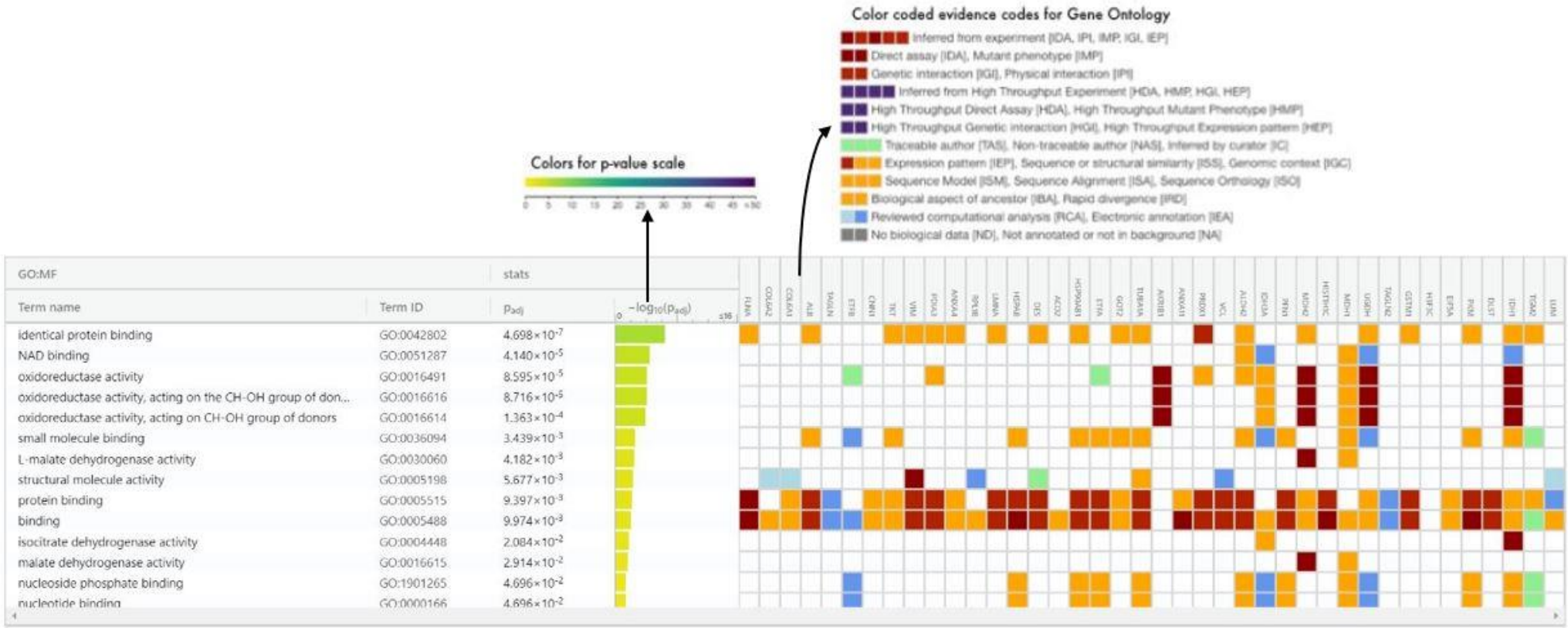

Figure 8.7: Functionally clustered proteins identified in GO:MF database. Colour coding of p-values and functionally enriched proteins is described above results. GO:MF, Gene Ontology: Molecular Function.

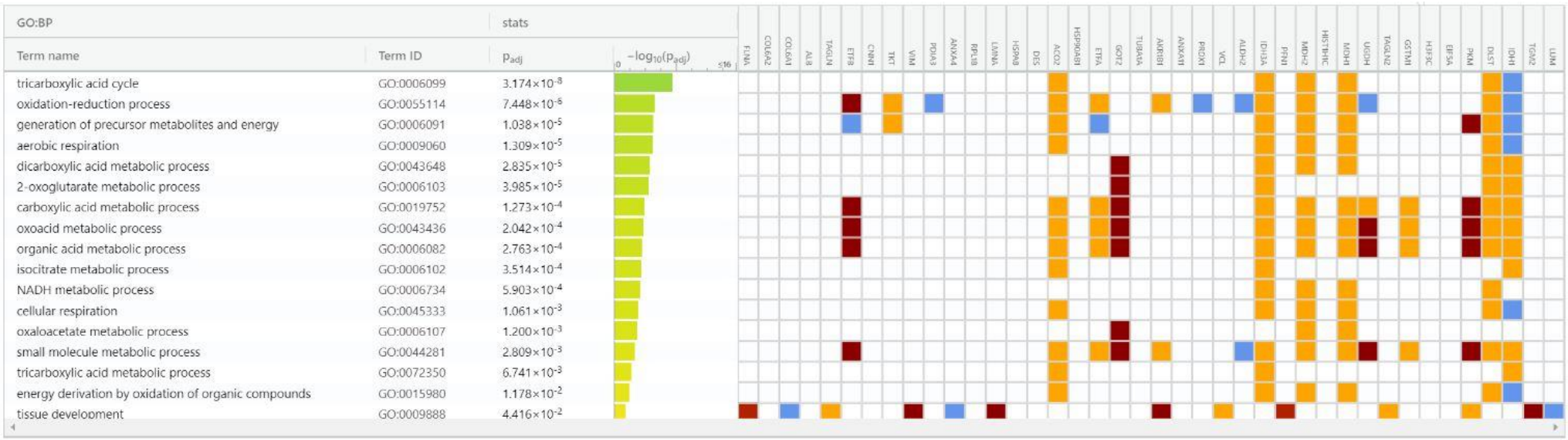

GO:BP		stats
Term name	Term ID	P_{adj}
tricarboxylic acid cycle	GO:0006099	3.174×10^{-8}
oxidation-reduction process	GO:0055114	7.448×10^{-6}
generation of precursor metabolites and energy	GO:0006091	1.038×10^{-5}
aerobic respiration	GO:0009060	1.309×10^{-5}
dicarboxylic acid metabolic process	GO:0043648	2.835×10^{-5}
2-oxoglutarate metabolic process	GO:0006103	3.985×10^{-5}
carboxylic acid metabolic process	GO:0019752	1.273×10^{-4}
oxoacid metabolic process	GO:0043436	2.042×10^{-4}
organic acid metabolic process	GO:0006082	2.763×10^{-4}
isocitrate metabolic process	GO:0006102	3.514×10^{-4}
NADH metabolic process	GO:0006734	5.903×10^{-4}
cellular respiration	GO:0045333	1.061×10^{-3}
oxaloacetate metabolic process	GO:0006107	1.200×10^{-3}
small molecule metabolic process	GO:0044281	2.809×10^{-3}
tricarboxylic acid metabolic process	GO:0072350	6.741×10^{-3}
energy derivation by oxidation of organic compounds	GO:0015980	1.178×10^{-2}
tissue development	GO:0009888	4.416×10^{-2}

Figure 8.8: Functionally clustered proteins identified in GO:BP database. GO:BP, Gene Ontology: Biological Process.

Figure 8.9: Functionally clustered proteins identified in GO:CC database. GO:CC, Gene Ontology: Cellular Component.

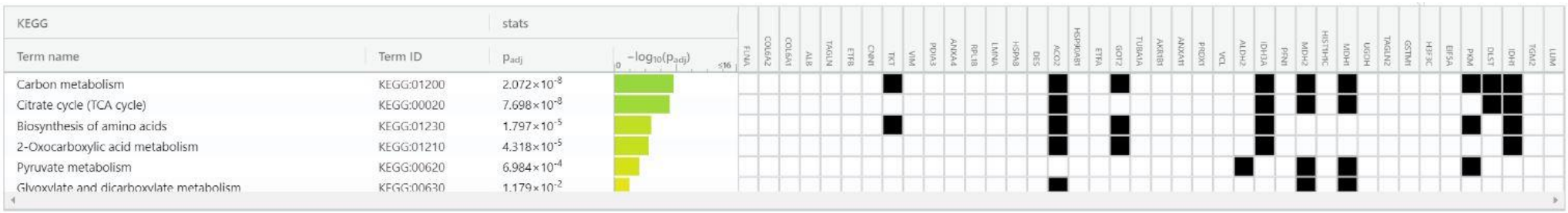

Figure 8.10: Functionally clustered proteins identified in KEGG database. KEGG, Kyoto Encyclopaedia of Genes and Genomes.

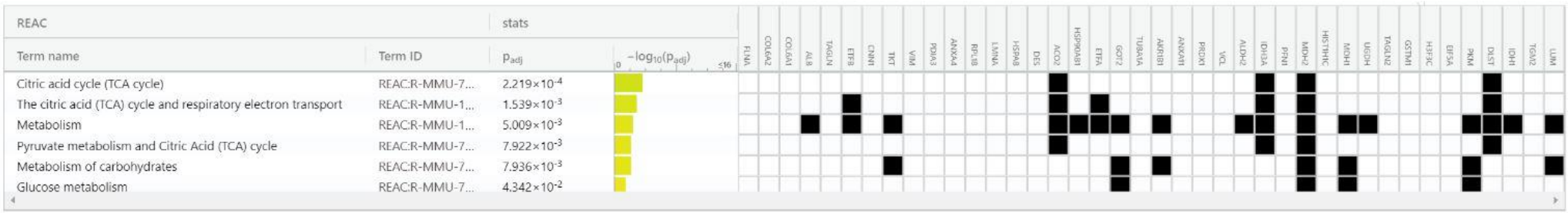

Figure 8.11: Functionally clustered proteins identified in REAC database. REAC, Reactome Pathways.

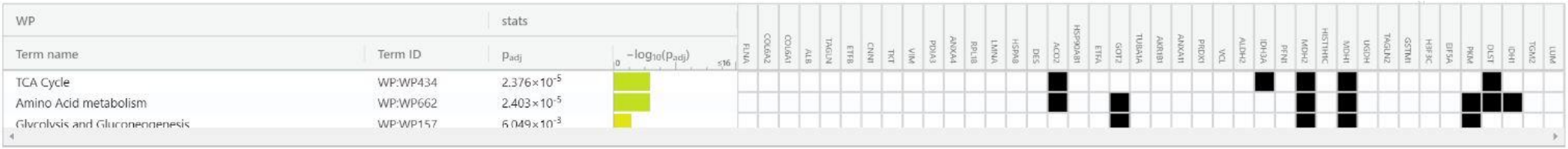

Figure 8.12: Functionally clustered proteins identified in WP database. WP, WikiPathways.

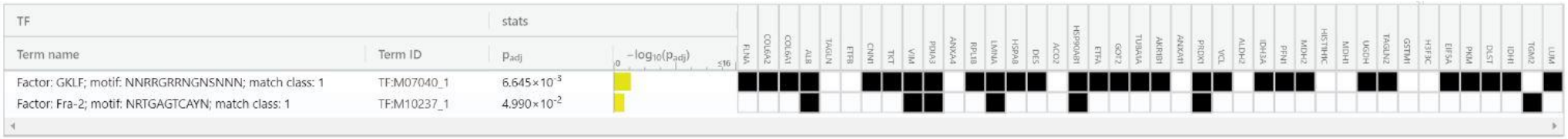

Figure 8.13: Functionally clustered proteins identified in TF database. TF, Transcription Factor.

CORUM		stats		FLNA	COL6A2	COL6A1	ALB	TAGLN	ETFB	CNN1	TKT	VIM	PDIA3	ANXA4	RPL18	LMNA	HSPA8	DES	ACO2	HSP90AB1	ETFA	GOT2	TUBA1A	AKR1B1	ANXA11	PRDX1	VCL	ALDH2	IDH3A	PRN1	MDH2	HIST1H1C	MDH1	UGDH	TAGLN2	GSTM1	HBF3C	EIF5A	PKM	DLST	IDH1	TGM2	LDHA
Term name	Term ID	p_{adj}	$-\log_{10}(p_{adj})$ 0 ≤16																																								
Profilin 1 complex	CORUM:2836	1.686×10^{-2}																																									

Figure 8.14: Functionally clustered proteins identified in CORUM Protein Complexes database.

APPENDIX G

Chapter 5 functional clustering of the three proteins that were downregulated with age in the mouse distal colon.

Figure 8.15 and *Figure 8.16* display proteins downregulated with age that were functionally clustered by each database. Gene nomenclature is used to label proteins. Proteins that are functionally enriched have a coloured box under gene nomenclature tag. P-values and functionally enriched proteins are colour coded as displayed in Figure 8.7.

GO:CC		stats				
Term name	Term ID	p_{adj}	$-\log_{10}(p_{adj})$ (0 – ≤16)	KRT5	KRT1	KRT79
keratin filament	GO:0045095	2.651×10^{-5}				
intermediate filament	GO:0005882	1.801×10^{-4}				
intermediate filament cytoskeleton	GO:0045111	2.941×10^{-4}				
polymeric cytoskeletal fiber	GO:0099513	8.587×10^{-3}				
supramolecular fiber	GO:0099512	1.888×10^{-2}				
supramolecular polymer	GO:0099081	1.927×10^{-2}				
supramolecular complex	GO:0099080	4.255×10^{-2}				

Figure 8.15: Functionally clustered proteins identified in GO:CC database. GO:CC, Gene Ontology: Cellular Component.

REAC		stats		KRT5	KRT1	KRT79
Term name	Term ID	p_{adj}	$-\log_{10}(p_{adj})$ 0 ≤16			
Formation of the cornified envelope	REAC:R-MMU-6...	2.559×10^{-4}				
Keratinization	REAC:R-MMU-6...	1.601×10^{-3}				
Developmental Biology	REAC:R-MMU-1...	2.554×10^{-2}				

Figure 8.16: Functionally clustered proteins identified in REAC database. REAC, Reactome Pathways.

APPENDIX H

Conference contributions and awards

July 2016: British society for research in Ageing (BSRA) poster submission

‘The effects of ageing on the distribution of inhibitory inputs to neurons modulating bladder activity in C57BL / 6J male mice’ (poster prize awarded)

Emily Doogan, Emily Slack, Hayley Tsang, Gary Black, Jill Saffrey, Rachel Ranson

May 2017: Three Minute Thesis (Northumbria University)

‘Ageing effects on central nervous control of the bladder and continence in male C57BL / 6J mice’ (presentation prize awarded)

Emily Doogan

May 2017: Three Minute Thesis (Sunderland University)

‘Ageing effects on central nervous control of the bladder and continence in male C57BL / 6J mice’

Emily Doogan

May 2017: Northumbria Research Conference

‘Ageing effects on central nervous control of the bladder and continence in male C57BL / 6J mice’

Emily Doogan

July 2017: BSRA poster submission

‘Ageing effects on the distribution of glutamate / GABA inputs to paraventricular neurons’

Emily Doogan, Gary Black, Jill Saffrey, Rachel Ranson